

# Flows of Nanomaterials by Stretching Boundaries



By

**Ikram Ullah**

**Department of Mathematics  
Quaid-i-Azam University  
Islamabad, Pakistan  
2020**

# Flows of Nanomaterials by Stretching Boundaries



By

**Ikram Ullah**

**Supervised By**

**Prof. Dr. Tasawar Hayat**

**Department of Mathematics  
Quaid-i-Azam University  
Islamabad, Pakistan  
2020**

# Flows of Nanomaterials by Stretching Boundaries



By

**Ikram Ullah**

A THESIS SUBMITTED IN THE PARTIAL FULFILLMENT OF THE REQUIREMENT FOR  
THE DEGREE OF  
DOCTOR OF PHILOSOPHY  
IN  
MATHEMATICS

Supervised By

**Prof. Dr. Tasawar Hayat**

**Department of Mathematics  
Quaid-i-Azam University  
Islamabad, Pakistan  
2020**

## **Author's Declaration**

I, **Ikram Ullah**, hereby state that my PhD thesis titled **Flows of Nanomaterials by Stretching Boundaries** is my own work and has not been submitted previously by me for taking any degree from the Quaid-I-Azam University Islamabad, Pakistan or anywhere else in the country/world.

At any time if my statement is found to be incorrect even after my graduate the university has the right to withdraw my PhD degree.

Name of Student: **Ikram Ullah**

Date: **17-Sep-2020**

## **Plagiarism Undertaking**

I solemnly declare that research work presented in the thesis titled "**Flows of Nanomaterials by Stretching Boundaries**" is solely my research work with no significant contribution from any other person. Small contribution/help wherever taken has been duly acknowledged and that complete thesis has been written by me.

I understand the zero tolerance policy of the HEC and **Quaid-i-Azam University** towards plagiarism. Therefore, I as an Author of the above titled thesis declare that no portion of my thesis has been plagiarized and any material used as reference is properly referred/cited.

I undertake that if I am found guilty of any formal plagiarism in the above titled thesis even afterward of PhD degree, the University reserves the rights to withdraw/revoke my PhD degree and that HEC and the University has the right to publish my name on the HEC/University Website on which names of students are placed who submitted plagiarized thesis.



Student/Author Signature

Name: **Ikram Ullah**

## Certificate of Approval

This is to certify that the research work presented in this thesis entitled **Flows of Nanomaterials by Stretching Boundaries** was conducted by **Mr. Ikram Ullah** under the kind supervision of **Prof. Dr. Tasawar Hayat**. No part of this thesis has been submitted anywhere else for any other degree. This thesis is submitted to the Department of Mathematics, Quaid-i-Azam University, Islamabad in partial fulfillment of the requirements for the degree of Doctor of Philosophy in field of Mathematics from Department of Mathematics, Quaid-i-Azam University Islamabad, Pakistan.

Student Name: **Ikram Ullah**

Signature: 

External committee:

a) **External Examiner 1:**

Signature: 

Name: **Prof. Dr. Saleem Asghar**

Designation: Professor

Office Address: Department of Mathematics, COMSATS University, Park Road Chak Shahzad, Islamabad.

b) **External Examiner 2:**

Signature: 

Name: **Dr. Rahmat Ellahi**

Designation: Associate Professor

Office Address: Department of Mathematics, Faculty of Basics Applied Sciences International Islamic University, Islamabad.

c) **Internal Examiner**

Signature: 

Name: **Prof. Dr. Tasawar Hayat**

Designation: Professor

Office Address: Department of Mathematics, Quaid-i-Azam University, Islamabad.

**Supervisor Name:**

Signature: 

**Prof. Dr. Tasawar Hayat**

**Name of Dean/ HOD**

Signature: 

**Prof. Dr. Sohail Nadeem**

# Flows of Nanomaterials by Stretching Boundaries

By

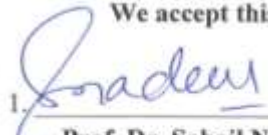
**Ikram Ullah**


CERTIFICATE

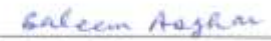
A THESIS SUBMITTED IN THE PARTIAL FULFILLMENT OF THE  
REQUIREMENTS FOR THE DEGREE OF THE

**DOCTOR OF PHILOSOPHY IN MATHEMATICS**

We accept this thesis as conforming to the required standard

1.   
Prof. Dr. Sohail Nadeem  
(Chairman)

2.   
Prof. Dr. Tasawar Hayat  
(Supervisor)

3.   
Prof. Dr. Saleem Asghar  
(External Examiner)

4.   
Dr. Rahmat Ellahi  
(External Examiner)

Department of Mathematics, COMSATS  
University, Park Road Chak Shahzad,  
Islamabad.

Department of Mathematics, Faculty of  
Basics Applied Sciences International  
Islamic University, Islamabad.

**Department of Mathematics  
Quaid-I-Azam University  
Islamabad, Pakistan  
2020**

*Dedicated*

to

*My beloved father (Anwar Said) and late mother.*



# Preface

Many non-linear materials (polymers, blood, sauce, drilling muds, sugar solutions, colloidal suspensions, shampoos, lubricants etc) deviates Newtonian's law of viscosity. The significance of topic can be perceived by its numerous industrial and engineering applications such as petroleum reservoirs, pharmaceutical industries, ceramics, polymer processing, metallurgy and many others. The fluids in all such applications are single type. Therefore viscous and non-Newtonian models like Sisko, Williamson and second grade materials are adopted here. Nanoliquid is further formed by adding nano-dimensions of tiny particles in traditional liquids. It remarkably intensifies low thermal efficiency of materials. It can be utilized in both non-Newtonian and viscous materials. Nanoparticles comprising of carbides, semiconductors, metals, oxides ceramics, CNTs and many other composites are submerged in traditional liquids like engine oil, water, kerosene oil and ethylene glycol to improve heat transport capability. Nanoliquids are extensively utilized in nanotechnologies such as atomic force microscope, conductive plastic, gas storing, nuclear power magnifying lens, electromechanical devices and industrial cooling applications. Hybrid nanoliquids consist of more than one type of nanoparticles. Novel concept of hybrid nanofluid greatly motivated the researchers due to its better thermal feature, excellent stability and physical strength. Therefore main emphasis here to given to inspect the flows of nano and hybrid nanoliquids by stretching boundaries. Phenomenon of heat transport is characterized via various mechanisms. Concept of thermodynamic second law is utilized for entropy production.

Thus intension here is to develop mathematical modelling for flows of nano and hybrid nanomaterials using various nanoparticles. The problems are addressed by preserving natural aspects intact and then tackled via different techniques. The chapter wise arrangement of this thesis is as follows.

Chapter one consists the expressions for fundamental laws and literature review. Mathematical development of Sisko, Williamson, second grade and Buongiorno models are addressed. Basic concept regarding the solution techniques is provided.

Chapter two explores the consequences of nanoparticles on three-dimensional mixed convention flow of Sisko fluid over a stretched surface. Salient aspects of thermophoresis and Brownian motion are addressed. Convective conditions are imposed at the boundary. Boundary layer concept is utilized for mathematical modelling. Homotopic technique is

implemented for solutions convergence. Graphs of embedded variables on velocity, temperature and concentration are deliberated. Finally heat and mass transfer rates are also studied. Findings of this chapter are reported in **International Journal of Mechanical Sciences**, **133 (2017) 273-282**.

Chapter three communicates the chemical reaction and double stratification in MHD stagnation point flow of Williamson nanoliquid towards a stretched sheet. Flow is generated due to non-linear stretching sheet of variable thickness. Non-uniform magnetic field is implemented in transverse direction. Aspects of Brownian motion, radiation, thermophoresis and viscous dissipation are addressed. Additionally chemical reaction is present. Relevant mathematical formulations are made through boundary layer concept. Homotopic technique is implemented for the solutions procedure. Rate of heat transfer is estimated. Research of this chapter is published in **Radiation Physics and Chemistry**, **152 (2018) 151–157**.

The aim of chapter four is in fourfolds. Firstly to formulate magnetized nanomaterials squeezed flow of viscoelastic (second grade) fluid between two parallel disks. Such consideration has relevance in industrial and biomedical utilizations like spintronic devices, catalysis and MEMS etc. Secondly to scrutinize nonlinear thermal radiation for heat transfer analysis. Flows through such consideration are useful in numerous processes like nuclear plants, combustion chambers and solar power technology. Thirdly, the novel chemical species model which elaborates activation energy impact. Activation energy describes least energy required through chemical shape with potential reactants to develop a chemical reaction. Fourth to compute solutions for nonlinear problems utilizing homotopic scheme. Graphical and tabular outcomes are portrayed and elaborated in detail for involved variables. The data of this research is publication in **Journal of Heat Transfer**, **142(2020) 082501**.

Chapter five addresses the comparative analysis for radiated flow of nano and hybrid nanomaterials by stretchable disk. Both thermal and velocity slips are considered. Water based liquid containing Aluminum alloy (AA7072–A7075) nanoparticles is considered. Further exponential heat source is present. Transformations are implemented for conversion of PDEs into ODEs. Non-linear problems are treated through NDSolve scheme. Features of sundry variables for both nano and hybrid nano phases are computed and discussed. Major outcomes are listed in conclusions. The contents of this research are published in **Physica Scripta**, **94 (2019) 125708**.

Chapter six discusses the nonlinear radiative flow of ethylene-glycol based CNTs suspended in Darcy-Forchheimer porous medium. Xue model is implemented for the transportation of nanomaterials. Ethylene-glycol (EG) is used as a base liquid. The characteristics of nanoparticles volume fraction have been considered. A concise depiction about the entropy of system is presented. Implementation of suitable variables yields dimensionless system. Numerical scheme is employed in order to solve the nonlinear systems. The behaviours of many regulatory flow variables are explained through plots. In addition, the variation of some valuable engineering quantities is interpreted via tabulated values. The results of this chapter are accepted in **Journal of Non-Equilibrium Thermodynamics**.

Chapter seven is generalized version of chapter six in view of hybridization of CNTs. Thus this chapter explicitly provides the comparative analysis for two different types of nanofluids namely regular nanofluid (SWCNT/engine oil) and hybrid nanofluids (SWCNT-MWCNT/engine oil) past a stretching cylinder. Xue model is modified for the modeling of hybrid nanofluid. Effects of melting, viscous dissipation and radiation are studied. To overcome the level of entropy production in a system and irreversibility arising due to pressure drop, mixing and heat transfer, an entropy number is utilized. Dimensionless variables convert the partial differential systems to ordinary one. The reduced systems are then solved numerically by means of NDSolve approach. Graphical analysis is made to visualize the physical characteristics of interesting variables. Moreover analysis of various parameters at surface in terms of skin friction and Nusselt number is also provided. Finding of this chapter is accepted in **Modern Physics Letters B**.

Main emphasis in chapter eight is to differentiate the heat transportation rate in hybrid nanofluid (SWCNT-MWCNT/kerosene oil) and regular nanofluid (SWCNT/kerosene oil) suspended in Darcy-Forchheimer porous space. Whole system is in a rotating frame. Entropy analysis is incorporated. Energy equation is modelled via heat source, convective condition and dissipation. Obtained non-linear systems are tackled by employing numerical approach (NDSolve shooting technique). The physical features of various sundry variables for both types of nanomaterials are depicted graphically and via table. It is noteworthy to point out that analytical model of hybrid nanofluid is novel achievement of available models based on single-nanoparticles. With great confidence this modified Xue model can be used to assess the heat transport and flow of hybrid nanomaterials in any configuration. The outcomes achieved in this study are important in industrial research, academics and discussion about entropy analysis for flow of two types of nanofluids by keeping the regular fluid fixed. The

outcomes of current chapter are accepted for publication in **Journal of Thermal Analysis and Calorimetry**.

# Contents

<b>1</b>	<b>Background and some basic laws</b>	<b>5</b>
1.1	Introduction . . . . .	5
1.2	Background . . . . .	5
1.3	Basic relations . . . . .	10
1.3.1	Mass conservation expression . . . . .	10
1.3.2	Linear momentum conservation relation . . . . .	11
1.3.3	Energy conservation relation . . . . .	11
1.3.4	Concentration conservation relation . . . . .	12
1.4	Fluid models . . . . .	13
1.4.1	Viscous liquid . . . . .	13
1.4.2	Non-Newtonian liquids . . . . .	13
1.5	Solution techniques . . . . .	15
1.5.1	ND-Solve scheme . . . . .	15
1.5.2	Homotopy analysis method (HAM) . . . . .	15
1.5.3	Optimal homotopy analysis method . . . . .	15
1.5.4	Bvp4c Matlab approach . . . . .	16
<b>2</b>	<b>Analysis of Sisko nanoliquid flow with convective conditions</b>	<b>17</b>
2.1	Model development . . . . .	17
2.2	Definitions and solutions . . . . .	20
2.3	Convergence analysis . . . . .	21
2.4	Result and discussion . . . . .	24

2.5	Concluding remarks . . . . .	39
<b>3</b>	<b>Analysis of magnetized Williamson nanoliquid subject to stratification</b>	<b>41</b>
3.1	Modeling . . . . .	41
3.2	Analysis of homotopic solutions . . . . .	45
3.3	Discussion . . . . .	47
3.4	Closing remarks . . . . .	57
<b>4</b>	<b>Non-linear radiative squeezed flow of nanoliquid with chemical reaction and activation energy</b>	<b>58</b>
4.1	Formulation . . . . .	58
4.2	Series solutions and convergence analysis . . . . .	63
4.3	Discussion . . . . .	65
4.4	Conclusions . . . . .	77
<b>5</b>	<b>Dissipative flow of hybrid nanoliquid (<math>H_2O</math>–aluminum alloy nanoparticles) with thermal radiation</b>	<b>78</b>
5.1	Problem description . . . . .	79
5.1.1	Formulation . . . . .	79
5.1.2	Governing equations . . . . .	79
5.1.3	Thermal energy . . . . .	80
5.1.4	Dimensionless systems . . . . .	81
5.1.5	Physical quantities . . . . .	82
5.2	Numerical technique and discussion . . . . .	83
5.3	Concluding remarks . . . . .	88
<b>6</b>	<b>Numerical simulation for irreversibility analysis of ethylene glycol (<math>C_2H_6O_2</math>) based carbon nanotubes flow in Darcy-Forchheimer porous medium</b>	<b>90</b>
6.1	Modeling . . . . .	91
6.1.1	Thermo-physical features of carbon nanotubes and ethylene glycol . . . . .	92
6.1.2	Boundary conditions . . . . .	93
6.1.3	Transformations . . . . .	93

6.1.4	Transformed systems . . . . .	93
6.1.5	Physical quantities . . . . .	94
6.2	Entropy analysis . . . . .	94
6.3	Computational procedure . . . . .	96
6.4	Discussion . . . . .	96
6.4.1	Velocity . . . . .	97
6.4.2	Variation in temperature . . . . .	97
6.4.3	Entropy generation and Bejan numbers . . . . .	98
6.4.4	Variations of non-dimensional drag forces and Nusselt number . . . . .	98
6.5	Final outcomes . . . . .	110
<b>7</b>	<b>Numerical treatment of melting heat transfer and entropy generation in stagnation point flow of hybrid nanomaterials (SWCNT-MWCNT/engine oil)</b>	<b>111</b>
7.1	Formulation . . . . .	112
7.1.1	Thermo-physical features for nanomaterials . . . . .	113
7.1.2	Dimensionless variables and transformed systems . . . . .	114
7.1.3	Physical quantities . . . . .	115
7.2	Entropy production ( $N_G$ ) and Bejan number (Be) . . . . .	116
7.3	Computational scheme and discussion . . . . .	117
7.4	Final remarks . . . . .	127
<b>8</b>	<b>Optimization of entropy production in flow of hybrid nanomaterials via porous space</b>	<b>128</b>
8.1	Mathematical formulation and modeling of hybrid nanofluid . . . . .	129
8.1.1	Empirical relations and thermo-physical features for nanomaterials . . . . .	130
8.1.2	Boundary conditions . . . . .	131
8.1.3	Dimensionless variables . . . . .	131
8.1.4	Transformed systems . . . . .	131
8.1.5	Physical quantities . . . . .	132
8.2	Second law analysis . . . . .	133
8.3	Computational scheme . . . . .	134

8.4	Outcomes and discussion . . . . .	134
8.4.1	Velocity . . . . .	135
8.4.2	Temperature . . . . .	135
8.4.3	Entropy generation . . . . .	136
8.4.4	Variations in physical quantities of interest ( $C_{fx}$ , $Nu_x$ ) . . . . .	137
8.5	Final outcomes . . . . .	146



# Chapter 1

## Background and some basic laws

### 1.1 Introduction

Review of some basic studies related to entropy, nanofluids, hybrid nanofluids, non-Newtonian fluid, thermal radiation and Darcy's law is incorporated in this chapter. Fundamental laws important for modeling momentum, concentration and energy expressions are also addressed. Mathematical modeling associated to viscous, Sisko, Williamson and second grade liquids are described for better understanding of upcoming chapters. Final section describes the analytical and numerical techniques which are being implemented for solving the governing systems considered here.

### 1.2 Background

Generally in any thermal process the amount of energy and quality are two main factors. The quantity of energy during heat exchange process can be seen by a tool know as entropy which was given by second law of thermodynamics. As stated by second law, amount of energy will be lost during conversion of energy which consequently reduces the efficiency of any thermal system. Such loss of energy enhances with the entropy production. In order to rise the capability of the system, we have to lower the production of energy. Therefore minimization of entropy production is important and is useful for the optimization of engineering tools to get high energy capability [1-3]. Entropy generation explores the importance of irreversible factors concerned

with friction, heat transfer and other non ideal processes inside a system. It is utilized to find out the upper limits for conductance of several engineering systems like refrigerators, internal combustion engines and chemical reactors. Few recent uses of entropy are solar energy collectors, cooling of new electronic systems, nuclear fuel rods cooling, slurry systems, solar heat exchangers in pseudo-optimization process, heat waste from steam pipes and nuclear swirl electromagnetic propulsion etc. Keeping in perspective the consequence of entropy production, many theoretical as well as experimental interrogation for entropy production are accomplished by numerous researchers. The problem of entropy generation in a fluid flow past a flat plate was investigated by Reveillere and Baytas [4]. Rashidi et al. [5] studied entropy analysis in MHD flow. They used numerical scheme for the problem. Survey of Entropy production in hydromagnetic slip flow with injection/suction was discussed by Ibanez [6]. He concluded that degradation of entropy can be accomplished by proper physical and geometrical variables. Jian [7] explored the entropy generation and hydromagnetic flow for micro-parallel channel. Butt et al. [8] explored the entropy generation in Blasius flow subject to radiative heat flux. Mustafa et al. [9] disclosed the radiation impact on B $\ddot{u}$ odewadt flow with entropy analysis. Hayat et al. [10] disclosed entropy generation features in MHD dissipative flow due to rotating disk. Khan et al. [11] examined irreversibility analysis in Williamson nanomaterials flow in presence of Joule heating. Currently Ganesh et al. [12] numerically treated the problem of slip by considering irreversibility analysis.

The traditional heat transport liquids such as ethylene glycol, water, propylene glycol and oil are crucial for various kinds of industrial purposes which cover considerable zones of fluid dynamics and heat transport. However the performance of these liquids are too much poor although they are utilized in various applications. But the saving energy, management of energy and obtaining higher efficiency are of very important. Advancements in electronics importantly the integration and miniaturization of latest electronic gadgets demand for long term operation, reliability and improved efficiency. Therefore Choi [13] presented the concept of nanoliquid. Here nanomaterials is formed by adding nano-dimensions of tiny particles in base liquid. This commencing experimental work noticed thermal conductivity increment of nanoliquid. Eastman et al. [14] indicated that a small quantity (volume fraction <1%) of carbon nanotubes or Cu nanoparticles dispersed in ethylene glycol or oil peculiarly improved the ther-

mal conductivity of regular liquid by (40%) and (50%) respectively. Impurities, corrosion and pressure drop are significantly reduced due to small size of nanoparticles. Furthermore stability of nanomaterials is remarkably improved versus sedimentation [15 – 16]. Thus nanofluids are considered more effectual in nano/micro heat exchangers, latest cooling systems, large scale systems thermal management through evaporators, electromechanical gadgets and industrial cooling uses. Nanomaterials are also used as a barrier to gasses. This avoids the foods from drying out or spoiling. Few recent studies related to nanomaterials are [17 – 27]. Materials of nanoscale have attracted worldwide consideration in ongoing technology since the exploration of carbon nanotubes by Iijima in (1991). CNTs are allotropes of atoms consisting of pure carbon that are thin, long and hexagonal nano-structure that have been shaped into cylinder. CNTs can be put into two classes i.e SWCNTs and MWCNTs. For the nanomaterials shape of the nanoparticles is very important. In view of heat transport, cylindrical shaped nanoparticles (nanotubes) is very efficient than the other particles like blade, bricks, spherical etc. These materials have variety of uses in optics, atomic force microscope, gas storing, extra strong fibers, basic composite materials, display of field emission, nuclear power magnifying lens, exhibition of flat-panel, antifouling shade, conductive plastic and many more. CNTs are additionally utilized as electrical contacts, warming source, high temperature refractories, biosensor in medical gadgets. In daily life the CNTs can be used as antennas for radios and some other important electromagnetic gadgets. Moreover CNTs don't have any danger to the environment because of carbon chain. In this regard Xue [28] presented the model for transportation of nanomaterials based on thermal conductivity. Wang et al. [29] examined aspect of pressure drop in nanoliquid consisting CNTs. Hayat et al. [30] studied Newtonian heating impact in stagnation point flow by considering CNTs. MHD flow of nanomaterials with CNTs dispersed in a salt water mixture was discussed by Ellahi et al. [31]. Imtiaz et al. [32] analytically treated the problem of convective and radiative flow of nanoliquid by adding CNTs. Farooq et al. [33] discussed the CNTs liquid model describing the peristalsis in a curved channel. Kumar et al. [34] investigated water based CNTs nanoliquid flow with quartic chemical reaction.

In all above mentioned studies, the researchers have discussed the features of nanomaterials which consists of just single type of nanoparticles in base liquid. No doubt these nanofluids have better rheological features and thermal performance but they do not have all the intended

properties that scientist needed. Some nanoparticles like silver, copper etc possess high thermal conductivities but these particles are unstable and chemically reactive. Lately, growing analysis has inaugurated the aspect of hybrid nanofluids. Hybrid nanomaterials are basically the addition of more than one kind of nanoparticles to the regular liquid. Basic purpose of hybridizing nanoparticles is to achieve higher heat transfer and thermos-physical features. They have good thermal features or rheological characteristics in comparison with single particle nanoliquid. These two useful features of hybrid nanomaterials make them highly desirable because it reduced the cost of heat exchange devices by enhancing its effectiveness. Thereafter various scientists studied flow analysis by incorporating hybrid nanomaterials in order to achieved excellent stability as well as better thermal conductivity. Although larger size of nanoparticles augments the density and viscosity compared to regular liquids. Furthermore it also forces sedimentation of particle which cause undesired aggravate the homogeneity and pressure drops [35]. Therefore it is very important to decide which type of based liquids and nanoparticles to be used [36 – 38]. There are several ingredients that are related to the properties of hybrid nanomaterials like viscosity, stability, liquid temperature, purity of nanoparticles, shape and size of nanoparticles, compatibility, preparation method, dispersion techniques that correspond to nanofluid harmonious mixture. Numerous investigators have remarked a tremendous improvement in density and viscosity by utilizing hybrid nanomaterials which are the major factor related to thermal utilizations. Suresh et al. [39] explored the characteristics of pressure drop and turbulent transportation of heat in  $\text{Al}_2\text{O}_3\text{-Cu}$ /water hybrid liquid. Harandi et al. [40] developed hybrid nanoliquid by hybridizing  $\text{Fe}_3\text{O}_4$  and FMWCNTs in ethylene glycol for enhancing the thermal features of regular liquid. They concluded that thermal conductivity of nanomaterials augmented by 30% comparative to base liquid by taking volume fraction of 2.3%. Ghadikolaei et al. [41] discussed the behavior of hybrid nanoparticles ( $\text{TiO}_2\text{-Cu}$ ) suspended in water base liquid. Rostamia et al. [42] find the dual solution for stagnation point flow of silica/alumina hybrid nanoliquid. They provided the comparative analysis of nanofluid and hybrid nanofluid and concluded that hybrid nanofluid has higher rate of transfer then ordinary one.

Numerous liquids (biological, industrial) like lubricating greases, printer inks, fruit juices, polymers, gypsum pastes, ceramics, blood, multi-grade oils and paints do not follow the tra-

ditional Newton's viscosity relation. Such liquids constantly alter their viscosities subject to shear stress application are identified as non-Newtonian materials. All such liquids have distinct thermal and physical features. Hence, it is impossible to elaborate all such liquids employing a solitary mathematical relation in comparison to Newtonian liquids [43, 44]. Thus several models for non-Newtonian liquid have been addressed. The adopted model (second grade liquid) falls in the category of differential type liquids. This model comprises both elastic and viscous properties [45]. It has significant utilization in industrial, technological and chemical like die swell, electronic devices, solar energy collectors, cooling of polymer films and many more. In addition this model accompanied magnetic attribute is extensive in biomedical area i.e wound treatment, heat removal processes, tumors elimination etc. Few researches reported recently are given through [46 – 49] and numerous studies therein. Sisko [50] liquid model is one the most significant non-Newtonian liquid. This model specifies both dilatant and pseudoplastic liquids depending on their shear thickening and shear thinning features. It can be regard more generalized form of power law model. It covers both power law and viscous models. Abelman et al. [51] analyzed the flow of Sisko liquid originated by a suddenly moved plate. The aspects of suction/injection on Sisko liquid is discussed by Hayat et al. [52]. Flow of Sisko liquid over a stretched surface is explored by Munir et al. [53]. Khan and Malik [54] analyzed the Sisko nanomaterials flow in the existence of variable aspects. Magnetizable Sisko nanoliquid is elaborated by Hayat et al. [55]. The Williamson liquid model [56] is another important non-Newtonian model capable to describes the feature of viscoelastic material. It also elaborates the attribute of various pseudo-plastic materials. It has the liability to exhibits the behavior of various physiological and biophysical materials having shear-thinning characteristics like polymer, blood, melts, paints and gastro-intestinal [57]. In light of aforementioned applications, not much has been discussed related to this liquid model. Some attempts of researchers are [58 – 60].

Heat transportation via thermal radiation aspect has utilizations in numerous technological activities comprising aircraft, satellites, glass production, gas turbines and numerous propulsion mechanisms for space vehicles, aircraft, missiles and satellites. No doubt linear type of thermal radiation is not effective for higher temperature gap as the non-dimensional variable that is utilized in linearized Rosseland estimation yields effective Prandtl number [61] however in nonlinear estimation, the modeled problem is managed through three factors like temperature

ratio variable, Prandtl number and radiation variable. Pantokratoras [62] initially introduced nonlinear radiative flux concept for mixed convective viscous material flow. Cortell [63] elaborated thermal radiation impact in laminar viscous liquid flow via moving surface. Analysis of nonlinear radiated mixed convective Walter-B nanoliquid flow by heated surface is modeled by Khan et al. [64]. Irfan et al. [65] reported variable conductivity impact in chemically reactive Carreau liquid flow considering revised Fourier modeling.

Numerous environmental and industrial processes comprising fibrous insulation, catalytic reactors, geothermal energy systems, geophysics, crude oils production and design of heat exchanger involve flows via porous space. Porous space in the area of biomechanical is very significant in the procedure for the small blood vessel movement, kidneys, gallbladder with stones, lungs, tissues in the body like bone, cartilage, muscle etc. Darcy's law is valid for smaller velocity and low porosity conditions and becomes insufficient in engineering and industrial frameworks because larger velocity and non-uniform porosity occur in such systems. Thus Darcy–Forchheimer model which include the boundary and inertia features can be used to overcome the limitation of Darcy's law. For such aspects in (1901) Forchheimer [66] added the squared velocity term in equation of motion. Later on the factor Forchheimer is designated by Muskat [67]. Significance of Darcy–Forchheimer porous space in nanomaterials flow in vertical duct is explored by Umavathi et al. [68]. Further analysis regarding this feature can be reviewed via [69 – 73].

## 1.3 Basic relations

### 1.3.1 Mass conservation expression

Mass conservation expression elaborates that mass neither be formed nor destroyed. Its differential form can be expressed as

$$\frac{\partial \rho_f}{\partial t} + \nabla \cdot (\rho_f \mathbf{V}) = 0, \quad (1.1)$$

where  $\rho_f$  stands for the liquid density,  $\nabla$  denotes the gradient operator and  $\mathbf{V}$  signifies the velocity. For incompressible liquid

$$\nabla \cdot \mathbf{V} = 0. \quad (1.2)$$

In cylindrical and Cartesian coordinates Eq. (1.2) yields

$$\frac{1}{r} \frac{\partial}{\partial r} (rv_r) + \frac{1}{r} \frac{\partial}{\partial \theta} (v_\theta) + \frac{\partial}{\partial x} (v_x) = 0, \quad (1.3)$$

$$\frac{\partial u}{\partial x} + \frac{\partial v}{\partial y} + \frac{\partial w}{\partial z} = 0. \quad (1.4)$$

### 1.3.2 Linear momentum conservation relation

This relation manifests that momentum persists conserved of whole system. Newton's second law is utilized to develop it. Generalized form of motion is

$$\rho_f \frac{d\mathbf{V}}{dt} = \text{div } \boldsymbol{\tau} + \rho_f \mathbf{f}, \quad (1.5)$$

where  $\rho_f \mathbf{f}$  depicts the body force and  $\boldsymbol{\tau} (= -p\mathbf{I} + \mathbf{S})$  represents Cauchy-stress tensor,  $\mathbf{S}$  the extra stress tensor,  $\mathbf{I}$  identity tensor and  $p$  the pressure. Momentum relation in terms of rotation is stated as

$$\rho_f \left( \frac{d\mathbf{V}}{dt} + \boldsymbol{\Omega} \times (\boldsymbol{\Omega} \times \mathbf{r}) + 2(\boldsymbol{\Omega} \times \mathbf{V}) \right) = \text{div } \boldsymbol{\tau} + \rho_f \mathbf{f}, \quad (1.6)$$

where  $2(\boldsymbol{\Omega} \times \mathbf{V})$  and  $(\boldsymbol{\Omega} \times (\boldsymbol{\Omega} \times \mathbf{r}))$  show the respective Coriolis and centrifugal force.

### 1.3.3 Energy conservation relation

It expresses that sum of all energies of whole system under observation remains invariant. It is obtained via thermodynamics first law. Mathematically

$$(\rho c)_f \frac{dT}{dt} = -\text{div } \mathbf{q} + Q_t. \quad (1.7)$$

In Eq. (1.6),  $\mathbf{q} (= -k \text{grad } T)$  designates Fourier's heat conduction,  $k$  the fluid's thermal conductivity,  $T$  the temperature and  $c_f$  declares specific heat. The term  $\left( (\rho c)_f \frac{dT}{dt} \right)$  symbolizes internal energy, on right side first and second term signify energy flux and source term associated to energy transport. Source term ( $Q_t$ ) is liable for alteration of heat transport features. It can be implemented for consideration of radiative heat flux, viscous dissipation and surface heating cooling. Further it also stands for other physical aspects like Dufour and Joule heating. In the

presence of nanoparticles, Eq. (1.6) takes the form

$$(\rho c)_f \frac{dT}{dt} = -\text{div } \mathbf{q} + h_p \nabla \cdot \mathbf{j}_p, \quad (1.8)$$

where  $\mathbf{j}_p$  and  $\mathbf{q}$  are stated as

$$\mathbf{j}_p = -\rho_p D_B \nabla C - \rho_p D_T \frac{\nabla T}{T_\infty}, \quad (1.9)$$

$$\mathbf{q} = -k \nabla T + h_p \mathbf{j}_p, \quad (1.10)$$

In view of above expression, Eq. (1.7) yields

$$(\rho c)_f \frac{dT}{dt} = k \nabla^2 T + (\rho c)_p \left( D_B \nabla C \cdot \nabla T + \frac{\nabla T \cdot \nabla T}{T_\infty} \right). \quad (1.11)$$

### 1.3.4 Concentration conservation relation

This relation is developed through Fick's second law. It demonstrates that total concentration of whole system remains unchanged. Let  $C$  denotes the liquid mass concentration per unit volume then expression of mass can be addressed as:

$$\frac{dC}{dt} = -\nabla \cdot \mathbf{j}, \quad (1.12)$$

with

$$\mathbf{j} = -D \nabla C. \quad (1.13)$$

Expression (1.12) yields

$$\frac{dC}{dt} = D \nabla^2 C, \quad (1.14)$$

where  $\mathbf{j}$  and  $D$  denote the characterizes mass flux and mass diffusivity respectively. In terms of nanoliquids we have

$$\frac{\partial C}{dt} + \mathbf{v} \cdot \nabla C = -\frac{1}{\rho_p} \nabla \cdot \mathbf{j}_p. \quad (1.15)$$



The above Eq. in view of Eq. (1.8) becomes

$$\frac{\partial C}{\partial t} + \mathbf{V} \cdot \nabla C = D_B \nabla^2 C + D_T \frac{\nabla^2 \mathbf{T}}{T_\infty}. \quad (1.16)$$

## 1.4 Fluid models

### 1.4.1 Viscous liquid

The stress strain expression for incompressible viscous liquid is

$$\boldsymbol{\tau} = -p\mathbf{I} + \mu\mathbf{A}_1, \quad (1.17)$$

$$\mathbf{A}_1 = \mathbf{L} + \mathbf{L}^{tr}, \quad \mathbf{L} = \nabla \mathbf{V} = \begin{bmatrix} \frac{\partial u}{\partial x} & \frac{\partial u}{\partial y} & \frac{\partial u}{\partial z} \\ \frac{\partial v}{\partial x} & \frac{\partial v}{\partial y} & \frac{\partial v}{\partial z} \\ \frac{\partial w}{\partial x} & \frac{\partial w}{\partial y} & \frac{\partial w}{\partial z} \end{bmatrix}, \quad (1.18)$$

where  $\mathbf{A}_1$  symbolized the first Rivlin-Ericksen tensor. In cylindrical coordinates

$$\mathbf{L} = \nabla \mathbf{V} = \begin{bmatrix} \frac{\partial u_r}{\partial r} & \frac{1}{r} \frac{\partial u_r}{\partial \theta} - \frac{v_\theta}{r} & \frac{\partial v_r}{\partial z} \\ \frac{\partial u_\theta}{\partial r} & \frac{1}{r} \frac{\partial u_r}{\partial \theta} + \frac{u_r}{r} & \frac{\partial v_\theta}{\partial z} \\ \frac{\partial w_z}{\partial r} & \frac{1}{r} \frac{\partial w_z}{\partial \theta} - \frac{v_\theta}{r} & \frac{\partial w_z}{\partial z} \end{bmatrix}. \quad (1.19)$$

### 1.4.2 Non-Newtonian liquids

The stress strain expression for incompressible non-Newtonian liquid is defined as

$$\boldsymbol{\tau} = -p\mathbf{I} + \mathbf{S}, \quad (1.20)$$

where  $\mathbf{S}$  denotes extra stress tensor varies for different materials.

#### Sisko liquid

The constitutive expressions for Sisko liquid model are:

$$\mathbf{S} = \left[ a + b \left| \sqrt{\frac{1}{2} \text{trace}(\mathbf{A}_1^2)} \right|^{n-1} \right] \mathbf{A}_1, \quad (1.21)$$

where  $a$  and  $b$  are the Sisko materials variables and  $n > 0$  describes the non-Newtonian aspects of liquid.

### Williamson liquid

The constitutive expressions for Williamson liquid model are:

$$\boldsymbol{\tau} = \left[ \mu_\infty + \left( \frac{\mu_0 - \mu_\infty}{1 - \Gamma \dot{\gamma}} \right) \right] \mathbf{A}_1, \quad (1.22)$$

$$\dot{\gamma} = \sqrt{\Pi/2}, \quad (1.23)$$

$$\Pi = \text{trace}(\mathbf{A}_1)^2. \quad (1.24)$$

Here  $\mu_0$  zero shear viscosity,  $\mu_\infty$  infinite shear rate viscosity,  $\Gamma$  constant of time-dependent material and  $\dot{\gamma}$  rate of deformation. By considering  $\Gamma \dot{\gamma} < 1$  and  $\mu_\infty = 0$ , Eq. (1.22) becomes

$$\boldsymbol{\tau} = \left[ \frac{\mu_0}{(1 - \Gamma \dot{\gamma})} \right] \mathbf{A}_1. \quad (1.25)$$

### Second grade liquid

For second grade liquid one write

$$\boldsymbol{\tau} = -p\mathbf{I} + \mu\mathbf{A}_1 + \alpha_1^* \mathbf{A}_2 + \alpha_2^* \mathbf{A}_1^2. \quad (1.26)$$

In above expression  $\mathbf{A}_1$  and  $\mathbf{A}_2$  characterize first and second Rivlin-Ericksen tensors i.e.

$$\mathbf{A}_1 = \mathbf{L} + \mathbf{L}^{tr},$$

$$\mathbf{A}_2 = \frac{d\mathbf{A}_1}{dt} + \mathbf{A}_1\mathbf{L} + \mathbf{L}\mathbf{A}_1, \quad (1.27)$$

where  $\frac{d}{dt}$  represents the material derivative. For liquid stability of thermodynamic survey, the following criteria must be fulfilled:

$$\mu \geq 0, \alpha_1^* \geq 0, \alpha_1^* + \alpha_2^* = 0. \quad (1.28)$$

Therefore Eq. (1.26) yields

$$\boldsymbol{\tau} = -p\mathbf{I} + \mu\mathbf{A}_1 + \alpha_1^*(\mathbf{A}_2 - \mathbf{A}_1^2). \quad (1.29)$$

## 1.5 Solution techniques

This section aims to elaborate different techniques (ND-Solve scheme, HAM, OHAM and bvp4c) which will be implemented to tackle the governing systems in upcoming chapters.

### 1.5.1 ND-Solve scheme

ND-Solve is built in command of Mathematica based on shooting scheme with 4th order R-K integration technique. This technique is a numerical solver of differential systems. With the aid of NDSolve we can tackle different ODEs and PDEs system as well as differential algebraic equations that mix differential equation with algebraic ones. General ODEs system possess number of equations  $n$  (i.e.  $q_1, q_2, q_3 \dots q_n$ ), independent variable  $x$ , number of dependent variable  $n$  (i.e.  $v_1, v_2, v_3 \dots v_n$ ) and boundary conditions according to order of PDEs system. By NDSolve technique this system can be computed as follows:

$$NDSolve[\{q_1, q_2, q_3 \dots q_n, \text{boundary conditions}\}, \{v_1, v_2, v_3 \dots v_n\}, \{x, x_{\min}, x_{\max}\}. \quad (1.30)$$

This technique attains exceptional accuracy and is stable unconditionally. Furthermore it provides us best outcomes in minimum CPU time and avoid the lengthy expressions.

### 1.5.2 Homotopy analysis method (HAM)

In 1992, Liao [120] firstly given the idea of homotopy. This technique is utilized to compute highly nonlinear problems. The continuous deformation of expression or a function is termed as homotopy. This technique is utilized more effectively for solutions of several non-linear problems [74 – 84]. The detail methodology of this technique is utilized in chapter two.

### 1.5.3 Optimal homotopy analysis method

The concept of minimization is employed by addressing average squared residual errors [85].

Mathematically

$$\varepsilon_{\hat{m}} = \frac{1}{k+1} \sum_{j=0}^k \left[ N \left( \sum_{i=0}^{\hat{m}} u_{\hat{m}}(\zeta) \right)_{\zeta=j\delta\zeta} \right]^2, \quad (1.31)$$

where  $\varepsilon_{\hat{m}}$  is total squared residual error.

#### 1.5.4 Bvp4c Matlab approach

The nonlinear flow problem is executed as built-in scheme known as bvp4c in Matlab [86 – 90]. Lobatto IIIA formula is utilized in present technique. To utilize this scheme it is important to convert the nonlinear and higher order system into first order ODEs by setting new variables. Considering

$$\mathbf{t}' = \mathbf{f}(x, \mathbf{t}, \mathbf{D}) \quad a \leq x \leq b, \quad (1.32)$$

with

$$\mathbf{h}(\mathbf{t}(a), \mathbf{t}(b), \mathbf{D}). \quad (1.33)$$

This technique attains exceptional accuracy and is stable unconditionally. It is used for highly nonlinear coupled problems. This technique is utilized for the problem in chapter 6.

## Chapter 2

# Analysis of Sisko nanoliquid flow with convective conditions

This chapter deals with a model to examine mixed convection flow of Sisko nanofluid driven by bidirectionally stretched surface. Features of thermophoresis and Brownian movement phenomena are accounted. Convective conditions are employed for heat and mass transfer process. Transformations yield ordinary differential systems. Convergence of derived series solutions for resulting problems is verified. Behavior of sundry variables is explored by plotting graphs. Computations for heat and mass transfer rates are declared and analyzed for the influence of emerging variables. It is inspected that higher mixed convection variable results to enhance the velocity distribution whereas it decays fluid temperature and concentration. The Present outcomes are compared with existing studies in particular cases and noticed in good agreement.

### 2.1 Model development

Here 3D mixed convection flow of Sisko nanofluid. The fluid movement is induced because of the stretching property of sheet. We choose system with Cartesian coordinate. Let  $U_w = cx$  and  $V_w = dy$  (where  $c$  and  $d$  are positive dimensional constants) indicate surface stretching velocities in the  $x$ - and  $y$ - direction respectively (see Fig. 2.1). Heat and mass transfer characteristics are explored when thermophoresis and Brownian diffusion are present. Stretched surface possesses the convective conditions. Convection from a hot liquid at temperature  $T_f$  leads to heat up the

flow surface. The nanoparticles concentration at the wall is characterized by  $C_f$ , coefficient of mass transport  $h_c$  and  $C_\infty$  liquid ambient concentration. The resulting expressions are

$$\frac{\partial u}{\partial x} + \frac{\partial v}{\partial y} + \frac{\partial w}{\partial z} = 0, \quad (2.1)$$

$$u \frac{\partial u}{\partial x} + v \frac{\partial u}{\partial y} + w \frac{\partial u}{\partial z} = \frac{1}{\rho_f} \left( a \frac{\partial^2 u}{\partial z^2} - b \frac{\partial}{\partial z} \left( -\frac{\partial u}{\partial z} \right)^n + g\beta_C(C - C_\infty) + g\beta_T(T - T_\infty) \right), \quad (2.2)$$

$$\rho_f \left( u \frac{\partial v}{\partial x} + v \frac{\partial v}{\partial y} + w \frac{\partial v}{\partial z} \right) = a \frac{\partial^2 v}{\partial z^2} + b \frac{\partial}{\partial z} \left( -\frac{\partial u}{\partial z} \right)^{n-1} \frac{\partial v}{\partial z}, \quad (2.3)$$

$$u \frac{\partial T}{\partial x} + v \frac{\partial T}{\partial y} + w \frac{\partial T}{\partial z} = \alpha_f \frac{\partial^2 T}{\partial z^2} + \left( \frac{(\rho c)_p}{(\rho c)_f} \right) \left( D_B \frac{\partial C}{\partial z} \frac{\partial T}{\partial z} + \frac{D_T}{T_\infty} \left( \frac{\partial T}{\partial z} \right)^2 \right), \quad (2.4)$$

$$u \frac{\partial C}{\partial x} + v \frac{\partial C}{\partial y} + w \frac{\partial C}{\partial z} = D_B \frac{\partial^2 C}{\partial z^2} + \frac{D_T}{T_\infty} \frac{\partial^2 T}{\partial z^2}. \quad (2.5)$$

with

$$u = U_w = cx, \quad v = V_w = dy, \quad w = 0, \quad -k \frac{\partial T}{\partial z} = h_f(T_f - T), \quad -D_B \frac{\partial C}{\partial z} = h_c(C_f - C) \text{ at } z = 0, \quad (2.6)$$

$$u \rightarrow 0, \quad v \rightarrow 0, \quad T \rightarrow T_\infty, \quad C \rightarrow C_\infty \text{ when } z \rightarrow \infty. \quad (2.7)$$

Here in  $(x, y, z)$  directions, the associated velocities are  $(u, v, w)$ ,  $\rho_f$  liquid density,  $\beta_T$  designates the coefficient of thermal expansion,  $T_\infty$  denotes liquid ambient temperature,  $g$  signifies acceleration due to gravity,  $T$  the temperature,  $\beta_C$  the coefficient of solutal expansion,  $\alpha_f$  manifests thermal diffusivity,  $(\rho c)_f$  the heat capacity of liquid,  $(\rho c)_p$  the nanofluid material effective heat capacity and  $(D_T, D_B)$  denote the coefficients of thermophoresis and Brownian diffusion. Here  $a$  and  $b$  are the Sisko material variables and  $n > 0$  describes the non-Newtonian aspects of liquid. It is significant to declare that for  $n = 1$  and  $b = 0$ , the liquid is viscous. For  $n > 1$  the situation is dilatant and when  $0 < n < 1$  then case corresponds to pseudoplastic. Furthermore for  $a = 0$ , the case of power law material is achieved (for detail [91 – 95]). We use the following transformations

$$\left. \begin{aligned} u = cx f'(\eta), \quad v = dy g'(\eta), \quad w = -c \left( \frac{c^{n-2}}{\rho/b} \right)^{1/(n+1)} \left( \frac{2n}{n+1} f + \frac{1-n}{n+1} \eta f' + g \right) x^{\frac{n-1}{n+1}}, \\ \theta(\eta) = \frac{T-T_\infty}{T_f-T_\infty}, \quad \phi(\eta) = \frac{C-C_\infty}{C_f-C_\infty}, \quad \eta = z \left( \frac{c^{2-n}}{\rho/b} \right)^{1/n+1} x^{\frac{1-n}{1+n}}. \end{aligned} \right\} \quad (2.8)$$

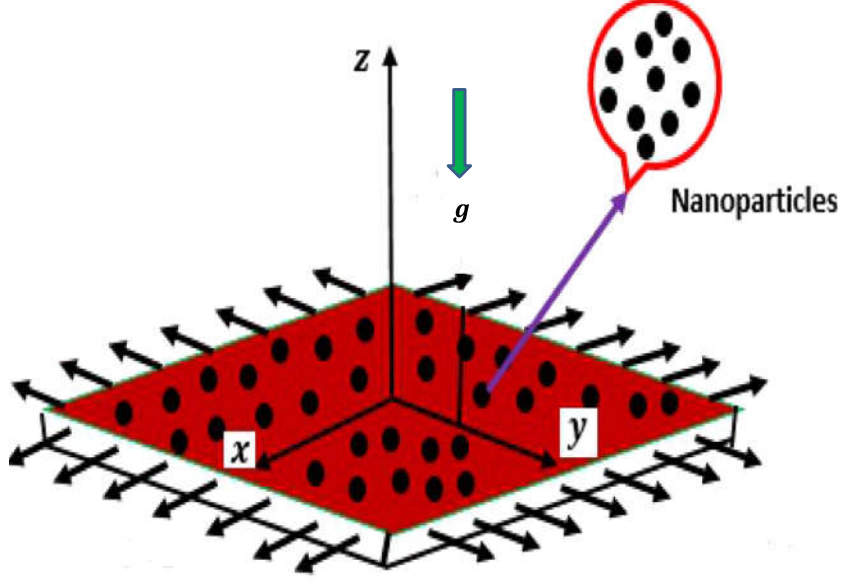


Fig. 2.1. Flow configuration and physical model.

Expression (2.1) is trivially verified and Eqs. (2.2) – (2.7) become

$$\beta f''' + (-f'')^{n-1} f''' + \left( \frac{2n}{n+1} \right) f f'' - (f')^2 + g f'' + \lambda(\theta + N\phi) = 0, \quad (2.9)$$

$$\beta g''' + (-f'')^{n-1} g''' - (n-1)g'' f''' (-f'')^{n-2} + \left( \frac{2n}{n+1} \right) f g'' - (g')^2 + g g'' = 0, \quad (2.10)$$

$$\theta'' + \text{Pr} \left( N_b \theta' \phi' + N_t (\theta')^2 + \left( \frac{2n}{n+1} \right) \theta' f + \theta' g \right) = 0, \quad (2.11)$$

$$\phi'' + Le \text{Pr} \left( g \phi' + \left( \frac{2n}{n+1} \right) f \phi' \right) + \left( \frac{N_t}{N_b} \right) \theta'' = 0, \quad (2.12)$$

$$f = 0, \quad g = 0, \quad f' = 1, \quad g' = \alpha, \quad \theta' = -\gamma(1 - \theta), \quad \phi' = -\gamma_1(1 - \phi) \quad \text{at } \eta = 0, \quad (2.13)$$

$$f' \rightarrow 0, \quad g' \rightarrow 0, \quad \theta \rightarrow 0, \quad \phi \rightarrow 0 \quad \text{as } \eta \rightarrow \infty. \quad (2.14)$$

Here  $\beta$  signifies the material variable of Sisko liquid,  $Re_b$  and  $Re_a$  show the local Reynolds numbers,  $\lambda$  indicates the mixed convection parameter,  $N$  represents the buoyancy ratio parameter,  $\alpha$  designates ratio parameter,  $Gr$  stands for Grashof number,  $N_b$  signifies Brownian motion variable,  $Pr$  denotes Prandtl number,  $N_t$  shows thermophoresis parameter,  $Le$  designates Lewis number,  $\gamma$  the temperature Biot number and  $\gamma_1$  the concentration Biot number.

The dimensionless variables are

$$\left. \begin{aligned} \beta &= \frac{\text{Re}_b^{\frac{2}{n+1}}}{\text{Re}_a}, \quad N_b = \tau \frac{D_B(C_f - C_\infty)}{\nu}, \quad \gamma = \frac{h_f}{k} x \text{Re}_b^{\frac{-1}{(n+1)}}, \quad \text{Re}_b = \frac{\rho_f x^n U^{2-n}}{b}, \\ N &= \frac{\beta C(T_f - T_\infty)}{\beta_T(C_f - C_\infty)}, \quad \alpha = \frac{d}{c}, \quad \lambda = \frac{g\beta_T(T_f - T_\infty)/\nu^2}{(xU)^2/\nu^2}, \quad \text{Pr} = \frac{xU \text{Re}_b^{\frac{-2}{n+1}}}{k/(\rho c)_f}, \\ \text{Re}_a &= \frac{\rho_f x U}{a}, \quad Le = \frac{\alpha_f}{D_B}, \quad N_t = \tau \frac{D_T(T_f - T_\infty)}{T_\infty \nu}, \quad \gamma_1 = \frac{h_c}{D_B} x \text{Re}_b^{\frac{-1}{(n+1)}}. \end{aligned} \right\} \quad (2.15)$$

It is noted that fluid here is non-Newtonian i.e Sisko fluid. Hence we found that presence of Sisko fluid and mixed convection terms in the momentum equations (2.9) and (2.10) and convective conditions for heat and mass transfer in (2.13) do not allow the problems to have self similar solutions. Consequently parameters  $\beta$ ,  $\lambda$ ,  $\gamma$  and  $\gamma_1$  are functions of  $x$  when  $n \neq 1$  i.e. for Sisko fluid case. The only possibility for similarity solutions corresponds to  $n = 1$  (for viscous liquid) and no mixed convection i.e.  $\lambda = 0$ . In this case the variables  $\beta = 0$  and  $\gamma$  and  $\gamma_1$  do not rely upon  $x$  i.e.  $\gamma$  and  $\gamma_1$  are constant. In light of these points, our purpose now is to establish local similar solutions [96 – 100]).

Skin frictions are given by

$$\left. \begin{aligned} \text{Re}_b^{\frac{1}{(n+1)}} C_{fx} &= \beta f''(0) + (f''(0))^n, \\ \text{Re}_b^{\frac{1}{(n+1)}} C_{fy} &= \frac{V_w}{U_w} (\beta g''(0) f(0) + (-f''(0))^{n-1} g''(0)). \end{aligned} \right\} \quad (2.16)$$

Expressions for  $(Nu_x)$  and  $(Sh_x)$  can be written as

$$\left. \begin{aligned} \text{Re}_b^{-1/(n+1)} Nu_x &= -\theta'(0), \\ \text{Re}_b^{-1/(n+1)} Sh_x &= -\phi'(0), \end{aligned} \right\} \quad (2.17)$$

where  $\text{Re}_b = \frac{\rho_f x^n U^{2-n}}{b}$  and  $\text{Re}_a = \frac{\rho_f x U}{a}$  elucidate local Reynolds numbers.

## 2.2 Definitions and solutions

Homotopic scheme is employed for given flow system. Therefore the initial approximations  $(f_0(\eta), g_0(\eta), \theta_0(\eta), \phi_0(\eta))$  and linear operators  $(\tilde{\mathcal{L}}_f, \tilde{\mathcal{L}}_g, \tilde{\mathcal{L}}_\theta, \tilde{\mathcal{L}}_\phi)$  are

$$f_0(\eta) = 1 - e^{-\eta}, \quad g_0(\eta) = \alpha(1 - e^{-\eta}), \quad \theta_0(\eta) = \frac{\gamma}{1 + \gamma} e^{-\eta}, \quad \phi_0(\eta) = \frac{\gamma_1}{1 + \gamma_1} e^{-\eta}, \quad (2.18)$$



$$\left. \begin{aligned} \tilde{\mathcal{L}}_f &= f''' - f', \\ \tilde{\mathcal{L}}_g &= g''' - g', \\ \tilde{\mathcal{L}}_\theta &= \theta'' - \theta, \\ \tilde{\mathcal{L}}_\phi &= \phi'' - \phi, \end{aligned} \right\} \quad (2.19)$$

$$\left. \begin{aligned} \tilde{\mathcal{L}}_f [c_1^{**} + c_2^{**} e^\eta + c_3^{**} e^{-\eta}] &= 0, \\ \tilde{\mathcal{L}}_g [c_4^{**} + c_5^{**} e^\eta + c_6^{**} e^{-\eta}] &= 0, \\ \tilde{\mathcal{L}}_\theta [c_7^{**} e^\eta + c_8^{**} e^{-\eta}] &= 0, \\ \tilde{\mathcal{L}}_\phi [c_9^{**} e^\eta + c_{10}^{**} e^{-\eta}] &= 0, \end{aligned} \right\} \quad (2.20)$$

where  $c_n^{**}$  ( $n = 1 - 10$ ) designates the constants. The general solutions are:

$$f_m(\eta) = f_m^*(\eta) + c_1^{**} + c_2^{**} e^\eta + c_3^{**} e^{-\eta}, \quad (2.21)$$

$$g_m(\eta) = g_m^*(\eta) + c_4^{**} + c_5^{**} e^\eta + c_6^{**} e^{-\eta}, \quad (2.22)$$

$$\theta_m(\eta) = \theta_m^*(\eta) + c_7^{**} e^\eta + c_8^{**} e^{-\eta}, \quad (2.23)$$

$$\phi_m(\eta) = \phi_m^*(\eta) + c_9^{**} e^\eta + c_{10}^{**} e^{-\eta}. \quad (2.24)$$

Where special solutions are presented by  $f_m^*(\eta)$ ,  $g_m^*(\eta)$ ,  $\theta_m^*(\eta)$  and  $\phi_m^*(\eta)$  and the constants  $c_n^{**}$  ( $n = 1 - 10$ ) are as follows.

$$\left. \begin{aligned} c_2^{**} = c_5^{**} = c_7^{**} = c_9^{**} = 0, \quad c_3^{**} &= \frac{\partial f_m^*(\eta)}{\partial \eta} \Big|_{\eta=0}, \\ c_1^{**} &= -c_3^{**} - f_m^*(0), \quad c_6^{**} = \frac{\partial g_m^*(\eta)}{\partial \eta} \Big|_{\eta=0}, \\ c_4^{**} &= -c_6^{**} - g_m^*(0), \quad c_8^{**} = \frac{1}{1+\gamma} \left( \frac{\partial \theta_m^*(\eta)}{\partial \eta} \Big|_{\eta=0} - \gamma \theta_m^*(0) \right), \\ c_{10}^{**} &= \frac{1}{1+\gamma_1} \left( \frac{\partial \phi_m^*(\eta)}{\partial \eta} \Big|_{\eta=0} - \gamma_1 \phi_m^*(0) \right). \end{aligned} \right\} \quad (2.25)$$

### 2.3 Convergence analysis

Homotopic technique warrants us about the solutions convergence. HAM incorporates an embedding auxiliary variable  $\hbar$  which provides flexibility to extend the convergence region. Here  $h$ -curves are interpreted in order to achieve acceptable ranges of these variables (see Figs. 2.1 & 2.2). Permissible ranges of  $\hbar_f$ ,  $\hbar_g$ ,  $\hbar_\theta$  and  $\hbar_\phi$  for  $n = 1$  are  $[-0.2 \leq \hbar_f \leq -1.6]$ ,

$[-0.2 \leq \hbar_g \leq -1.5]$ ,  $[-0.2 \leq \hbar_\theta \leq -1.9]$  and  $[-0.5 \leq \hbar_\phi \leq -1.7]$  whereas for  $n = 2$  we have  $[-0.2 \leq \hbar_f \leq -0.6]$ ,  $[-0.2 \leq \hbar_g \leq -0.65]$ ,  $[-0.1 \leq \hbar_\theta \leq -0.9]$  and  $[-0.2 \leq \hbar_\phi \leq -0.9]$ . Noted that the convergence region at  $n = 1$  is larger when compared to  $n = 2$ . Further homotopic solutions also converge when  $\hbar_f = -0.9 = \hbar_g$  and  $\hbar_\theta = -1.0 = \hbar_\phi$ . Table 2.1 demonstrates that 45<sup>th</sup> order of estimations are essential for the convergence scrutiny.

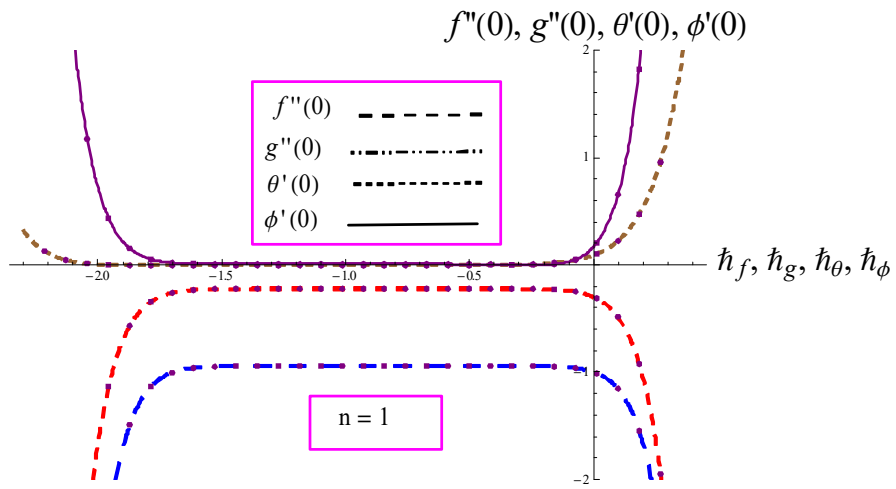


Fig.(2.2). The  $\hbar$ -curves for  $f, g, \theta$  and  $\phi$  when  $n = 1$ .

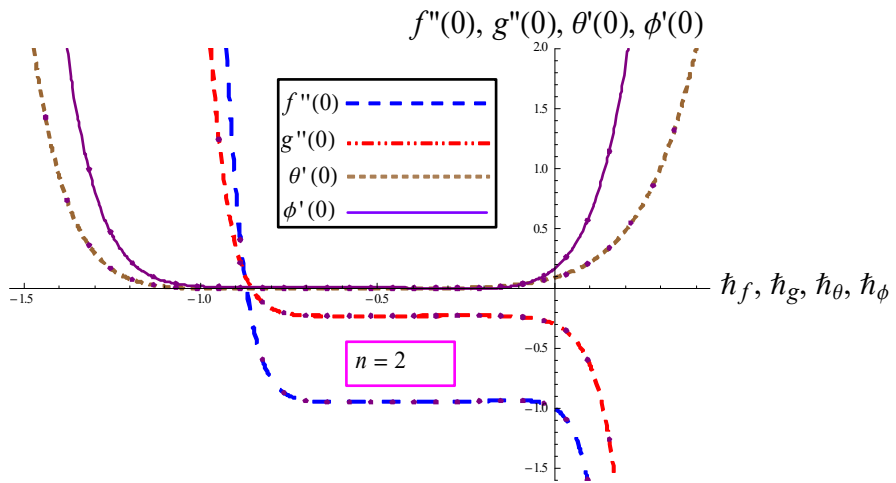


Fig.(2.3). The  $\hbar$ -curves for  $f, g, \theta$  and  $\phi$  when  $n = 2$ .

**Table 2.1:** Solutions convergence when  $Pr = 1.0$ ,  $\beta = N_b = 0.2 = \gamma_1$ ,  $N = 0.1 = \gamma$ ,  $N_t = 0.3 = \alpha = \lambda$ , and  $Le = 1.2$ .

Order of estimations	$-f''(0)$		$-g''(0)$		$-\theta'(0)$		$-\phi'(0)$	
	$n = 1$	$n = 2$	$n = 1$	$n = 2$	$n = 1$	$n = 2$	$n = 1$	$n = 2$
1	0.9404	0.9113	0.2235	0.2408	0.0884	0.0898	0.1486	0.1585
5	0.9431	0.9439	0.2228	0.2256	0.0870	0.0884	0.1434	0.1489
10	0.9432	0.9487	0.2229	0.2296	0.0871	0.0881	0.1435	0.1469
15	0.9432	0.9478	0.2229	0.2297	0.0870	0.0880	0.1435	0.1464
20	0.9432	0.9474	0.2229	0.2294	0.0870	0.0880	0.1435	0.1464
25	0.9432	0.9475	0.2229	0.2294	0.0870	0.0880	0.1435	0.1464
30	0.9432	0.9475	0.2229	0.2294	0.0870	0.0880	0.1435	0.1464
35	0.9432	0.9475	0.2229	0.2294	0.0870	0.0880	0.1435	0.1464
40	0.9432	0.9475	0.2229	0.2294	0.0870	0.0880	0.1435	0.1464

## 2.4 Result and discussion

Here outcomes of numerous variables are explored for  $f'(\eta)$ ,  $g'(\eta)$ ,  $\theta(\eta)$  and  $\phi(\eta)$ . Figs. (2.4) – (2.23) have been interpreted for such motivation. Effect of buoyancy ratio variable  $N$  on  $f'(\eta)$  is shown in Fig. 2.4. It is declared that  $f'(\eta)$  enhances when  $N$  increased. Buoyancy force due to concentration is a cause of velocity enhancement. Features of  $\lambda$  on  $f'(\eta)$  is depicted in Fig. 2.5. Here we found that  $f'(\eta)$  augments through larger  $\lambda$ . In fact buoyancy force rises for higher  $\lambda$  which augments  $f'(\eta)$ . Impacts of material parameter  $\beta$  on velocity distributions  $f'(\eta)$  and  $g'(\eta)$  are reported through in (Figs. 2.6 and 2.7). It is noticed that an increment in  $\beta$  enhances  $f'(\eta)$  along the  $x$ - and  $y$ -directions. Characteristics of  $\alpha$  on  $f'(\eta)$  is demonstrated in Fig. 2.8. Here increment in  $\alpha$  causes decay in the velocity distribution. Salient characteristics of  $\alpha$  on  $g'(\eta)$  is displayed in Fig. 2.9. Comparative study with Fig. 2.8 explores that  $f'(\eta)$  reduces while  $g'(\eta)$  enhances when  $\alpha$  has higher values. When  $\alpha$  starts to rise from zero then sidewise surface undergoes to move in  $y$ -direction and hence the velocity  $g'(\eta)$  enhances while the velocity  $f'(\eta)$  decays. Moreover these figures indicate that there is no flow and the fluid velocity is zero when  $\alpha = 0$ . Fig. 2.10 provides mixed convection parameter effect on temperature field. Clearly

fluid temperature diminished by  $\lambda$ . In physical sense, buoyancy forces dominates the inertial forces which enhance the heat transport. As a results  $\theta(\eta)$  decays. It is inferred from Fig. 2.11 that fluid temperature is reduced by higher  $N$ . This feature  $\theta(\eta)$  is because of temperature differences. Fig. 2.12 depicts the contribution of  $\alpha$  on  $\theta(\eta)$ . It is obvious that  $\theta(\eta)$  decays for higher estimations of  $\alpha$ . Influence of  $\gamma$  on  $\theta(\eta)$  is addressed in Fig. 2.13. Higher  $N_t$  cause  $\theta(\eta)$  enhancement (see Fig. 2.14). Here nanomaterials temperature upgraded for larger  $N_t$ . This feature is due to association of thermophoresis phenomenon which extracts heated particles towards cold zone from heated one. Fig. 2.15 elucidates that liquid temperature rises against higher  $N_b$ . Higher  $N_b$  enhance the collision between fluid particles which create more heat and consequently  $\theta(\eta)$  increases. Fig. 2.16 exhibits feature of Pr on  $\theta(\eta)$ . Here  $\theta(\eta)$  is increasing function of Pr. It is expected physically because small estimation of Pr ( $< 1$ ) corresponds to fluid materials having low viscosity and high thermal diffusivity. High viscosity liquids are demonstrated by Pr ( $> 1$ ). An increment in  $\lambda$  decays the concentration  $\phi(\eta)$  (see Fig. 2.17). Physically, buoyancy force acts as favorable pressure gradient thus stronger buoyancy force assists in upward direction due to which concentration decreases. Fig. 2.18 illustrates behavior of  $N$  on  $\phi(\eta)$ . Here larger  $N$  decays the concentration distribution. In fact higher concentration buoyancy force is associated with larger buoyancy ratio parameter which results in lower concentration. Fig. 2.19 is drawn to see the characteristics of  $\alpha$  on  $\phi(\eta)$ . It is found that concentration distribution diminishes via  $\alpha$ . Variation of  $\gamma_1$  on concentration distribution is depicted in Fig. 2.20. One can see that liquid concentration enhances with an increase of  $\gamma_1$ . Biot number due to concentration has a great dependence on mass transfer coefficient  $h_c$ . The coefficient of mass transfer  $h_c$  is increased for higher solutal Biot number  $\gamma_1$  due to which the temperature and thickness of concentration layer are enhanced. The consequences of  $N_t$  on the concentration field is declared in Fig. 2.21. Here  $\phi(\eta)$  enhances via thermophoresis parameter  $N_t$ . Such circumstances is observed because of consistent development in percentage of nanoparticles for  $N_t$ . Feature of  $N_b$  on  $\phi(\eta)$  is depicted in Fig. 2.22. An improvement in  $N_b$  enhances the concentration  $\phi(\eta)$ . Due to movement of nanoparticles in nanomaterials, the Brownian movement occurs. Thus an enhancement greatly affected the Brownian movement and as a result  $\phi(\eta)$  decays. Fig. 2.23 clearly demonstrates that concentration decays when  $Le$  is enhanced. It is interesting to note from Figs. (2.4) – (2.23) that all physical variables

has similar behavior for  $n = 1$  and  $n = 2$ . The numerical outcome of  $(-f''(0))$ ,  $(-g''(0))$ ,  $(-\theta'(0))$  and  $(-\phi'(0))$  is declared in Table 2.1 when  $\beta = 0.2 = N_b$ ,  $N = 0.1 = \gamma$ ,  $\text{Pr} = 1.0$ ,  $\alpha = N_t = 0.3 = \lambda$ ,  $Le = 1.2$ ,  $\hbar_f = -0.9 = \hbar_g$  and  $\hbar_\theta = -1.0 = \hbar_\phi$ . It is reported that 45<sup>th</sup> order of estimations are quite appropriate for solutions convergence. The characteristics of local Nusselt  $(\frac{1}{2} \text{Re}_b^{-1/(n+1)} Nu_x)$  and local Sherwood  $(\frac{1}{2} \text{Re}_b^{-1/(n+1)} Sh_x)$  numbers via  $\lambda$ ,  $\beta$ ,  $\alpha$ ,  $\text{Pr}$ ,  $N$ ,  $N_t$ ,  $N_b$ ,  $Le$ ,  $\gamma_1$  and  $\gamma$  are given in Tables 2.3(a) and 2.3(b). Here we revealed that local Nusselt number enhances via  $\beta$ ,  $\lambda$ ,  $\alpha$ ,  $\text{Pr}$  and  $N_b$  and it diminishes via  $N_t$  and  $\gamma_1$ . Further  $(\frac{1}{2} \text{Re}_b^{-1/(n+1)} Sh_x)$  enhances against  $\beta$ ,  $\lambda$ ,  $\alpha$ ,  $\text{Pr}$  and  $N_b$  and it reduces via  $N_t$ . Table 2.3 explores the comparison of presented analysis with Ariel [101] and Munir et al. [102] for  $\alpha$ . A good agreement is noticed.

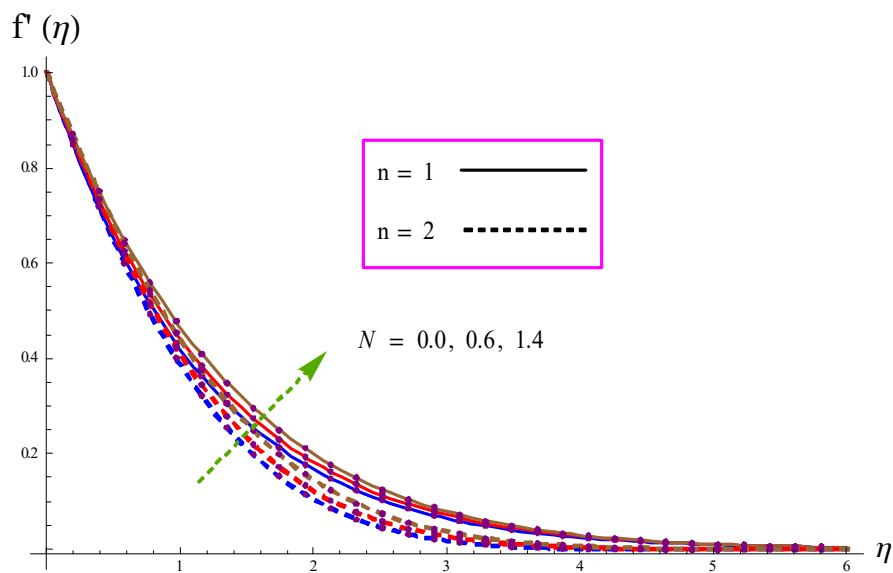


Fig. 2.4. Variation of  $f'(\eta)$  via  $N$ .

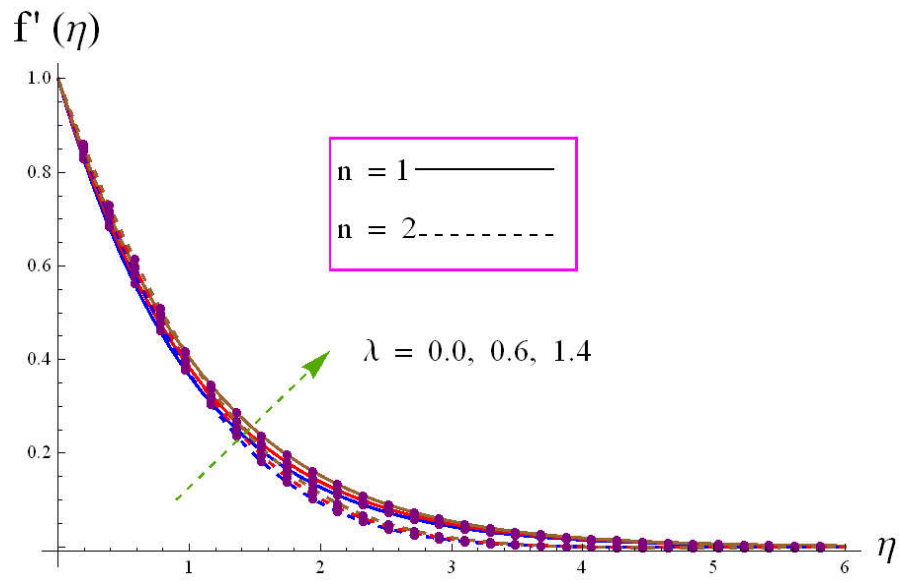


Fig. 2.5. Variation of  $f'(\eta)$  via  $\lambda$ .

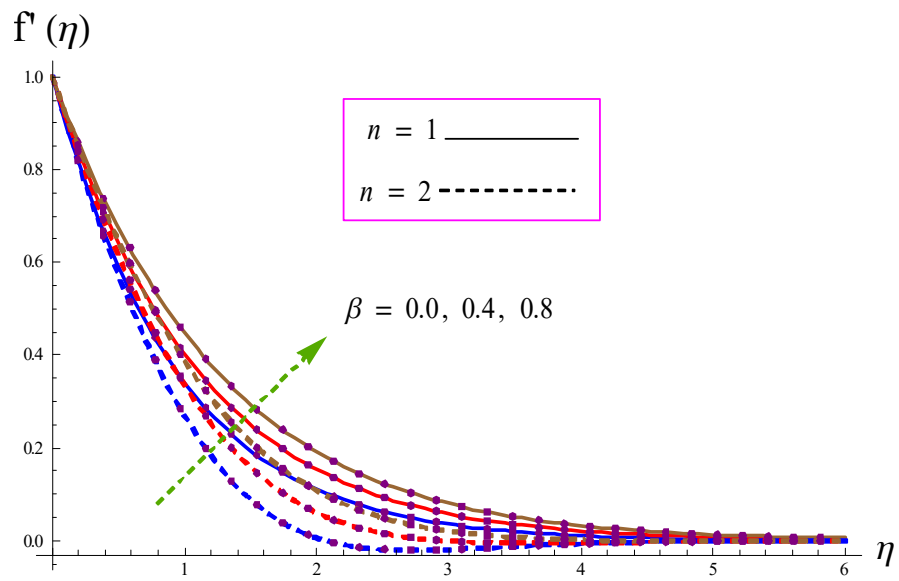


Fig. 2.6. Variation of  $f'(\eta)$  via  $\beta$ .

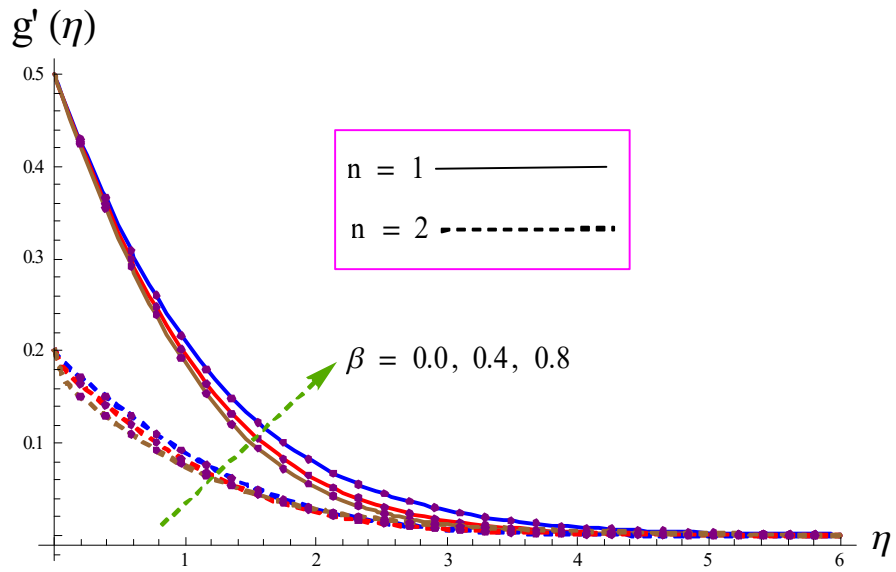


Fig. 2.7. Variation of  $g'(\eta)$  via  $\beta$ .

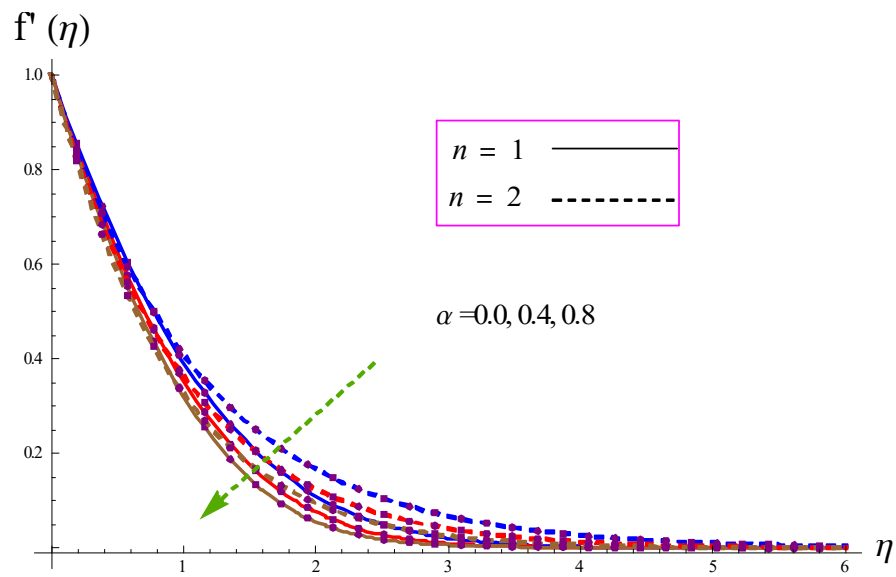


Fig. 2.8. Variation of  $f'(\eta)$  via  $\alpha$ .



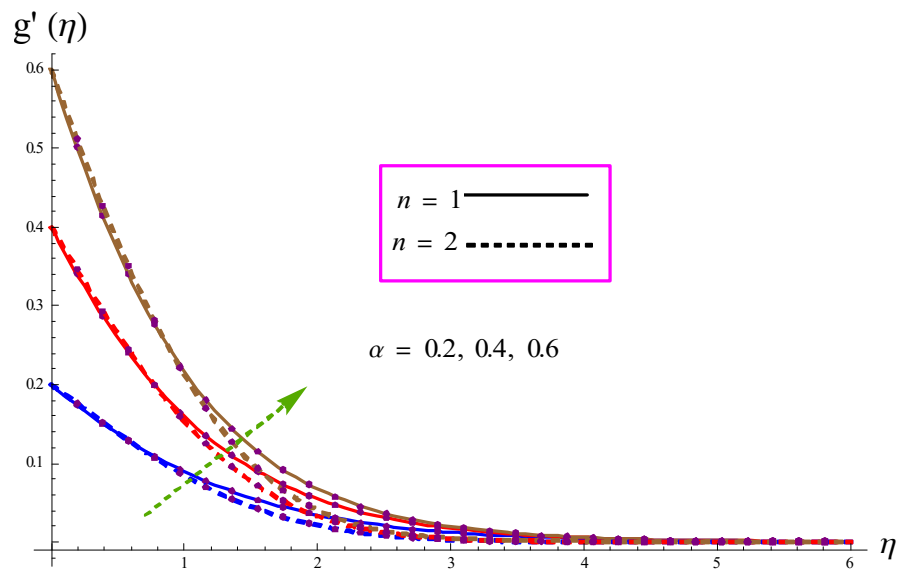


Fig. 2.9. Variation of  $g'(\eta)$  via  $\alpha$ .

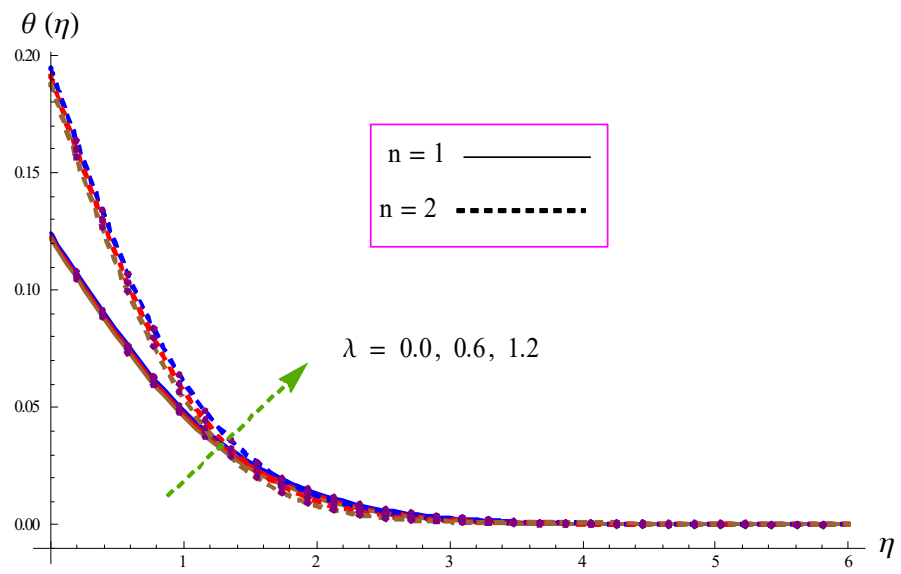


Fig. 2.10. Variation of  $\theta(\eta)$  via  $\lambda$ .

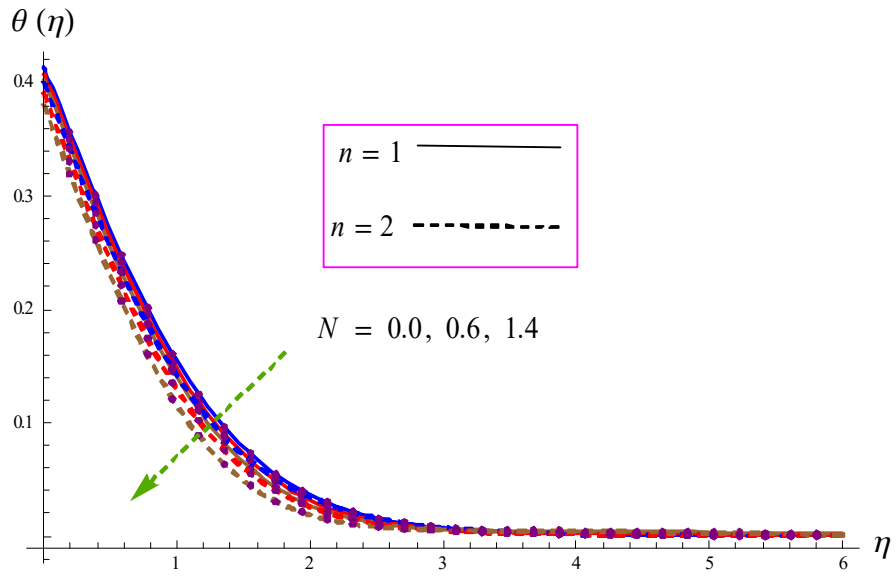


Fig. 2.11. Variation of  $\theta(\eta)$  via

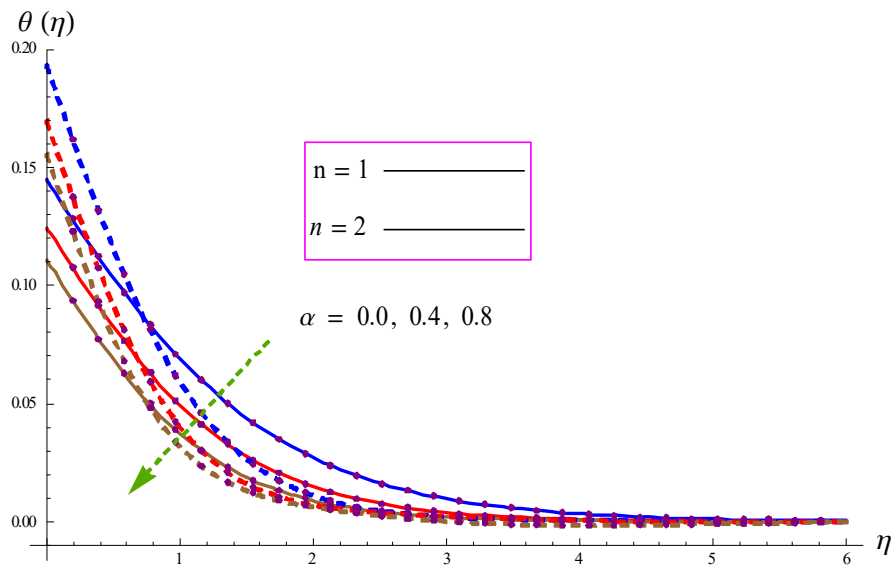


Fig. 2.12. Variation of  $\theta(\eta)$  via  $\alpha$ .

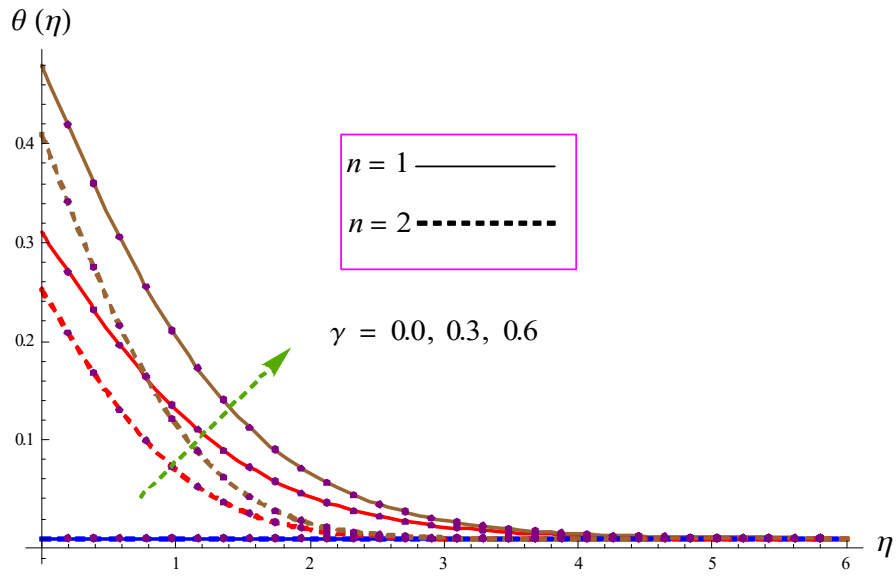


Fig. 2.13. Variation of  $\theta(\eta)$  via  $\gamma$ .

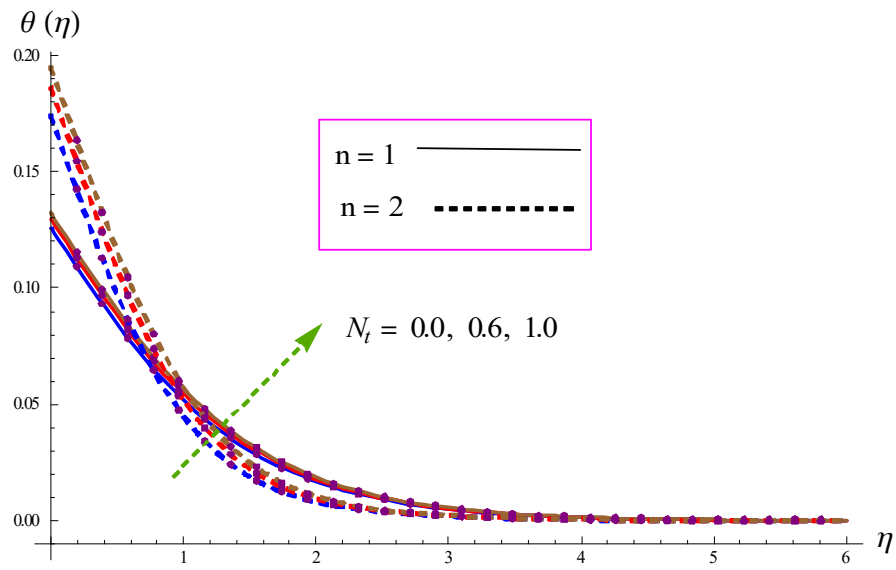


Fig. 2.14. Variation of  $\theta(\eta)$  via  $N_t$ .

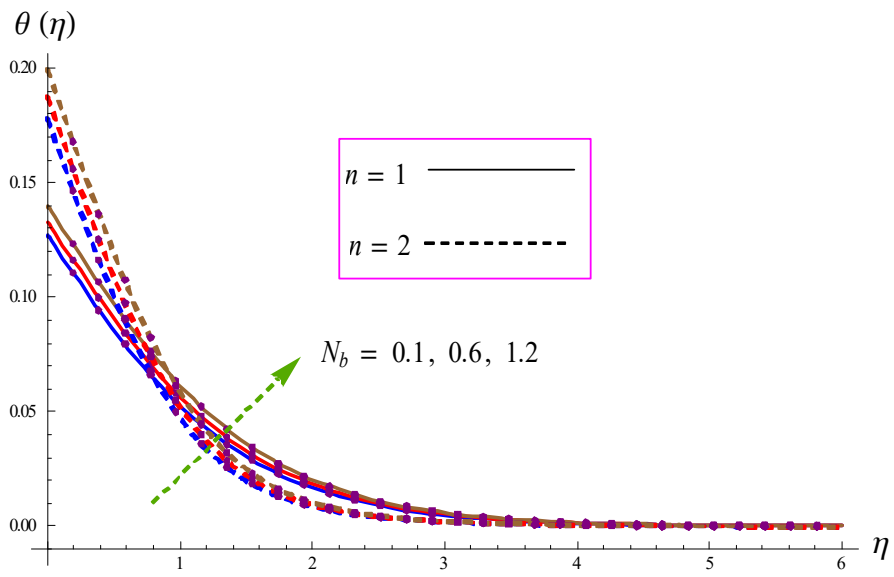


Fig. 2.15. Variation of  $\theta(\eta)$  via  $N_b$ .

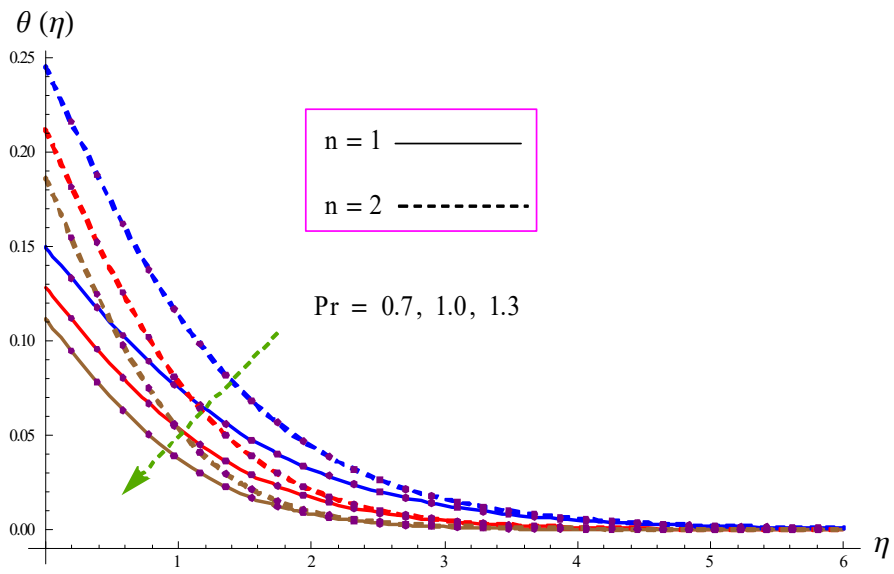


Fig. 2.16. Variation of  $\theta(\eta)$  via  $Pr$ .

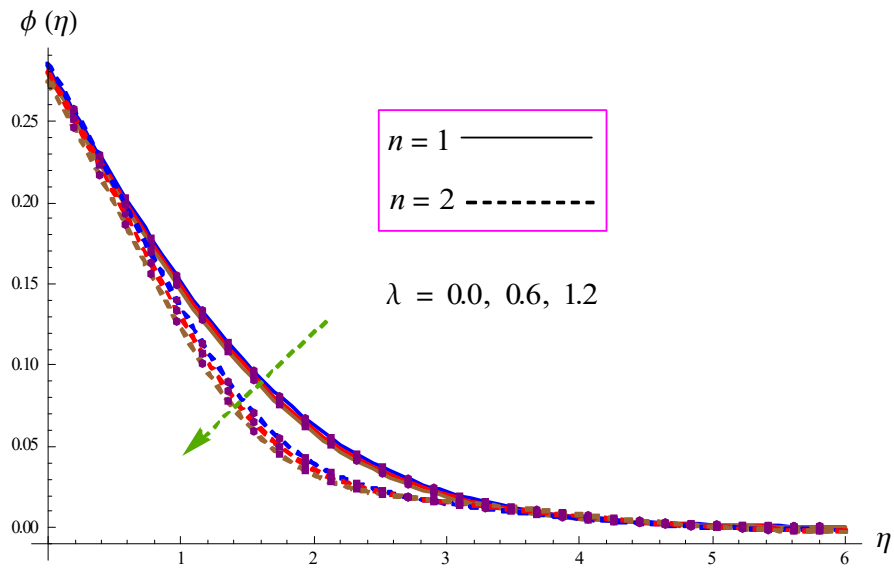


Fig. 2.17. Variation of  $\phi(\eta)$  via  $\lambda$ .

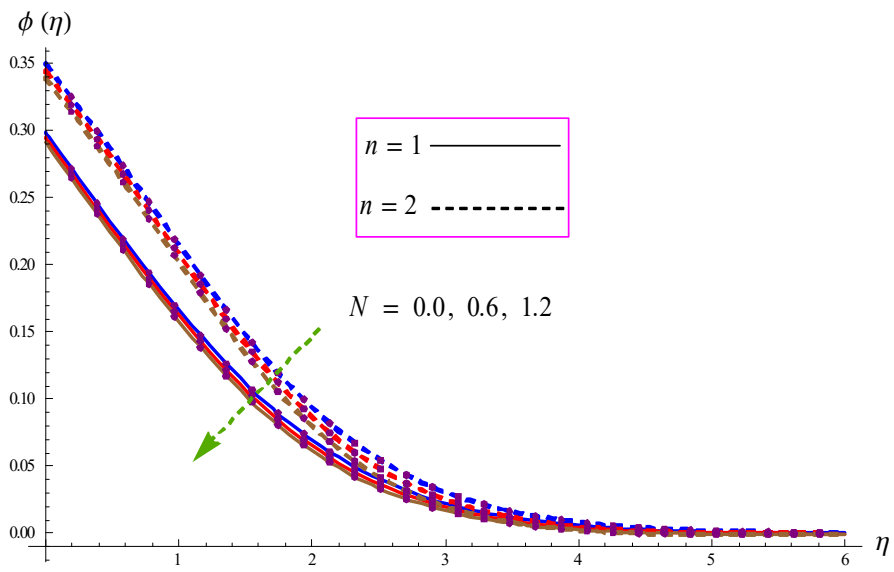


Fig. 2.18. Variation of  $\phi(\eta)$  via  $N$ .

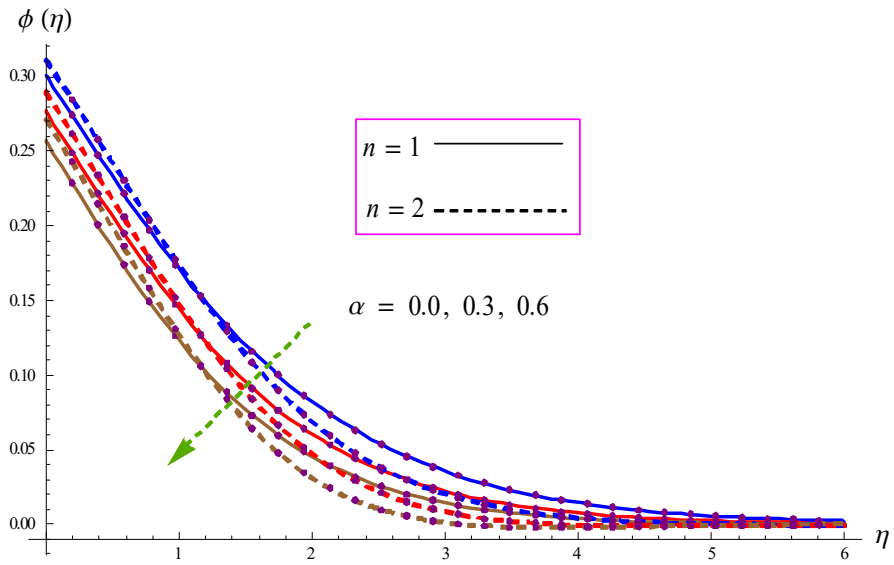


Fig. 2.19. Variation of  $\phi(\eta)$  via  $\alpha$ .

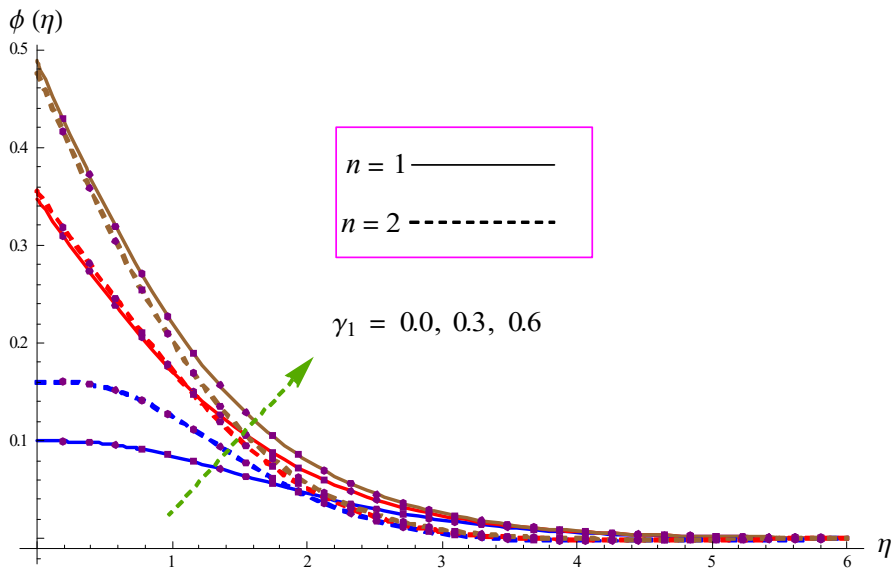


Fig. 2.20. Variation of  $\phi(\eta)$  via  $\gamma_1$ .

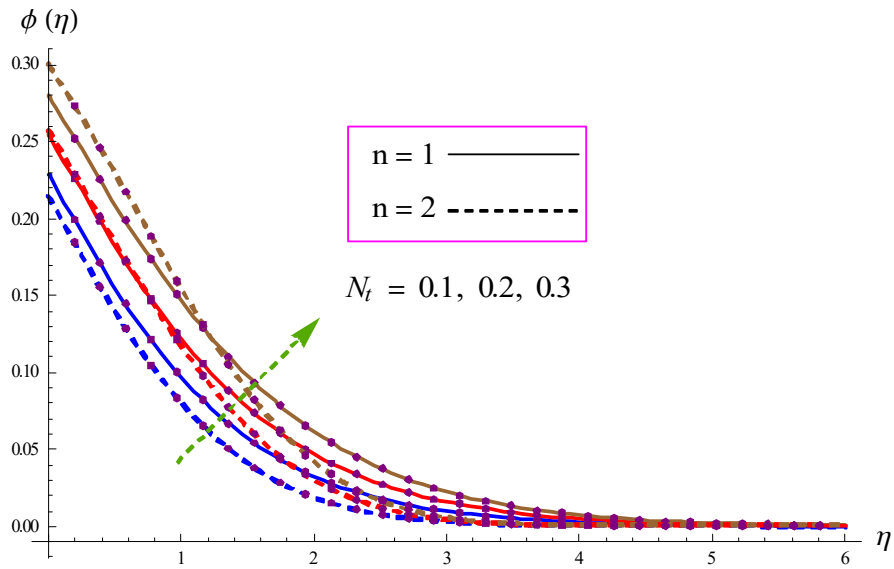


Fig. 2.21. Variation of  $\phi(\eta)$  via  $N_t$ .

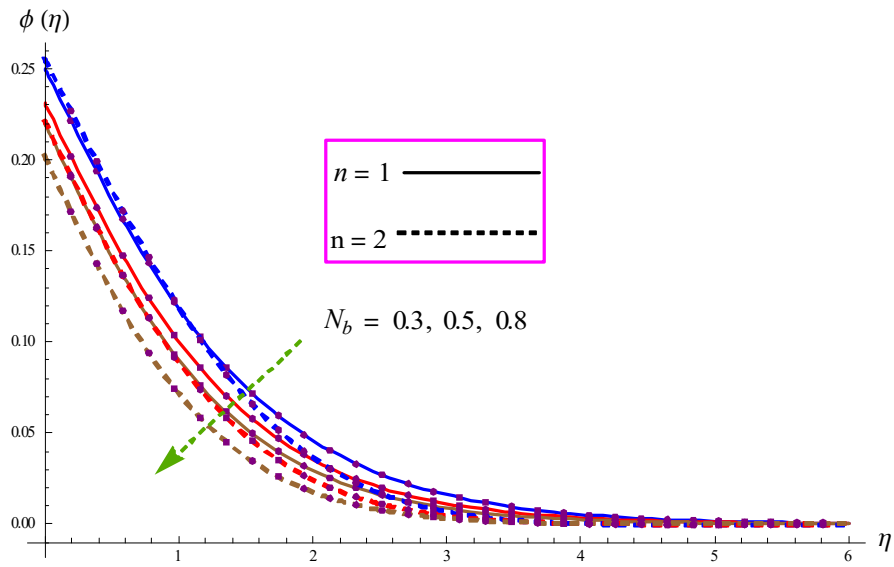


Fig. 2.22. Variation of  $\phi(\eta)$  via  $N_b$ .

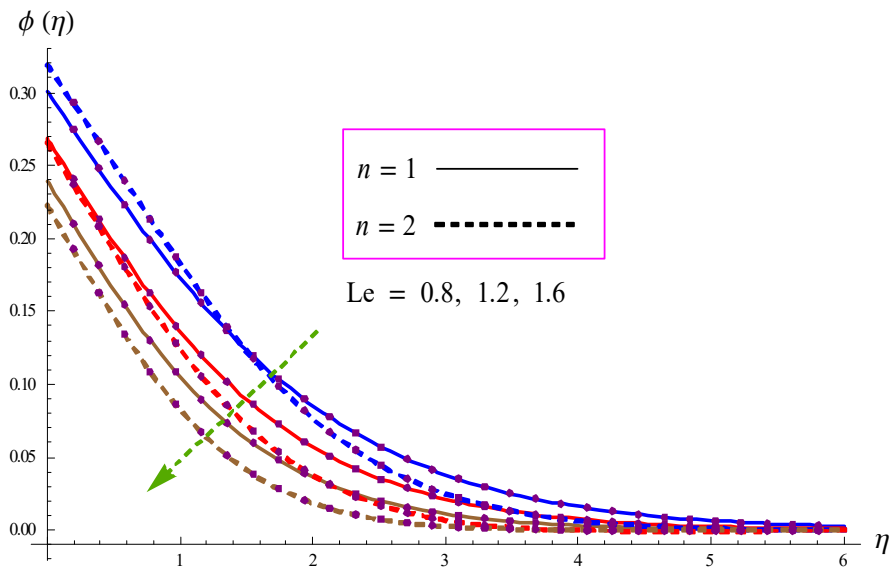


Fig. 2.23. Variation of  $\phi(\eta)$  via  $Le$ .



**Table 2.2 (a):** Numerical data of  $(-\theta'(0))$  and  $(-\phi'(0))$  via  $\beta$ ,  $\lambda$ ,  $\alpha$ ,  $N$  and  $\text{Pr}$  when  $N_b = 0.2 = \gamma_1$ ,  $\gamma = 0.1$ ,  $N_t = 0.3$ , and  $Le = 1.2$ .

$\beta$	$\lambda$	$\alpha$	$N$	$\text{Pr}$	$-\theta'(0)$		$-\phi'(0)$	
					$n = 1$	$n = 2$	$n = 1$	$n = 2$
0.0	0.3	0.3	0.1	1.0	0.0868	0.0890	0.1421	0.1441
	0.3				0.0873	0.0895	0.1447	0.1474
	0.8				0.0877	0.0898	0.1463	0.1494
0.2	0.0	0.3	0.1	1.0	0.0870	0.0891	0.1433	0.1457
		0.5			0.0871	0.0892	0.1437	0.1458
		0.8			0.0872	0.0893	0.1440	0.1462
0.2	0.3	0.0	0.1	1.0	0.0852	0.0880	0.1368	0.1405
		0.3			0.0871	0.0893	0.1436	0.1461
		0.6			0.0883	0.0902	0.1481	0.1499
0.2	0.3	0.3	0.0	1.0	0.0871	0.0893	0.1435	0.1459
			0.2		0.0871	0.0893	0.1436	0.1460
			0.5		0.0871	0.0893	0.1438	0.1462
0.2	0.3	0.3	0.1	0.7	0.0844	0.0856	0.1322	0.1275
				1.0	0.0871	0.0881	0.1436	0.1401
				1.2	0.0888	0.0897	0.1507	0.1484

**Table 2.2 (b):** Numerical data of  $(-\theta'(0))$  and  $(-\phi'(0))$  via  $N_b$ ,  $\gamma_1$ ,  $\gamma$ ,  $N_t$ , and  $Le$  when  $Pr = 1.2$ ,  $\beta = 0.2$ ,  $\lambda$ ,  $N = 0.1$  and  $\alpha = 0.3 = \lambda$ .

$N_b$	$N_t$	$\gamma$	$\gamma_1$	$Le$	$-\theta'(0)$		$-\phi'(0)$	
					$n = 1$	$n = 2$	$n = 1$	$n = 2$
0.1	0.3	0.1	0.2	1.2	0.0872	0.0894	0.1273	0.1292
	0.3				0.0870	0.0892	0.1490	0.1516
	0.5				0.0867	0.0889	0.1533	0.1560
0.2	0.0	0.1	0.2	1.2	0.0873	0.0895	0.1596	0.1625
		0.3			0.0871	0.0893	0.1436	0.1460
		0.6			0.0869	0.0891	0.1278	0.1296
0.2	0.3	0.0	0.2	1.2	0.000	0.000	0.1595	0.1625
		0.4			0.2482	0.0892	0.1152	0.1140
		0.6			0.3111	0.2667	0.1045	0.1141
0.2	0.3	0.1	0.0	1.2	0.000	0.0895	0.0873	0.0000
			0.3		0.0870	0.0892	0.1957	0.2002
			0.5		0.0869	0.0891	0.2759	0.2851
0.2	0.3	0.1	0.2	0.7	0.0871	0.0893	0.1230	0.1326
				1.0	0.0871	0.0893	0.1373	0.1461
				1.4	0.0871	0.0893	0.1484	0.1561

**Table 2.3:** A comparison of  $(C_{fx}, C_{fy})$  for different values of  $\alpha$  when  $n = 1.0$ ,  $\beta = N_b = N_t = Le = 0$ ,  $\gamma_1 \rightarrow \infty$  and  $\gamma \rightarrow \infty$ .

	$\alpha$	$f''(0)$	$g''(0)$
Ariel [101]	0.00	-1.00000	0.0
Munir et al. [102]	0.00	-1.00000	0.0
Present study	0.00	-1.00000	0.0
Ariel [101]	0.25	-1.048813	-0.194565
Munir et al. [102]	0.25	-1.048818	-0.194567
Present study	0.25	-1.048825	-0.194570
Ariel [101]	0.50	-1.93097	-0.465206
Munir et al. [102]	0.50	-1.93098	-0.465207
Present study	0.50	-1.93105	-0.465210
Ariel [101]	0.75	-1.134485	-0.794619
Munir et al. [102]	0.75	-1.134486	-0.794619
Present study	0.75	-1.134489	-0.794622
Ariel [101]	1.00	-1.173720	-1.173721
Munir et al. [102]	1.00	-1.173721	-1.173721
Present study	1.00	-1.173724	-1.173723

## 2.5 Concluding remarks

Model for 3D mixed convection flow of Sisko nanoliquid generated by stretched surface is elaborated. The key outcomes are given below.

- Influences of  $\lambda$  and  $N$  on the velocity  $f'(\eta)$  are quite similar.
- An increment in  $\lambda$  results in decrease of temperature and concentration.
- Temperature is enhanced via  $N_t$  and  $N_b$ .
- Impact of  $N_b$  on  $\phi(\eta)$  is qualitatively contrary to that of  $N_t$ .
- Effect of  $\alpha$  leads to decay in temperature and concentration.

- Temperature is increased for larger  $\gamma$ .

## Chapter 3

# Analysis of magnetized Williamson nanoliquid subject to stratification

This chapter explores the stratification phenomenon in flow of Williamson magnetized-nanoliquid. Flow is stretched in a non-linear way. Aspects of viscous dissipation and radiation are accounted. Chemical reaction having order one is also considered. Resultant problems are solved via homotopic technique. Convergent solutions are obtained. Graphs and table are arranged to disclose the behavior of distinct influential variables. Present pointed out that stratification diminishes the temperature and concentration. Moreover skin friction decays for higher magnetic parameter. Finally conclusion of current investigations are listed in the last section.

### 3.1 Modeling

Let us consider non-Newtonian (Williamson liquid) nanomaterials flow by stretching sheet of variable thickness. Stretching of sheet is taken in  $x$ -direction. Let  $U_w = U_0(x + b)^n$  be the sheet stretching velocity. Also  $n = 1$  leads to linear stretching. Flow geometry is assumed at  $y = \delta(x + b)^{\frac{1-n}{2}}$ , where  $\delta$  being small constant which specifies that sheet is adequately thin. Magnetic field  $B_0$  is implemented. Stratification, thermophoresis and Brownian motion aspects are accounted for modeling concentration and energy expressions. Dissipation and radiation effects are further included in energy expression. In addition concentration expression accounts chemical reaction. Geometrical configuration is captured in Fig. 3.1. Using boundary layer

approach the governing expressions for present analysis are

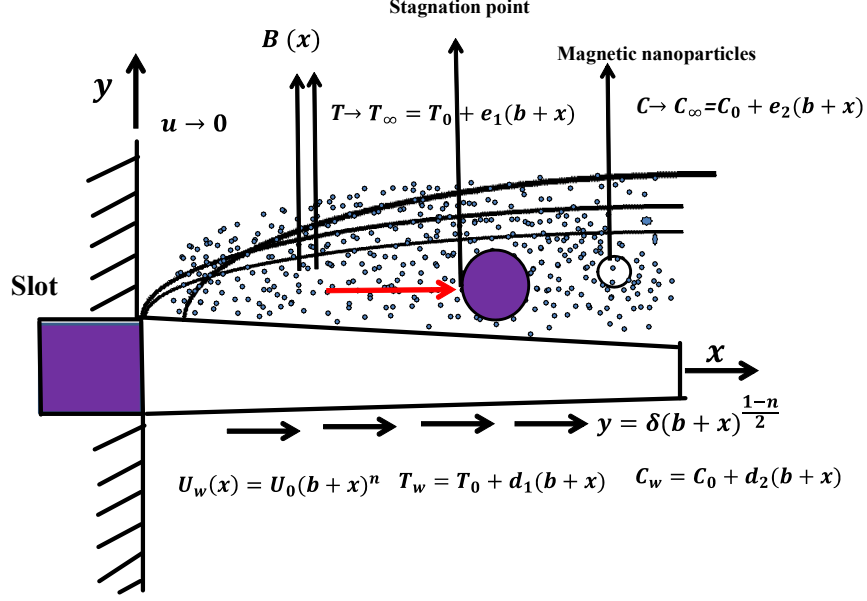


Fig. 3.1. Schematic diagram.

$$\frac{\partial u}{\partial x} + \frac{\partial v}{\partial y} = 0, \quad (3.1)$$

$$u \frac{\partial u}{\partial x} + v \frac{\partial u}{\partial y} = \nu \frac{\partial^2 u}{\partial y^2} + 2\nu\Gamma \frac{\partial^2 u}{\partial y^2} \frac{\partial u}{\partial y} + \frac{\sigma B_0^2}{\rho} (U_e - u) + U_e \frac{\partial U_e}{\partial x}, \quad (3.2)$$

$$\left. \begin{aligned} u \frac{\partial T}{\partial x} + v \frac{\partial T}{\partial y} &= \alpha_f \frac{\partial^2 T}{\partial y^2} + \tau \left( D_B \frac{\partial C}{\partial y} \frac{\partial T}{\partial y} + \frac{D_T}{T_\infty} \left( \frac{\partial T}{\partial y} \right)^2 \right) \\ &\quad - \frac{1}{(\rho c)} \frac{\partial q_r}{\partial y} + \frac{\mu_0}{(\rho c)_f} \Gamma \left( \frac{\partial u}{\partial y} \right)^3 + \frac{\mu_0}{(\rho c)_f} \left( \frac{\partial u}{\partial y} \right)^2, \end{aligned} \right\} \quad (3.3)$$

$$u \frac{\partial C}{\partial x} + v \frac{\partial C}{\partial y} = D_B \frac{\partial^2 C}{\partial y^2} + \frac{D_T}{T_\infty} \frac{\partial^2 T}{\partial y^2} - k_1 (C_w - C_0), \quad (3.4)$$

$$\left. \begin{aligned} y = \delta(b+x)^{\frac{1-n}{2}}, \quad u = U_w = U_0(b+x)^n, \quad v = 0, \\ T = T_w = T_0 + d_1(b+x), \quad C = C_w = C_0 + d_2(b+x), \end{aligned} \right\} \quad (3.5)$$

$$\left. \begin{aligned} y \rightarrow \infty, \quad u \rightarrow U_e = U_\infty(x+b)^n, \quad T \rightarrow T_\infty = T_0 + e_1(b+x), \\ C \rightarrow C_\infty = C_0 + e_2(b+x), \end{aligned} \right\} \quad (3.6)$$

where  $(u, v)$  stand for respective components of velocity parallel to  $(x, y)$  directions,  $\Gamma$  for time constant,  $\rho_f$  for base liquid density,  $U_e$  for free stream velocity,  $\mu_0$  for dynamic viscosity,

$\nu = \frac{\mu_0}{\rho_f}$  for kinematic viscosity,  $b$  for constant,  $(d_1, d_2, e_1, e_2)$  for non-dimensional constants,  $\sigma$  for electrical conductivity,  $n$  for velocity power index,  $\tau = (\rho c)_p/(\rho c)_f$  for heat capacities ratio,  $(T, T_0)$  for liquid and reference temperatures,  $k_1$  for chemical reaction rate,  $(C_0, C)$  for liquid and reference concentrations,  $D_T$  for coefficient of thermophoresis diffusion,  $(T_\infty, C_\infty)$  for ambient fluid temperature and concentration,  $U_0$  for reference velocity and  $D_B$  for diffusion coefficient. Radiated heat flux  $q_r$  is

$$q_r = -\frac{16\sigma^*T_\infty^3}{3m^*} \frac{\partial^2 T}{\partial y^2}, \quad (3.7)$$

in which  $\sigma^*$  symbolized Stefan-Boltzman constant and  $m^*$  indicates coefficient of mean absorption. Using Eq. (3.7) in Eq. (3.3) one obtains

$$\left. \begin{aligned} u \frac{\partial T}{\partial x} + v \frac{\partial T}{\partial y} &= \alpha_f \frac{\partial^2 T}{\partial y^2} + \tau \left( D_B \frac{\partial C}{\partial y} \frac{\partial T}{\partial y} + \frac{D_T}{T_\infty} \left( \frac{\partial T}{\partial y} \right)^2 \right) \\ &+ \frac{1}{(\rho c)_f} \frac{16\sigma^*T_\infty^3}{3m^*} \frac{\partial^2 T}{\partial y^2} + \frac{\mu_0}{(\rho c)_f} \Gamma \left( \frac{\partial u}{\partial y} \right)^3 + \frac{\mu_0}{(\rho c)_f} \left( \frac{\partial u}{\partial y} \right)^2. \end{aligned} \right\} \quad (3.8)$$

By considering the variables

$$\left. \begin{aligned} u &= U_0 (x+b)^n F'(\eta), \quad v = -\sqrt{\frac{(n+1)}{2}} \nu U_0 (x+b)^{n-1} \left[ F(\eta) + \eta F'(\eta) \left( \frac{n-1}{n+1} \right) \right], \\ \Theta(\eta) &= \frac{T-T_\infty}{T_w-T_0}, \quad \Phi(\eta) = \frac{C-C_\infty}{C_w-C_0}, \quad \eta = y \sqrt{\frac{(n+1)}{2}} \frac{U_0(x+b)^{n-1}}{\nu}, \end{aligned} \right\} \quad (3.9)$$

continuity equation is trivially satisfied while other Eqs. (3.2) – (3.8) become

$$F''' + FF'' + We \sqrt{\frac{n+1}{2}} F'' F''' - \left( \frac{2n}{n+1} \right) F'^2 + \left( \frac{2n}{n+1} \right) \lambda^2 + \left( \frac{2}{n+1} \right) M^2(\lambda - F') = 0, \quad (3.10)$$

$$\left. \begin{aligned} (1 + Rd) \Theta'' + \text{Pr} \left( F\Theta' + N_t \Theta'^2 + N_b' \Theta' \Phi' - \left( \frac{2}{n+1} \right) (\Theta + \epsilon_1) F' \right) \\ + \text{Pr} Ec F''^2 + We \text{Pr} Ec F''^3 = 0, \end{aligned} \right\} \quad (3.11)$$

$$\Phi'' + Sc \left( \Phi' F - \frac{2}{n+1} \epsilon_2 F' \right) - \left( \frac{2}{n+1} \right) Sc \gamma_1 \Phi + \left( \frac{N_t}{N_b} \right) \Theta'' = 0, \quad (3.12)$$

$$\left. \begin{aligned} F(\alpha) &= \alpha \left( \frac{1-n}{1+n} \right), \quad F'(\alpha) = 1, \quad \Theta(\alpha) = 1 - \epsilon_1, \quad \Phi(\alpha) = 1 - \epsilon_2, \\ F'(\infty) &\rightarrow \lambda, \quad \Theta(\infty) \rightarrow 0, \quad \Phi(\infty) \rightarrow 0, \end{aligned} \right\} \quad (3.13)$$

where prime designates derivative via  $\eta$  and  $\alpha = \delta\sqrt{\left(\frac{n+1}{2}\right)\frac{U_0}{\nu}}$  signifies wall thickness variable and  $\eta = \alpha = \delta\sqrt{\left(\frac{n+1}{2}\right)\frac{U_0}{\nu}}$ .

Now considering

$$\left. \begin{aligned} F(\eta) &= f(\eta - \alpha) = f(\xi), \\ \Theta(\eta) &= \theta(\eta - \alpha) = \theta(\xi), \\ \Phi(\eta) &= \phi(\eta - \alpha) = \phi(\xi), \end{aligned} \right\} \quad (3.14)$$

Eqs.(3.10) – (3.13) are reduced to the form

$$f''' + ff'' + We\sqrt{\frac{n+1}{2}}f''f''' - \left(\frac{2n}{n+1}\right)f'^2 + \left(\frac{2n}{n+1}\right)\lambda^2 + \left(\frac{2}{n+1}\right)M^2(\lambda - f') = 0, \quad (3.15)$$

$$\left. \begin{aligned} (1 + Rd)\theta'' + Pr\left(f\theta' + N_b\theta'\phi' + N_t\theta'^2 - \left(\frac{2}{n+1}\right)(\epsilon_1 + \theta)f'\right) \\ + WePrEc f''^3 + PrEc f''^2 = 0, \end{aligned} \right\} \quad (3.16)$$

$$\phi'' + Sc\left(f\phi' - \frac{2}{n+1}\epsilon_2 f'\right) - \frac{2}{n+1}Sc\gamma_1\phi + \left(\frac{N_t}{N_b}\right)\theta'' = 0, \quad (3.17)$$

$$\left. \begin{aligned} f(0) &= \alpha\left(\frac{1-n}{1+n}\right), \quad f'(0) = 1, \quad \theta(0) = 1 - \epsilon_1, \quad \phi(0) = 1 - \epsilon_2 \\ f'(\infty) &\rightarrow \lambda, \quad \theta(\infty) \rightarrow 0, \quad \phi(\infty) \rightarrow 0. \end{aligned} \right\} \quad (3.18)$$

Here  $Ec (= \frac{U_w^2}{c_p(T_w - T_0)})$  shows Eckert number,  $M^2 (= \frac{\sigma B_0^2}{\rho U_0(x+b)^{n-1}})$  magnetic parameter,  $N_b (= \frac{(\rho c)_p D_B(C_w - C_0)}{(\rho c)_f \nu})$  Brownian motion parameter,  $We (= \Gamma\sqrt{\frac{(n+1)U_0^3(x+b)^{3n-1}}{\nu}})$  Weissenberg number,  $\gamma_1 (= \frac{k_1}{U_0}(x+b)^{1-n})$  chemical reaction,  $(Pr = \frac{\nu}{\alpha_f})$  Prandtl number,  $\lambda (= \frac{U_\infty}{U_0})$  ratio of velocities,  $Rd (= \frac{16\sigma^* T_\infty^3}{3m^* k})$ ,  $N_t (= \frac{(\rho c)_p D_T(T_w - T_0)}{(\rho c)_f T_\infty \nu})$  thermophoresis parameter,  $\epsilon_2 (= \frac{e_2}{d_2})$  solutal stratified parameter,  $Sc (= \frac{\nu}{D_B})$  Schmidt number and  $\epsilon_1 (= \frac{e_1}{d_1})$  thermal stratified variable. Skin friction and temperature and concentration gradients are

$$\left. \begin{aligned} C_{fx} &= \frac{\tau_{yx}|_{y=\delta(b+x)\frac{1-n}{2}}}{1/2\rho U_w^2} \Big| \\ &= \frac{\mu_0\left(\frac{\partial u}{\partial y} + \frac{\Gamma}{2}\left(\frac{\partial u}{\partial y}\right)^2\right)_{y=\delta(x+b)\frac{1-n}{2}}}{1/2\rho U_w^2}, \end{aligned} \right\} \quad (3.19)$$

$$\left. \begin{aligned} Nu_x &= \frac{(x+b)q_w|_{y=\delta(b+x)\frac{1-n}{2}}}{k_\infty(T_w - T_\infty)} \\ &= -\frac{\left(\frac{\partial T}{\partial y}\right)_{y=\delta(x+b)\frac{1-n}{2}}}{(T_w - T_\infty)} + q_r, \end{aligned} \right\} \quad (3.20)$$



$$\left. \begin{aligned}
Sh_x &= \frac{(x+b)q_m \Big|_{y=\delta(b+x)\frac{1-n}{2}}}{D_B(C_w - C_\infty)} \\
&= -\frac{\left(\frac{\partial C}{\partial y}\right)_{y=\delta(b+x)\frac{1-n}{2}}}{(C_w - C_\infty)}.
\end{aligned} \right\} \quad (3.21)$$

In dimensionless form

$$(\text{Re}_x)^{\frac{1}{2}} C_{f_x} = \left(\frac{n+1}{4}\right) We f''(0) + \sqrt{\frac{(n+1)}{2}} f''(0), \quad (3.22)$$

$$\frac{Nu_x}{(\text{Re}_x)^{\frac{1}{2}}} = -\sqrt{\left(\frac{n+1}{2}\right)} (1 + Rd) \theta'(0), \quad (3.23)$$

$$\frac{Sh_x}{(\text{Re}_x)^{\frac{1}{2}}} = -\sqrt{\left(\frac{n+1}{2}\right)} \phi'(0), \quad (3.24)$$

in which local Reynolds number is symbolized as  $\text{Re}_x = U_w(b+x)/\nu$ .

### 3.2 Analysis of homotopic solutions

We choose

$$\left. \begin{aligned}
f_0(\xi) &= (1 - e^{-\xi})(1 - \lambda) + \alpha \left(\frac{1-n}{1+n}\right) + \lambda\xi, \\
\theta_0(\xi) &= (1 - \epsilon_1)e^{-\xi}, \quad \phi_0(\xi) = (1 - \epsilon_2)e^{-\xi},
\end{aligned} \right\} \quad (3.25)$$

with characteristics

$$\left. \begin{aligned}
\tilde{\mathcal{L}}_f [C_1^{**} + C_2^{**} e^\xi + C_3^{**} e^{-\xi}] &= 0, \\
\tilde{\mathcal{L}}_\theta [C_4^{**} e^\xi + C_5^{**} e^{-\xi}] &= 0, \\
\tilde{\mathcal{L}}_\phi [C_6^{**} e^\xi + C_7^{**} e^{-\xi}] &= 0,
\end{aligned} \right\} \quad (3.26)$$

where  $C_i^{**}$  ( $i = 1 - 7$ ) symbolized arbitrary constants.

To obtain the solutions via homotopic technique it is mandatory to look-over the convergence of required solutions. Such solutions comprise embedding variables ( $\hbar_f$ ,  $\hbar_\theta$  and  $\hbar_\phi$ ). For convergence the  $h$ -curves are declared through Figs. 3.2 & 3.3. Acceptable ranges of ( $\hbar_f$ ,  $\hbar_\theta$  and  $\hbar_\phi$ ) are  $[-1.20 \leq \hbar_f \leq -2.23]$ ,  $[-0.50 \leq \hbar_\theta \leq -1.52]$  and  $[-0.42 \leq \hbar_\phi \leq -1.35]$ . Furthermore

table 3.1 pointed out that homotopic solutions converge for  $\hbar_\phi = -0.6$  and  $\hbar_\theta = -5.0 = \hbar_f$ .

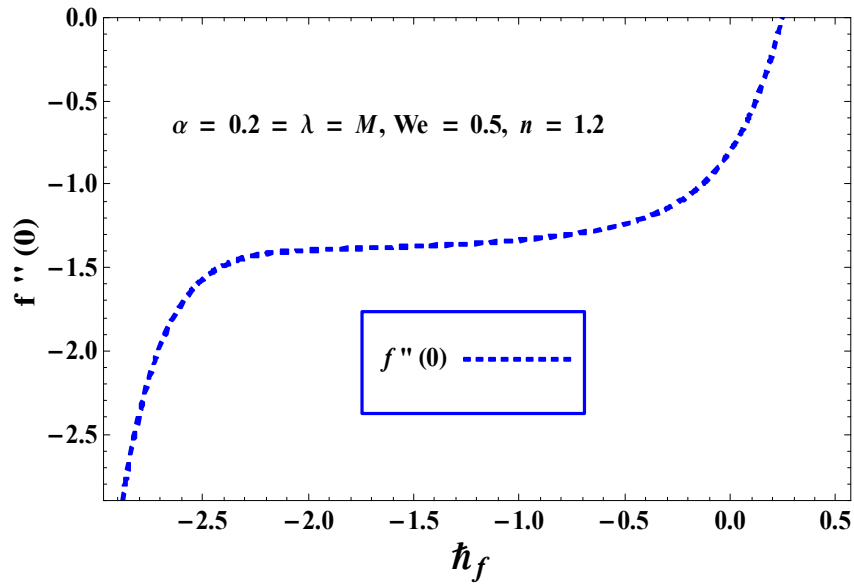


Fig. 3.2.  $\hbar$ -curve for  $f$ .

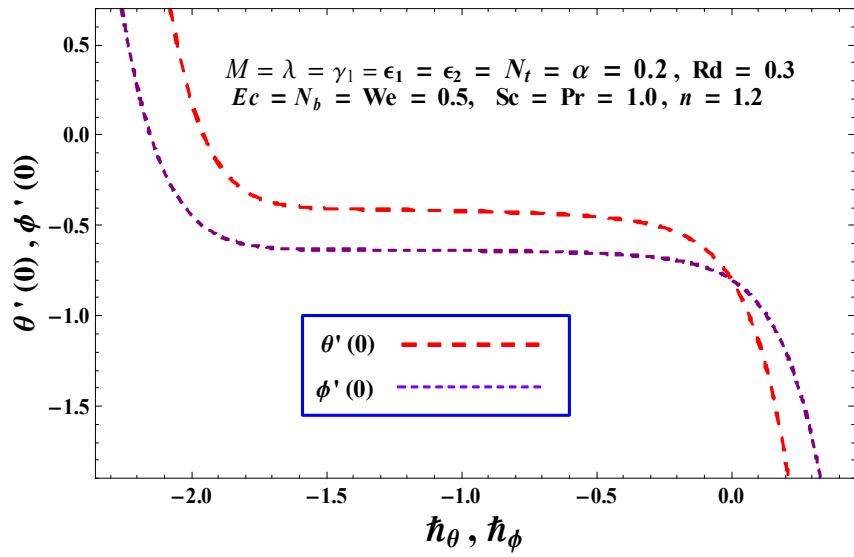


Fig. 3.3 :  $\hbar$ -curves for  $\theta$  and  $\phi$ .

**Table 3.1:** HAM solution convergence when  $\lambda = \alpha = \epsilon_2 = M = \epsilon_1 = N_t = \gamma_1 = n = 0.2$ ,  $N_b = We = 0.5 = Ec$ ,  $Rd = 0.3$  and  $Sc = 1.0 = Pr$ .

Estimations order	$(-f''(0))$	$(-\theta'(0))$	$(-\phi'(0))$
1	0.88576	0.73619	0.6937
5	1.0957	0.64235	0.5267
15	1.2885	0.59561	0.4498
25	1.3446	0.58512	0.4338
30	1.3470	0.58412	0.4328
35	1.3470	0.58412	0.4328
50	1.3470	0.58412	0.4328

### 3.3 Discussion

This portion reported the physical illustration of emerging variables i.e magnetic parameter ( $M$ ), Weissenberg number ( $We$ ), Eckert number ( $Ec$ ), velocity ratio variable ( $\lambda$ ), Brownian motion parameter ( $N_b$ ), Prandtl number ( $Pr$ ), velocity power index ( $n$ ), radiation variable ( $Rd$ ), thermophoresis variable ( $N_t$ ), chemical reaction ( $\gamma_1$ ), wall thickness variable ( $\alpha$ ) thermal and solutal stratified variables ( $\epsilon_1$  and  $\epsilon_2$ ) on  $(f')$ ,  $(\theta)$ ,  $(\phi)$ ,  $(Nu_x Re_x^{-0.5})$ ,  $(Sh_x Re_x^{-0.5})$  and  $(- (Re)^{0.5} C_f)$ . Here Figs. (3.4) – (3.19) are organized for velocity, temperature, concentration, local Sherwood and Nusselt numbers. Attributes of ( $\lambda$ ) against  $(f')$  are declared in Fig. 3.4. Here velocity  $(f')$  increases with enhancement of ( $\lambda$ ). Noted that momentum layer thickness strengthens for  $(\lambda) < 1$ . It is due to fact that stretched velocity influences the free stream velocity. Behavior of  $(We)$  on  $(f')$  is presented in Fig. 3.5. Here  $(We)$  improves the liquid thickness and thus  $(f')$  diminishes. Fig. 3.6 and 3.7 declared impact of ( $\alpha$ ) on velocity  $(f')$ . It is observed that  $(f')$  near surface decays for  $(n) < 1$  (see Fig. 3.6), where as reverse feature is noted for  $(n) > 1$  (see Fig. 3.7). Fig. 3.8 depicts graphical illustration of  $(f')$  for  $(M)$ . Here strengthen in magnetic field decays the nanoliquid velocity. Fig. 3.9 is designed to interpret how the temperature  $(\theta)$  gets influence by  $(N_t)$ . Clearly larger  $(N_t)$  correspond to improvement in  $(\theta)$ . Physically nanoparticles are extracted towards the cold liquid from hot boundary layer. That is why thermal field turns out to be thicker in the presence of  $(N_t)$ . Impact of  $(Rd)$  on

$(\theta)$  is displayed in Fig. 3.10. It is found that  $(\theta)$  is higher for against  $(Rd)$ . In fact coefficient of mean absorption  $(m^*)$  declines by higher  $(Rd)$  which is responsible for  $(\theta)$  augmentation. Salient characteristics of  $(Ec)$  on  $(\theta)$  is depicted in Fig. 3.11. Here  $(\theta)$  increases when  $(Ec)$  is enhanced. Physically larger  $(Ec)$  leads to frictional heating which ultimately increases thermal field  $(\theta)$ . Aspect of  $(Pr)$  on  $(\theta)$  is displayed in Fig. 3.12. This Fig. declares that  $(Pr)$  has higher nanoliquids temperature. Since the liquid diffusivity arises in  $(Pr)$  which becomes weaker for higher  $(Pr)$ . Thus reduction in  $(\theta)$  is associated with such weaker diffusivity. Characteristics of  $(\epsilon_1)$  on  $(\theta)$  are displayed in Fig. 3.13. Obviously stratification variable  $(\epsilon_1)$  reduces the temperature. It is due to a reason that difference of temperature declines between the ambient liquid and sheet. Figs. 3.14 and 3.15 interpret  $N_t$  and  $N_b$  impacts on  $(\phi)$ . Here an improvement in  $(\phi)$  is seen when  $(N_t)$  is incriminated. However reverse trend is noticed for  $(N_b)$ . Contribution of  $(\epsilon_2)$  versus  $(\phi)$  is exhibited in Fig. 3.16. It is found that  $(\phi)$  is decreasing function of  $(\epsilon_2)$ . It is because of small difference of ambient and surface concentration. Variation of  $(\gamma_1)$  on  $(\phi)$  is designed through Fig. 3.17. Strengthen in  $(\gamma_1)$  leads to decay  $(\phi)$  and corresponding layer becomes thin. The reason behind this argument is that distractive chemical rate  $(\gamma_1 > 1)$  increases the mass transport rate and consequently  $(\phi)$  reduces. Curves for  $(N_t)$  and  $(N_b)$  on  $(Nu_x Re_x^{-0.5})$  is drawn in Fig. 3.18. Temperature gradient decays for  $(N_b)$  whereas it enhances for  $(N_t)$ . Higher estimation of  $(n)$  and  $(Sc)$  boost  $(Sh_x Re_x^{-0.5})$ . This behavior is noted in Fig. 3.19. Numerical estimations of  $(-\theta'(0))$ ,  $(-f''(0))$  and  $(-\phi'(0))$  for distinct order of estimations are depicted in Table 3.1. It is identified that 30<sup>th</sup>-order of approximations are adequate for solutions convergence. Numerical outcomes of skin friction for  $(We)$ ,  $(\lambda)$ ,  $(n)$ ,  $(M)$  and  $(\alpha)$  are illustrated in Table 3.2. This Table certifies that skin friction is incriminated through  $(n)$  and

( $M$ ) while it diminishes for ( $\lambda$ ) and ( $\alpha$ ).

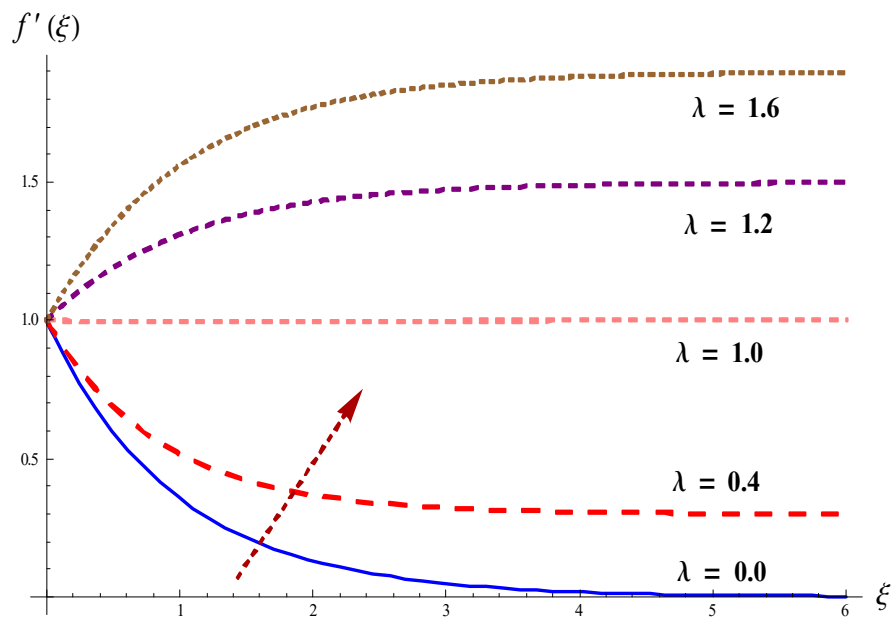


Fig. 3.4. Effect for  $f'$  through  $\lambda$ .

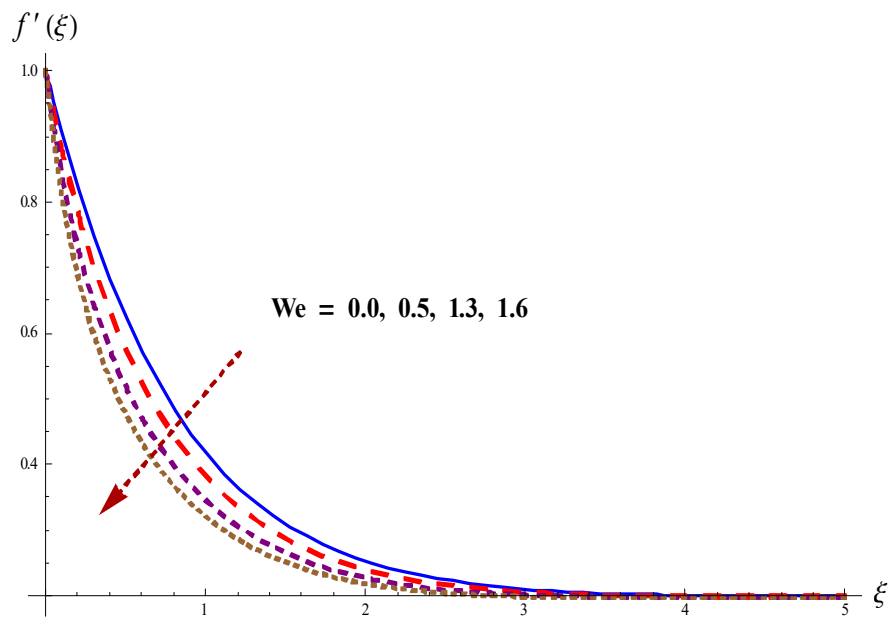


Fig. 3.5. Effect for  $f'$  through  $We$ .

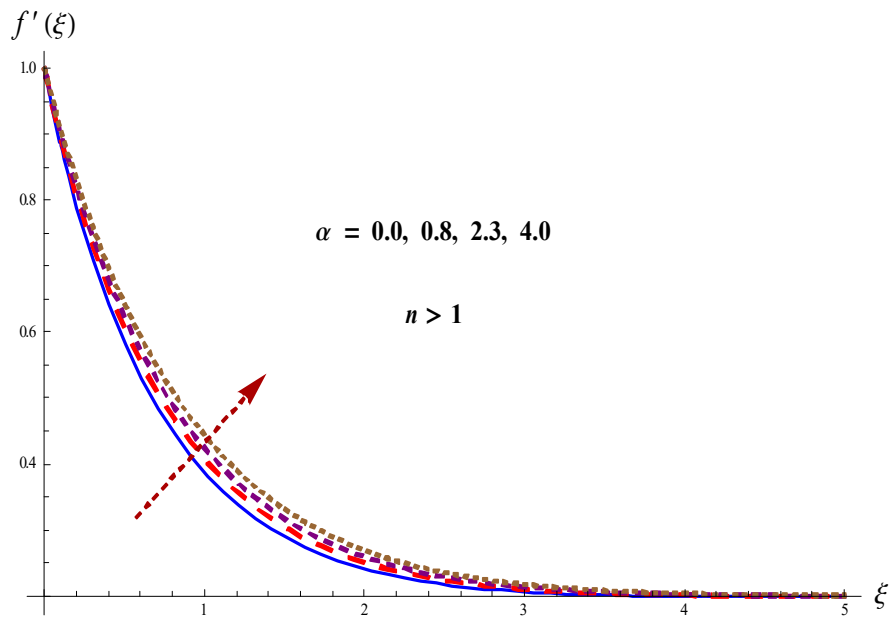


Fig. 3.6.  $f'$  through  $\alpha$  ( $n > 1$ ).

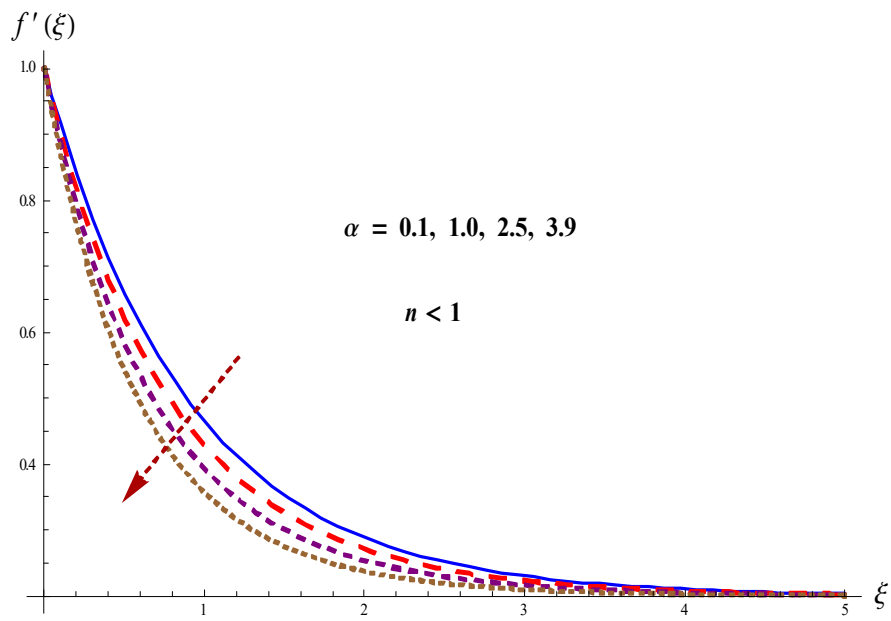


Fig. 3.7. Effect for  $f'$  through  $\alpha$  ( $n < 1$ ).

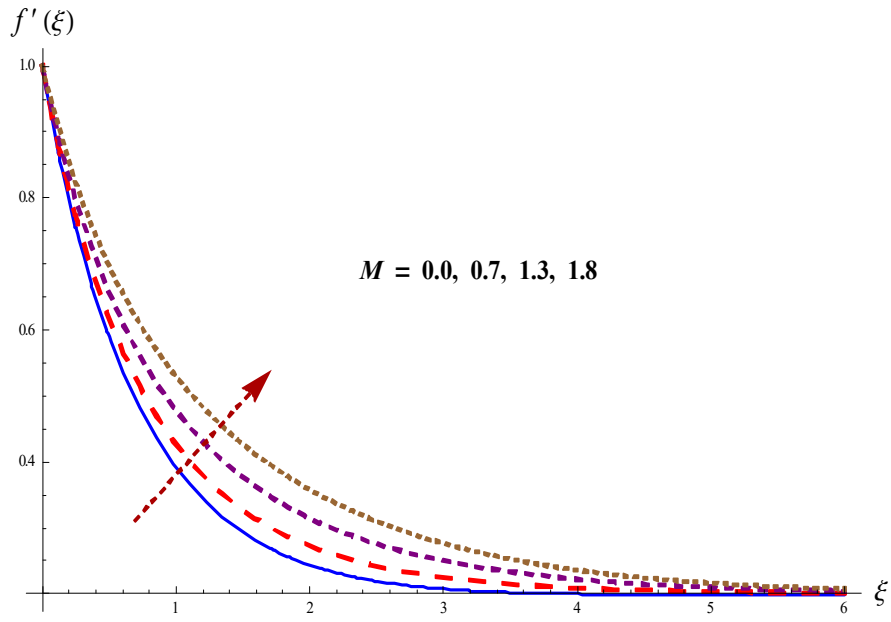


Fig. 3.8. Effect for  $f'$  through  $M$ .

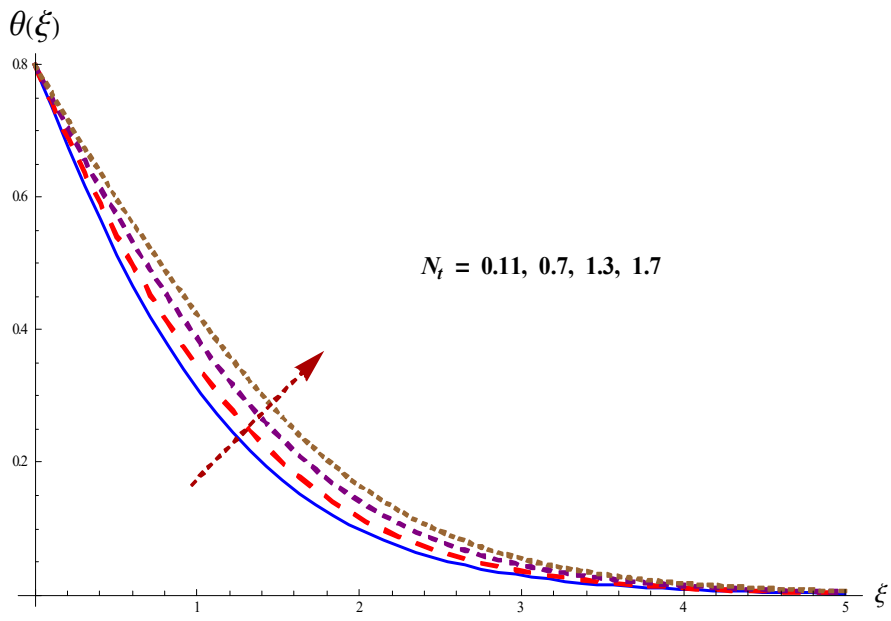


Fig. 3.9. Effect for  $\theta$  through  $N_t$ .

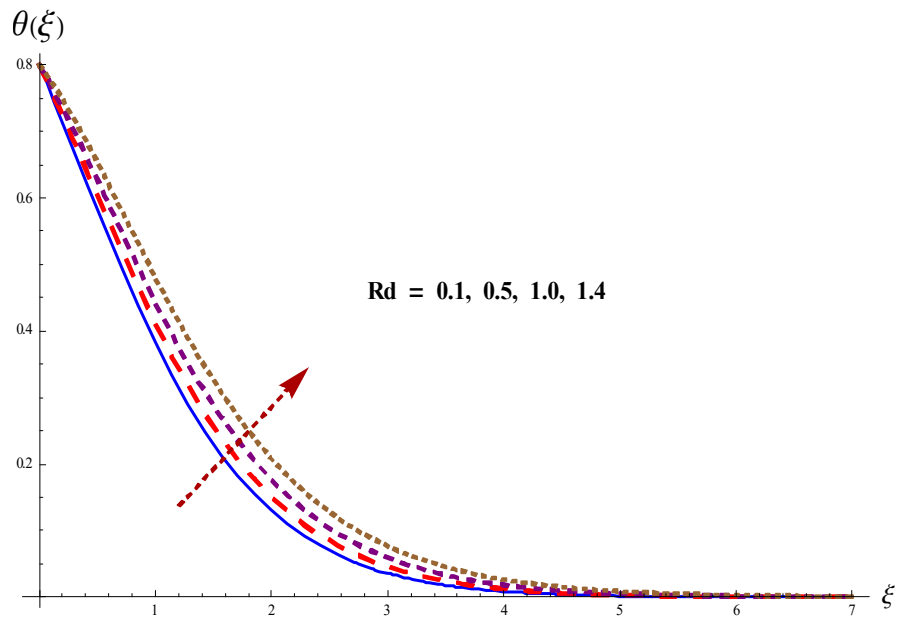


Fig. 3.10. Effect for  $\theta$  through  $Rd$ .

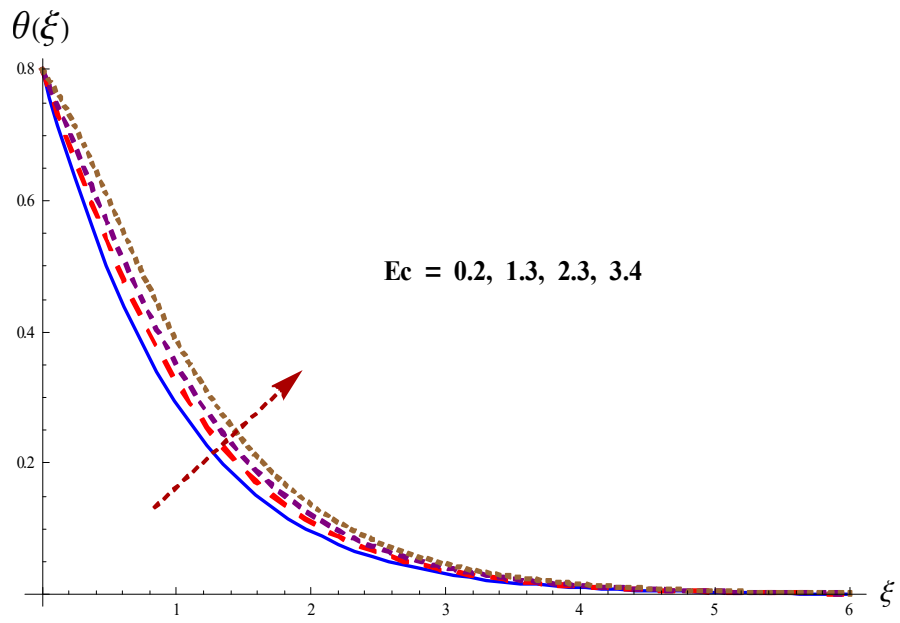


Fig. 3.11. Effect for  $\theta$  through  $Ec$ .



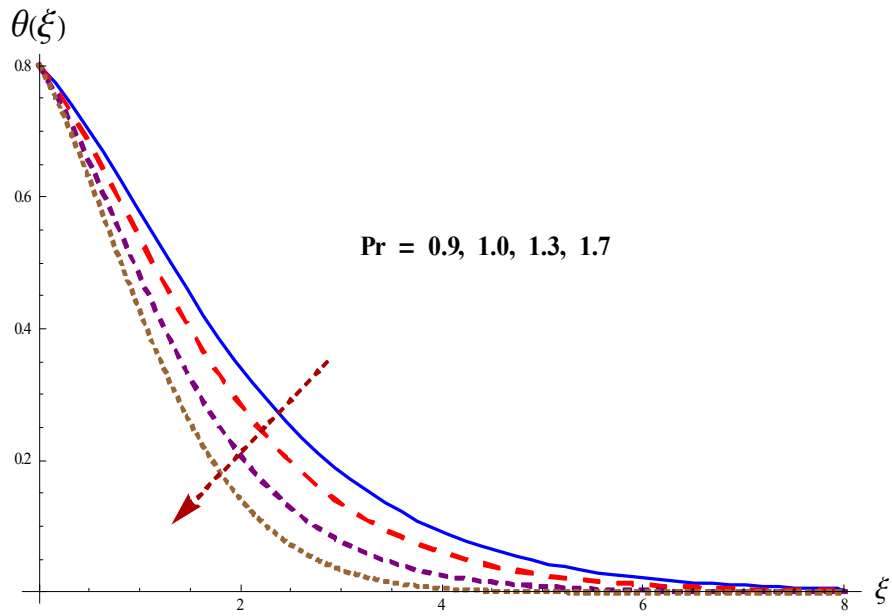


Fig. 3.12. Effect for  $\theta$  through Pr.

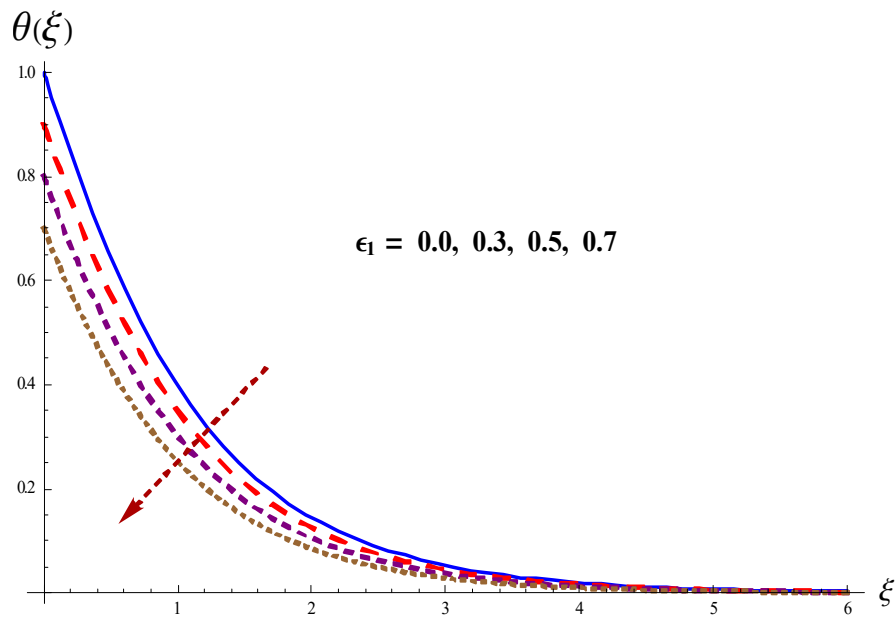


Fig. 3.13.  $\theta$  through  $\epsilon_1$ .

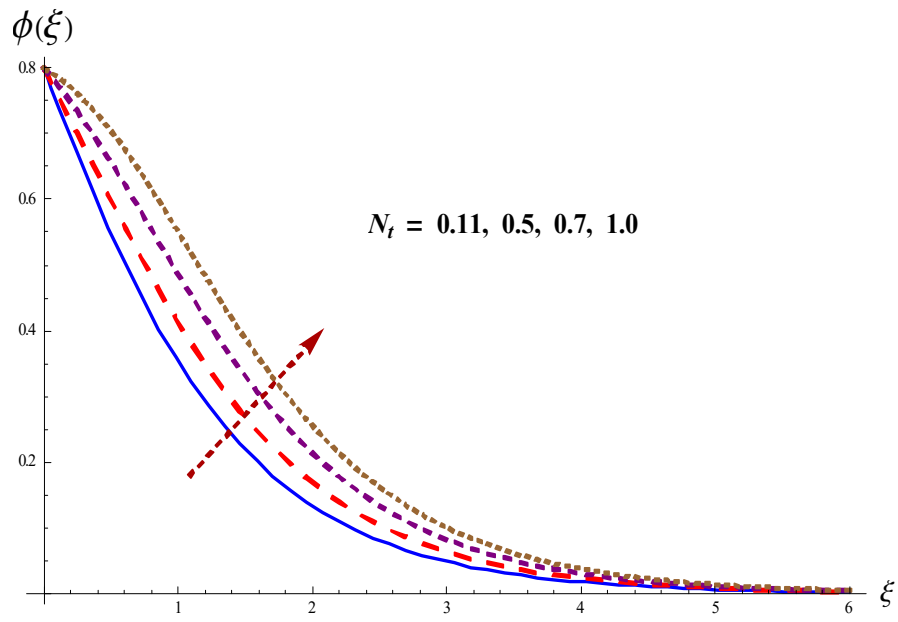


Fig. 3.14.  $\phi$  through  $N_t$ .

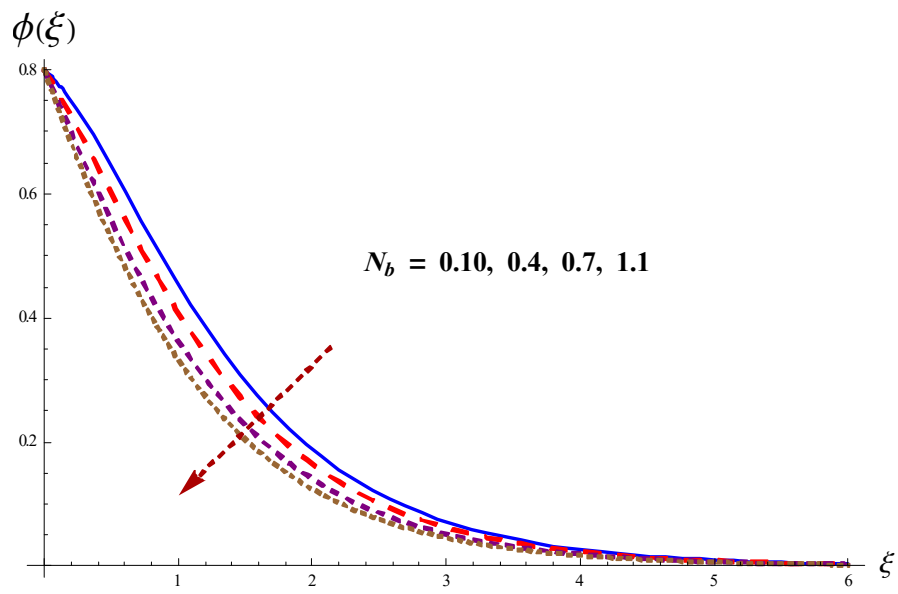


Fig. 3.15.  $\phi$  via  $N_b$ .

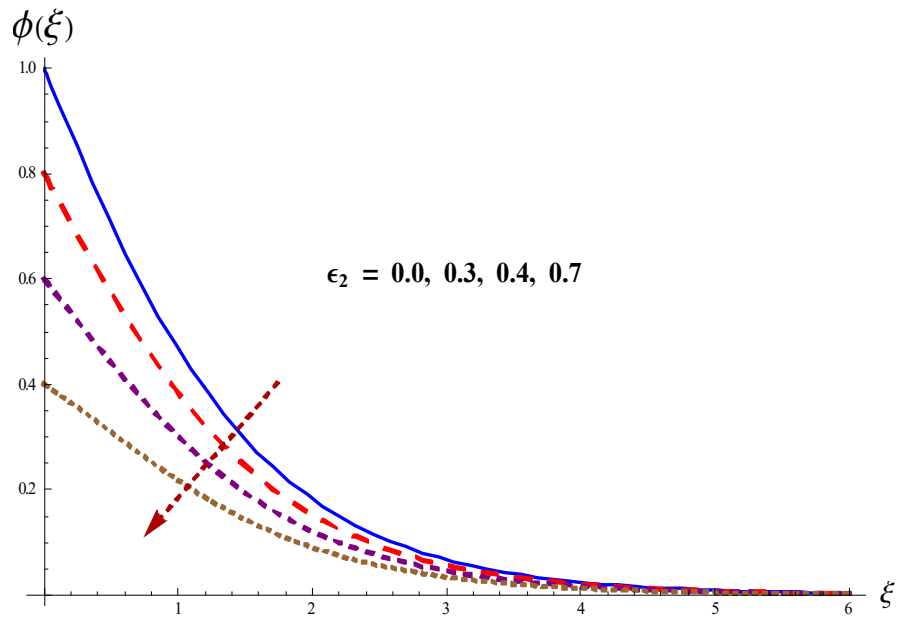


Fig. 3.16.  $\phi$  via  $\epsilon_2$ .

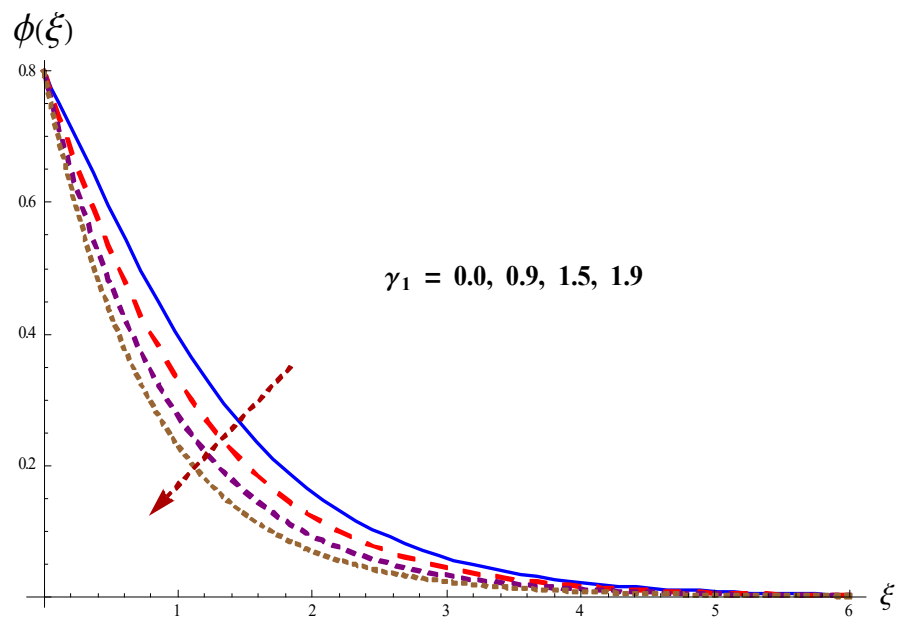


Fig. 3.17. Effect for  $\phi$  through  $\gamma_1$ .

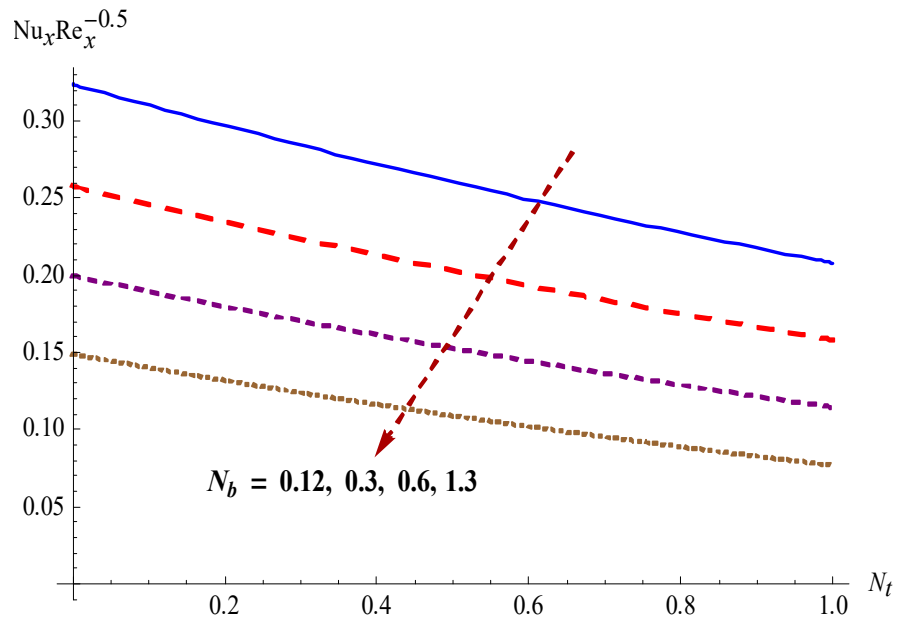


Fig. 3.18. Effect for  $N_t$  through  $N_b$  on  $Nu_x Re_x^{-\frac{1}{2}}$ .

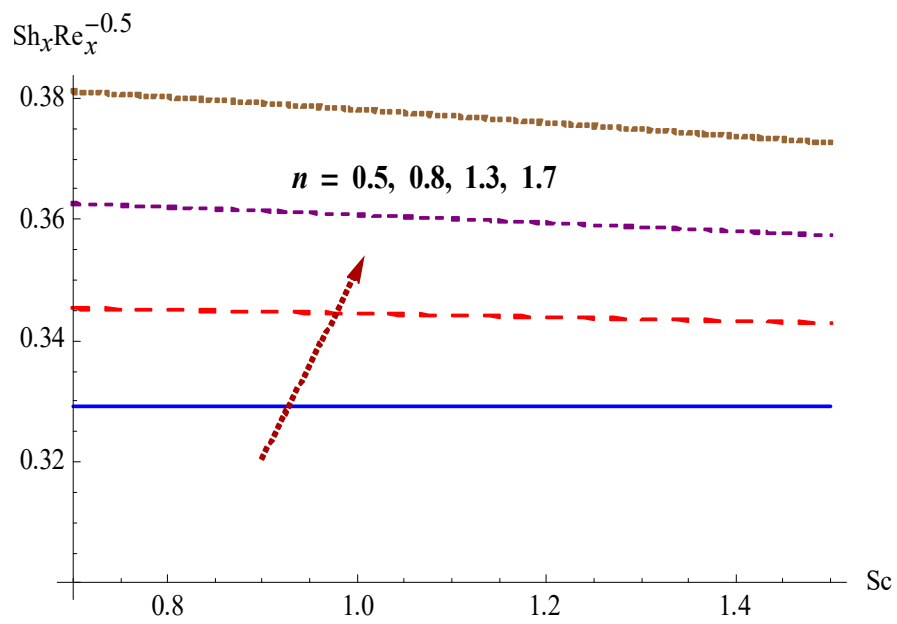


Fig. 3.19. Effect for  $n$  through  $Sc$  on  $Sh_x Re_x^{-\frac{1}{2}}$ .

**Table 3.2:** Numerical data of  $-(\text{Re})^{0.5} C_f$  for various estimations of  $We$ ,  $\lambda$ ,  $\alpha$ ,  $M$  and  $n$ .

Fixed values of parameters	Parameters		$-\text{Re}^{\frac{1}{2}} C_f$
$n = \lambda = \alpha = \epsilon_2 = \epsilon_1 = \gamma_1 = N_t = 0.2,$ $We = N_b = Ec = 0.5, Sc = Pr = 1, Rd = 0.3$	$M$	0.0	0.939939
		0.4	0.975113
		0.7	0.993821
$\lambda = M = \alpha = \epsilon_2 = \epsilon_1 = \gamma_1 = N_t = 0.2,$ $We = N_b = Ec = 0.5, Sc = Pr = 1, Rd = 0.3$	$n$	0.5	0.864361
		1.1	1.00641
		1.4	1.02899
$n = \lambda = M = \epsilon_2 = \epsilon_1 = \gamma_1 = N_t = 0.2,$ $We = N_b = Ec = 0.5, Sc = Pr = 1, Rd = 0.3$	$\alpha$	0.2	0.957556
		0.5	0.954224
		0.8	0.938785
$n = M = \alpha = \epsilon_2 = \epsilon_1 = \gamma_1 = N_t = 0.2,$ $We = N_b = Ec = 0.5, Sc = Pr = 1, Rd = 0.3$	$\lambda$	0.0	0.920663
		0.4	0.913273
		0.9	0.713070

### 3.4 Closing remarks

Here MHD impact in stratified radiated flow of Williamson nanomaterials with chemical reaction is investigated. Key outcomes of present study are given below:

- Higher ( $We$ ) decays the nanoliquid velocity.
- Larger ( $\alpha$ ) shows similar feature for both ( $f'$ ) and ( $\theta$ ).
- Higher estimations of ( $Rd$ ) and ( $N_t$ ) augment liquid temperature.
- Higher ( $\epsilon_1$ ) and ( $\epsilon_2$ ) decay ( $\phi$ ) and ( $\theta$ ).
- Larger ( $N_t$ ) and ( $N_b$ ) show reverse trend for Nusselt number.
- Drag force is higher for ( $M$ ) and  $n$ .

## Chapter 4

# Non-linear radiative squeezed flow of nanoliquid with chemical reaction and activation energy

This chapter explores the flow of magnetized nanomaterials between two parallel disks. Novel aspects of activation energy and non-linear radiation are explored. Non-linear system of ODEs is obtained via proper transformations. Homotopic scheme determines the convergence interval for the solution. Plots have been interpreted against various physical variables. Further surface drag forces and heat and mass transfer rates are numerically computed. Our computed analysis depicts that influence of squeezed and magnetic parameters have reverse effects on temperature.

### 4.1 Formulation

Here we intend to discuss second grade nanomaterials squeezed flow between two parallel disks. The distance between the parallel disks is  $h(t) = \sqrt{\frac{\nu(1-\alpha t)}{a}}$ . The upper disk is at  $z = h(t) = \sqrt{\frac{\nu(1-\alpha t)}{a}}$  while the lower permeable disk at  $z = 0$  ( see Fig. 4.1). Here  $\alpha$  denotes dimensional constant and  $\nu$  the kinematic viscosity. Lower disk is permeable and stretching with velocity  $\left(u = \frac{ar}{2(1-\alpha t)}\right)$  ( $a$  stands for stretching rate) while upper disk is squeezed towards the permeable moving lower disk with velocity  $w = \frac{-\alpha}{2} \sqrt{\frac{\nu}{a(1-\alpha t)}}$ . An incompressible liquid is electrically conducted. The generalized Ohm's law [103] in term of Hall current and

electric field is expressed as  $J = \frac{\sigma}{1+m_1^2} \left( E + V \times B - \frac{1}{\sigma n_e} J \times B \right)$ . Here  $B$  signifies magnetic induction,  $E$  denotes electric field,  $\sigma$  the electrical conductivity,  $J$  the electric current density,  $m_1$  the Hall current parameter and  $n_e$  the electron number density [104]. A magnetic field  $B(t) = B_0(1 - \alpha t)^{-1/2}$  is utilized transverse to flow. Electric field and Hall current aspects are disregarded. Since the flow presumes low velocity and uniform magnetic field, therefore magnetic Reynolds number have lower values. Such less values of Reynolds number assists assumption of negligible induced magnetic [105]. Brownian and thermophoresis diffusion attributes are retained in energy expression. Moreover chemical reaction and activation energy aspects are incorporated. The relevant problems have following statements.

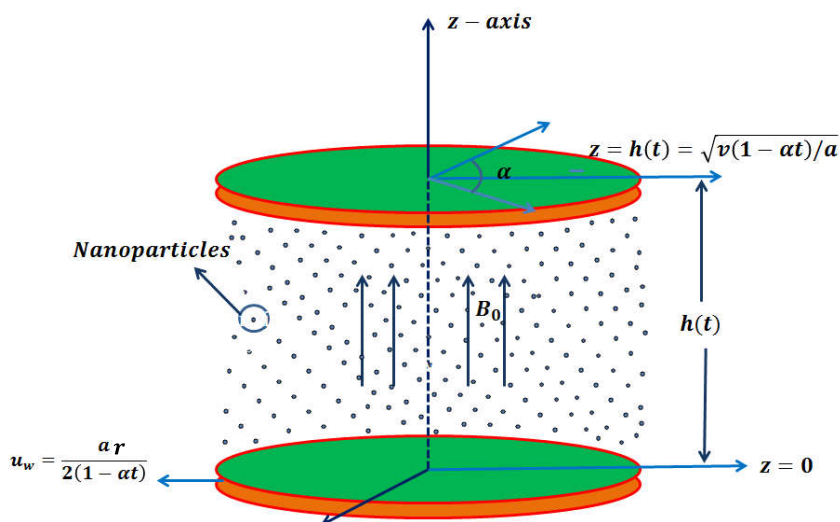


Fig. 4.1. Geometry of problem.

$$\frac{\partial u}{\partial r} + \frac{u}{r} + \frac{\partial w}{\partial r} = 0, \quad (4.1)$$

$$\left. \begin{aligned}
& \frac{\partial u}{\partial t} + u \frac{\partial u}{\partial r} + w \frac{\partial u}{\partial z} = -\frac{1}{\rho} \frac{\partial p}{\partial r} + \frac{\mu}{\rho} \left( \frac{\partial^2 u}{\partial r^2} + \frac{\partial^2 u}{\partial z^2} + \frac{1}{r} \frac{\partial u}{\partial r} - \frac{u}{r^2} \right) \\
& + \frac{\alpha_1^*}{\rho} \left( \begin{aligned}
& \frac{2}{r} \frac{\partial^2 u}{\partial t \partial r} - \frac{2}{r^2} \frac{\partial u}{\partial t} + 2 \frac{\partial^3 u}{\partial t \partial r^2} + \frac{\partial^3 u}{\partial t \partial z^2} + \frac{\partial^3 w}{\partial t \partial r \partial z} \\
& + 2 \frac{u^2}{r^3} - 2 \frac{w}{r^2} \frac{\partial u}{\partial z} - \frac{1}{r} \left( \frac{\partial u}{\partial z} \right)^2 - \frac{\partial u}{\partial z} \frac{\partial^2 w}{\partial z^2} + w \frac{\partial^3 u}{\partial z^3} - 2 \frac{u}{r^2} \frac{\partial u}{\partial t} \\
& + \frac{\partial u}{\partial r} \frac{\partial^2 u}{\partial z^2} + \frac{\partial w}{\partial r} \frac{\partial^2 w}{\partial z^2} + \frac{1}{r} \left( \frac{\partial w}{\partial r} \right)^2 + 2 \frac{w}{r} \frac{\partial^2 u}{\partial z \partial r} + \frac{\partial w}{\partial r} \frac{\partial^2 u}{\partial z \partial r} \\
& + \frac{\partial w}{\partial z} \frac{\partial^2 w}{\partial z \partial r} - \frac{\partial u}{\partial r} \frac{\partial^2 w}{\partial z \partial r} + u \frac{\partial^3 u}{\partial r \partial z^2} + w \frac{\partial^3 u}{\partial r \partial z^2} + 2 \frac{u}{r} \frac{\partial^2 u}{\partial r^2} + \frac{\partial u}{\partial r} \frac{\partial^2 u}{\partial r^2} \\
& + \frac{\partial u}{\partial z} \frac{\partial^2 w}{\partial r^2} + 2 \frac{\partial w}{\partial r} \frac{\partial^2 w}{\partial r^2} + 2w \frac{\partial^3 u}{\partial z \partial r^2} + u \frac{\partial^3 w}{\partial z \partial r^2} + 2u \frac{\partial^3 u}{\partial r^3} \\
& - \frac{\sigma B^2 u}{\rho},
\end{aligned} \right) \quad (4.2)
\end{aligned} \right\}$$

$$\left. \begin{aligned}
& \frac{\partial w}{\partial t} + u \frac{\partial w}{\partial r} + w \frac{\partial w}{\partial z} = -\frac{1}{\rho} \frac{\partial p}{\partial z} + \frac{\mu}{\rho} \left( \frac{\partial^2 w}{\partial r^2} + \frac{\partial^2 w}{\partial z^2} + \frac{1}{r} \frac{\partial w}{\partial r} \right) \\
& + \frac{\alpha_1^*}{\rho} \left( \begin{aligned}
& \frac{1}{r} \frac{\partial^2 u}{\partial t \partial z} + \frac{1}{r} \frac{\partial^2 w}{\partial t \partial r} + \frac{\partial^3 w}{\partial t \partial r^2} + \frac{\partial^3 u}{\partial t \partial r \partial z} + 2 \frac{\partial^3 w}{\partial t \partial z^2} - \frac{1}{r} \frac{\partial u}{\partial z} \frac{\partial w}{\partial z} \\
& + \frac{w}{r} \frac{\partial^2 u}{\partial z^2} + \frac{\partial u}{\partial z} \frac{\partial^2 w}{\partial z^2} + 2 \frac{\partial w}{\partial z} \frac{\partial^2 w}{\partial z^2} + 2u \frac{\partial w^3}{\partial z^3} + \frac{1}{r} \frac{\partial u}{\partial z} \frac{\partial u}{\partial r} \\
& + \frac{1}{r} \frac{\partial w}{\partial z} \frac{\partial w}{\partial r} + \frac{\partial w}{\partial r} \frac{\partial^2 u}{\partial z^2} - \frac{1}{r} \frac{\partial u}{\partial r} \frac{\partial w}{\partial r} + \frac{u}{r} \frac{\partial^2 u}{\partial z \partial r} - \frac{\partial w}{\partial z} \frac{\partial^2 u}{\partial z \partial r} \\
& + 2 \frac{\partial u}{\partial r} \frac{\partial^2 u}{\partial z \partial r} + \frac{w}{r} \frac{\partial^2 w}{\partial z \partial r} + \frac{\partial u}{\partial z} \frac{\partial^2 w}{\partial z \partial r} + w \frac{\partial^3 u}{\partial r \partial z^2} + 2u \frac{\partial^3 w}{\partial r \partial z^2} + \frac{\partial u}{\partial z} \frac{\partial^2 u}{\partial r^2} \\
& - \frac{\partial w}{\partial r} \frac{\partial^2 u}{\partial r^2} + \frac{u}{r} \frac{\partial^2 w}{\partial r^2} + \frac{\partial w}{\partial z} \frac{\partial^2 w}{\partial r^2} + u \frac{\partial^3 u}{\partial z \partial r^2} + w \frac{\partial^3 w}{\partial z \partial r^2} + u \frac{\partial^3 w}{\partial r^3}
\end{aligned} \right) \quad (4.3)
\end{aligned} \right\}$$

$$\left. \begin{aligned}
& \frac{\partial T}{\partial t} + u \frac{\partial T}{\partial r} + w \frac{\partial T}{\partial z} = \alpha^* \left( \frac{\partial^2 T}{\partial r^2} + \frac{1}{r} \frac{\partial T}{\partial r} + \frac{\partial^2 T}{\partial z^2} \right) \\
& + (\rho c)_p / (\rho c)_f \left( \begin{aligned}
& D_B \left( \frac{\partial C}{\partial r} \frac{\partial T}{\partial r} + \frac{\partial C}{\partial z} \frac{\partial T}{\partial z} \right) \\
& + \frac{D_T}{T_m} \left( \left( \frac{\partial T}{\partial r} \right)^2 + \left( \frac{\partial T}{\partial z} \right)^2 \right)
\end{aligned} \right) - \frac{1}{(\rho c)_f} \frac{\partial q_r}{\partial z}, \quad (4.4)
\end{aligned} \right\}$$

$$\left. \begin{aligned}
& \frac{\partial C}{\partial t} + u \frac{\partial C}{\partial r} + w \frac{\partial C}{\partial z} = D_B \left( \frac{\partial^2 C}{\partial r^2} + \frac{1}{r} \frac{\partial C}{\partial r} + \frac{\partial^2 C}{\partial z^2} \right) \\
& + \frac{D_T}{T_m} \left( \frac{\partial^2 T}{\partial r^2} + \frac{1}{r} \frac{\partial T}{\partial r} + \frac{\partial^2 T}{\partial z^2} \right) - k_r^2 (C - C_h) \left( \frac{T}{T_h} \right)^m \exp \left( \frac{-E_a}{\kappa T} \right), \quad (4.5)
\end{aligned} \right\}$$

$$\left. \begin{aligned}
& u = u_w = \frac{ar}{2(1-\alpha t)}, \quad w = -w_0, \quad T = T_w, \quad C = C_w \quad \text{at } z = 0, \\
& u = 0, \quad w = \frac{dh}{dt} = \frac{-\alpha}{2} \sqrt{\frac{\nu}{a(1-\alpha t)}}, \quad T = T_h, \quad C = C_h \quad \text{at } z = h(t). \quad (4.6)
\end{aligned} \right\}$$

Here  $u$  and  $w$  denote respective velocities of liquid in  $r$ - and  $z$ - directions,  $\sigma$  the electrical conductivity,  $p$  the pressure,  $\nu$  kinematic viscosity,  $\rho$  density of base liquid,  $\alpha_1^*$  the moduli for normal stress,  $\mu$  the dynamic viscosity,  $T$  the temperature,  $(\rho c)_f$  heat capacity of liquid,  $(\rho c)_p$  nanoparticles effective heat capacity,  $T_h$  upper disk temperature,  $C$  the concentration,  $\alpha^* = k/(\rho c)_f$  the thermal diffusivity,  $D_B$  the coefficient of Brownian diffusion,  $k$  the thermal conductivity and  $D_T$  the coefficient of thermophoretic diffusion. In Eq. (4.5) the term  $[k_r^2 (T/T_h)^m \exp(-E_a/\kappa T)]$  shows the modified Arrhenius function, where  $(\kappa = 8.61 \times 10 \text{ eV/K})$



is the Boltzmann constant,  $m$  ( $-1 < m < 1$ ) the constant of fitted rate and  $k_r^2$  rate of reaction. The radiative heat flux  $q_r$  is [84]:

$$q_r = -\frac{4\sigma^{**}}{3m^{**}} \frac{\partial(T^4)}{\partial z} = -\frac{16\sigma^{**}T^3}{3m^{**}} \frac{\partial T}{\partial z}, \quad (4.7)$$

where  $\sigma^{**}$  Stefan-Boltzman and  $m^{**}$  coefficient of mean absorption. From Eqs. (4.7) and (4.5) one has

$$\left. \begin{aligned} & \frac{\partial T}{\partial t} + u \frac{\partial T}{\partial r} + w \frac{\partial T}{\partial z} = \alpha^* \left( \frac{\partial^2 T}{\partial r^2} + \frac{1}{r} \frac{\partial T}{\partial r} + \frac{\partial^2 T}{\partial z^2} \right) \\ & + (\rho c)_p / (\rho c)_f \left( \begin{aligned} & D_B \left( \frac{\partial C}{\partial r} \frac{\partial T}{\partial r} + \frac{\partial C}{\partial z} \frac{\partial T}{\partial z} \right) \\ & + \frac{D_T}{T_m} \left( \left( \frac{\partial T}{\partial r} \right)^2 + \left( \frac{\partial T}{\partial z} \right)^2 \right) \end{aligned} \right) + \frac{1}{(\rho c)_f} \frac{16\sigma^{**}}{3m^{**}} \frac{\partial}{\partial z} \left( T^3 \frac{\partial T}{\partial z} \right), \end{aligned} \right\} \quad (4.8)$$

The transformations can be expressed as

$$\left. \begin{aligned} u &= \frac{ar}{2(1-\alpha t)} f'(\eta), \quad w = -\sqrt{\frac{av}{1-\alpha t}} f(\eta), \quad \eta = \frac{z}{h(t)}, \\ \theta(\eta) &= \frac{T-T_h}{T_w-T_h}, \quad \phi(\eta) = \frac{C-C_h}{C_w-C_h}. \end{aligned} \right\} \quad (4.9)$$

Expressions (4.2) – (4.6) and (4.8) after elimination of pressure gradient lead to

$$\left. \begin{aligned} & f^{iv} - S_q (\eta f''' + 3f'' - 2ff''') \\ & + \frac{K}{2} (\eta f^v + 5f^{iv} - 2ff^v) - M^2 f'' = 0, \end{aligned} \right\} \quad (4.10)$$

$$\left. \begin{aligned} & (1 + \frac{4}{3}Rd)\theta'' + \frac{4}{3}Rd[(\theta_w - 1)^3(3\theta'^2\theta^2 + \theta^3\theta'') + 3(\theta_w - 1)^2(2\theta'^2\theta + \theta^2\theta'')] \\ & + 3(\theta_w - 1)(\theta'^2 + \theta\theta'') + \text{Pr } S_q (f\theta' - \theta'\eta) + N_b \text{Pr } \theta'\phi' + \text{Pr } N_t\theta'^2 = 0, \end{aligned} \right\} \quad (4.11)$$

$$\phi'' + \text{Pr } Le S_q (f\phi' - \eta\phi') + \frac{N_t}{N_b} \theta'' - \text{Pr } Le \alpha_1 (1 + \delta\theta)^m \phi \exp\left(\frac{-E}{1 + \delta\theta}\right) = 0, \quad (4.12)$$

$$f(0) = S, \quad f'(0) = 1, \quad \theta(0) = 1, \quad \phi(0) = 1, \quad (4.13)$$

$$f(1) = \frac{S_q}{2}, \quad f'(1) = 0, \quad \theta(1) = 0, \quad \phi(1) = 0. \quad (4.14)$$

In above expressions  $\delta$  denotes the temperature difference parameter,  $\alpha_1$  the dimensionless reaction parameter,  $Rd$  the radiation variable,  $\text{Pr}$  the Prandtl number,  $N_b$  the Brownian motion variable,  $Le$  the Lewis number,  $S$  the blowing/suction variable,  $N_t$  the thermophoresis variable,  $K$  second grade variable,  $M$  the magnetic variable,  $E$  the activation energy variable and  $S_q$  the

squeezing variable. The steady flow between parallel plates can be recovered for  $S_q = 0$ . These dimensionless quantities can be defined as follows:

$$\left. \begin{aligned} \text{Pr} &= \frac{\nu}{\alpha^*}, \quad Le = \frac{\alpha^*}{D_B}, \quad N_b = \frac{\tau D_B}{\nu} (C_w - C_h), \quad S = \frac{w_0}{\alpha H}, \quad H = \sqrt{\frac{\nu}{a}}, \\ S_q &= \frac{\alpha H^2}{2\nu}, \quad N_t = \frac{\tau D_T}{\nu T_m} (T_w - T_h), \quad M = HB_0 \sqrt{\frac{\sigma}{\mu}}, \quad K = \frac{\alpha \alpha^*}{\mu(1-\alpha t)} \\ E &= \frac{E_a}{\kappa T}, \quad \alpha_1 = \frac{k_r^2}{a}, \quad \delta = \frac{T_w - T_h}{T_h}, \quad Rd \left( = \frac{4\sigma^{**} T_\infty^3}{km^{**}} \right), \end{aligned} \right\} \quad (4.15)$$

Skin frictions ( $C_{f0}, C_{f1}$ ) at both disks are

$$C_{f0} = \frac{\tau_{rz}|_{z=0}}{1/2\rho(u_w)^2}, \quad (4.16)$$

and

$$C_{f1} = \frac{\tau_{rz}|_{z=h(t)}}{\rho \left( \frac{\alpha H}{2(1-\alpha t)^{1/2}} \right)^2}, \quad (4.17)$$

$$\begin{aligned} \tau_{rz} &= \mu \left( \frac{\partial u}{\partial z} + \frac{\partial w}{\partial r} \right) \\ &+ \alpha_1 \left( \begin{aligned} &\frac{\partial^2 u}{\partial t \partial z} + \frac{\partial^2 w}{\partial t \partial r} + u \left( \frac{\partial^2 u}{\partial r \partial z} + \frac{\partial^2 w}{\partial r^2} \right) + w \left( \frac{\partial^2 u}{\partial z^2} + \frac{\partial^2 w}{\partial z \partial r} \right) \\ &- \frac{\partial w}{\partial z} \frac{\partial u}{\partial r} + \frac{\partial w}{\partial z} \frac{\partial w}{\partial r} + \frac{\partial u}{\partial z} \frac{\partial u}{\partial r} - \frac{\partial w}{\partial r} \frac{\partial u}{\partial r} \end{aligned} \right). \end{aligned} \quad (4.18)$$

The dimensionless forms of skin frictions are

$$\left. \begin{aligned} \text{Re}_0 C_{f0} &= \left( 1 + \frac{3}{2}K \right) f''(0), \\ \frac{H^2}{r^2} \text{Re}_r C_{f1} &= \left( 1 + \frac{3}{2}K \right) f''(1), \end{aligned} \right\} \quad (4.19)$$

with

$$\text{Re}_r^{-1} = \frac{2\nu}{r\alpha H(1-\alpha t)^{1/2}}, \quad \text{Re}_0 = \frac{ar^2}{2\nu(1-\alpha t)}. \quad (4.20)$$

Expressions of ( $Nu_{r0}$  and  $Nu_{r1}$ ) at both disks are

$$Nu_{r0} = -\frac{H}{(T_w - T_h)} \frac{\partial T}{\partial z} \Big|_{z=0} + (q_r)_{z=0} = -\frac{1}{\sqrt{1-\alpha t}} \left( 1 + \frac{4Rd}{3} (1 + (\theta_w - 1)\theta(0))^3 \right) \theta'(0), \quad (4.21)$$

$$Nu_{r1} = -\frac{H}{(T_w - T_h)} \frac{\partial T}{\partial z} \Big|_{z=h(t)} + (q_r)_{z=h(t)} = -\frac{1}{\sqrt{1-\alpha t}} \left( 1 + \frac{4Rd}{3} (1 + (\theta_w - 1)\theta(1))^3 \right) \theta'(1). \quad (4.22)$$

Expressions of  $(Sh_{r0}$  and  $Sh_{r1})$  at both disks are

$$Sh_{r0} = -\frac{H}{(C_w - C_h)} \frac{\partial C}{\partial z} \Big|_{z=0} = -\frac{1}{\sqrt{1-\alpha t}} \phi'(0), \quad (4.23)$$

$$Sh_{r1} = -\frac{H}{(C_w - C_h)} \frac{\partial C}{\partial z} \Big|_{z=h(t)} = -\frac{1}{\sqrt{1-\alpha t}} \phi'(1). \quad (4.24)$$

## 4.2 Series solutions and convergence analysis

The solution development require following initial guesses and linear operators

$$f_0(\eta) = (1 + 2S - S_q) \eta^3 + \left( \frac{2}{3} S_q - 2 - 3S \right) \eta^2 + S + \eta, \quad \theta_0(\eta) = 1 - \eta, \quad \phi_0(\eta) = 1 - \eta, \quad (4.25)$$

$$\left. \begin{aligned} \bar{\mathcal{L}}_f(f) &= \frac{d^4 f}{d\eta^4}, \\ \bar{\mathcal{L}}_\theta(\theta) &= \frac{d^2 \theta}{d\eta^2}, \\ \bar{\mathcal{L}}_\phi(\phi) &= \frac{d^2 \phi}{d\eta^2}, \end{aligned} \right\} \quad (4.26)$$

$$\left. \begin{aligned} \bar{\mathcal{L}}_f [B_1^* + B_2^* \eta + B_3^* \eta^2 + B_4^* \eta^3] &= 0, \\ \bar{\mathcal{L}}_\theta [B_5^* + B_6^* \eta] &= 0, \\ \bar{\mathcal{L}}_\phi [B_7^* + B_8^* \eta] &= 0, \end{aligned} \right\} \quad (4.27)$$

Here  $B_i^*$  ( $i = 1 - 8$ ) are the arbitrary constants. These constants have the following values

$$\left. \begin{aligned} B_1^* &= f_m^*(\eta)|_{\eta=0}, \quad B_2^* = \frac{\partial f_m^*(\eta)}{\partial \eta} \Big|_{\eta=0}, \\ B_3^* &= -3 f_m^*(\eta)|_{\eta=1} + \frac{\partial f_m^*(\eta)}{\partial \eta} \Big|_{\eta=1} - 3B_1^* - 2B_2^*, \\ B_4^* &= 2 f_m^*(\eta)|_{\eta=1} - \frac{\partial f_m^*(\eta)}{\partial \eta} \Big|_{\eta=1} + 2B_1^* + B_2^*, \\ B_5^* &= -\theta_m^*(\eta)|_{\eta=0}, \quad B_6^* = \theta_m^*(\eta)|_{\eta=0} - \theta_m^*(\eta)|_{\eta=1}, \\ B_7^* &= -\phi_m^*(\eta)|_{\eta=0}, \quad B_8^* = \phi_m^*(\eta)|_{\eta=0} - \phi_m^*(\eta)|_{\eta=1}. \end{aligned} \right\} \quad (4.46)$$

The nonzero auxiliary variables  $\hbar_f$ ,  $\hbar_\theta$  and  $\hbar_\phi$  have major role in the convergence of series solutions. Convergence region is region parallel to  $\hbar$ -axis. To acquire the acceptable values of

$\bar{h}_f$ ,  $\bar{h}_\theta$  and  $\bar{h}_\phi$ , the  $\bar{h}$ -curves are depicted at 20th order of estimations. Fig. 4.2 elaborates that convergence zone is inside the ranges  $-1.0 \leq \bar{h}_f \leq -0.2$ ,  $-1.34 \leq \bar{h}_\theta \leq -0.13$  and  $-1.30 \leq \bar{h}_\phi \leq -0.35$ . Table 4.1 shows that 10th order of estimations are enough concerning the convergence. Table 4.2. demonstrates total average squared residual errors computed via OHAM.

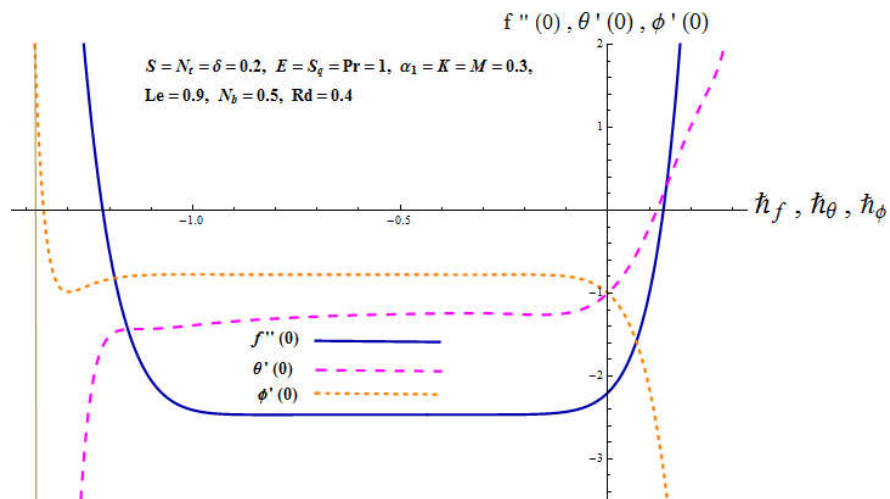


Fig. 4.2. give  $\bar{h}$ -curves for  $f$ ,  $\theta$  and  $\phi$  at lower disk.

**Table 4.1.** HAM convergence when  $\alpha_1 = K = 0.3$ ,  $\delta = M = Nt = 0.2 = S$ ,  $Nb = 0.5 = Rd$  and  $E = Le = S_q = 1.0 = Pr$ .

Deformations order	$(-f''(0))$	$(-\theta'(0))$	$(-\phi'(0))$
1	2.4048	0.8108	1.1275
5	2.4669	0.7078	1.1146
10	2.4670	0.7070	1.1140
15	2.4670	0.7070	1.1140
20	2.4670	0.7070	1.1140
25	2.4670	0.7070	1.1140

**Table 4.2:** Numerical iteration for average squared residual errors.

$\hat{m}$	$\varepsilon_{\hat{m}}^f$	$\varepsilon_{\hat{m}}^\theta$	$\varepsilon_{\hat{m}}^\phi$
2	0.00100263	0.000144278	0.00235891
6	0.0000720172	0.00005336	0.00055329
10	0.0000315963	0.000029575	0.000263673
16	0.000019137	0.000015455	0.000116424
18	0.0000178315	0.0000128735	0.0000923398
20	0.000017134	0.0000108436	0.0000743351

### 4.3 Discussion

Our intention here is to predict the features of various sundry variables on temperature and concentration. The ranges of physical parameters are  $0.0 \leq S \leq 1.1$ ,  $0.1 \leq Nt \leq 2.9$ ,  $0.4 \leq S_q \leq 4.5$ ,  $0.6 \leq Pr \leq 4.2$ ,  $0.0 \leq E \leq 3.5$ ,  $0.1 \leq K \leq 1.2$ ,  $0.0 \leq M \leq 1.5$ ,  $0.6 \leq Le \leq 4.0$ ,  $0.1 \leq Nb \leq 1.4$ ,  $0.0 \leq Rd \leq 2.4$ ,  $0.0 \leq \theta_w \leq 2.0$ ,  $0.1 \leq \alpha_1 \leq 2.1$ . The behavior of temperature  $\theta(\eta)$  for various estimations of thermophoresis parameter  $Nt$ , magnetic variable  $M$ , radiation variable  $Rd$ , Prandtl number  $Pr$ , Brownian motion variable  $Nb$ , Squeezing parameter  $S_q$ , temperature ratio parameter  $\theta_w$  is explained in Figs. (4.3)-(4.9). Variation of magnetic parameter  $M$  on  $\theta(\eta)$  is depicted in Fig. 4.3. Temperature is enhanced for larger magnetic parameter  $M$ . Physically

Lorentz force is direct contact with applications of magnetic field. More resistance is provided to liquid particles and  $\theta(\eta)$  rises. Further  $M = 0$  recovers the hydrodynamic situation. Outcome of thermophoresis variable  $N_t$  on  $\theta(\eta)$  is declared in Fig. 4.4. Higher  $N_t$  pronounces  $\theta(\eta)$  for movement of nanoparticles from hot regime to cold one. Fig. 4.5 highlights effect of  $Rd$  versus  $\theta(\eta)$ . Clearly rise in  $Rd$  enhances  $\theta(\eta)$ . Since in radiation process the more heating to working fluid corresponds in an enhancement of temperature field  $\theta(\eta)$ . Behavior of temperature ratio parameter  $\theta_w$  on thermal field  $\theta(\eta)$  is exhibited in Fig. 4.6. Here an increment in  $\theta_w$  improves thermal state of liquid which boosts  $\theta(\eta)$ . Fig. 4.7 declares the impact of  $N_b$  on temperature  $\theta(\eta)$ . Here  $\theta(\eta)$  rises for  $N_b$ . Since higher  $N_b$  has less viscous force and higher diffusion due to which more heat is produced. That is why higher  $N_b$  enhanced temperature. Fig. 4.8 manifests the variation in thermal field  $\theta(\eta)$  versus  $Pr$ . Since thermal diffusivity decays versus higher  $Pr$  so  $\theta(\eta)$  decreases. Fig. 4.9 is designed to report impact of  $S_q$  on temperature  $\theta(\eta)$ . Higher  $S_q$  augments  $\theta(\eta)$ . Curves of  $\phi(\eta)$  via  $N_t$  is displayed in Fig. 4.10. An enhancement in  $\phi(\eta)$  is noticed for higher  $N_t$ . In fact thermophoresis induces the migration of nanoparticles in direction reverse to temperature gradient which provides non-constant concentration and therefore  $\phi(\eta)$  enhances. Fig. 4.11 is captured to understand the change of  $\phi(\eta)$  against  $N_b$ . Concentration is reduced for larger  $N_b$ . Physically addition magnitude of  $N_b$  increases the rate at which nanoparticles proceed with various velocities in random movement because of Brownian diffusion. Fig. 4.12 presents that larger  $S_q$  lead to higher  $\phi(\eta)$ . It is interesting to visualize that ( $S_q$ ) narrates the plates movement, therefore ( $S_q > 0$ ) represents that the plates moving apart, where as  $S_q < 0$  manifests that plates moving towards each other). Fig. 4.13 exhibits the feature of  $Le$  on concentration distribution. Here  $\phi(\eta)$  diminishes via  $Le$ , since  $N_b$  and  $Le$  have inverse link with each other. Higher  $Le$  correspond to low Brownian diffusivity. Such lower Brownian diffusivity decays concentration. Impact of  $E$  on  $\phi(\eta)$  is captured in Fig. 4.14. Higher  $E$  lead to an enhancement in concentration field. It is due to high activation energy and low temperature which decay the rate of reaction and ultimately slows down the process of chemical reaction. That is why  $\phi(\eta)$  increases. Variation in  $\phi(\eta)$  with variation of  $\alpha_1$  is captured in Fig. 4.15. It is found that increase in  $\alpha_1$  corresponds to destructive chemical reaction due to which  $\phi(\eta)$  rises. Tables (4.3)-(4.5) are framed to visualize the feature of sundry variables on physical quantities. Skin frictions at both disks are declared in Table 4.3. Here ( $C_{f0}$  and  $C_{f1}$ ) at both disks are

enhanced via  $K$  and magnetic parameter  $M$  while reverse trend is noted for  $S$ . Since  $K$  and viscosity vary inversely, thus larger  $K$  yield low viscosity which rises the nanoliquid velocity. Therefore skin friction enhances. It is crucial to remind that ( $K = 0$ ) gives viscous liquid. Table 4.4 is designed to elaborate the numerical outcomes of ( $Nu_{r0}$  and  $Nu_{r1}$ ) at the lower and upper disks via  $S$ ,  $S_q$ ,  $M$ ,  $N_b$ ,  $N_t$ ,  $Le$  and  $Pr$ . Clearly ( $Nu_{r0}$  and  $Nu_{r1}$ ) decreases via  $S_q$  and  $Le$  while it rises for  $Pr$  and  $M$ . Table 4.5 is constructed for ( $Sh_{r0}$  and  $Sh_{r1}$ ) at the lower and upper disks for distinct embedding variables. Concentration gradient shows reverse behavior by strengthening values of suction/injection, Brownian motion and thermophoresis at lower and upper disk. Moreover it enhances for higher estimations of squeezing parameter and Lewis and Prandtl numbers.

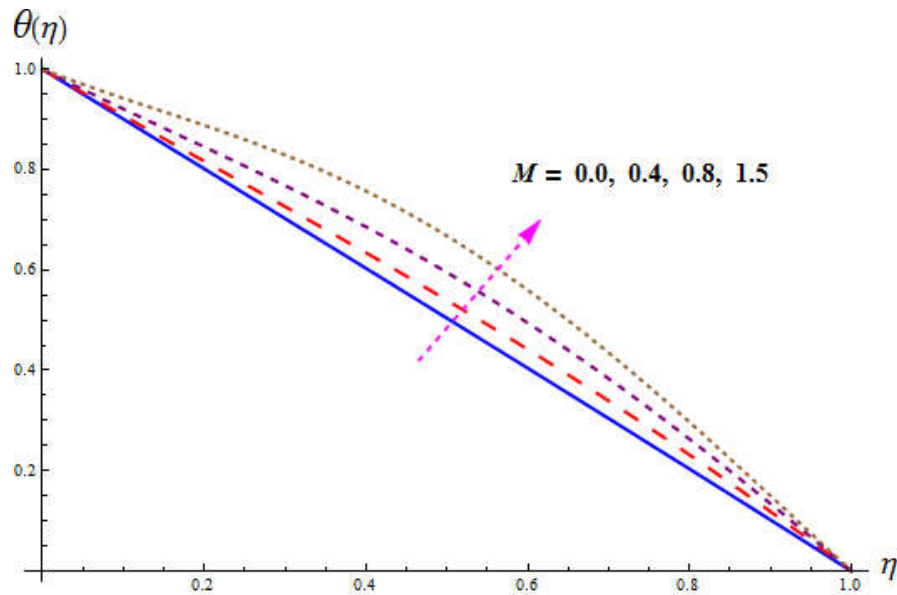


Fig. 4.3. Behavior of  $M$  on  $\theta(\eta)$ .

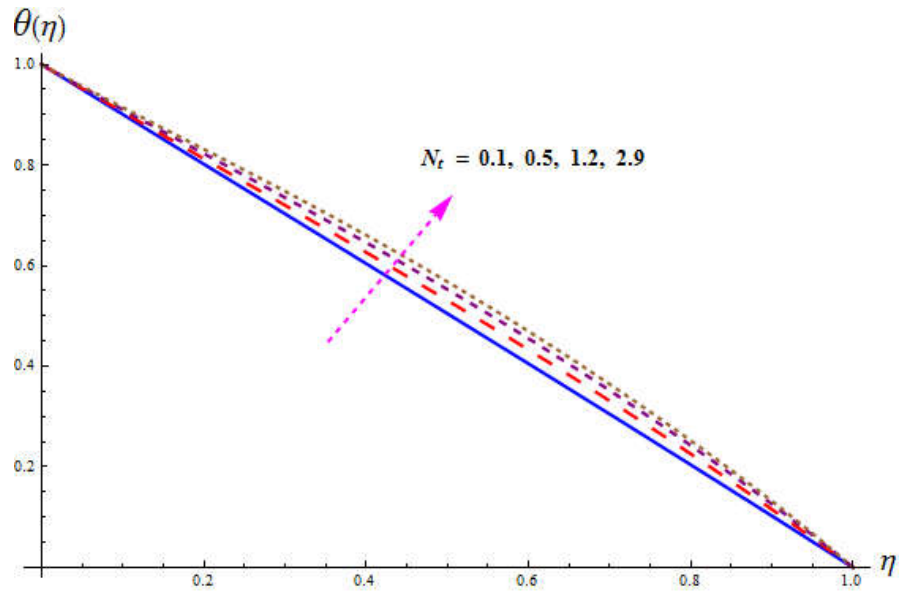


Fig. 4.4. Behavior of  $N_t$  on  $\theta(\eta)$ .

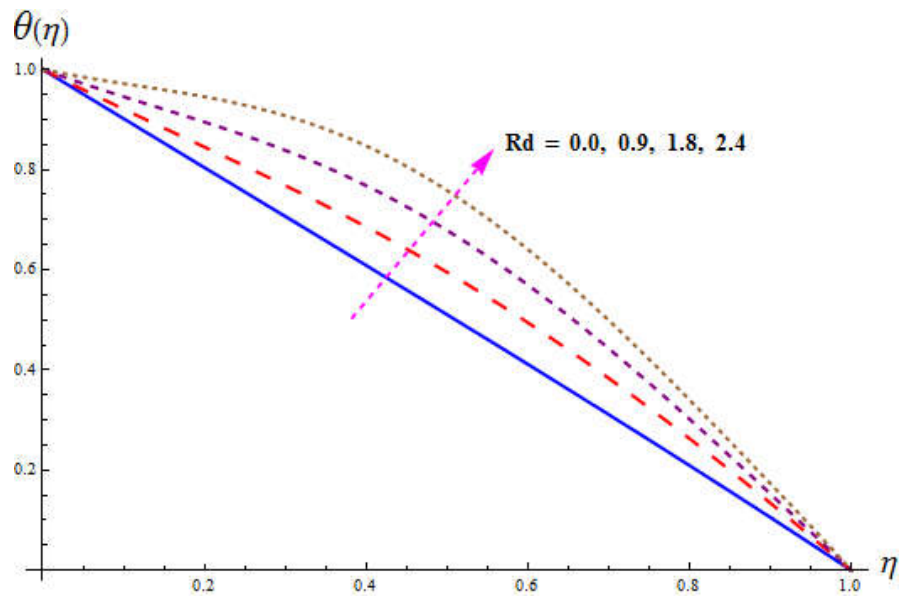


Fig. 4.5. Behavior for  $Rd$  on  $\theta(\eta)$ .



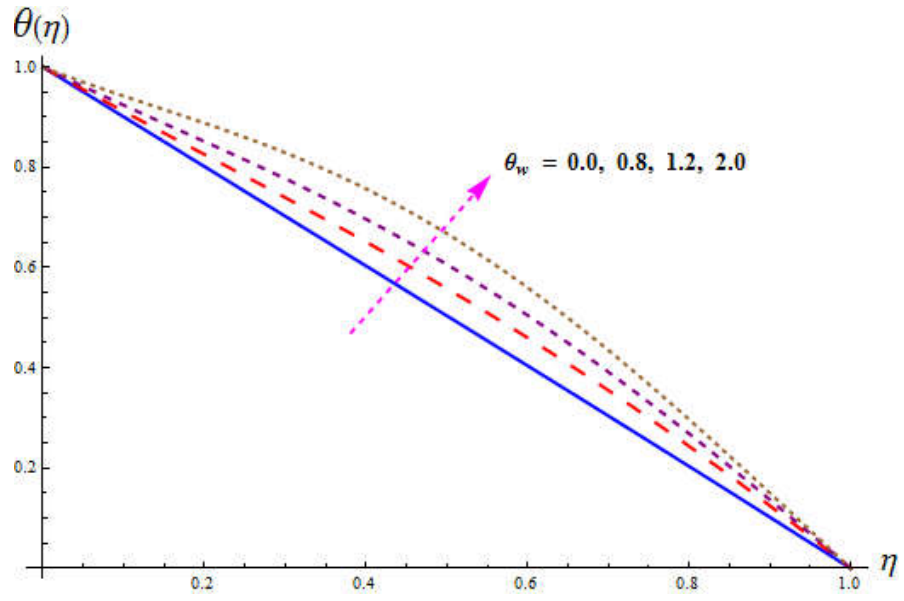


Fig. 4.6. Behavior of  $\theta_w$  on  $\theta(\eta)$ .

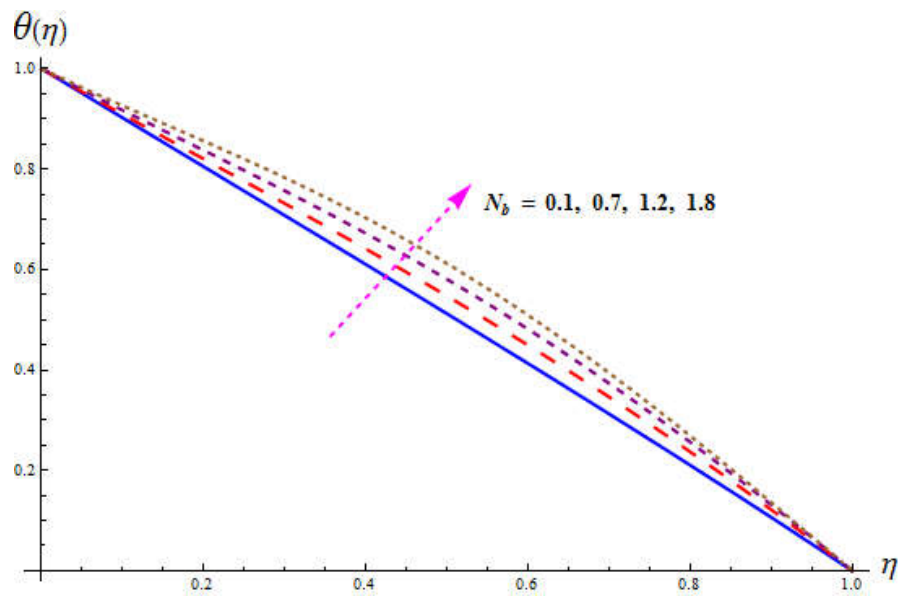


Fig. 4.7. Behavior of  $N_b$  on  $\theta(\eta)$ .

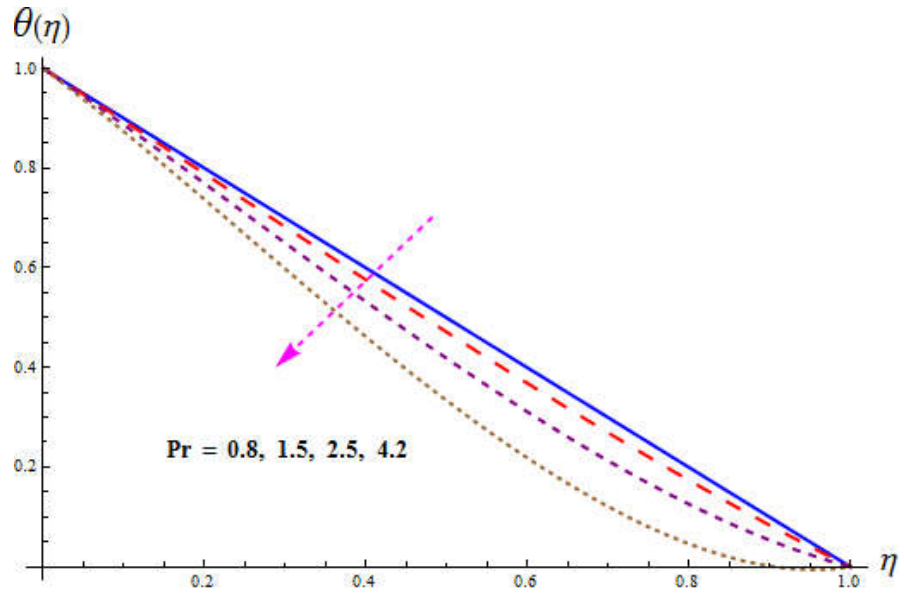


Fig. 4.8. Behavior of Pr on  $\theta(\eta)$ .

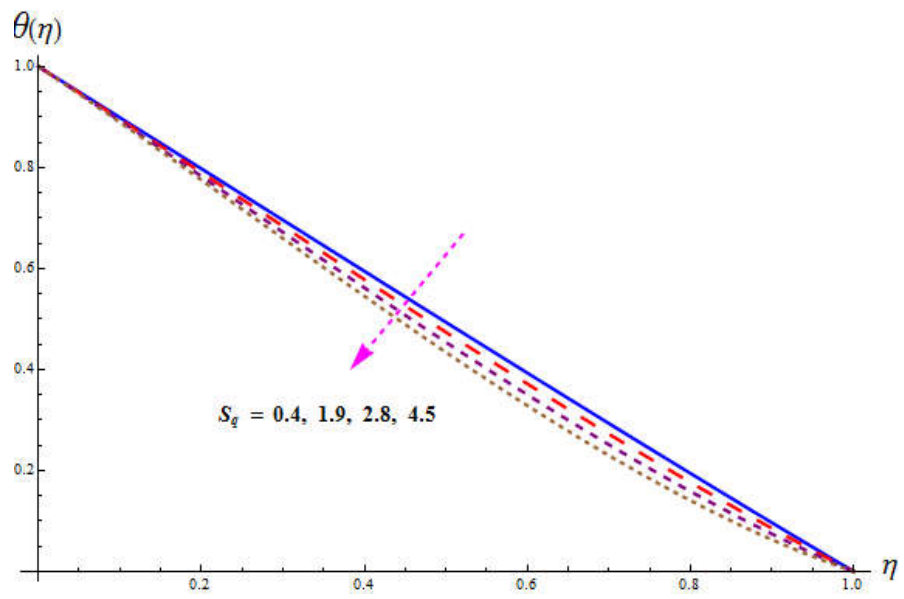


Fig. 4.9. Behavior of  $S_q$  on  $\theta(\eta)$ .

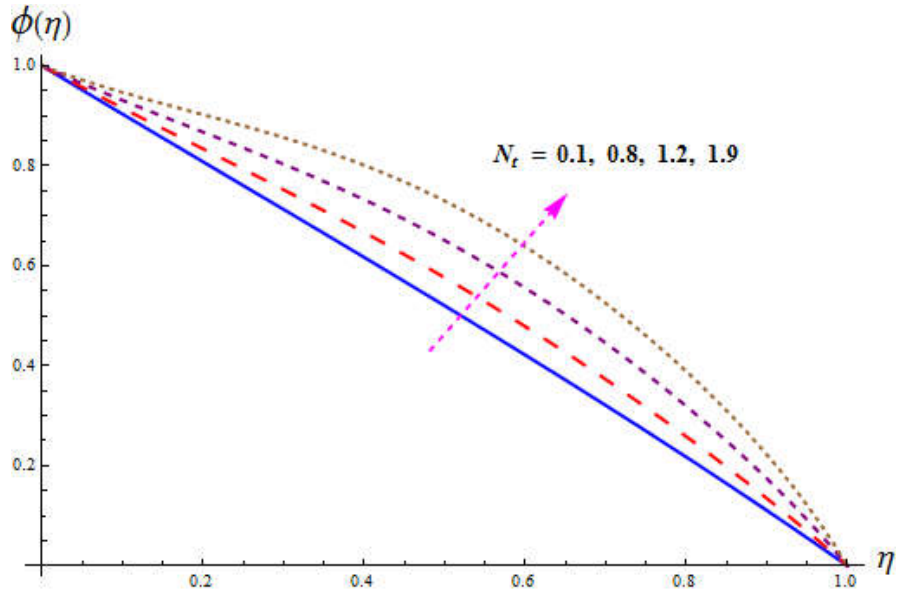


Fig. 4.10. Behavior of  $N_t$  on  $\phi(\eta)$ .

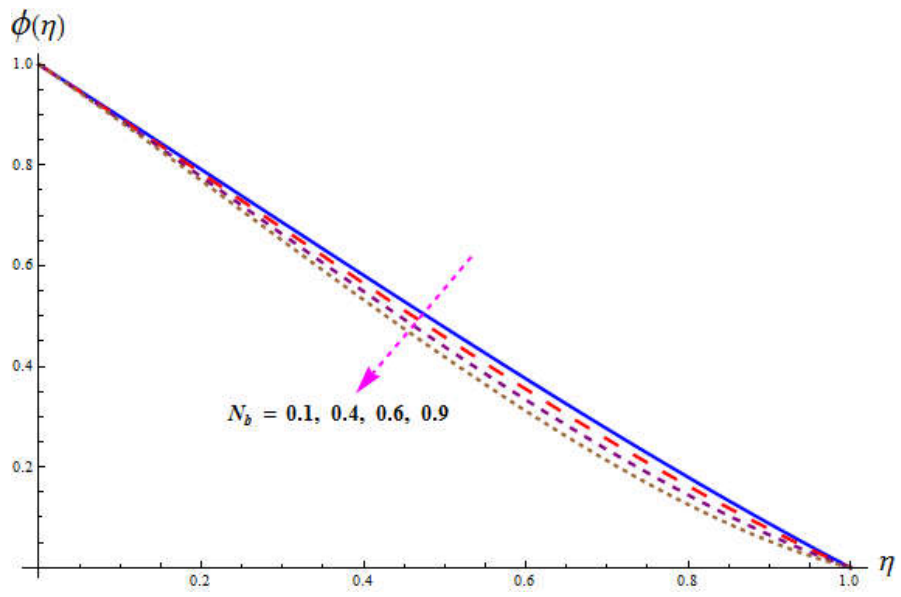


Fig. 4.11. Behavior of  $N_b$  on  $\phi(\eta)$ .

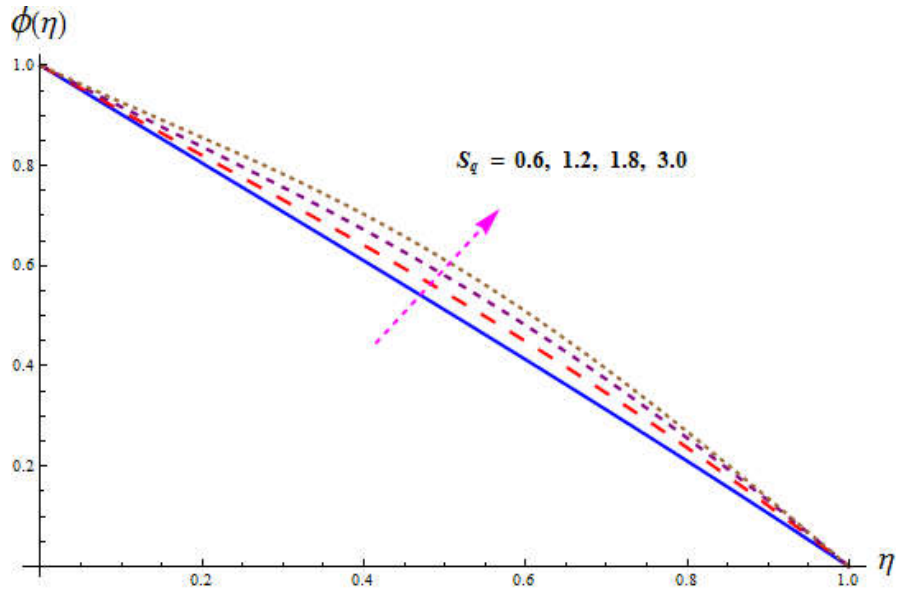


Fig. 4.12. Behavior of  $S_q$  on  $\phi(\eta)$ .

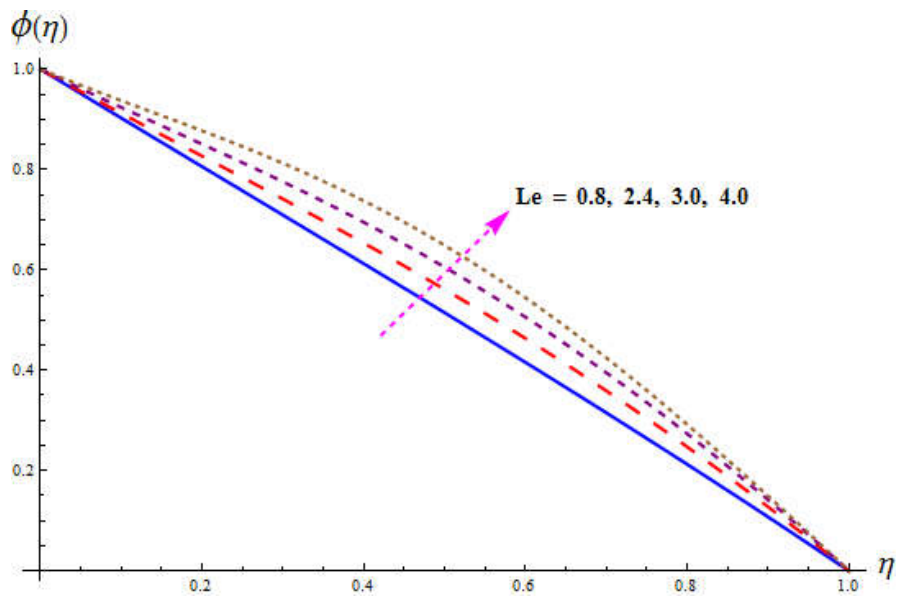


Fig. 4.13. Behavior of  $Le$  on  $\phi(\eta)$ .

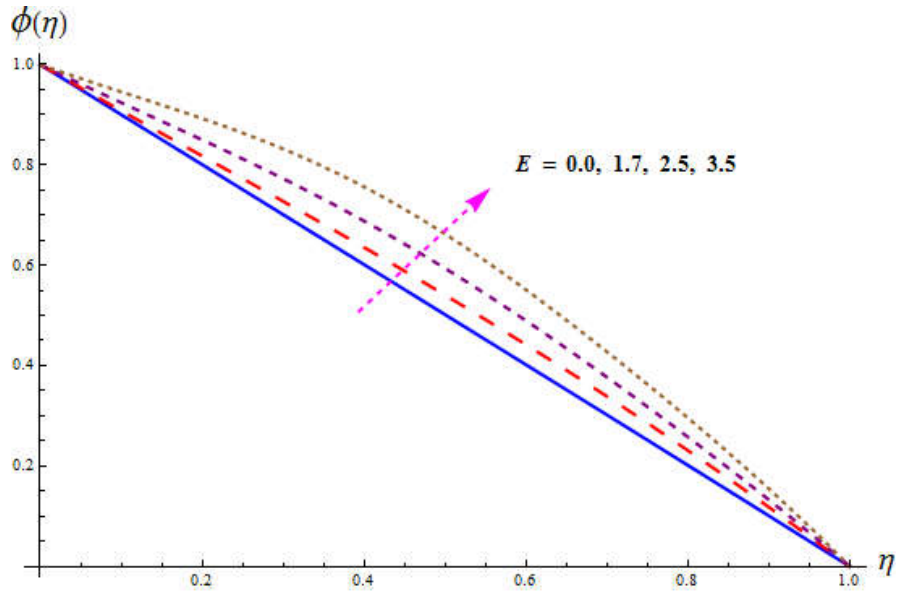


Fig. 4.14. Behavior of  $E$  on  $\phi(\eta)$ .

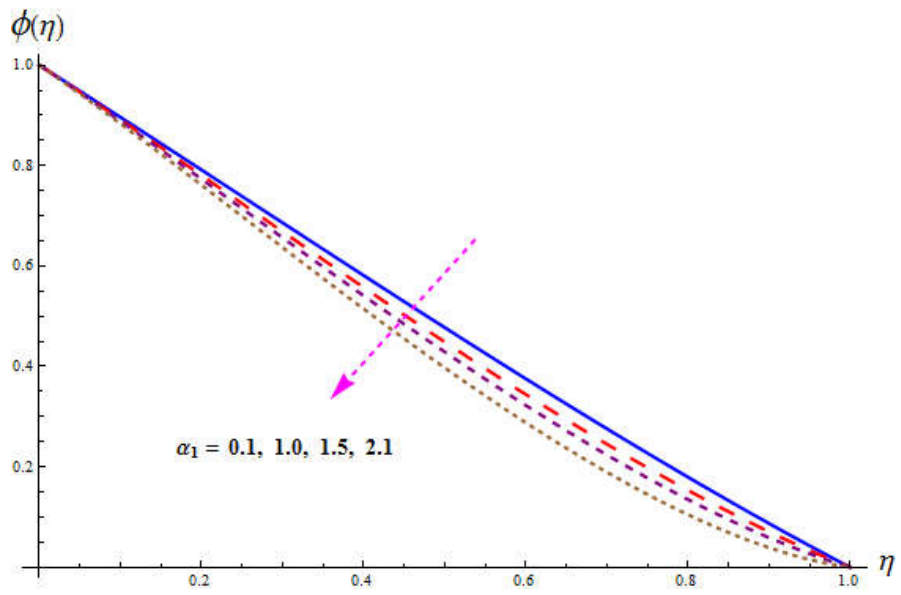


Fig. 4.15. Behavior of  $\alpha_1$  on  $\phi(\eta)$ .

**Table 4.3.** Skin friction ( $C_{f0}$  and  $C_{f1}$ ) via  $S$ ,  $K$ ,  $M$  and  $S_q$ .

$K$	$M$	$S$	$S_q$	$C_{f0}$	$C_{f1}$
0.1	0.2	0.2	1.0	2.192644	2.087126
0.2				2.426313	2.343562
0.3				2.659187	2.604499
0.3	0.0	0.2	1.0	2.657925	2.603901
		0.5		2.665798	2.607639
		0.9		2.683339	2.616023
0.3	0.2	0.0	1.0	4.498153	4.414397
			0.3	1.759886	1.721182
			0.5	0.8736101	0.8528635
0.3	0.2	0.2	0.6	2.596938	2.606282
			1.0	2.659187	2.604499
			1.5	2.736807	2.603390

**Table 4.4.** Nusselt numbers ( $Nu_{r0}$  and  $Nu_{r1}$ ) via  $Rd$ ,  $S$ ,  $M$ ,  $S_q$ ,  $\theta_w$ ,  $N_t$ ,  $N_b$ ,  $Le$  and  $Pr$ .

$S$	$K$	$M$	$S_q$	$N_t$	$N_b$	$Le$	$Pr$	$Rd$	$\theta'(0)$	$\theta'(1)$	
0.0	0.3	0.2	1.0	0.2	0.5	1.0	1.0	0.5	0.77444	1.21516	
									0.61257	1.29577	
									0.50356	1.35632	
0.2	0.1	0.2	1.0	0.2	0.5	1.0	1.0	0.5	0.63707	1.28291	
									0.63707	1.28291	
									0.63707	1.28291	
0.8	0.3	0.0	1.0	0.2	0.5	1.0	1.0	0.5	0.56634	1.32075	
									0.56636	1.32075	
									0.56640	1.32074	
0.2	0.3	0.2	0.0	0.2	0.5	1.0	1.0	0.5	0.69050	1.39050	
									0.63707	1.28291	
									0.58798	1.18403	
0.2	0.3	0.2	1.0	0.2	0.5	1.0	1.0	0.5	0.63707	1.28291	
									0.50761	1.52494	
									0.35291	1.79063	
0.2	0.3	0.2	1.0	0.2	0.4	1.0	1.0	0.5	0.67273	1.22579	
									0.50888	1.52875	
									0.37849	1.87469	
0.2	0.3	0.2	1.0	0.2	0.5	0.6	1.0	0.5	0.63610	1.28133	
									0.63687	1.28250	
									0.63794	1.28465	
0.2	0.3	0.2	1.0	0.2	0.5	1.0	0.6	0.5	0.76580	1.16552	
									0.63707	1.28291	
									0.48055	1.47280	
0.2	0.3	0.2	1.0	0.2	0.5	1.0	1.0	0.0	0.21314	1.23568	
									0.5	0.28249	1.35975
									0.9	0.32458	1.49867

**Table 4.5.** Sherwood numbers ( $Sh_{r0}$  and  $Sh_{r1}$ ) via  $S$ ,  $M$ ,  $S_q$ ,  $Nt$ ,  $Nb$ ,  $Le$  and  $Pr$  when  $Rd = 0.5$  and  $\theta_w = 0.3$ .

$S$	$K$	$M$	$S_q$	$Nt$	$Nb$	$Le$	$Pr$	$\phi'(0)$	$\phi'(1)$
0.0	0.3	0.2	1.0	0.2	0.5	1.0	1.0	0.99833	1.10367
0.6								1.28577	1.01903
1.1								1.54546	0.95317
0.2	0.1		1.0	0.2	0.5	1.0	1.0	1.23601	1.03275
	0.5							1.23601	1.03275
	1.2							1.23601	1.03275
0.8	0.3	0.0		0.2	0.5	1.0	1.0	1.38749	0.99212
		0.6						1.38746	0.99212
		1.2						1.38737	0.99213
0.2	0.3	0.2	0.0		0.5	1.0	1.0	1.12380	0.84379
			1.0					1.23601	1.03275
			2.0					1.33266	1.19929
0.5		0.2	1.0	0.2		1.0	1.0	1.23601	1.03275
				0.6				1.72340	0.58836
				1.2				2.79345	0.26742
0.2	0.3	0.2	1.0	0.2	0.4		1.0	1.25507	1.02590
					0.9			1.19987	1.05856
					1.4			1.18165	1.08931
0.2	0.3	0.2	1.0	0.2	0.5	0.6		1.19159	0.97583
						0.9		1.22724	1.01864
						1.4		1.27042	1.08837
0.2	0.3	0.2	1.0	0.2	0.5	1.0	0.6	1.14657	1.16552
							1.0	1.23601	1.09275
							1.6	1.35846	1.03665



## 4.4 Conclusions

The key attributes associated with this analysis are:

- Higher  $M$  rise the liquid temperature.
- Temperature is improved for higher thermophoresis and Brownian motion parameters.
- Behavior of squeezing variable on  $\phi(\eta)$  and  $\theta(\eta)$  is quite contrary.
- Concentration is reduced for  $N_b$ .
- $C_{f0}$  and  $C_{f1}$  are higher for  $M$  and  $K$  whereas reverse is noticed for  $S$ .
- Viscous fluid outcomes can be recovered for  $K = 0$ .
- Magnitude of temperature gradient enhances via  $S$  and  $N_b$  for lower disk while opposite trend is observed for upper disk. Further it reduces for higher thermophoresis parameter  $N_t$ .

## Chapter 5

# Dissipative flow of hybrid nanoliquid ( $H_2O$ –aluminum alloy nanoparticles) with thermal radiation

An improvement in heat transfer fluid is one of the important tasks which can be achieved through implementation of hybrid nanoparticles. Hence the aim of this chapter is to communicate flow of hybrid nanoliquid by stretchable rotating infinite disk. The considered hybrid nanoliquid is a combination of and nanoparticles and water. Law of energy incorporates the nonlinear radiation, dissipation and irregular heat source terms. Von Karman variables lead to dimensionless problem under consideration. Reduced system is tackled numerically via NDSolve based Shooting scheme. Graphical descriptions are made against various physical variables of interest. Moreover rate of heat transfer at disk is estimated. Present work pointed out that local heat transfer rate accelerates for higher thermal radiation and thermal slip parameters whereas decaying trend is seen for higher estimations of Eckert number and (ESHS) parameter. It is noted that fluid velocity reduces for higher volumetric fraction. Furthermore hybrid nanomaterials have great influence throughout our analysis when compared with regular nanomaterials. The peculiar outcomes achieved in this study are important in industrial research, academics and discussion about heat transfer analysis in flow of two types of nanoliquids by keeping the regular fluid fixed. Finally key points of present analysis are included.

## 5.1 Problem description

### 5.1.1 Formulation

We consider flow of nanoliquid comprising of hybrid nanoparticles (AA7072, AA7075) by an infinite disk. Two-dimensional steady flow of viscous liquid is considered. Physical interpretation of considered problem is presented in Fig. 5.1. Non-linear thermal radiation and space dependent heat source are addressed. No relative motion exists between nanoparticles and base liquid. Furthermore it is assumed that nanoparticles have uniform shape and size and uniformly distributed in the base liquid. Problem statement with dissipation effect has following equations [106]:

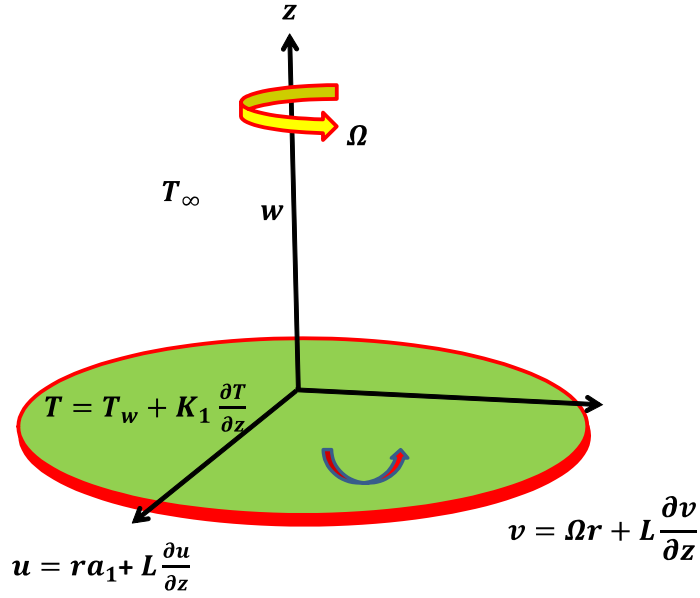


Fig. 5.1. Flow configuration.

### 5.1.2 Governing equations

Continuity equation:

$$\frac{\partial u}{\partial r} + \frac{u}{r} + \frac{\partial w}{\partial z} = 0, \quad (5.1)$$

Momentum equation:

$$\rho_{hnf} \left( u \frac{\partial u}{\partial r} - \frac{v^2}{r} + w \frac{\partial u}{\partial z} \right) = \mu_{hnf} \left( \frac{1}{r} \frac{\partial u}{\partial r} + \frac{\partial^2 u}{\partial z^2} - \frac{u}{r^2} + \frac{\partial^2 u}{\partial r^2} \right), \quad (5.2)$$

$$\rho_{hnf} \left( u \frac{\partial v}{\partial r} + \frac{uv}{r} + w \frac{\partial v}{\partial z} \right) = \mu_{hnf} \left( \frac{1}{r} \frac{\partial v}{\partial r} + \frac{\partial^2 v}{\partial z^2} - \frac{v}{r^2} + \frac{\partial^2 v}{\partial r^2} \right), \quad (5.3)$$

$$\rho_{hnf} \left( u \frac{\partial u}{\partial r} - w \frac{\partial u}{\partial z} \right) = \mu_{hnf} \left( \frac{\partial^2 w}{\partial z^2} + \frac{1}{r} \frac{\partial w}{\partial r} + \frac{\partial^2 w}{\partial r^2} \right), \quad (5.4)$$

where  $\rho_{hnf}$  denotes the hybrid nanoliquid density,  $(u, w)$  being the velocity components in  $(r, z, \Phi)$  directions and  $\mu_{hnf}$  hybrid nanoliquid. Relevant conditions are:

$$\left. \begin{aligned} u = ra_1 + L \frac{\partial u}{\partial z} \Big|_{z=0}, \quad v = r\Omega + L \frac{\partial v}{\partial z} \Big|_{z=0}, \quad w|_{z=0} = 0, \\ u|_{z \rightarrow \infty} = 0, \end{aligned} \right\} \quad (5.5)$$

### 5.1.3 Thermal energy

The energy expression is given by:

$$\left. \begin{aligned} (\rho c_p)_{hnf} \left( u \frac{\partial T}{\partial r} + w \frac{\partial T}{\partial z} \right) = k_{hnf} \frac{\partial^2 T}{\partial z^2} + Q_0 (T_w - T_\infty) \exp\left(-n \sqrt{\frac{\Omega}{\nu_f}} z\right) \\ + \left( \frac{16\sigma^*}{3k^*} T_\infty^3 \frac{\partial T}{\partial z} \right) + \mu_{hnf} \left( \left( \frac{\partial u}{\partial z} \right)^2 + \left( \frac{\partial v}{\partial z} \right)^2 \right), \end{aligned} \right\} \quad (5.6)$$

with

$$T|_{z=0} = T_\infty + K_1 \frac{\partial T}{\partial z}, \quad T|_{z \rightarrow \infty} = T_\infty, \quad (5.7)$$

where  $n$  depicts the exponential index,  $(\rho c_p)_{hnf}$  the hybrid nanoliquid heat capacitance,  $k_{hnf}$  the thermal conductivity of hybrid nanoliquid,  $T$  the temperature,  $k^*$  the mean absorption coefficient,  $Q_0$  heat generation/absorption variable,  $\sigma^*$  Stefan-Boltzmann constant and  $(T_w, T_\infty)$  the wall and ambient liquid temperatures.

**Table 5.1:** Thermo-physical features of nanofluid ( $AA7075/H_2O$ ) and hybrid nanoliquid  $AA7072 - A7075/H_2O$ .

Properties	Nanofluid	Hybrid nanofluid
Density	$\rho_{nf} = \rho_f \left( (1 - \phi) + \phi \left( \frac{\rho_s}{\rho_f} \right) \right)$	$\rho_{hnf} = \rho_f (1 - \phi_2) \left( (1 - \phi_1) + \phi_1 \left( \frac{\rho_{s1}}{\rho_f} \right) \right) + \phi_2 \left( \frac{\rho_{s2}}{\rho_f} \right)$
Viscosity	$\mu_{nf} = \frac{\mu_f}{(1-\phi)^{2.5}}$	$\mu_{hnf} = \frac{\mu_f}{(1-\phi_1)^{2.5}(1-\phi_2)^{2.5}}$
Heat capacity	$(\rho c_p)_{nf} = (\rho c_p)_f \left( (1 - \phi) + \phi \left( \frac{\rho c_p}_s \right) \right)$	$(\rho c_p)_{nf} = \phi_2 \left( \frac{\rho c_p}_2 \right) + (\rho c_p)_f (1 - \phi_2) \left( (1 - \phi_1) + \phi_1 \left( \frac{\rho c_p}_{s1} \right) \right)$
Thermal conductivity	$\frac{k_{nf}}{k_f} = \frac{k_s + (s-1)k_f - (s-1)\phi(k_f - k_s)}{k_s + (s-1)k_f + \phi(k_f - k_s)}$	$\frac{k_{hnf}}{k_bf} = \frac{k_{s2}(s-1)k_{bf} - (s-1)\phi_2(k_{bf} - k_{s2})}{k_{s2} + (s-1)k_{bf} + \phi_2(k_{bf} - k_{s2})}$ where $\frac{k_{bf}}{k_f} = \frac{k_{s1}(s-1)k_f - (s-1)\phi_1(k_f - k_{s1})}{k_{s1} + (s-1)k_f + \phi_1(k_f - k_{s1})}$

#### 5.1.4 Dimensionless systems

Following Karman similarity variables:

$$u = \Omega r f'(\eta), \quad u = \Omega r g(\eta), \quad w = -\sqrt{2\Omega\nu_f} f(\eta), \quad T = T_\infty + (T_w - T_\infty)\theta(\eta), \quad \eta = z\sqrt{\frac{\Omega}{\nu_f}}, \quad (5.8)$$

Eqs. (5.1) – (5.7) become

$$\frac{1}{A_1 A_2} 2f''' + 2ff'' - f'^2 + g^2 = 0, \quad (5.9)$$

$$\frac{1}{A_1 A_2} 2g'' + 2g'f - 2f'g = 0, \quad (5.10)$$

$$\frac{1}{\text{Pr}} \left( \frac{A_4}{k_f} + \frac{4}{3} Rd \right) \theta'' + \frac{1}{A_1} Ec(f''^2 + g'^2) + \theta Q_T \exp(-n\eta) - 2A_3 f\theta' = 0, \quad (5.11)$$

$$\left. \begin{aligned} f'(\eta)|_{\eta=0} &= \beta f'(0) + \gamma_s f''(\eta)|_{\eta=0}, \\ g(\eta)|_{\eta=0} &= 1 + \gamma_s g(\eta)|_{\eta=0}, \\ \theta(\eta)|_{\eta=0} &= 1 + \gamma_T \theta'(\eta)|_{\eta=0}, \\ f'(\eta)|_{\eta=\infty} &= 0, \quad \theta(\eta)|_{\eta=\infty} = 0, \end{aligned} \right\} \quad (5.12)$$

where

$$A_1 = (1 - \phi_1)^{2.5}(1 - \phi_2)^{2.5}, \quad (5.13)$$

$$A_2 = (1 - \phi_2) \left( (1 - \phi_1) + \phi_1 \left( \frac{\rho_{s1}}{\rho_f} \right) \right) + \phi_2 \left( \frac{\rho_{s2}}{\rho_f} \right), \quad (5.14)$$

$\infty$

$$A_3 = (1 - \phi_2) \left( (1 - \phi_1) + \phi_1 \frac{(\rho c_p)_{s1}}{(\rho c_p)_f} \right) + \phi_2 \left( \frac{(\rho c_p)_2}{(\rho c_p)_f} \right), \quad (5.15)$$

$$A_4 = \frac{k_{s2}(s-1)k_{bf} - (s-1)\phi_2(k_{bf} - k_{s2})}{k_{s2} + (s-1)k_{bf} + \phi_2(k_{bf} - k_{s2})} \frac{k_{s1}(s-1)k_f - (s-1)\phi_1(k_f - k_{s1})}{k_{s1} + (s-1)k_f + \phi_1(k_f - k_{s1})}. \quad (5.16)$$

Here  $\gamma_s$  denotes the velocity slip parameter,  $\beta$  stretching variable,  $Rd$  radiation parameter,  $Ec$  the Eckert number,  $Pr$  Prandtl number,  $\gamma_T$  thermal slip parameter and  $Q_T$  (ESHS) variable.

We set

$$\left. \begin{aligned} \gamma_s &= L\sqrt{\frac{2\Omega}{\nu_f}}, \quad Ec = \frac{r^2\Omega^2}{(c_p)_f(T_w - T_\infty)}, \quad Q_T = \frac{Q_0}{\Omega\beta(\rho c_p)_f}, \\ Pr &= \frac{(c_p)_f\mu_f}{k_f}, \quad Rd = \frac{4\sigma^*T_\infty^3}{k^*\nu_f(\rho c_p)_f}, \quad \gamma_T = K_1\sqrt{\frac{2\Omega}{\nu_f}}, \quad \beta = \frac{a_1}{\Omega}. \end{aligned} \right\} \quad (5.17)$$

### 5.1.5 Physical quantities

For practical and engineering purposes we are concerned with the exploration of physical quantity i.e. temperature gradient ( $Nu_r$ ) which gives rate of heat transfer at disk and is expressed by:

$$Nu_r = \frac{rq_w}{k_f(T_w - T_\infty)}, \quad (5.18)$$

where

$$q_w = - \left( \left. \frac{\partial T}{\partial z} \right|_{z=0} - q_r|_{z=0} \right). \quad (5.19)$$

The above expression yield

$$Re^{-0.5} Nu_r = - \frac{k_{hmf}}{k_f} \left[ 1 + \frac{4}{3} Rd \right] \theta'(0), \quad (5.20)$$

where local Reynolds number is  $Re_r = \frac{r^2\Omega}{\nu_f}$ .

**Table 5.2:** Physical and thermal features of AA7072 and AA7075 nanoparticles and water ( $H_2O$ ) [107, 108].

Constituents	$\rho(kg/m^3)$	$c_p(J/kgK)$	$k(W/mk)$
AA7072	2720	893	222
AA7075	2810	960	173
$H_2O$	997.1	4179	0.613

## 5.2 Numerical technique and discussion

The reduced problem defined in Eqs. (5.9)–(5.12) has been solved numerically by NDSolve technique. The simulation of non-linear problems has been performed through employing computer software Mathematica. Thermo-physical characteristics of water and hybrid nanomaterials are depicted in Tables 5.1 and 5.2. Temperature  $\theta(\eta)$  and velocity  $f'(\eta)$  are disclosed in graphical form for various estimations of sundry variables i.e radiation parameter ( $Rd$ ), velocity slip parameter ( $\gamma_s$ ), thermal slip parameter ( $\gamma_T$ ), Prandtl number (Pr), Eckert number ( $Ec$ ) and (ESHS) parameter ( $Q_T$ ) (see Figs. 5.2 – 5.8). In these Figs. solid lines show the behavior of AA7072 – A7075/ $H_2O$  hybrid nanoliquid and dashed lines present features of AA7075/ $H_2O$  nanofluid. Further engineering quantity of curiosity namely heat transfer rate is also estimated and discussed. The values used for involved variables are  $s = 3.7$ ,  $Q_T = n = Ec = 0.1$ ,  $Pr = 6.2$ ,  $Rd = 0.3 = \gamma_s$ ,  $\phi_1 = 0.3$ ,  $\phi_2 = 0.5$  and  $\gamma_T = 0.2$ .

Consequences of  $\gamma_s$  (i.e. velocity slip parameter) on  $f'(\eta)$  are pointed out in Fig. 5.2. From this Fig. it is identified that larger  $\gamma_s$  partially shifted the stretching velocity. As a result the velocity is diminished. Further in case of AA7072 – A7075/ $H_2O$  hybrid nanoliquid the velocity is more than AA7075/ $H_2O$  nanofluid. Characteristics of  $\phi_1/\phi_2$  on  $F(\eta)$  is declared in Fig. 5.3. It is scrutinized that  $f'(\eta)$  gives less layer thickness for hybrid nanoliquid (AA7072 – A7075/ $H_2O$ ) when compared to nanoliquid (AA7075/ $H_2O$ ). An enhancement in  $\phi_2$  leads to decay of velocity  $f'(\eta)$ .

Influences of embedded flow variables on temperature of hybrid nanoliquid (AA7072 – A7075/ $H_2O$ ) and nanoliquid (AA7075/ $H_2O$ ) are depicted in Figs. 5.4 – 5.8. Effect of  $Ec$  on  $\theta(\eta)$  is shown in Fig. 5.4. Higher  $Ec$  increases the frictional heating which generates more heat.

That is why the temperature increases. Moreover hybrid nanoliquid ( $AA7072 - A7075/H_2O$ ) has higher temperature than nanoliquid ( $AA7075/H_2O$ ). Fig. 5.5 declared the importance of  $\gamma_T$  on  $\theta(\eta)$ . Temperature is higher for higher  $\gamma_T$ . Fig. 5.6 is disclosed to understand the feature of (ESHS) parameter  $Q_T$  on  $\theta(\eta)$ . Here increasing estimations of  $Q_T$  augment the temperature  $\theta(\eta)$ . In fact strength of heat source process increases which generates more heat into fluid and thus  $\theta(\eta)$  rises. For hybrid nanoliquid ( $AA7072 - A7075/H_2O$ ) an increment in thermal field is rapid when compared with nanoliquid ( $AA7075/H_2O$ ). An enlargement in  $\phi_2$  corresponds to rise of temperature. This behavior is depicted in Fig. 5.7. Moreover immediate improvement in  $\theta(\eta)$  is due to ( $AA7072 - A7075/H_2O$ ) hybrid nanofluid. Changes in  $\theta(\eta)$  via  $Rd$  are portrayed in Fig. 5.8. Clearly  $\theta(\eta)$  increases for larger  $Rd$ . Physically higher  $Rd$  supplies more heat in liquid and consequently rise  $\theta(\eta)$ . A sudden improvement in  $\theta(\eta)$  is due to hybrid nanoliquid ( $AA7072 - A7075/H_2O$ ). Aspect of various embedding variables on local Nusselt number of nanofluid ( $AA7075 - H_2O$ ) and hybrid nanofluid ( $AA7072 - AA7075 - H_2O$ ) is reported in Table 5.3. Heat transfer rate ( $Nu_x$ ) is increasing function of  $Rd$  and  $\gamma_T$ . However it indicates reverse behavior via  $Q_T$  and  $Ec$ . Further it is noteworthy to mention that for hybrid nanomaterials ( $AA7072 - AA7075$ ) the heat transfer rate is more than nanoparticles ( $AA7075$ ).

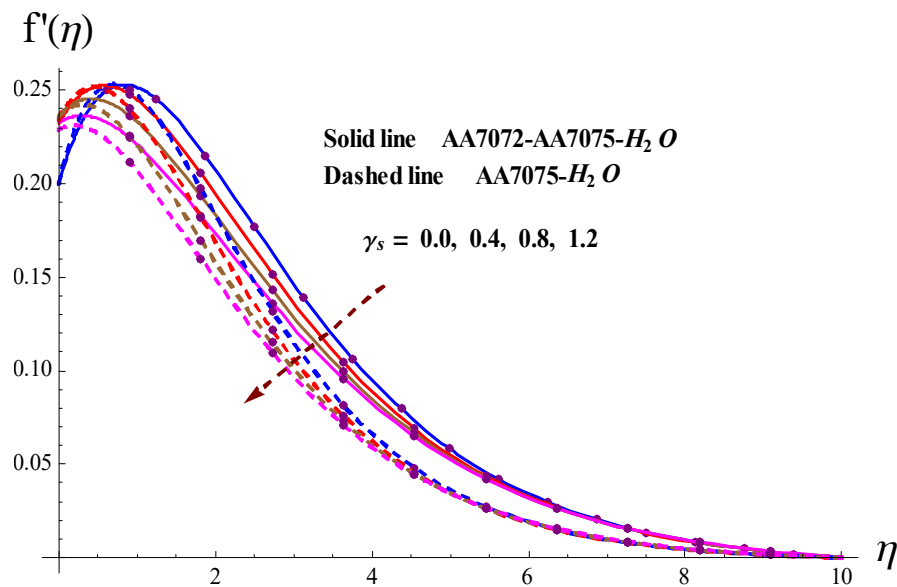


Fig. 5.2. Variation of  $f'(\eta)$  via  $\gamma_s$ .



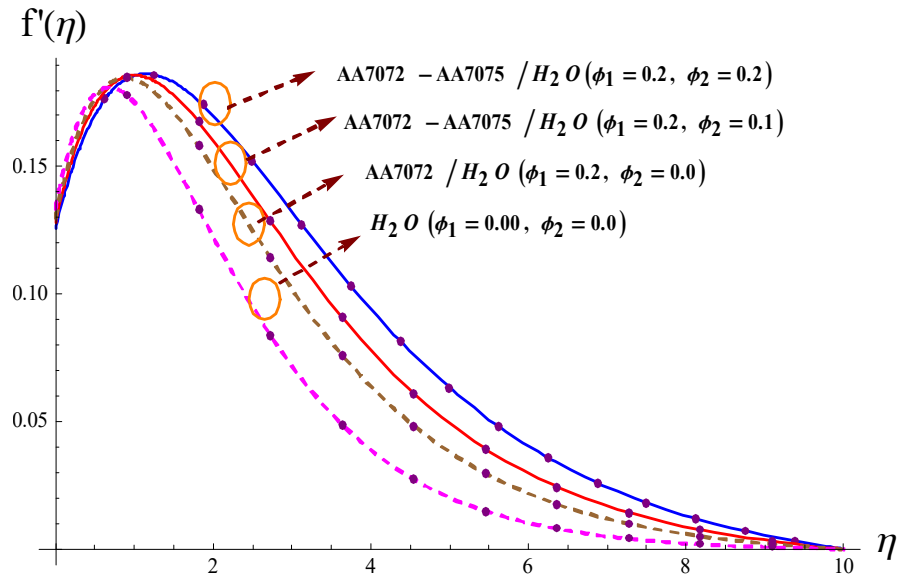


Fig. 5.3. Variation of  $f'(\eta)$  via  $\phi_1/\phi_2$ .

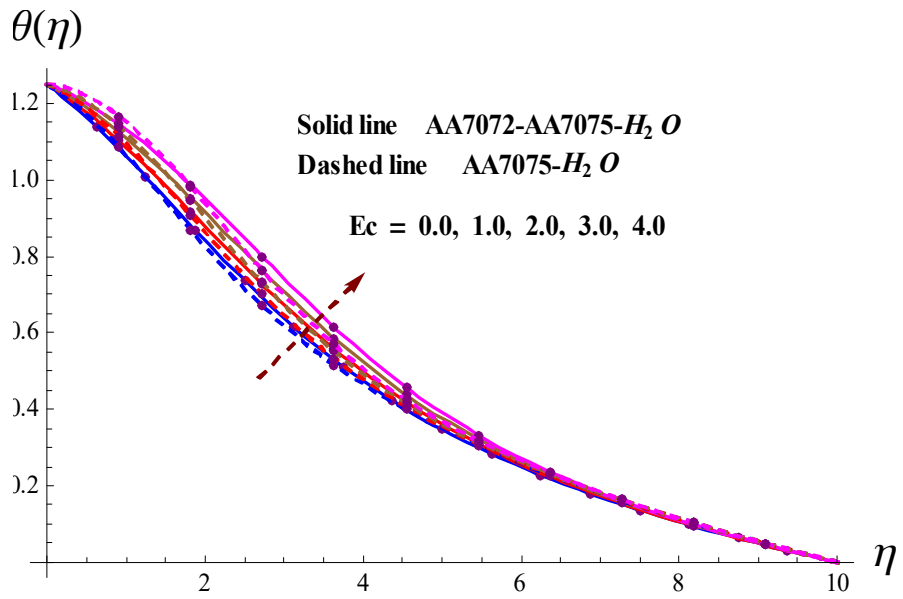


Fig. 5.4. Variation of  $\theta(\eta)$  via  $Ec$ .

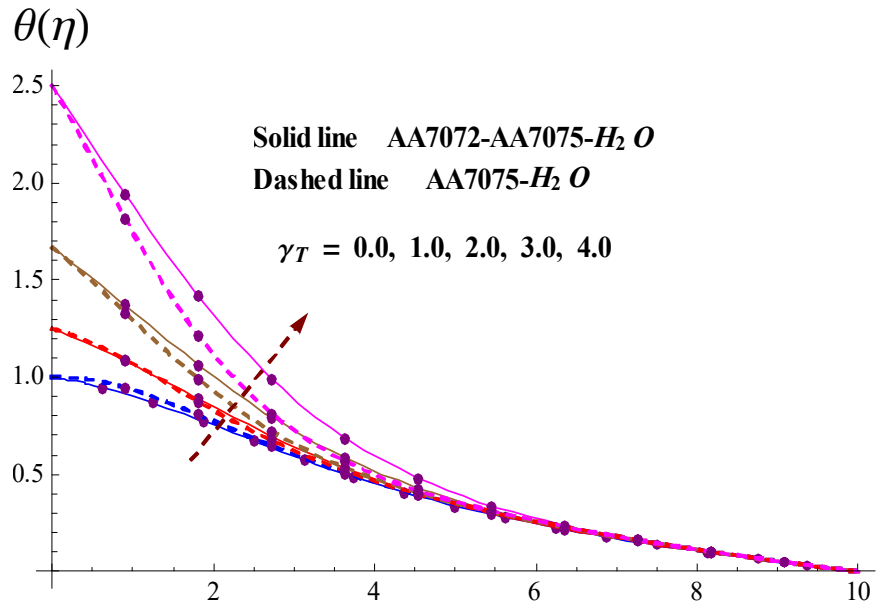


Fig. 5.5. Variation of  $\theta(\eta)$  via  $\gamma_T$ .

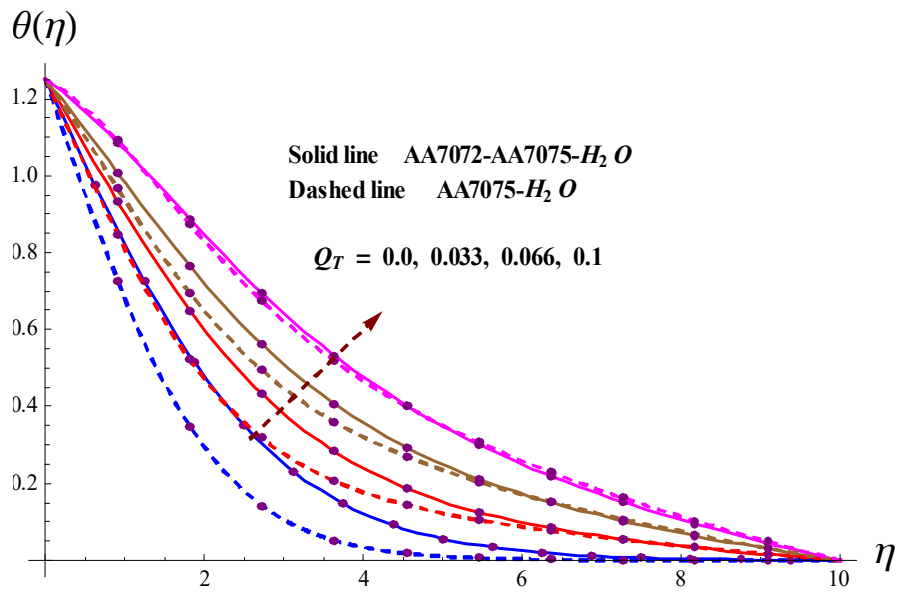


Fig. 5.6. Variation of  $\theta(\eta)$  via  $Q_T$ .

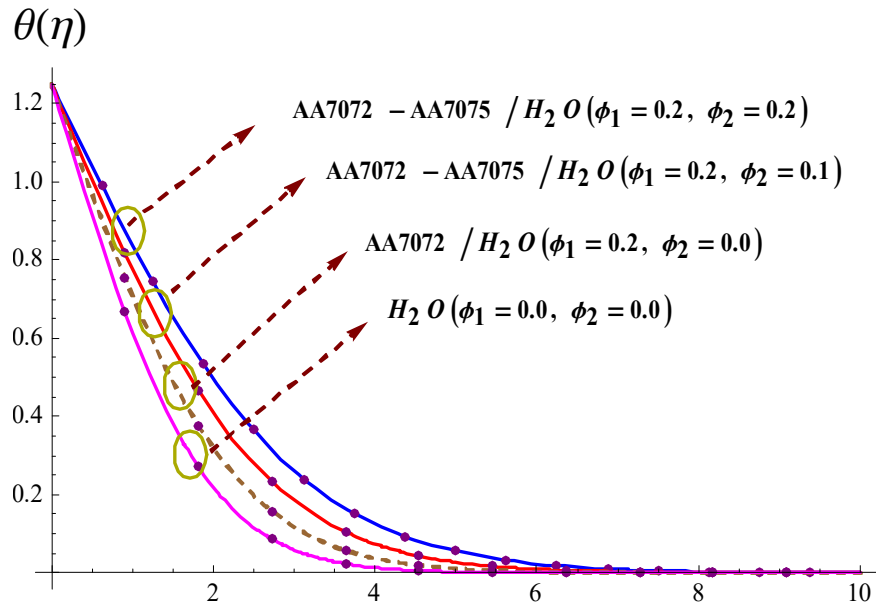


Fig. 5.7. Variation of  $\theta(\eta)$  via  $\phi_1/\phi_2$ .

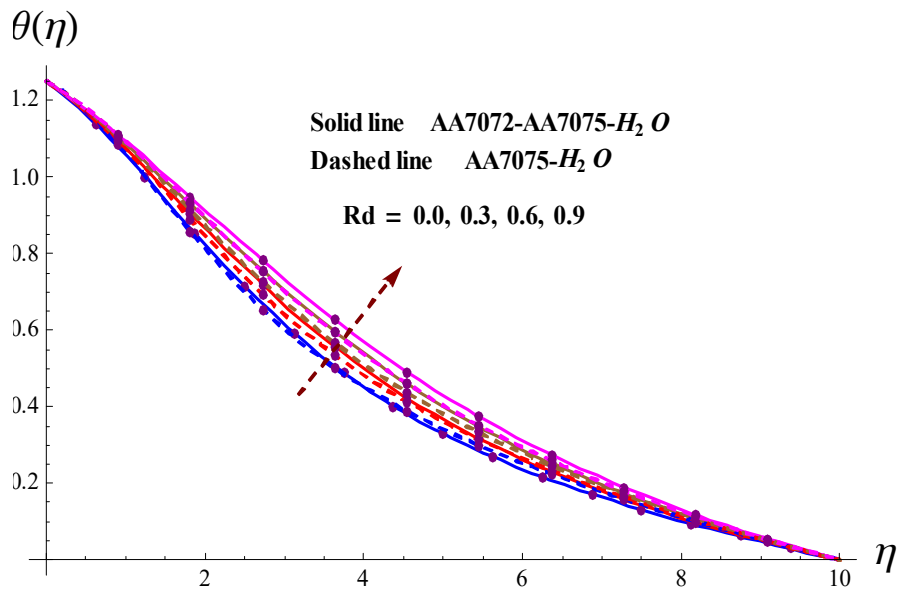


Fig. 5.8. Variation of  $\theta(\eta)$  via  $Rd$ .

**Table 5.3:** Nusselt number for nano ( $AA7075 - H_2O$ ) and hybrid nanofluid ( $AA7072 - AA7075 - H_2O$ ).

$Rd$	$\gamma_T$	$Ec$	$Q_T$	$AA7075 - H_2O$	$AA7072 - AA7075 - H_2O$
				$Nu_x$	$Nu_x$
0.0	0.3	0.1	0.1	0.293774	0.720721
0.3				0.374094	0.852325
0.6				0.524971	1.09989
0.3	0.0		0.1	0.044318	0.327675
	0.3			0.67296	1.22708
	0.6			2.46616	3.47558
0.3	0.3	0.0	0.1	0.394669	0.879845
		0.2		0.374094	0.852325
		0.4		0.353518	0.824806
0.3	0.3	0.1	0.0	2.07149	2.59573
			0.01	1.90175	2.42139
			0.1	0.374094	0.852325

### 5.3 Concluding remarks

Radiated flow of nanoliquid comprising of hybrid nanoparticles ( $AA7072, AA7075$ ) by an infinite disk is addressed numerically. Salient aspects of various emerging variables like velocity and thermal slip parameters, nanofluid volumetric fraction, thermal radiation and Eckert number on Nusselt number, velocity and temperature are studied. Following key points are important.:

- Outcomes of slip parameter and nanoparticles volume fraction on radial velocity are opposite.
- Temperature has increasing effect for larger values Eckert number and ESHS parameter.
- Temperature is qualitatively similar for nanoparticles volumetric fraction and radiation parameter.

- Heat transmission rate is enhanced by thermal slip and radiation parameter whereas reverse holds for higher Eckert number and ESHS parameter.
- For *AA7072 – AA7075* nanoparticles, the heat transfer rate is lower when compared with *AA7075* nanoparticles.
- Hybrid nanomaterials have great influence throughout the analysis when compared with regular nanomaterials.

## Chapter 6

# Numerical simulation for irreversibility analysis of ethylene glycol ( $C_2H_6O_2$ ) based carbon nanotubes flow in Darcy-Forchheimer porous medium

Here Darcy-Forchheimer stretched flow of CNTs in a rotating frame. Two types of CNTs known as multiple wall (MWCNT) and single wall (SWCNT) carbon nanotubes are accounted. Ethylene glycol (EG) is treated as base liquid. Xue's model is utilized for the physical features of density, thermal conductivity and specific heat. Entropy analysis is the main focus of this study. Heat transfer is modeled through non-linear thermal radiation, viscous dissipation and convective condition. The governing flow problems have been computed via numerical approach. Obtained solutions are presented for various estimations of embedded variables. Outcomes for single-walled and multi-walled CNTs are arranged and compared. Our findings depict that entropy generation has increasing trend for Brinkman number and temperature ratio parameter. Thermal field boosts up with an enhancement of radiative and convective variables. Moreover temperature gradient has marginally higher values in case of SWCNT when compared with

MWCNT.

## 6.1 Modeling

Here entropy generation in 3D rotating ethylene glycol CNTs nanoliquid flow by stretching surface is scrutinized. Darcy-Forchheimer model is implemented to explain the flow in porous space. The system rotates with angular velocity  $\omega$  (see Fig. 6.1). Here  $U_w = ax$  (with constant  $a > 0$ ) denotes the stretching velocity. Temperature at the surface is controlled by means of convection which is portrayed by hot liquid at temperature  $T_f$  below the sheet and heat transfer coefficient  $h_f$ . In addition irreversibility of viscous dissipation and non-linear thermal radiation are addressed. The governing expressions in view of aforementioned considerations are:

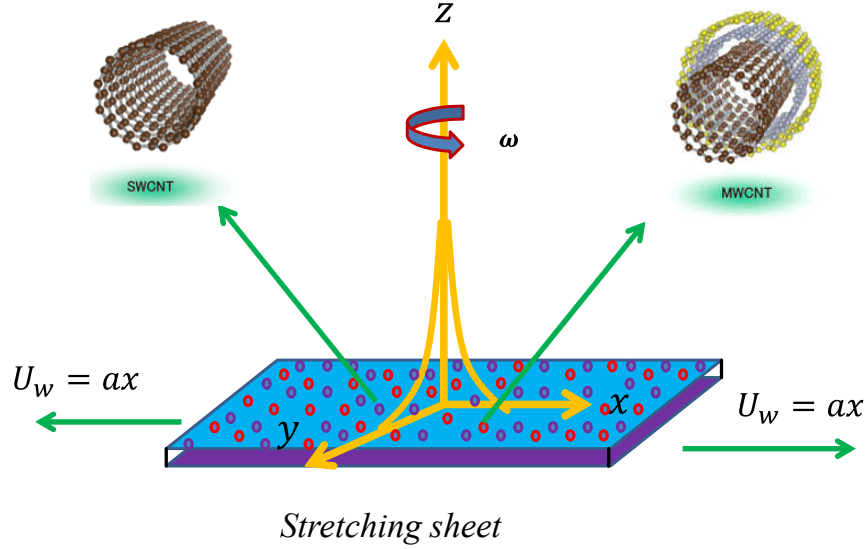


Fig. 6.1. Flow configuration..

$$\frac{\partial u}{\partial x} + \frac{\partial v}{\partial y} + \frac{\partial w}{\partial z} = 0, \quad (6.1)$$

$$u \frac{\partial u}{\partial x} + v \frac{\partial u}{\partial y} + w \frac{\partial u}{\partial z} - 2\omega v = \nu_{nf} \left( \frac{\partial^2 u}{\partial z^2} \right) - \frac{\nu_{nf}}{K_p} u - F u^2, \quad (6.2)$$

$$u \frac{\partial v}{\partial x} + v \frac{\partial v}{\partial y} + w \frac{\partial v}{\partial z} + 2\omega u = \nu_{nf} \left( \frac{\partial^2 v}{\partial z^2} \right) - \frac{\nu_{nf}}{K_p} v - F v^2, \quad (6.3)$$

$$u \frac{\partial T}{\partial x} + v \frac{\partial T}{\partial y} + w \frac{\partial T}{\partial z} = \alpha_{nf} \frac{\partial^2 T}{\partial z^2} + \frac{\nu_{nf}}{K_p (c_p)_{nf}} (u^2 + v^2) + \frac{1}{(\rho c_p)_{nf}} \frac{\partial}{\partial z} \left( \frac{16\sigma^* T^3}{3m^*} \frac{\partial T}{\partial z} \right) + \frac{\nu_{nf}}{(c_p)_{nf}} \left[ \left( \frac{\partial u}{\partial z} \right)^2 + \left( \frac{\partial v}{\partial z} \right)^2 \right], \quad (6.4)$$

where  $(u, v, w)$  show velocity components along  $(x, y, z)$ ,  $F = \frac{C_b}{x\sqrt{K_p}}$  the porous medium non-uniform inertia coefficient,  $\nu_{nf}$  the nanofluid kinematic viscosity,  $K_p$  the porous space permeability,  $C_b$  the drag coefficient,  $\alpha_{nf}$  the thermal diffusivity of nanofluid,  $(T, T_\infty)$  the liquid and ambient temperatures,  $m^*$  manifests coefficient of mean absorption and  $\sigma^*$  the Stefan-Boltzmann constant.

### 6.1.1 Thermo-physical features of carbon nanotubes and ethylene glycol

Model for nanofluid accorded by Xue [16] is

$$\left. \begin{aligned} \frac{k_{nf}}{k_f} &= \frac{1-\phi+2\phi \frac{k_{CNT}}{k_{CNT}-k_f} \ln \frac{k_{CNT}+k_f}{2k_f}}{1-\phi+2\phi \frac{k_f}{k_{CNT}-k_f} \ln \frac{k_{CNT}+k_f}{2k_f}}, \quad \rho_{nf} = \rho_f(1-\phi) + \rho_{CNT}\phi, \quad \nu_{nf} = \frac{\mu_{nf}}{\rho_{nf}}, \\ \alpha_{nf} &= \frac{k_{nf}}{(\rho c_p)_{nf}}, \quad \mu_{nf} = \frac{\mu_f}{(1-\phi)^{25/10}}, \quad (\rho c_p)_{nf} = (\rho c_p)(1-\phi) + (\rho c_p)_{CNT}\phi, \end{aligned} \right\} \quad (6.5)$$

where  $nf$  manifests nanofluid,  $\phi$  the solid volume fraction of CNTs,  $(\rho_f, \rho_{nf}, \rho_{CNT})$  the base fluid, nanofluid and carbon nanotubes densities,  $(\mu_f, \mu_{nf})$  the nanofluid effective and base liquids dynamic viscosity,  $(\rho c_p)_{nf}$  the nanofluid effective heat capacity and  $(k_{nf}, k_f)$  the thermal conductivities of carbon nanotubes and base liquid.

**Table 6.1:** Physical and thermal features of carbon nanotubes (SWCNT and MWCNT) and ethylene glycol ( $C_2H_6O_2$ ) [109, 110].

Constituents	$\rho(kg/m^3)$	$c_p(J/kgK)$	$k(W/mk)$
<i>CWNT</i>	2600	425	6600
<i>MWNT</i>	1600	796	3000
$C_2H_6O_2$	1115	2430	0.253



### 6.1.2 Boundary conditions

The related conditions are

$$\left. \begin{aligned} u = U_w(x) = ax, \quad v = 0, \quad w = 0, \quad -k_{nf} \frac{\partial T}{\partial z} = h_f(T_f - T) \text{ at } z = 0, \\ u \longrightarrow 0, \quad v \longrightarrow 0, \quad T \longrightarrow T_\infty \text{ as } z \longrightarrow \infty. \end{aligned} \right\} \quad (6.7)$$

### 6.1.3 Transformations

The non-dimensional variables for considered problem are expressed by

$$\left. \begin{aligned} u = axf'(\eta), \quad v = -axg(\eta), \quad w = -(a\nu_f)^{1/2}f(\eta), \\ \theta(\eta) = (T - T_\infty)/(T_f - T_\infty), \quad \eta = \left(\frac{a}{\nu_f}\right)^{1/2}z. \end{aligned} \right\} \quad (6.8)$$

Insertion of  $u = axf'(\eta)$ ,  $v = -axg(\eta)$  and  $w = -(a\nu_f)^{1/2}f(\eta)$  fulfills expression (6.1) automatically.

### 6.1.4 Transformed systems

Now using Eq. (6.8) in Eqs. (6.2) – (6.3) one obtains

$$\frac{1}{(1-\phi)^{2.5} \left(1 - \phi + \frac{\rho_{CNT}}{\rho_f} \phi\right)} (f''' - \lambda f') + ff'' + 2\Omega g - (1 + F_r)f'^2 = 0, \quad (6.9)$$

$$\frac{1}{(1-\phi)^{2.5} \left(1 - \phi + \frac{\rho_{CNT}}{\rho_f} \phi\right)} (g''' - \lambda g) + fg' - f'g - 2\Omega f' - F_r g^2 = 0, \quad (6.10)$$

$$\left. \begin{aligned} \frac{1}{\text{Pr}} \left(\frac{k_{nf}}{k_f}\right) \theta'' + \frac{Rd}{\text{Pr}} (\theta(\theta_w - 1))^2 (3\theta'^2(\theta_w - 1) + (\theta(\theta_w - 1) + 1)\theta'') \\ + \left(1 - \phi + \frac{\rho_{CNT}}{\rho_f} \phi\right) (f + g)\theta' + \frac{Br}{\text{Re}} \lambda (f'^2 + g^2) = 0, \end{aligned} \right\} \quad (6.11)$$

$$\left. \begin{aligned} f(0) = 0, \quad f'(0) = 1, \quad g(0) = 0, \quad \theta'(0) = \frac{k_f}{k_{nf}} \gamma \theta(0), \\ f'(0) \rightarrow 0, \quad f''(0) \rightarrow 0, \quad \theta(0) \rightarrow 0, \end{aligned} \right\} \quad (6.12)$$

where prime symbolizes differentiation via  $\eta$ ,  $\gamma = \frac{h_f}{k_f} \sqrt{\frac{\nu_f}{a}}$  the Biot number,  $F_r = \frac{C_b}{K_p^{1/2}}$  the inertia coefficient,  $\lambda = \frac{\nu_f}{aK_p}$  the porosity parameter,  $Rd = \frac{16\sigma^* T_\infty^3}{3m^* k_f}$  the radiation variable,  $\text{Pr} = \frac{(\rho c_p)_f}{k_f}$  the Prandtl number,  $\Omega = \frac{\omega}{a}$  refers to rotation variable and  $\theta_w = \frac{T_f}{T_\infty}$  the temperature ratio

variable.

### 6.1.5 Physical quantities

For engineering curiosity, we are concerned for drag force ( $C_{fx}$ ) and temperature gradient ( $Nu_x$ ) given by

$$\left. \begin{aligned} C_{fx} &= \frac{2\tau_{wx}}{\rho_f U_w^2}, \\ Nu_x &= \frac{xq_w}{(T_f - T_\infty)k_f}, \end{aligned} \right\} \quad (6.13)$$

in which ( $\tau_{wx}$ ) and ( $q_w$ ) are

$$\left. \begin{aligned} \tau_{wx} &= \mu_{nf} \left( \frac{\partial u}{\partial z} \right) \Big|_{z=0}, \\ q_w &= - \frac{k_f}{k_{nf}} \left( \frac{\partial T}{\partial z} \right) \Big|_{z=0} + \frac{4\sigma^*}{3m^*} \frac{\partial T^4}{\partial z} \Big|_{z=0}. \end{aligned} \right\} \quad (6.14)$$

Invoking Eq. (6.14) in Eq. (6.13) we have

$$\left. \begin{aligned} \text{Re}_x^{0.5} C_{fx} &= k \frac{1}{(1-\phi)^{25/10}} f''(0), \\ Nu_x &= - \left( \frac{K_{nf}}{k_f} + \text{Rd}(\theta(0)(\theta_w - 1) + 1)^3 \right) \theta'(0), \end{aligned} \right\} \quad (6.15)$$

where local Reynolds number is symbolized as  $\text{Re}_x = \frac{xU_w}{\nu_f}$ . It is important to highlight that conventional liquid situation is recovered when  $\phi = 0$ .

## 6.2 Entropy analysis

Analysis of entropy production is very important about irreversibility of thermal energy of a certain system. Following Bejan the volumetric rate of entropy production satisfies

$$E_G = \frac{k_f}{T_\infty^2} \left[ \frac{k_{nf}}{k_f} + \frac{16\sigma^*}{3m^*k_f} \right] \left( \frac{\partial T}{\partial z} \right)^2 + \frac{\mu_{nf}}{T_\infty} \Psi + \frac{\mu_{nf}}{T_\infty K_p} (u^2 + v^2), \quad (6.16)$$

where  $\Psi$  represents viscous dissipation as

$$\Psi = \left( \frac{\partial u}{\partial z} \right)^2 + \left( \frac{\partial v}{\partial z} \right)^2. \quad (6.17)$$

Using Eq. (6.17) in Eq. (6.16) one has

$$E_G = \left( \frac{k_f}{T_\infty^2} \right) \left[ \frac{k_{nf}}{k_f} + \frac{16\sigma^*}{3m^*k_f} \right] \left( \frac{\partial T}{\partial z} \right)^2 + \left( \frac{\mu_{nf}}{T_\infty} \right) \left[ \left( \frac{\partial v}{\partial z} \right)^2 + \left( \frac{\partial u}{\partial z} \right)^2 \right] + \left( \frac{\mu_{nf}}{T_\infty K_p} \right) (v^2 + u^2). \quad (6.18)$$

Let us define entropy generation number ( $N_G$ ) which is equal to generation rate of volumetric entropy ( $E_G$ ) to generation rate of characteristic entropy ( $E_0 = \frac{k_{nf}(T_f - T_\infty)}{T_\infty l^2}$ ) ratio. Mathematically this relation

$$N_G = \frac{E_G}{E_0}. \quad (6.19)$$

On utilizing transformation (6.8) Eqs. (6.18) and (6.19) take the form

$$N_G = \left[ \frac{k_{nf}}{k_f} + Rd(\theta(\theta_w - 1) + 1)^3 \right] \theta'^2 \alpha_1 + \lambda Br \frac{1}{(1-\phi)^{25/10}} (f'^2 + g^2) + \frac{Br}{(1-\phi)^{25/10}} (f''^2 + g'^2). \quad (6.20)$$

For the sake of relative significance of entropy generation by heat transfer, we define another essential parameter known as Bejan number i.e

$$Be = \frac{\text{Entropy generation due to heat and mass transfer}}{\text{Total entropy generation}}, \quad (6.21)$$

or

$$Be = \frac{\left[ \frac{k_{nf}}{k_f} + Rd(\theta(\theta_w - 1) + 1)^3 \right] \theta'^2 \alpha_1}{\left[ \frac{k_{nf}}{k_f} + Rd(\theta(\theta_w - 1) + 1)^3 \right] \theta'^2 \alpha_1 + \lambda Br \frac{1}{(1-\phi)^{25/10}} (f'^2 + g^2) + \frac{Br}{(1-\phi)^{25/10}} (f''^2 + g'^2)}, \quad (6.22)$$

where  $Br = \frac{U_w^2 \mu_f}{k_f \Delta T}$  denotes the Brinkman number and  $\alpha_1 = \frac{(T_f - T_\infty)}{T_\infty}$  the temperature ratio variable due to entropy generation.

It is important to highlight that for  $Be = 1$  the heat transfer irreversibility effects become dominant whereas for case  $Be = 0$ , the entropy due to liquid friction dominates. Furthermore  $Be = 0.5$  represents that production of entropy because of liquid friction and heat transfer are similar.

### 6.3 Computational procedure

Numerical solutions to the proposed non-linear coupled problems (6.9) – (6.11) and (6.12) are obtained by employing `bvp4c` technique (based on FDM). For this objective we reduced Eqs. (6.9 – 6.12) to first ODEs. The mesh and error control selection is developed on the residual of progressive computations. The boundary layer region is attained for each collection of parametric values. The iterative error is set  $10^{-6}$ . The main algorithm are given as follows:

$$y_1 = f, y_2 = f', y_3 = f'', y_4 = g, y_5 = g', y_6 = \theta, y_7 = \theta', \quad (6.23)$$

$$\begin{bmatrix} y_1' \\ y_2' \\ y_3' \\ y_4' \\ y_5' \\ y_6' \\ y_7' \end{bmatrix} = \begin{bmatrix} y_2 \\ y_3 \\ \frac{((1+F_r)y_2^2 - y_1y_3 - 2\Omega y_4) + \lambda y_2}{(1-\phi)^{2.5} \left(1 - \phi + \frac{\rho_{CNT}}{\rho_f} \phi\right)} \\ y_5 \\ \frac{(F_r y_4^2 + y_2 y_4 + 2\Omega y_2 - y_1 y_5) + \lambda y_4}{(1-\phi)^{2.5} \left(1 - \phi + \frac{\rho_{CNT}}{\rho_f} \phi\right)} \\ y_7 \\ \frac{\left[-\left(1 - \phi + \frac{\rho_{CNT}}{\rho_f} \phi\right)(y_1 + y_4)y_7 - Rd(y_6(\theta_w - 1) + 1)^2(3(\theta_w - 1)y_7^2)\right]}{\left[\frac{k_{nf}}{k_f} + Rd[y_6(\theta_w - 1) + 1]\right]} \end{bmatrix} \quad (6.24)$$

with initial conditions

$$\begin{bmatrix} y_1(0) \\ y_2(0) \\ y_2(\infty) \\ y_4(0) \\ y_4(\infty) \\ y_6(\infty) \\ y_7 \end{bmatrix} = \begin{bmatrix} 0 \\ 1 \\ 0 \\ 0 \\ 0 \\ 0 \\ -\frac{k_{nf}}{k_f} y_6(0) \end{bmatrix} \quad (6.25)$$

### 6.4 Discussion

This portion is dedicated to interpret physical feature of embedding variables on flow quantities namely velocities ( $f'(\eta)$  and  $g'(\eta)$ ), temperature  $\theta(\eta)$ , entropy production  $N_G$  and Bejan

number  $Be$  against SWCNTs and MWCNTs. These outcomes are well explained and presented graphically (see Figs. 6.2 – 6.17). In these graphs the dotted lines present the feature of SWCNTs and the solid lines show the behavior of MWCNTs. Skin frictions ( $(Re_x^{0.5} f_x)$  and  $(Re_x^{0.5} f_y)$ ) and Nusselt numbers ( $Re^{-0.5} Nu_x$ [MWCNTs] and  $Re^{-0.5} Nu_x$ [SWCNTs]) are also computed and analyzed (see Tables 6.2 and 6.3). Further physical and thermal features of carbon nanotubes (SWCNT and MWCNT) and ethylene glycol ( $C_2H_6O_2$ ) are shown in Table 6.1. The assigned values to the physical variables in our whole analysis are  $Fr = \lambda = \theta_w = Br = 0.1$ ,  $\Omega = 0.3$ ,  $Pr = 40.36$ ,  $\gamma = 5.0$ ,  $Rd = 2.5$  and  $\alpha_1 = 0.5$ .

#### 6.4.1 Velocity

Figs. (6.2–6.9) disclosed the variations of interesting physical variables on velocity distributions ( $f'(\eta)$  and  $g'(\eta)$ ). Effect of  $\phi$  in the range of  $0.1 \leq \phi \leq 0.5$  for both SWCNTs and MWCNTs on velocity distributions ( $f'(\eta)$  and  $g'(\eta)$ ) are shown in Figs. (6.2 and 6.3). It is found that larger estimations of nanoparticles volume fraction led to enhance ( $f'(\eta)$  and  $g'(\eta)$ ) in both cases of CNTs. Figs. (6.4 and 6.5) enlighten the behavior of  $Fr$  on ( $f'(\eta)$  and  $g'(\eta)$ ). Here higher  $Fr$  decay the fluid velocities ( $f'(\eta)$  and  $g'(\eta)$ ). Physically for higher  $Fr$  the internal force enhances and thus velocity decays. Plots of  $\lambda$  for ( $f'(\eta)$  and  $g'(\eta)$ ) are depicted in Figs. (6.6 and 6.7). It is clear from these Figs. that velocities ( $f'(\eta)$  and  $g'(\eta)$ ) increase for higher  $\lambda$ . In fact resistive force increases in the nanoliquid motion due to porous medium. Thus velocities ( $f'(\eta)$  and  $g'(\eta)$ ) are reduced. Figs. (6.8 and 6.9) portray the aspect of rotation parameter  $\Omega$  on velocities ( $f'(\eta)$  and  $g'(\eta)$ ). These Figs. pointed out that  $\Omega$  decayed the velocity distribution in both directions. Higher estimations of  $\Omega$  make more rotation rate when compared with stretching rate. Therefore influence of higher rotation gives a decay in liquid velocity. Further Figs. (6.2 and 6.9) also indicate that SWCNTs have lower velocity when compared with MWCNTs. Physically SWCNTs has higher density than MWCNTs.

#### 6.4.2 Variation in temperature

To investigate the behavior of dimensionless temperature verses  $\phi$ ,  $\theta_w$ ,  $Rd$  and  $\gamma$  the Figs. (6.10 – 6.14) are interpreted. Feature of  $\phi$  on thermal field is displayed in Fig. 6.10. Here temperature significantly decays for higher  $\phi$ . Also thermal field  $\theta(\eta)$  is more in case of MWCNTs

when compared with SWCNTs. Behavior of thermal field  $\theta(\eta)$  for larger  $\theta_w$  is disclosed in Fig. 6.11. Here thermal field and layer thickness are increased for both CNTs. Here  $\theta(\eta)$  is less in case of SWCNTs than MWCNTs. Fig. 6.12 is designed to examine how thermal field is effected by  $Rd$ . An increment in temperature for  $Rd$  is perceived. In physical sense this phenomenon is anticipated, since temperature rises as radiation variable supplies more heat to the nanoliquid. Fig. 6.13 displayed variation of  $\gamma$  on  $\theta(\eta)$ . Temperature increases abruptly by Biot number  $\gamma$ . This behavior is due to higher convection which enhanced the surface temperature.

### 6.4.3 Entropy generation and Bejan numbers

Figs. (6.14 – 6.21) describe the aspects of various embedding variables ( $Br$ ,  $\alpha$ ,  $Rd$  and  $\gamma$ ) in the range of  $0 \leq \eta \leq 5.0$  on  $N_G$  and  $Be$  for both MWCNTs and SWCNTs. Consequences of  $Br$  on  $N_G$  and  $Be$  are declared in Figs. 6.14 and 6.15. Higher Brinkman number significantly enhance thermal energy irreversibility. This behavior is seen in Fig. 6.14. From Fig. 6.15 it is noted that entropy generation rate  $N_G$  shows crossover point at  $\eta = 3.5$ . Before this variation, the entropy is increased and then it starts to fall. Characteristics of temperature ratio variable due to entropy  $\alpha_1$  on  $Be$  and  $N_G$  are reported in Figs. 6.16 and 6.17. Here we observed that entropy and Bejan number are intensified for both (SWCNTs) and (MWCNTs). Further  $Be$  is higher in case of (MWCNTs) than (SWCNTs). Figs. 6.18 and 6.19 are depicted to see how  $Rd$  effects the  $Be$  and  $N_G$ . Here we see that both  $Be$  and  $N_G$  are increasing functions of  $Rd$ . Physically higher  $Rd$  rise the internal heat generation in moving liquid which consequently enhance  $Be$  and  $N_G$ . Fig. 6.20 and 6.21 show outcomes for  $Be$  and  $N_G$  in response to  $\gamma$ . It is found that larger estimations of  $\gamma$  insist an increment in both  $Be$  and  $N_G$ . In physical sense, an enhancement in  $\gamma$  corresponds to rise the stretching surface thermal energy irreversibility. This fact declared the decaying features of  $Be$  and  $N_G$ .

### 6.4.4 Variations of non-dimensional drag forces and Nusselt number

Tables 6.2 and 6.3 are organized numerically to examined the behavior of physical quantities (skin frictions and Nusselt number) for both SWCNTs and MWCNTs. Table 6.2 declared that skin friction is increased via  $\phi$ ,  $\lambda$  and  $\Omega$ . Also higher estimations of  $F_r$  increases primary skin friction ( $-\text{Re}_x^{0.5} C_{fx}$ ) whereas slowly reduction is occurs in secondary skin friction

$(-\text{Re}_x^{0.5} C_{fy})$ . Table 6.3 manifests that Nusselt number enhances for higher  $\phi$ ,  $\theta_w$ ,  $\gamma$  and  $Rd$ . Furthermore Nusselt number has marginally higher values in case of SWCNTs when compared with MWCNTs.

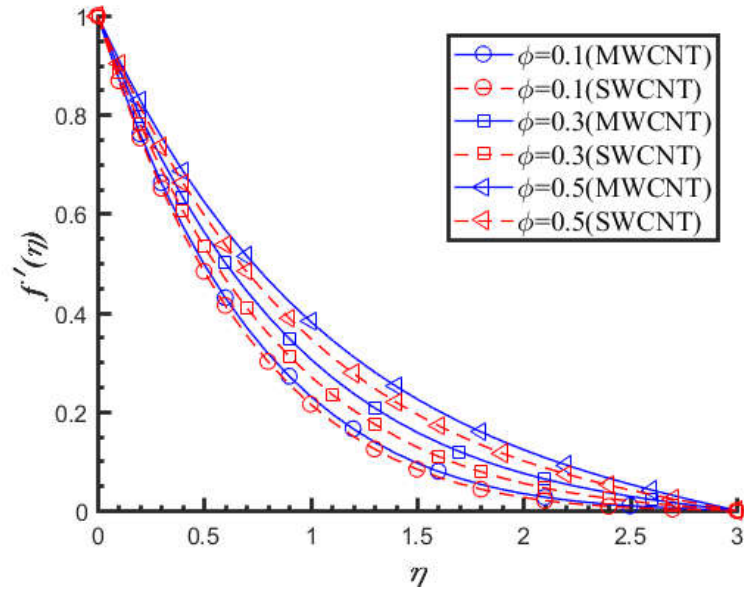


Fig. 6.2.  $f'(\eta)$  vs  $\phi$ .

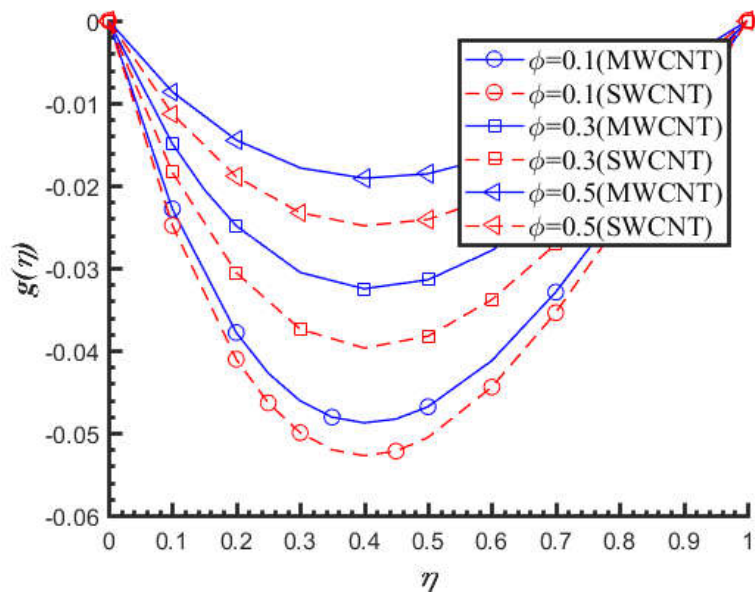


Fig. 6.3.  $g(\eta)$  vs  $\phi$ .

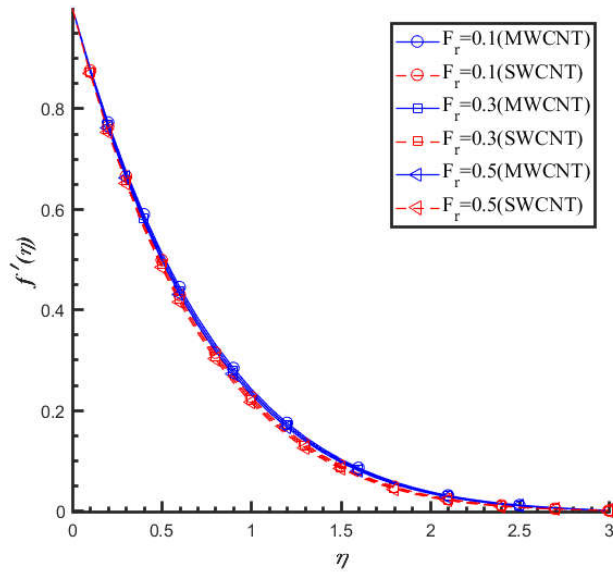


Fig. 6.4.  $f'(\eta)$  vs  $F_r$ .

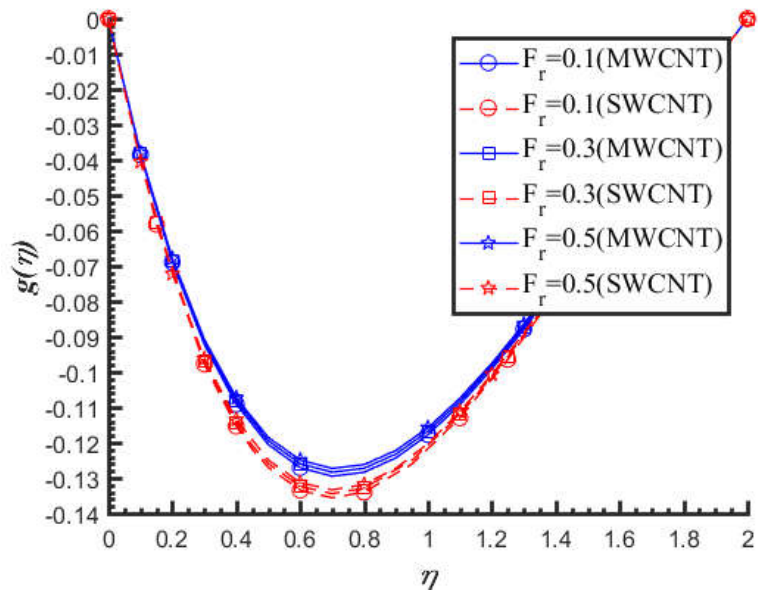


Fig. 6.5.  $g(\eta)$  vs  $F_r$ .



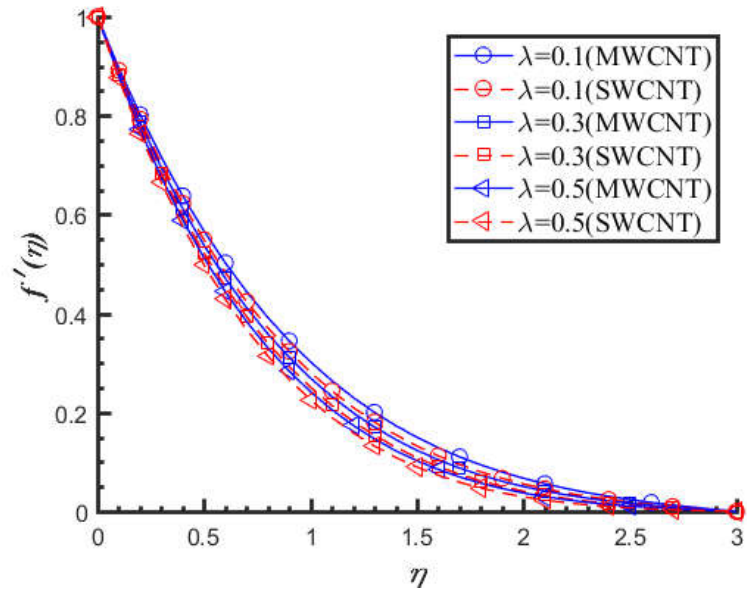


Fig. 6.6.  $f'(\eta)$  vs  $\lambda$ .

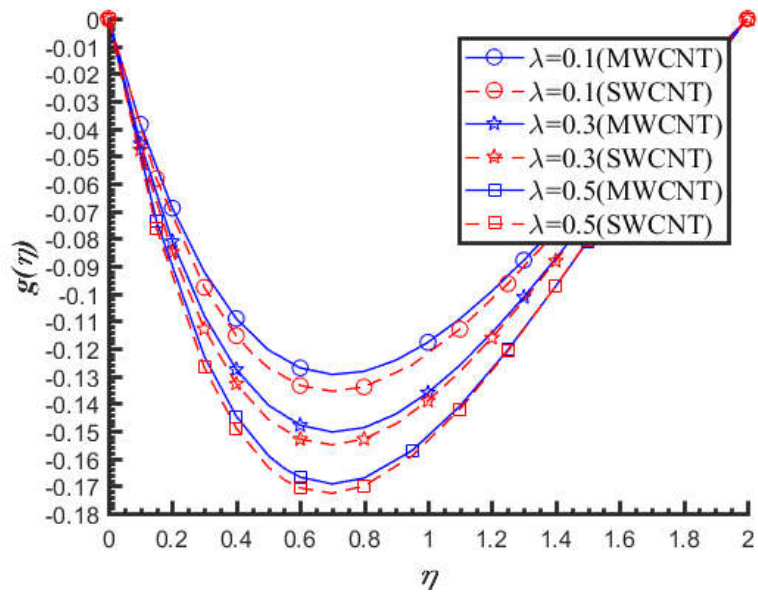


Fig. 6.7.  $g(\eta)$  vs  $\lambda$ .

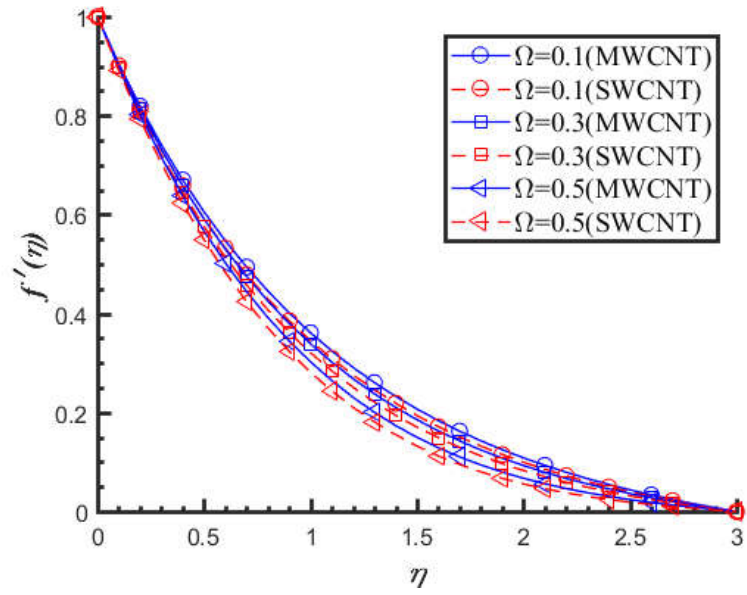


Fig. 6.8.  $f'(\eta)$  vs  $\Omega$ .

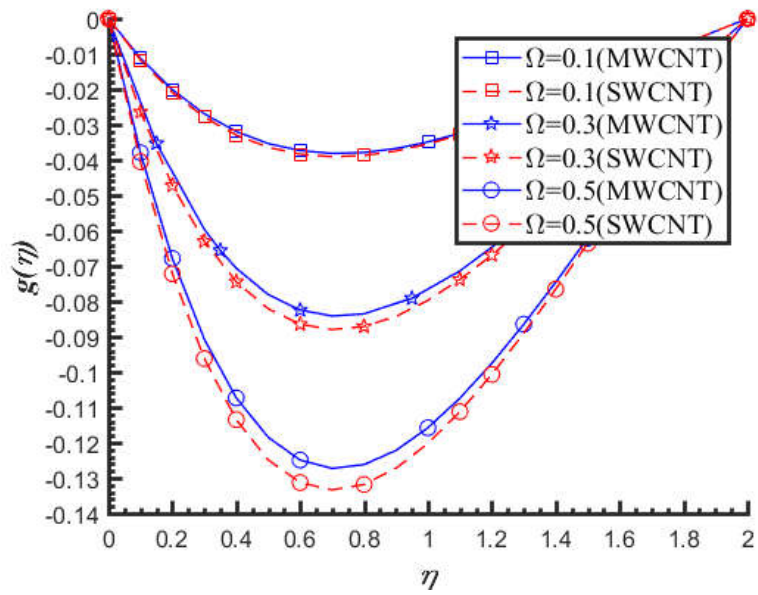


Fig. 6.9.  $g(\eta)$  vs  $\Omega$ .

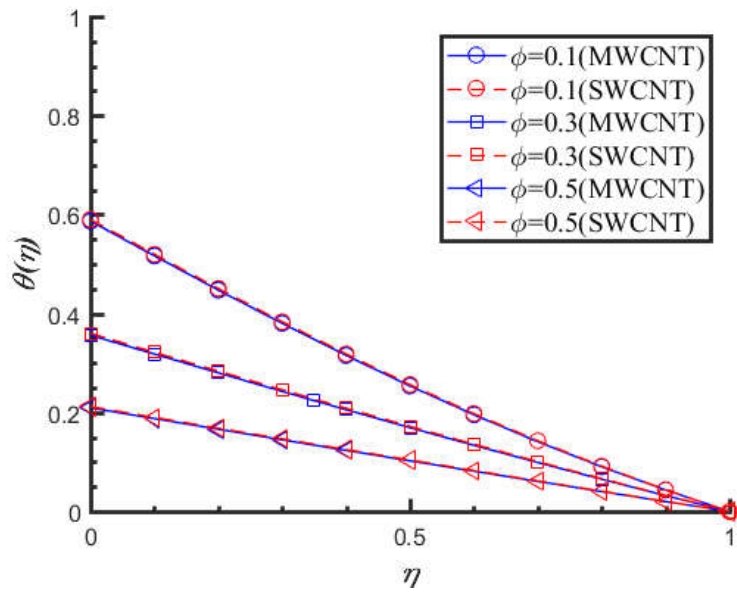


Fig. 6.10.  $\theta(\eta)$  vs  $\phi$ .

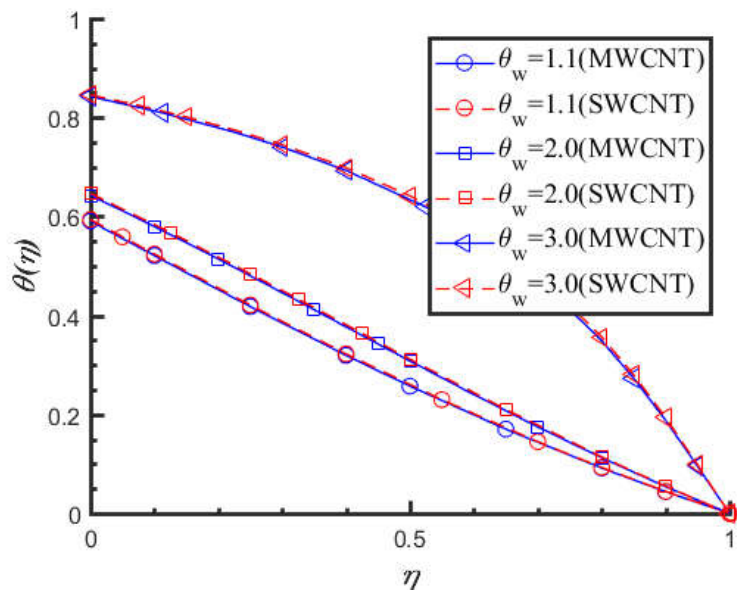


Fig. 6.11.  $\theta(\eta)$  via  $\theta_w$ .

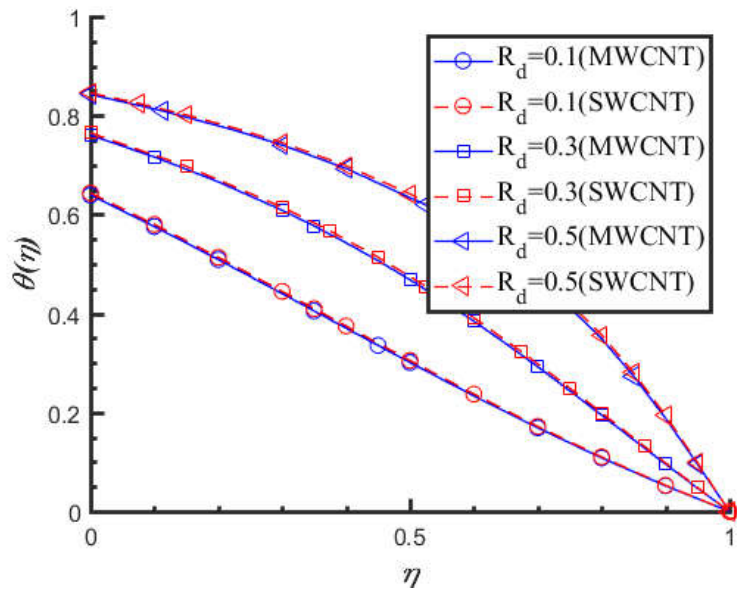


Fig. 6.12.  $\theta(\eta)$  via  $R_d$ .

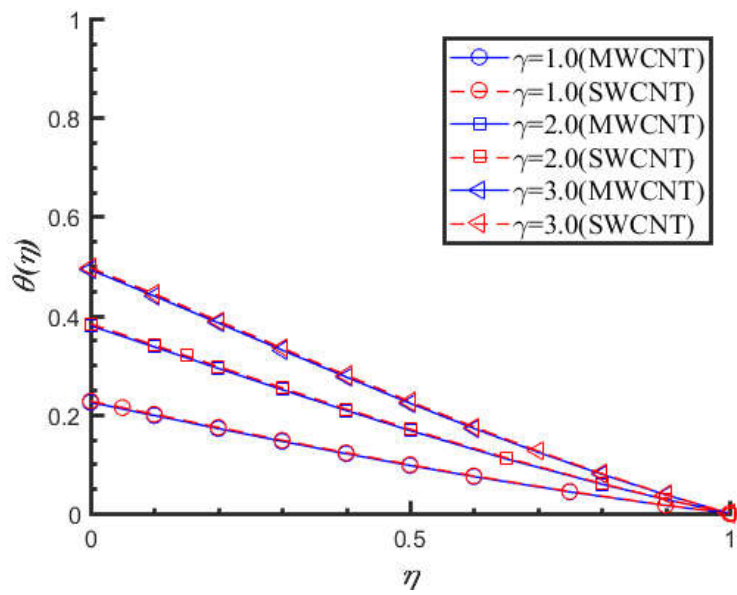


Fig. 6.13.  $\theta(\eta)$  via  $\gamma$ .

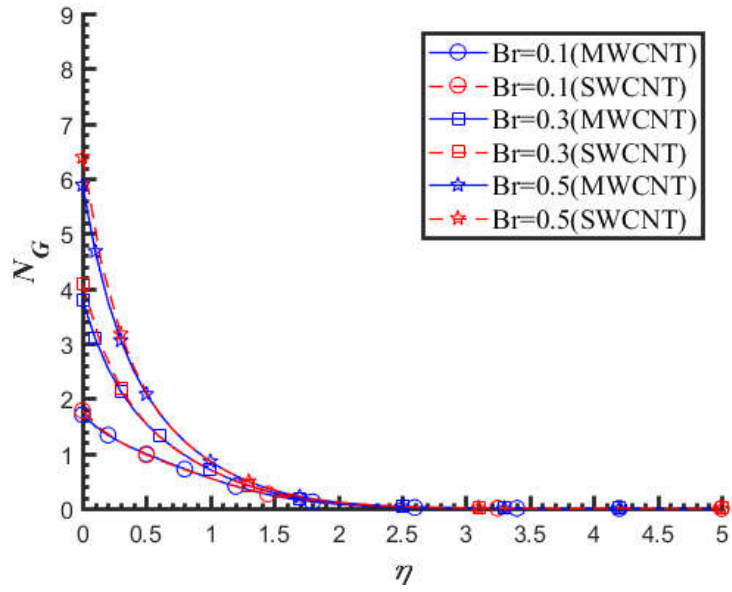


Fig. 6.14.  $N_G$  via  $Br$ .

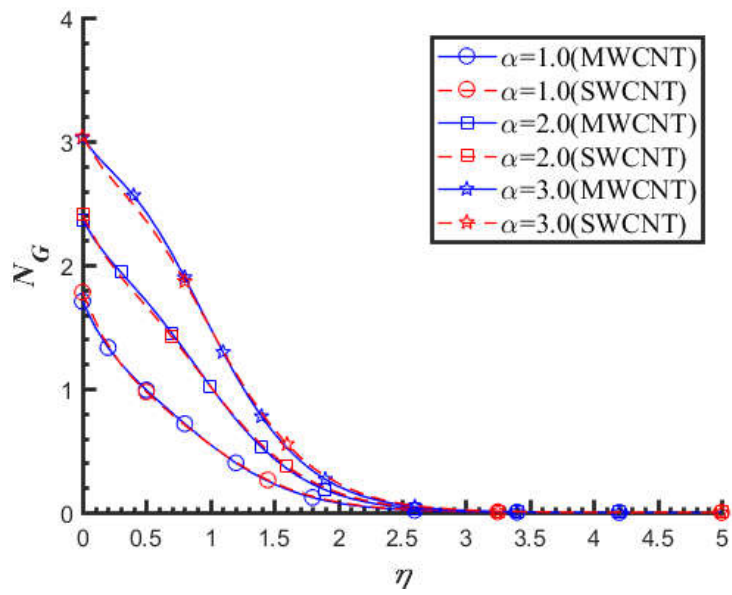


Fig. 6.15.  $N_G$  via  $\alpha$ .

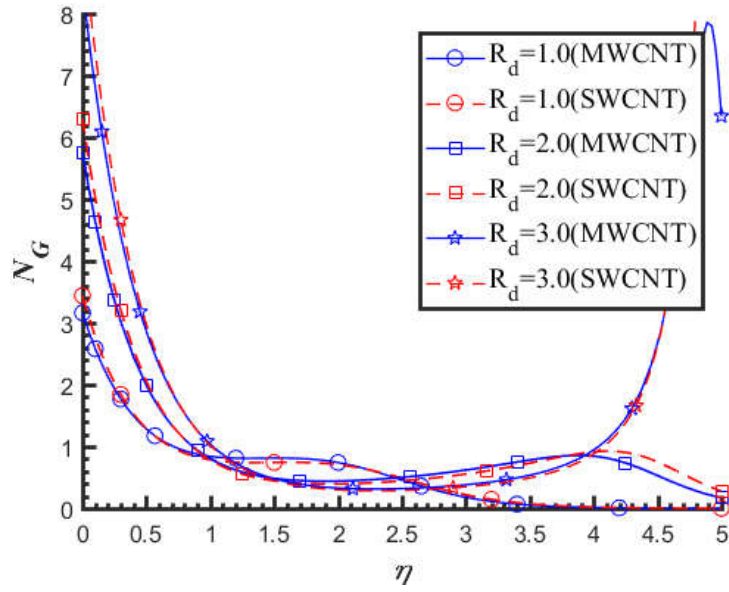


Fig. 6.16.  $N_G$  via  $R_d$ .

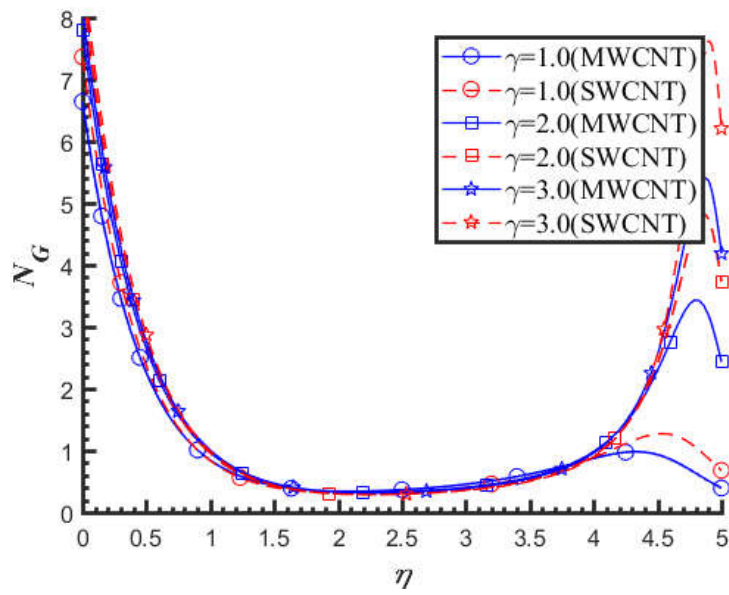


Fig. 6.17.  $N_G$  via  $\gamma$ .

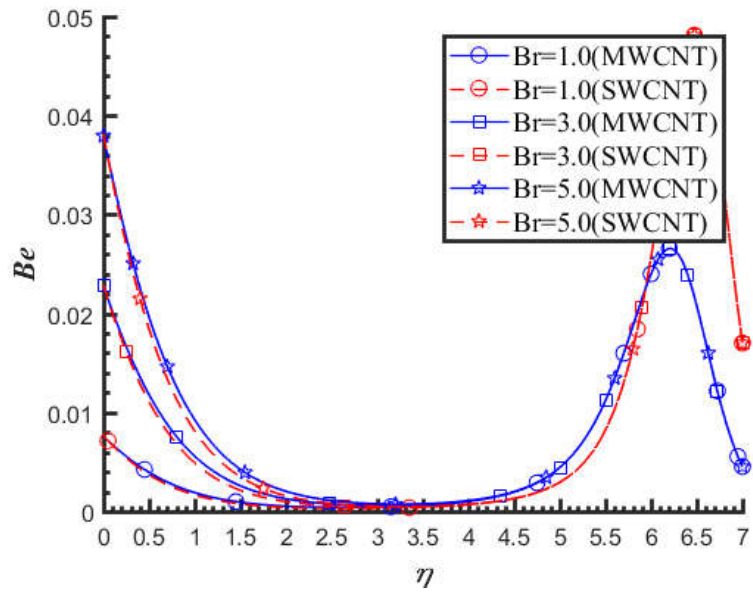


Fig. 6.18.  $Be$  via  $Br$ .

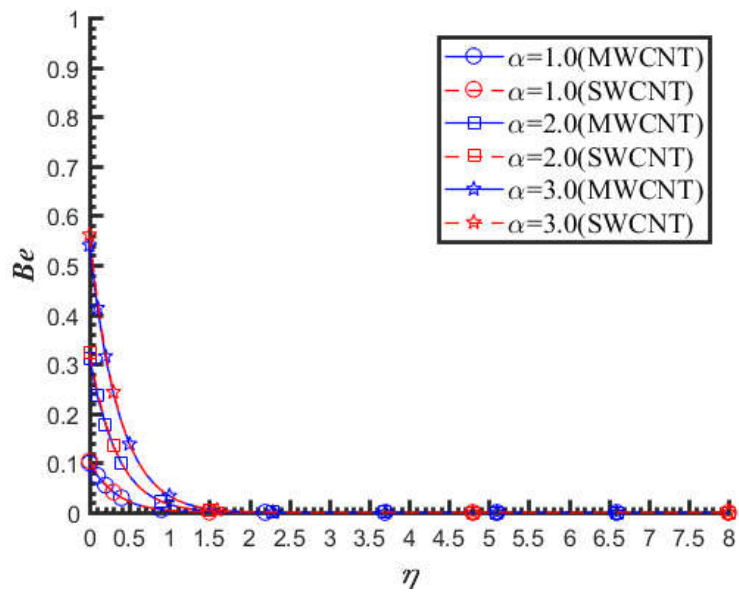


Fig. 6.19.  $Be$  via  $\alpha$ .

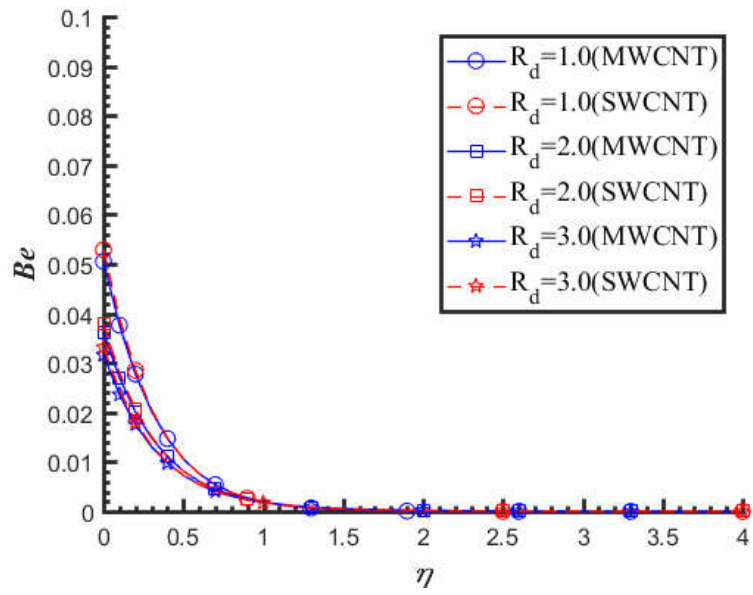


Fig. 6.20.  $Be$  via  $R_d$ .

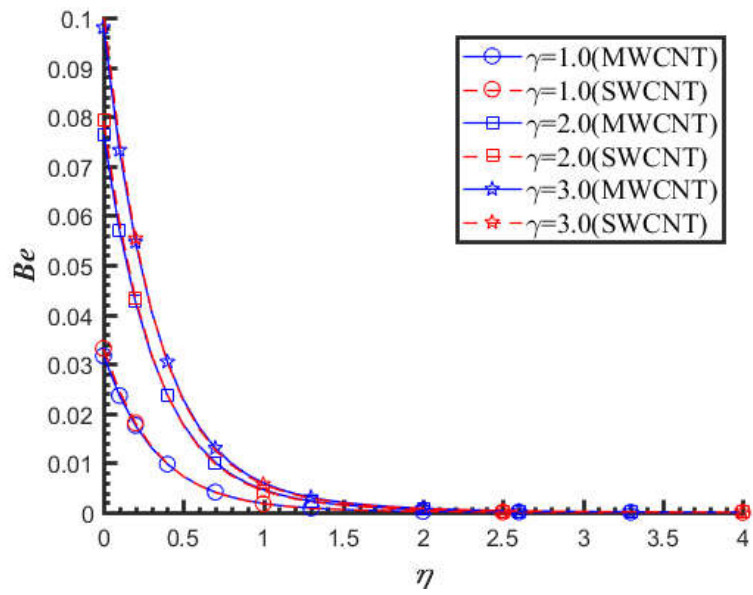


Fig. 6.21.  $Be$  via  $\gamma$ .



**Table 6.2:** Computation of  $(\text{Re}_x^{0.5} C_{fx})$  and  $(\text{Re}_x^{0.5} C_{fy})$  via  $\phi$ ,  $F_r$ ,  $\lambda$  and  $\Omega$  for both MW-CNTs and SWCNTs.

40.36		MWCNTs		SWCNTs	
Parameters (fixed values)	Variables	$(-\text{Re}_x^{\frac{1}{2}} C_{fx})$	$(-\text{Re}_x^{\frac{1}{2}} C_{fy})$	$(-\text{Re}_x^{\frac{1}{2}} C_{fx})$	$(-\text{Re}_x^{\frac{1}{2}} C_{fy})$
$Fr = \lambda = \theta_w = Br = 0.1,$	$\phi = 0.1$	2.3676	0.1888	2.3557	0.2050
$Pr = 40.36, \Omega = 0.3,$	0.2	3.0515	0.2092	3.0670	0.2423
$Rd = 2.5, \alpha_1 = 0.5, \gamma = 5.0,$	0.3	4.1012	0.2361	4.1334	0.2870
$\lambda = \theta_w = Br = 0.1, \Omega = 0.3,$	$F_r = 0.1$	1.9827	0.1888	2.0179	0.2050
$Pr = 40.36, \gamma = 5.0$	0.2	2.0012	0.1884	2.0380	0.2046
$Rd = 2.5, \phi = 0.1, \alpha_1 = 0.5,$	0.3	2.0195	0.1881	2.0580	0.2042
$Fr = \theta_w = Br = 0.1, \alpha_1 = 0.5,$	$\lambda = 0.1$	2.1267	0.1888	2.1756	0.2050
$Pr = 40.36, \gamma = 5.0, \Omega = 0.3,$	0.2	2.1576	0.2204	2.2062	0.2364
$Rd = 2.5, \phi = 0.1$	0.3	2.1882	0.2518	2.2365	0.2675
$Fr = \lambda = \theta_w = Br = 0.1,$	$\Omega = 0.1$	1.9743	0.0846	2.0077	0.0899
$Pr = 40.36, \alpha_1 = 0.5,$	0.2	1.9754	0.1367	2.0091	0.1475
$Rd = 2.5, \phi = 0.1, \gamma = 5.0,$	0.3	1.9772	0.1888	2.0113	0.2050

**Table 6.3:** Variation of  $\text{Re}^{-0.5} Nu_x[\text{MWCNTs}]$  and  $\text{Re}^{-0.5} Nu_x[\text{SWCNTs}]$  via  $\phi$ ,  $F_r$ ,  $\lambda$  and  $\Omega$ .

Parameters (fixed values)	Variables	MWCNTs		SWCNTs	
			$\text{Re}^{-0.5} Nu_x$		$\text{Re}^{-0.5} Nu_x$
$F_r = \lambda = \theta_w = Br = 0.1, \Omega = 0.3,$ $Pr = 40.36, \gamma = 5.0, Rd = 2.5, \alpha_1 = 0.5$	$\phi$	0.1	0.9061	0.1	0.9126
		0.2	2.8954	0.2	2.9213
		0.3	7.1033	0.3	7.1730
$F_r = \lambda = \theta_w = Br = 0.1, \Omega = 0.3, \alpha_1 = 0.5,$ $Pr = 40.36, Rd = 2.5, \phi = 0.1$	$\gamma$	0.1	0.9061	0.1	0.9126
		0.2	1.7678	0.2	1.7799
		0.3	2.5881	0.3	2.6051
$F_r = \lambda = Br = 0.1, \Omega = 0.3, \alpha_1 = 0.5,$ $Pr = 40.36, \gamma = 5.0, Rd = 2.5, \phi = 0.1$	$\theta_w$	0.1	0.9061	0.1	0.9126
		0.2	0.9064	0.2	0.9128
		0.3	0.9066	0.3	0.9130
$F_r = \lambda = \theta_w = Br = 0.1, \alpha_1 = 0.5,$ $Pr = 40.36, \gamma = 5.0, \phi = 0.1, \Omega = 0.3$	$Rd$	0.1	0.9061	0.1	0.9126
		0.2	0.9975	0.2	1.0045
		0.3	1.0947	0.3	1.1025

## 6.5 Final outcomes

Here thermodynamic second law is utilized to calculate the total entropy production. The governing expressions are modeled including the Darcy-Forchheimer model, viscous dissipation, ethylene glycol CNTs and nonlinear thermal radiation. Main findings are summed below.

- Higher  $\Omega$ ,  $\lambda$  and  $F_r$  lead to decay the liquid velocities for both CNTs.
- Higher  $\theta_w$ ,  $Rd$  and  $\gamma$  strengthen thermal field.
- $\Omega$ ,  $\lambda$  and  $\phi$  decay the skin frictions for both CNTs.
- Temperature gradient is enhanced via  $\theta_w$ ,  $Rd$ ,  $\phi$  and  $\gamma$ .
- Higher  $\alpha$  and  $\gamma$  boost up the Bejan number  $Be$ .
- Generation rate of entropy shows increasing impact for  $Br$ ,  $\gamma$  and  $\alpha$ .

## Chapter 7

# Numerical treatment of melting heat transfer and entropy generation in stagnation point flow of hybrid nanomaterials (SWCNT-MWCNT/engine oil)

Present chapter addresses the entropy analysis and melting effect in flow of hybrid nanomaterials consisting of CNTs nanoparticles and engine oil mixture. Flow is by a stretching cylinder. Formulation accounting the viscous dissipation, velocity slip and thermal radiation impacts is made. In order to estimate the disorder within the thermo-physical frame, second order analysis has been used. The governing system with the imposed boundary condition is dimensionless via proper variables and then tackled through numerical scheme. Numerical outcomes are expressed graphically and analyzed. Comparison of hybrid nanomaterials, nanomaterials and regular liquid are expressed graphically. Outcomes indicate that hybrid nanomaterials have great impact throughout the inspection than common nanomaterials.

## 7.1 Formulation

Fig. 7.1. presents the flow configuration. Consider stagnation point flow of hybrid nanomaterials (dispersion of SWCNT and MWCNT in engine oil) past a stretching cylinder. Nanoparticles SWCNT and MWCNT are treated as first and second particles respectively. Cylindrical coordinates  $(x, r)$  are used for the development of relevant expressions. The laminar and incompressible nanomaterials are assumed to be in thermal equilibrium. A single phase concept is employed for nanofluid modeling. Further no relative motion exists between liquid and nanoparticles. Irreversibility analysis in porous space is considered. In addition velocity slip and melting effects are accounted. Governing flow problems are:

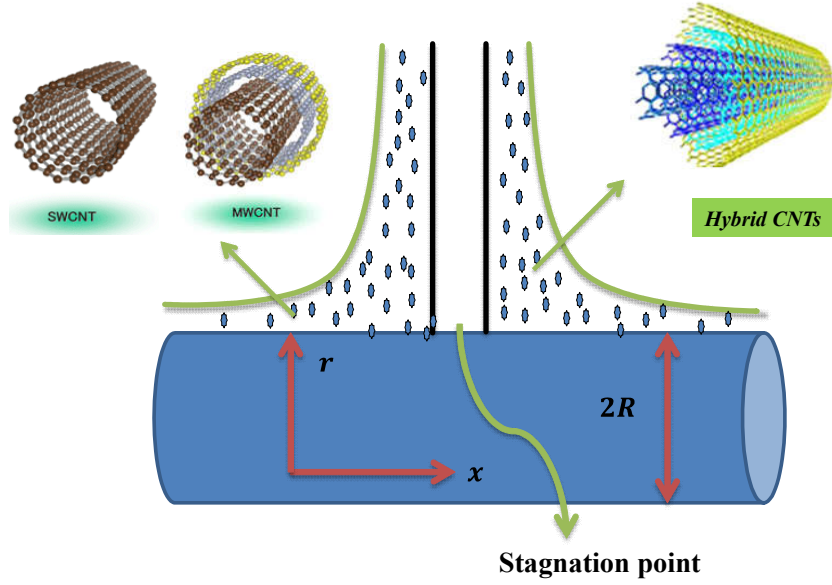


Fig. 7.1. Flow model.

$$\frac{\partial}{\partial r}(rv) + \frac{\partial}{\partial x}(ru) = 0, \quad (7.1)$$

$$v \frac{\partial u}{\partial r} + u \frac{\partial u}{\partial x} = \nu_{hnf} \left( \frac{\partial^2 u}{\partial r^2} + \frac{1}{r} \frac{\partial u}{\partial r} \right) + U_e \frac{dU_e}{dx}, \quad (7.2)$$

$$\left. \begin{aligned} u \frac{\partial T}{\partial x} + v \frac{\partial T}{\partial r} &= \left( \frac{\mu_{hnf}}{(\rho c_p)_{hnf}} \right) \left( \frac{\partial u}{\partial r} \right)^2 + \left( \frac{k_{hnf}}{(\rho c_p)_{hnf}} \right) \left( \frac{\partial^2 T}{\partial r^2} + \frac{1}{r} \frac{\partial T}{\partial r} \right) \\ &+ \frac{1}{(\rho c_p)_{hnf}} \frac{16\sigma^* T_\infty^2}{3k^*} \left( \frac{1}{r} \frac{\partial T}{\partial r} + \frac{\partial^2 T}{\partial r^2} \right), \end{aligned} \right\} \quad (7.4)$$

with boundary conditions:

$$\left. \begin{aligned} v = 0, \quad u = U_w(x) + \delta_1 \frac{\partial u}{\partial r}, \quad T = T_m \text{ at } r = R, \\ u \longrightarrow U_e(x) = \frac{U_\infty x}{l}, \quad T \longrightarrow T_\infty \text{ as } r \longrightarrow \infty, \end{aligned} \right\} \quad (7.5)$$

$$k_{hnf} \left( \frac{\partial T}{\partial r} \right)_{r=R} = \rho_{hnf} [\lambda_1 + c_s(T_m - T_0)] v(R, x). \quad (7.6)$$

Slip condition is prescribed at cylinder i.e. velocity of adjacent liquid particles and cylinder are not same due to low adhesive forces. The conditions (7.5) are imposed at  $r = R$  and  $r \rightarrow \infty$ . Here  $U_w = \frac{U_0 x}{l}$  denotes the stretching velocity,  $\delta_1 \frac{\partial u}{\partial r}$  represents the effect of velocity slip,  $U_e(x) = \frac{U_\infty x}{l}$  the free stream velocity, ( $v = 0$ ) means no injection/suction and ( $T_0, T_m, T_\infty$ ) denote the respective surface, melting and ambient temperatures. Condition (7.6) physically manifests that heat conducted to the surface is equal to heat of melting and sensible heat need to ascent surface temperature ( $T_0$ ) to its melting temperature ( $T_m$ ). Furthermore  $c_s$  surface heat capacity and  $\lambda_1$  the fluid latent heat.

### 7.1.1 Thermo-physical features for nanomaterials

Researchers proposed different nanofluid models but these models are solely valid for elliptical rotational and share particles with low axial ratio. Furthermore these models do not predict features of space distribution of CNTs on thermal conductivity. However CNTs can be considered as elliptical rotational particles along with higher axial ratio. In order to overcome these issues, Xue recommended a theoretical model depending upon Maxwell theory which confidently describes impact of space distributions on CNTs and elliptical rotational nanotubes with large axial ratio. The effective characteristics of CNTs and hybrid CNTs may be presented in terms of regular liquid (engine oil) as follows:

$$\left. \begin{aligned} \rho_{nf} = \rho_f(1 - \phi) + \rho_{CNT}\phi, \quad (\rho c_p)_{nf} = (\rho c_p)_f(1 - \phi) + (\rho c_p)_{CNT}\phi, \\ \mu_{nf} = \frac{\mu_f}{(1 - \phi_1)^{2.5/10}}, \quad \frac{k_{nf}}{k_f} = \frac{1 - \phi + 2\phi \frac{k_{CNT}}{k_{CNT} - k_f} \ln \frac{k_{CNT} + k_f}{2k_f}}{1 - \phi + 2\phi \frac{k_f}{k_{CNT} - k_f} \ln \frac{k_{CNT} + k_f}{2k_f}}, \end{aligned} \right\} \quad (7.7)$$

and

$$\left. \begin{aligned}
 \rho_{hnf} &= \rho_f(1 - \phi_2) \left( (1 - \phi_1) + \phi_1 \left( \frac{\rho_{SWCNT}}{\rho_f} \right) \right) + \phi_2 \left( \frac{\rho_{MWCNT}}{\rho_f} \right), \\
 (\rho c_p)_{hnf} &= \phi_2 \left( \frac{(\rho c_p)_{MWCNT}}{(\rho c_p)_f} \right) + (\rho c_p)_f(1 - \phi_2) \left( (1 - \phi_1) + \phi_1 \frac{(\rho c_p)_{SWCNT}}{(\rho c_p)_f} \right), \\
 \frac{k_{hnf}}{k_{bf}} &= \frac{1 - \phi_2 + 2\phi_2 \frac{k_{MWCNT}}{k_{MWCNT} - k_f} \ln \frac{k_{MWCNT} + k_f}{2k_f}}{1 - \phi_2 + 2\phi_2 \frac{k_f}{k_{MWCNT} - k_f} \ln \frac{k_{MWCNT} + k_f}{2k_f}}, \quad \mu_{hnf} = \frac{\mu_f}{(1 - \phi_1)^{2.5}(1 - \phi_2)^{2.5}}, \\
 \frac{k_{bf}}{k_f} &= \frac{1 - \phi_1 + 2\phi_1 \frac{k_{SWCNT}}{k_{SWCNT} - k_f} \ln \frac{k_{SWCNT} + k_f}{2k_f}}{1 - \phi_1 + 2\phi_1 \frac{k_f}{k_{SWCNT} - k_f} \ln \frac{k_{SWCNT} + k_f}{2k_f}}.
 \end{aligned} \right\} \quad (7.8)$$

In Eqs. (7.7) and (7.8),  $(\phi_1, \phi_2)$  denote the solid volume fractions of CNTs and hybrid CNTs,  $(\rho_f, \rho_{nf}, \rho_{CNT})$  the base fluid, nanofluid and carbon nanotubes densities,  $(nf, hnf)$  exhibit nanofluid and hybrid nanofluid,  $(\mu_f, \mu_{nf}, \mu_{hnf})$  the base liquids, effective nanofluid and hybrid nanofluid dynamic viscosity,  $(k_{hnf}, k_{nf}, k_f)$  the thermal conductivities of CNTs and hybrid CNTs and base liquid and  $((\rho c_p)_{nf}, (\rho c_p)_{hnf})$  the nanoliquid and hybrid nanoliquid effective heat capacities.

**Table 7.1:** Thermo-physical characteristics of carbon nanotubes (SWCNT and MWCNT) and engine oil.

Constituents	$\rho(kg/m^3)$	$c_p(J/kgK)$	$k(W/mk)$
<i>SWCNT</i>	2600	425	6600
<i>MWCNT</i>	1600	796	3000
Engine oil	884	1910	0.144

### 7.1.2 Dimensionless variables and transformed systems

Transformations are expressed as follows:

$$\left. \begin{aligned}
 \psi &= \sqrt{U_w \nu_f x R} f(\eta), \quad u = \frac{U_0 x}{l} f'(\eta), \quad v = -\sqrt{\frac{\nu_f U_0}{l} \frac{R}{r}} f(\eta), \\
 \theta(\eta) &= (T - T_m)/(T_\infty - T_m), \quad \eta = \sqrt{\frac{U_0}{l \nu_f}} \left( \frac{r^2 - R^2}{2R} \right).
 \end{aligned} \right\} \quad (7.9)$$

After implementing the above transformations Eq. (7.1) is verified and other Eqs. become

$$\left. \begin{aligned} & \frac{1}{(1-\phi_1)^{2.5}(1-\phi_2)^{2.5}(1-\phi_2)} \left( (1-\phi_1) + \phi_1 \left( \frac{\rho_{SWCNT}}{\rho_f} \right) \right) + \phi_2 \left( \frac{\rho_{MWCNT}}{\rho_f} \right) \left[ (1 + 2\eta\gamma_c) f''' + 2\gamma_c f'' \right] \\ & + f f'' + A^2 - f'^2 = 0, \end{aligned} \right\} \quad (7.10)$$

$$\left. \begin{aligned} & \frac{1}{\text{Pr}} \left( \frac{\frac{k_{hnf}}{k_f} + Rd}{(1-\phi_2) \left( (1-\phi_1) + \phi_1 \left( \frac{\rho_{c_p} SWCNT}{(\rho_{c_p})_f} \right) \right) + \phi_2 \left( \frac{\rho_{c_p} MWCNT}{(\rho_{c_p})_f} \right)} \right) \left[ (1 + 2\eta\gamma_c) \theta'' + 2\gamma_c \theta' \right] \\ & - \text{Pr} f \theta' + \frac{1}{(1-\phi_1)^{2.5}(1-\phi_2)^{2.5}(1-\phi_2)} \left( (1-\phi_1) + \phi_1 \left( \frac{\rho_{c_p} SWCNT}{(\rho_{c_p})_f} \right) \right) + \phi_2 \left( \frac{\rho_{c_p} MWCNT}{(\rho_{c_p})_f} \right) \text{Pr} Ec (1 + 2\eta\gamma_c) f''^2 = 0, \end{aligned} \right\} \quad (7.11)$$

$$\left. \begin{aligned} & f'(0) = 1 + \gamma_s f''(0), \quad \theta(0) = 0, \\ & f'(\infty) \rightarrow A, \quad \theta(\infty) \rightarrow 1, \\ & \text{Pr} \left( (1 - \phi_2) \left( (1 - \phi_1) + \phi_1 \left( \frac{\rho_{c_p} SWCNT}{(\rho_{c_p})_f} \right) \right) + \phi_2 \left( \frac{\rho_{c_p} MWCNT}{(\rho_{c_p})_f} \right) \right) f(0) + Me \frac{k_{hnf}}{k_f} \theta'(0) = 0, \end{aligned} \right\} \quad (7.12)$$

where  $\text{Pr} \left( = \frac{(\rho_{c_p})_f}{k_f} \right)$  signifies the Prandtl number,  $\gamma_c \left( = \sqrt{\frac{l\nu_f}{U_0 R^2}} \right)$  manifests curvature variable,  $A = \left( \frac{U_\infty}{U_0} \right)$  the ratio of velocities,  $Me = \frac{c_p(T_\infty - T_m)}{\lambda_1 + c_s(T_m - T_0)}$  the melting variable,  $Rd = \frac{16\sigma^* T_\infty^3}{k_f k^*}$  the radiation parameter,  $\gamma_s = \sqrt{\frac{\mu_f U_0 \rho_f}{l}}$  the slip parameter,  $Ec = \frac{U_w^2}{(c_p)_f (T_f - T_\infty)}$  the Eckert number and prime symbolizes differentiation via  $\eta$ . It is important to disclose that for  $\phi_1 = \phi_2 = 0$ , the conventional liquid (engine oil) situation is recovered. When  $\phi_1 \neq 0$  and  $\phi_2 = 0$ , then engine oil based CNTs nanomaterials has been achieved. The relation  $\phi_2 \neq \phi_1 \neq 0$  must be satisfied for SWCNT-MWCNT/engine oil hybrid nanofluid. Furthermore  $c_p(T_\infty - T_m)$  and  $\lambda_1 + c_s(T_m - T_0)$  denote the Stefan numbers of solid and liquid phases respectively.

### 7.1.3 Physical quantities

Physical quantities such as drag force ( $C_{fx}$ ) and temperature gradient ( $Nu_x$ ) are given by:

$$\left. \begin{aligned} C_{fx} &= \frac{2\tau_{wx}}{\rho_f U_w^2}, \\ Nu_x &= \frac{r q_w}{k_f (T_\infty - T_m)}, \end{aligned} \right\} \quad (7.13)$$

where  $(\tau_{wx})$  and  $(q_w)$  are the wall shear stress and heat flux i.e.,

$$\left. \begin{aligned} \tau_{wx} &= \mu_{hnf} \left( \frac{\partial u}{\partial r} \right) \Big|_{r=R}, \\ q_w &= -k_{nf} \left( \frac{\partial T}{\partial r} \right) + q_r \Big|_{r=R}. \end{aligned} \right\} \quad (7.14)$$

Dimensionless versions of  $(C_{fx})$  and  $(Nu_x)$  are

$$\left. \begin{aligned} \text{Re}_x^{0.5} C_{fx} &= \frac{1}{(1-\phi_1)^{25/10}(1-\phi_2)^{25/10}} f''(0), \\ \text{Re}_x^{-0.5} Nu_x &= - \left( \frac{K_{hnf}}{k_f} + Rd \right) \theta'(0), \end{aligned} \right\} \quad (7.15)$$

in which local Reynolds number is symbolized as  $\text{Re}_x = \frac{xU_w}{\nu_f}$ .

## 7.2 Entropy production ( $N_G$ ) and Bejan number (Be)

Following Bejan the volumetric rate of entropy production for flow of nano and hybrid nanofluid past a stretching cylinder is communicated. In present study the generation of entropy is due to two factors i.e. irreversibility due to liquid friction and irreversibility due to heat transport. All other factors of irreversibility like diffusive, porosity, permeability and magnetic irreversibility are neglected. Additionally the system is considered in a state of local thermodynamic equilibrium. The volumetric rate of entropy is

$$E_G = \frac{\mu_{hnf}}{T_\infty} \left( \frac{\partial u}{\partial r} \right)^2 + \left( \frac{k_f}{T_\infty^2} \right) \left[ \left( \frac{k_{hnf}}{k_f} \right) \left( \frac{\partial T}{\partial r} \right)^2 + \frac{16\sigma^* T_\infty^2}{3k^*} \left( \frac{\partial T}{\partial r} \right)^2 \right]. \quad (7.16)$$

Entropy generation quantity ( $N_G$ ) can be stated as

$$N_G = \frac{\text{Generation rate of volumetric entropy}}{\text{Generation rate of characteristic entropy}}, \quad (7.17)$$

or

$$N_G = \frac{E_G}{E_0}, \quad (7.18)$$

where generation rate of characteristic entropy is  $E_0 = \frac{k_f(T_\infty - T_m)^2}{T_\infty^2 l^2}$ .



On utilizing variables (7.9), Eqs. (7.16) and (7.18) take the form

$$N_G = \frac{\text{Re}_l}{X} \left( \frac{k_{hnf}}{k_f} + Rd \right) (1 + 2\eta\gamma_c)\theta'^2 + \frac{\text{Re}_l Br}{X \alpha_T} \frac{(1 + 2\eta\gamma_c)}{(1 - \phi_1)^{25/10}(1 - \phi_2)^{25/10}} f''^2, \quad (7.19)$$

where  $X = x/l$ ,  $\alpha_T = \frac{(T_\infty - T_m)}{T_\infty}$  the non-dimensional temperature difference,  $Br = \text{Pr} Ec$  the Brinkman number and  $\text{Re}_l = \frac{U_w l}{\nu_f}$  the Reynolds number. Let us define another essential dimensionless variable known as Bejan number which is employed to check whether entropy generation due to heat dominates over liquid friction or vice versa. It is defined as

$$Be = \frac{\text{Entropy generation due to heat}}{\text{Total entropy generation}}, \quad (7.20)$$

or

$$Be = \frac{\frac{\text{Re}_l}{X} \left( \frac{k_{hnf}}{k_f} + Rd \right) (1 + 2\eta\gamma_c)\theta'^2}{\frac{\text{Re}_l}{X} \left( \frac{k_{hnf}}{k_f} + Rd \right) (1 + 2\eta\gamma_c)\theta'^2 + \frac{\text{Re}_l Br}{X \alpha_T} \frac{(1 + 2\eta\gamma_c)}{(1 - \phi_1)^{25/10}(1 - \phi_2)^{25/10}} f''^2}. \quad (7.21)$$

The values of  $Be$  more or less than  $\frac{1}{2}$  elucidates that the contribution of irreversibility due to heat transfer to a total entropy generation is higher/less when compared with irreversibility due to liquid friction. Both effects are same when  $Be = \frac{1}{2}$ . Besides that for  $Be = 0$ , the entropy production due to liquid friction dominates while for  $Be = 1$  the heat transfer irreversibility effects become predominates.

### 7.3 Computational scheme and discussion

After utilization of transformations the governing systems are solved through NDSolve technique. Numerical approximations are performed to obtain the outcomes by considering different values of physical variables i.e.  $\gamma_c = \gamma_s = A = Rd = 0.2$ ,  $Me = 0.3$  and  $\phi_2 = \phi_1 = 0.04$ . These values remain unchanged throughout analysis except some variations in respective figures. Figs. (7.2) – (7.17) show the entropy generation ( $N_G$ ), Nusselt number ( $Nu_x$ ), temperature ( $\theta(\eta)$ ), skin friction ( $C_{f_x}$ ) and velocity ( $f'(\eta)$ ) of hybrid nanofluid and nanofluid for distinct variables of interest. We select  $\text{Pr} = 6450$  (for engine oil) in present work. Thermo-physical attributes of both types of CNTs and engine oil are displayed in Tables (7.1). Additionally it is presumed that nano and hybrid nanofluids have same concentration. Fig. (7.2) explores that how veloc-

ity of fluid is effected by  $\gamma_s$  for both hybrid nanomaterials (SWCNT-MWCNT/engine oil) and nanomaterials (SWCNT/engine oil). Here velocity curves enhance for higher  $\gamma_s$ . Velocity  $f'(\eta)$  is less in case of SWCNT/engine oil) situation. Physically an increment in  $\gamma_s$  means liquid gains partially stretching velocity which decays the fluid velocity. Influence of  $Me$  on  $f'(\eta)$  is expressed in Fig. 7.3. Velocity enhances for both nano and hybrid phases by increasing  $Me$ . In fact temperature gap between ambient and melting surface increases due to enhancement of sensible heat. Therefore velocity  $f'(\eta)$  increases. Furthermore the impact of hybrid nanofluid dominates over nanofluid. Fig. (7.4) elucidates variation in  $f'(\eta)$  against  $\gamma_c$ . It is noted that velocity near the surface reduces whereas it enhances far away from stretching cylinder. The outcomes of volumetric fraction on  $f'(\eta)$  is arranged in Fig. (7.5). Velocity  $f'(\eta)$  grows up for larger volumetric fraction for both cases due to higher convective flow. This Fig. also explores that velocity curves are remarkably more for hybrid nanomaterials rather than nanomaterials. Fig. (7.6) presents the feature of temperature  $\theta(\eta)$  with variation of  $Rd$ . One can see that  $\theta(\eta)$  enhances for both nano and hybrid phases. In fact rise in strength of thermal layer is because of transport of radiant energy to liquid particles by higher  $Rd$ . Thermal field  $\theta(\eta)$  improves for higher  $Ec$  in both nano and hybrid phases (see Fig. 7.7). Physically higher  $Ec$  contribute more dissipative energy to nanomaterials which causes to augment the thermal field  $\theta(\eta)$ . Furthermore this Fig. also declared that hybrid nanofluid provided more dissipative energy than nanoliquid. Fig. (7.8) exhibits the outcomes of  $\gamma_c$  on  $\theta(\eta)$ . Intensification in  $\gamma_c$  significantly enhances  $\theta(\eta)$  in both cases. It is also found that hybrid nanomaterials show best performance in comparison with nanomaterials. Higher  $\gamma_c$  leads to decay the cylinder surface due to which less nanomaterials are stick to surface. Since conduction process is more near the surface, therefore  $\theta(\eta)$  enhances. Effect of  $Me$  on  $\theta(\eta)$  is illustrated in Fig. (7.9). From this Fig. initially the temperature decays because temperature difference between melting surface and ambient liquid enhances. After that  $\theta(\eta)$  starts to enhance. Fig. (7.10) exhibits that how  $\theta(\eta)$  of fluid is effected by nanoparticles volumetric fraction ( $\phi_2$ ). Temperature enhances for higher  $\phi_2$ . Furthermore this Fig. provides the comparative study of nanomaterials, hybrid non-material and base liquid. Clearly it is found that hybrid nanomaterials have more contribution to increase  $\theta(\eta)$  than nanomaterials.

The concept of  $(N_G(\eta))$  in liquid is included because of viscosity and thermal diffusion. Thus

it is important to explore the disorderedness in system to compute its capability. Fig. (7.10) – (7.12) are displayed to study the behaviors of  $Rd$ ,  $\alpha_1$  and  $\phi_1/\phi_2$  on  $N_G(\eta)$ . Fig. (7.10) depicts the variation in  $N_G(\eta)$  due to  $\alpha_1$ . Since entropy is directly linked with temperature. Therefore an increase in  $\alpha_1$  corresponds to more temperature (which causes entropy to enhance). Moreover reasonable performance is displayed by hybrid nanomaterials followed by nanomaterials and regular liquid. Fig. (7.11) reveals that an increment  $Rd$  decays the entropy  $N_G(\eta)$  for both cases of nanomaterials. Fig. (7.12) provides the comparative study of engine oil ( $\phi_1 = \phi_2 = 0$ ), nanofluid ( $\phi_1 \neq, \phi_2 = 0$ ) and hybrid nanoliquid ( $\phi_1 \neq \phi_2 \neq 0$ ). This Fig. witnesses that hybrid nanomaterials greatly effect the entropy  $N_G(\eta)$  when compared with common nanomaterials and based liquid. An intensification in volumetric fraction ( $\phi_2$ ) reduces the skin friction  $C_{fx}$ . This behavior is shown via Fig. (7.13). Further this Fig. reflects that reduction in skin friction is more in case of hybrid nanomaterials than nanomaterials and base liquid. It is observed from Figs. (7.14) and (7.15) that  $C_{fx}$  shows a reverse tendency towards  $\gamma_c$  and  $\gamma_s$ . The values of skin friction  $C_{fx}$  are higher for (SWCNT-MWCNT/engine oil) than (SWCNT/engine oil). Fig. (7.16) is drawn to explore the feature of volumetric fraction  $\phi_2$  on  $Nu_x$ . It is found that  $Nu_x$  decays for  $\phi_2$ .  $Nu_x$  is also higher for hybrid nanoliquid when compared with common nanofluid and base liquid.

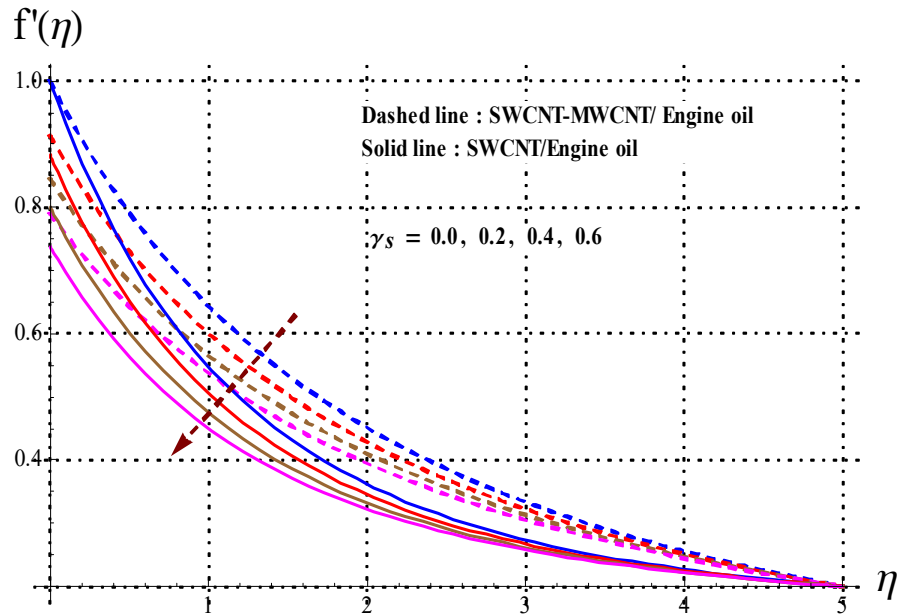


Fig. 7.2.  $f'(\eta)$  vs  $\gamma_s$ .

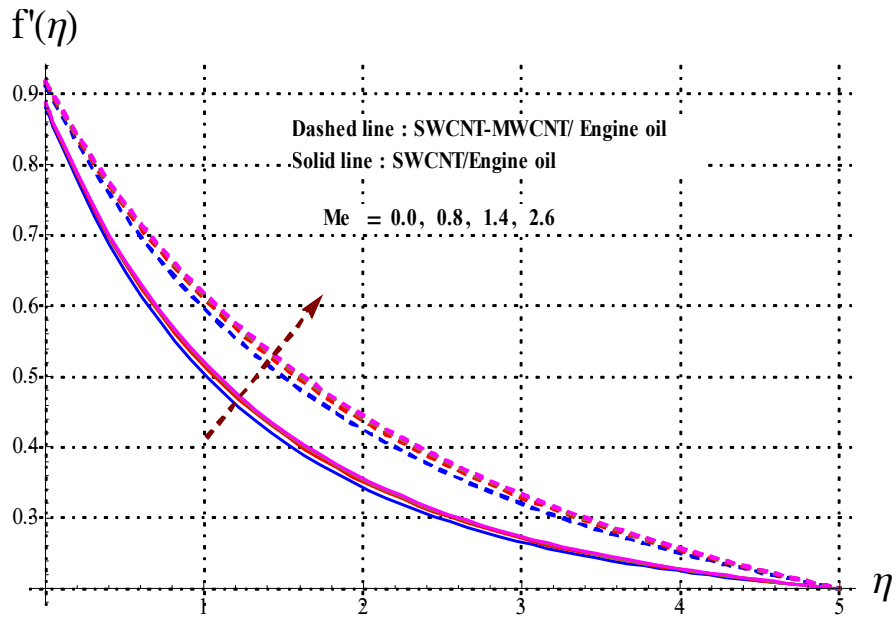


Fig. 7.3.  $f'(\eta)$  vs  $Me$ .

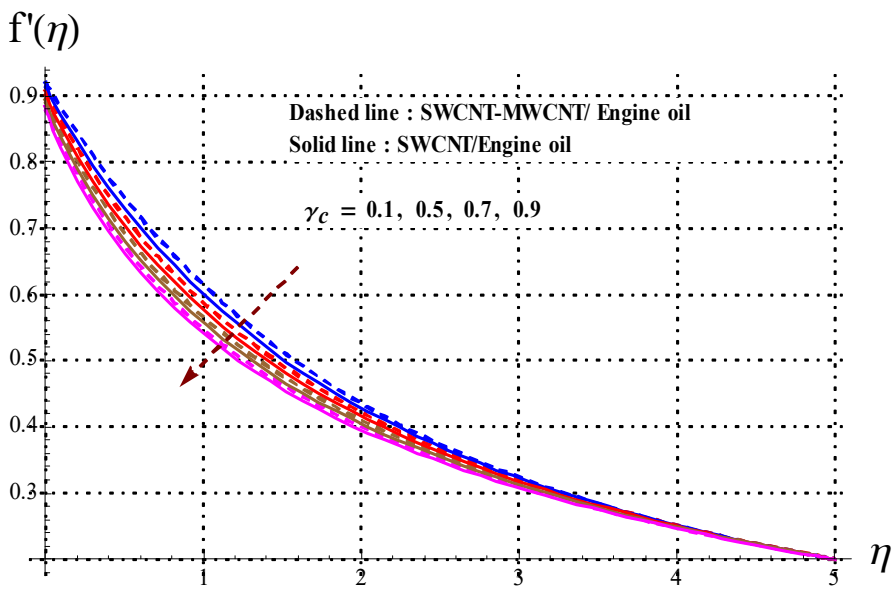


Fig. 7.4.  $f'(\eta)$  vs  $\gamma_c$ .

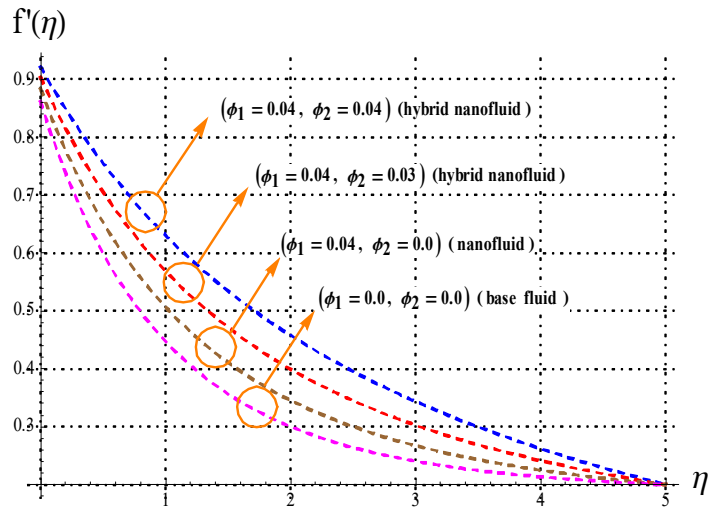


Fig. 7.5.  $f'(\eta)$  vs  $\phi_1/\phi_2$ .

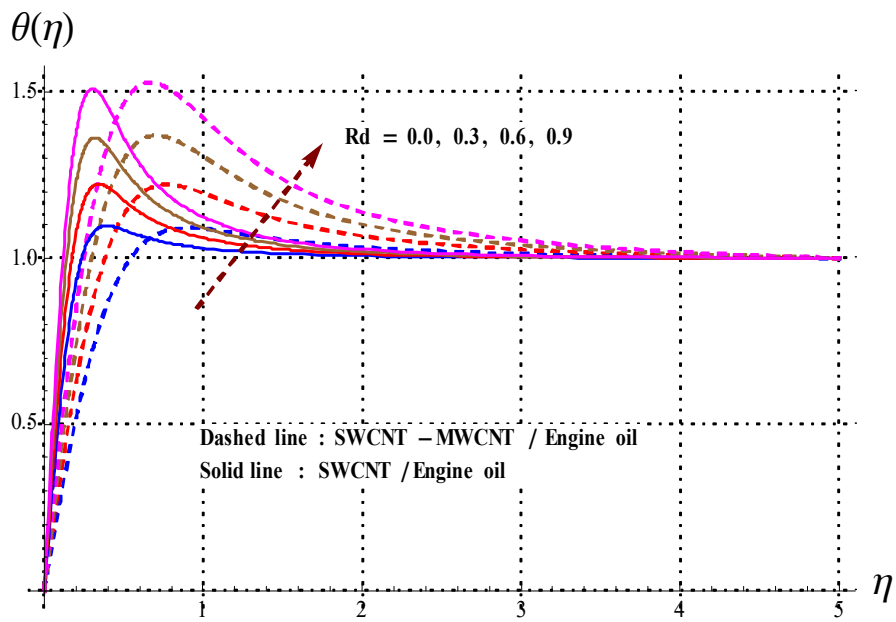


Fig. 7.6.  $\theta(\eta)$  vs  $Rd$ .

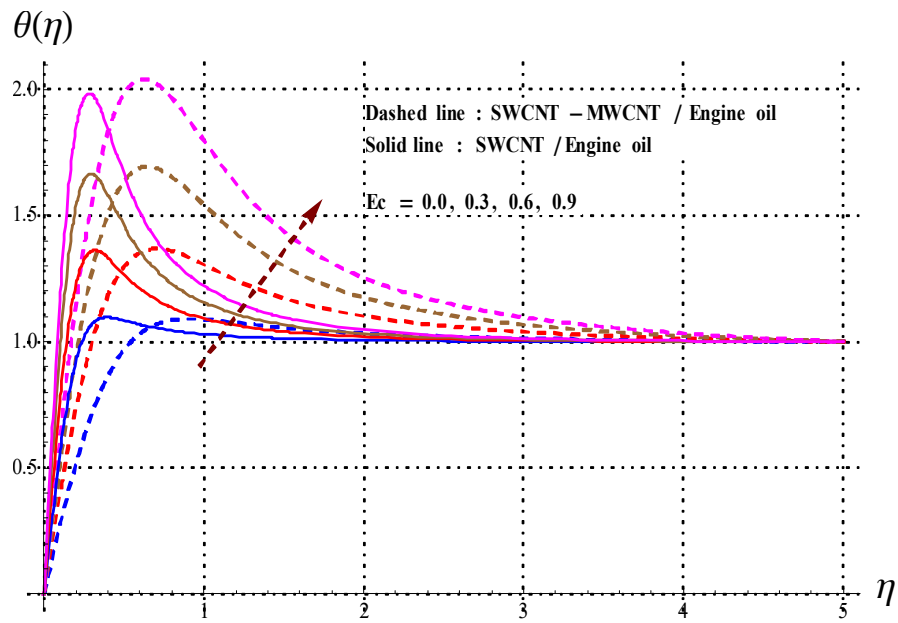


Fig. 7.7.  $\theta(\eta)$  vs  $Ec$ .

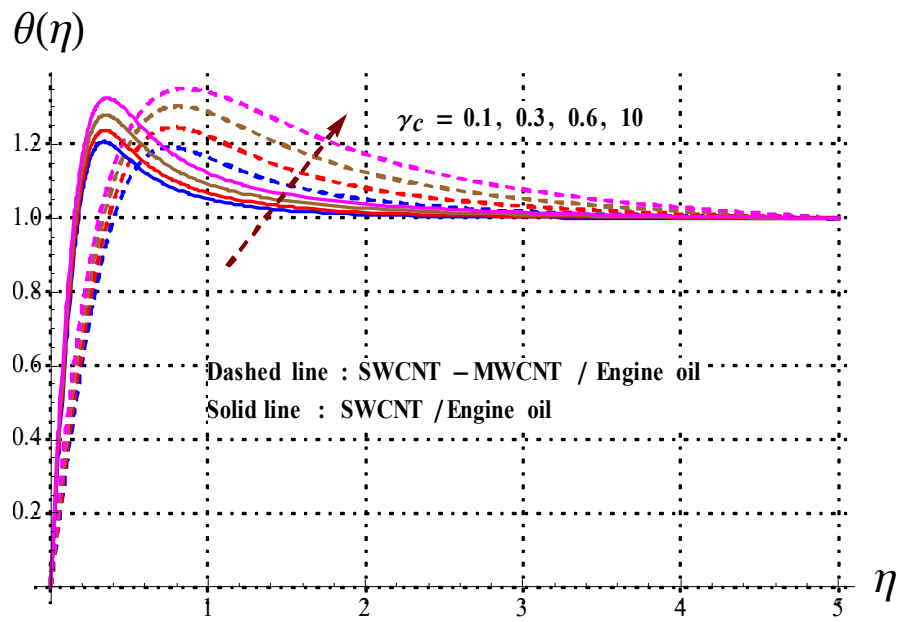


Fig. 7.8.  $\theta(\eta)$  vs  $\gamma_c$ .

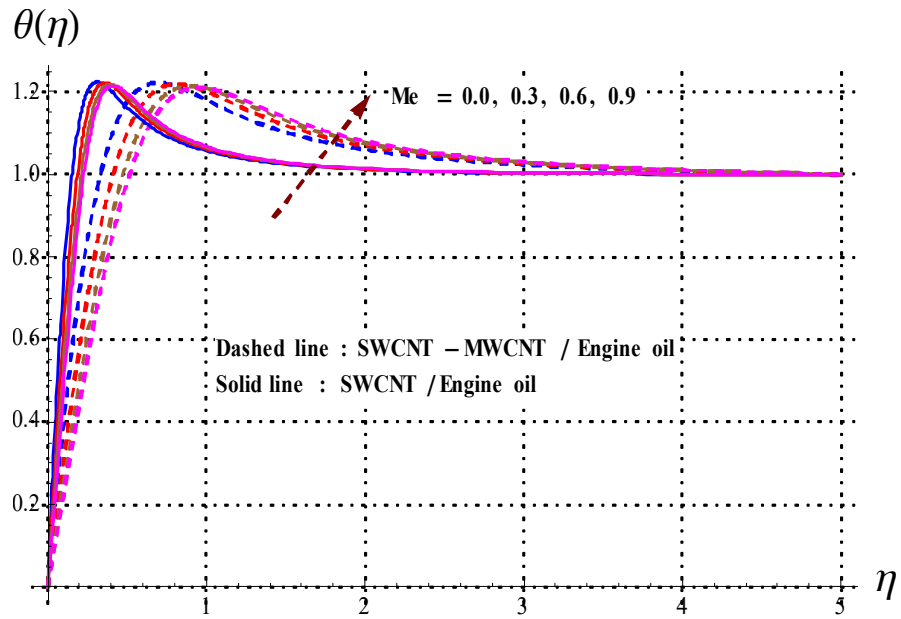


Fig. 7.9.  $\theta(\eta)$  vs  $Me$ .

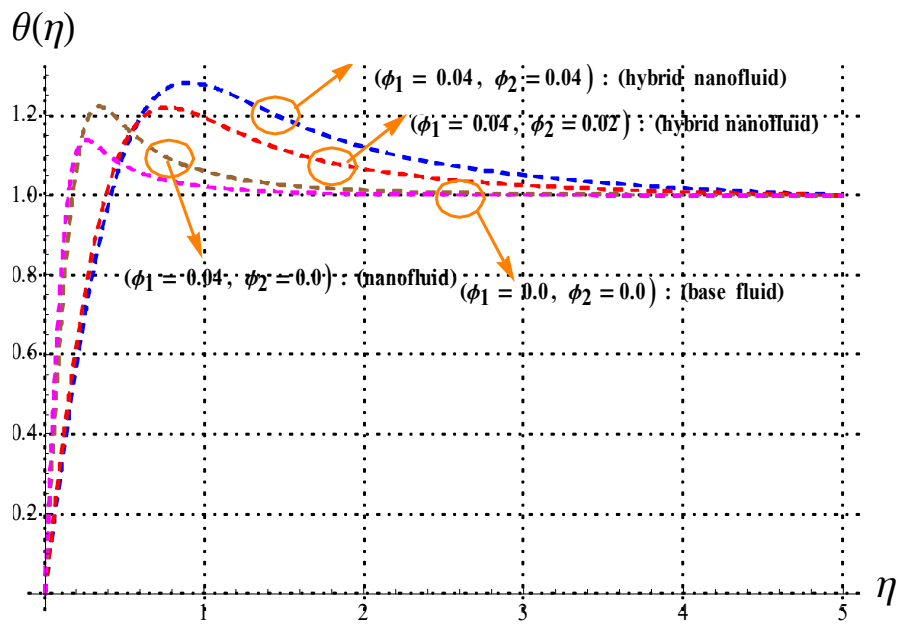


Fig. 7.10.  $\theta(\eta)$  vs  $\phi_1/\phi_2$ .

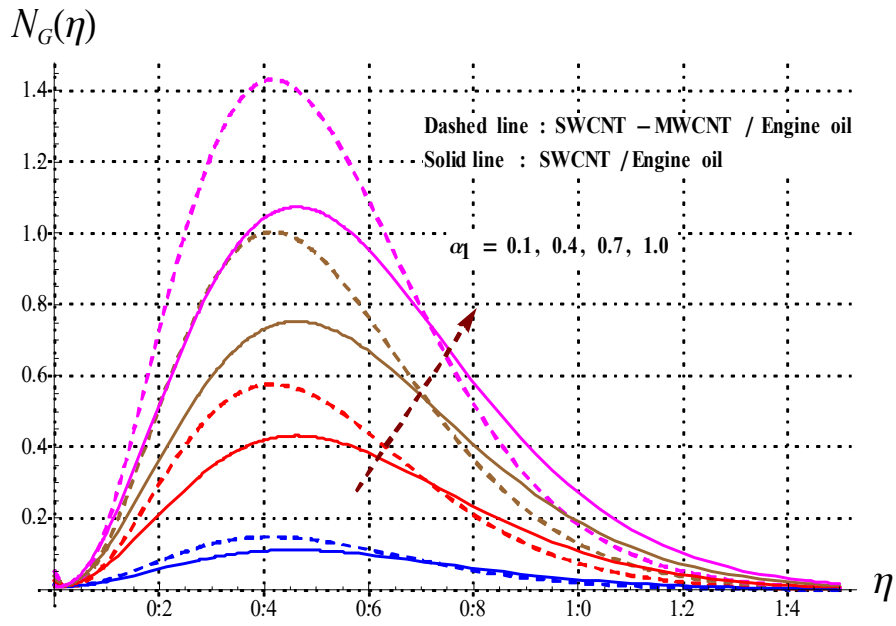


Fig. 7.11.  $N_G(\eta)$  vs  $\alpha_1$ .

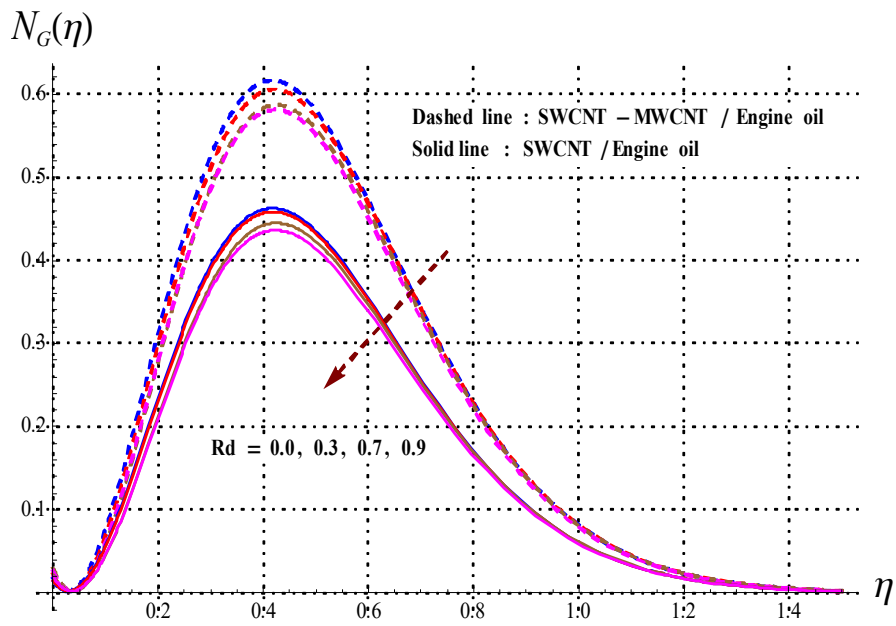


Fig. 7.12.  $N_G(\eta)$  vs  $Rd$ .



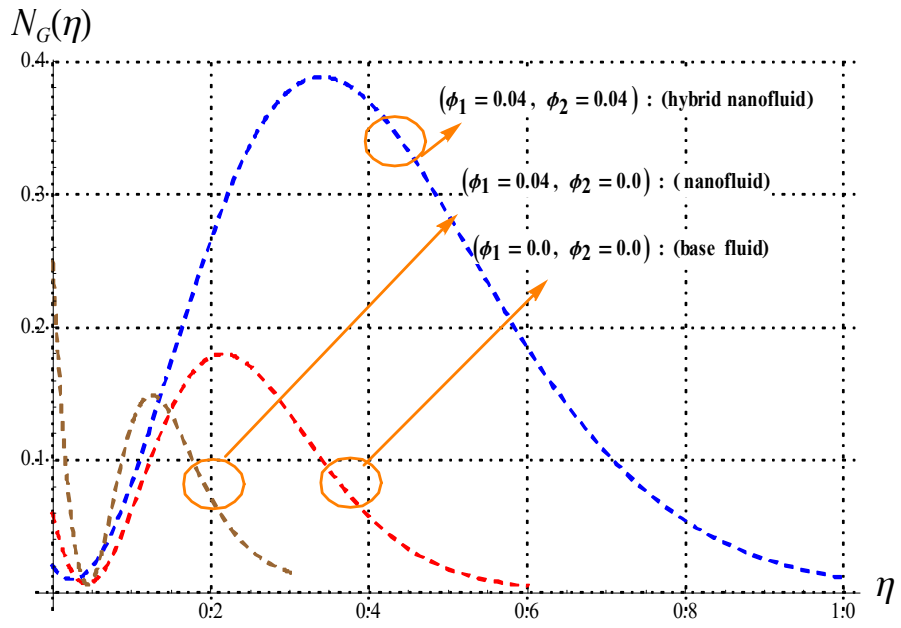


Fig. 7.13.  $N_G(\eta)$  vs  $\phi_1/\phi_2$ .

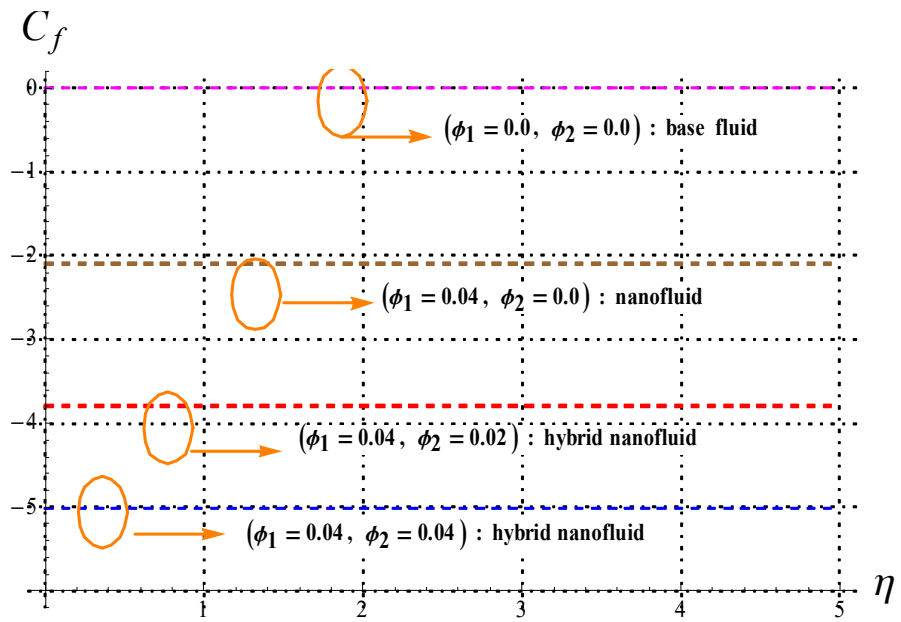


Fig. 7.14.  $C_{fx}$  vs.  $\phi_1/\phi_2$ .

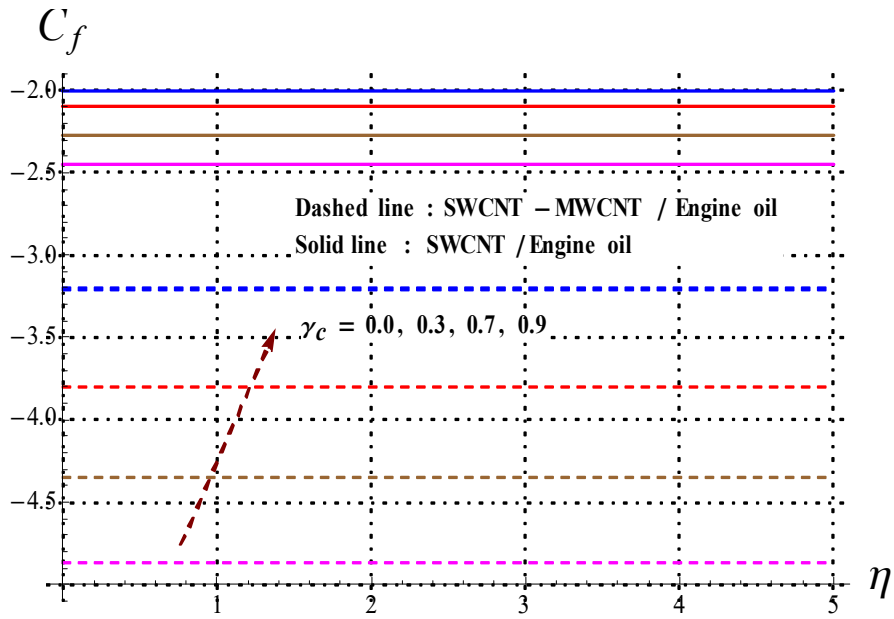


Fig. 7.15.  $C_{fx}$  vs.  $\gamma_c$ .

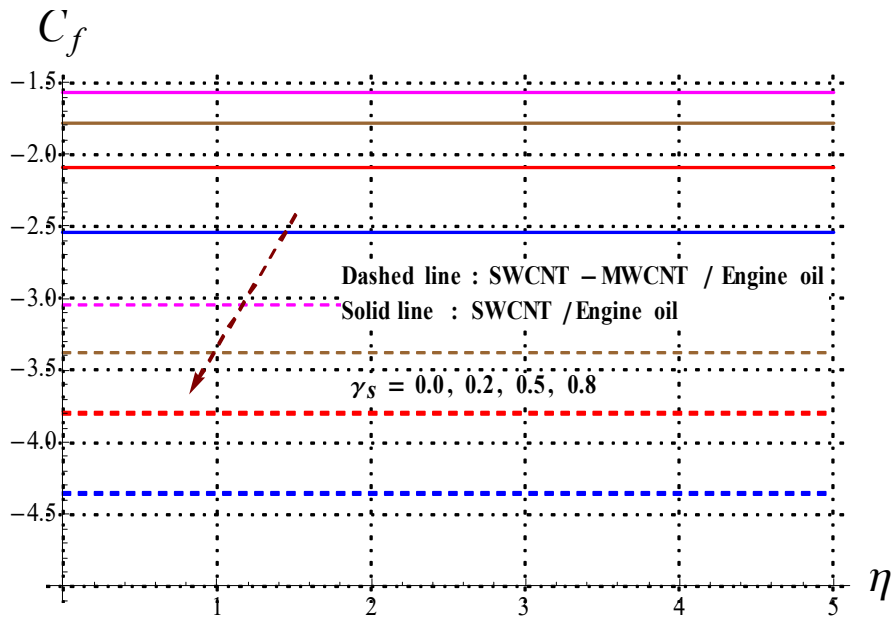


Fig. 7.16.  $C_{fx}$  vs.  $\gamma_s$ .

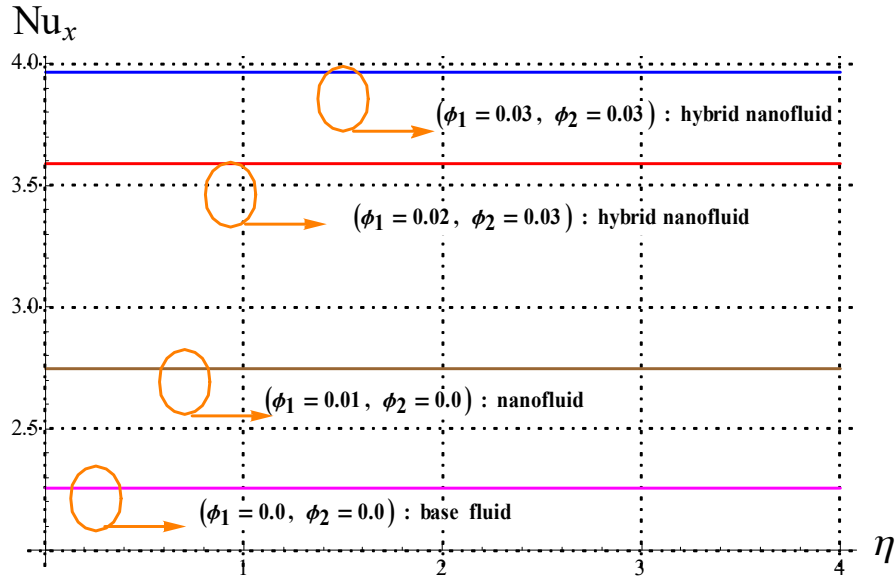


Fig. 7.17.  $Nu_x$  vs.  $\phi_1/\phi_2$ .

## 7.4 Final remarks

- The key outcomes of current chapter are:
- Velocity has decaying behavior for larger curvature and slip variables.
- Intensification in  $(\theta(\eta))$  is observed for larger  $Rd$ ,  $Me$ ,  $Ec$ ,  $\phi_2$  and  $\phi_1$ .
- Decay in entropy production rate ( $N_G$ ) is noted for larger  $Rd$  whereas opposite trend is seen for higher  $\phi_1$  and  $\alpha_1$ .
- Skin friction manifests reverse tendency towards  $\gamma_c$  and  $\gamma_s$ .
- Nusselt number ( $Nu_x$ ) inversely varies with  $\phi_2$ .
- As expected hybrid nanomaterials impact is more in whole analysis than nanomaterials and base liquid.

## Chapter 8

# Optimization of entropy production in flow of hybrid nanomaterials via porous space

Irreversibility analysis in Darcy-Forchheimer flow of nanomaterials with (SWCNT) and (MWCNT) hybrid nanoparticles/kerosene oil mixture is presented. Xue's and newly modified Xue's models are implemented for physical feature of empirical relations (thermal conductivity, density and specific heat). Analysis of entropy is performed to estimate the disorder within the thermo-physical frame. The governing flow expressions have been computed through numerical scheme. Graphical illustrations and tables are made to investigate the effects of noteworthy embedding variables on various physical distributions. Moreover, detailed analysis for temperature and velocity gradients against pertinent parameters are provided. Our findings reflect that temperature upgraded for both nanoliquid and hybrid nanoliquid by higher Eckert number and heat source parameter while a contrary trend is seen for temperature gradient. Skin friction escalates for inertia coefficient, rotation parameter and porosity parameter. There is remarkable increase for SWCNT-MWCNT/kerosene oil hybrid nanofluid when compared with SWCNT/kerosene oil nanoliquid. As a whole hybrid nanomaterials have great influence throughout our analysis when compared with regular nanomaterials.

## 8.1 Mathematical formulation and modeling of hybrid nanofluid

Present problem comprises a mixture of hybrid nanomaterials SWCNT and MWCNT which are dispersed in kerosene oil as a regular liquid. Thermo-physical features of hybrid liquid are considered to rely on volumetric fraction of nanoparticles ( $\phi_1, \phi_2$ ). Flow is considered in porous space by utilizing Darcy-Forchheimer model. The wall velocity is expressed as  $U_w = ax$  (with constant  $a > 0$ ) along x-axis while stretching along y-axis is ignored ( $v = 0$ ). Additionally whole system rotates with angular velocity ( $\omega$ ). The surface temperature is controlled via convection. Irreversibility analysis in porous space is considered. The graphical view of current problem has been disclosed in Fig. 8.1. Expressions that model present problem in view of above mentioned considerations are:

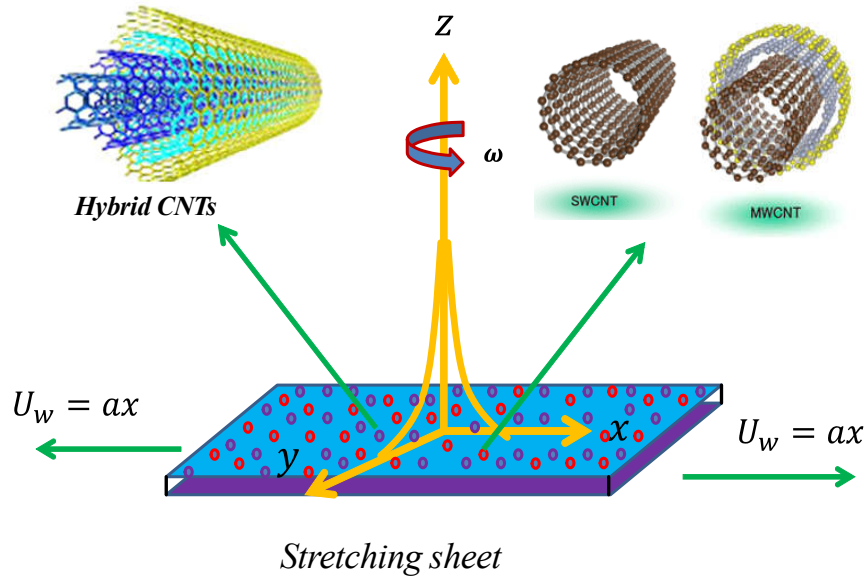


Fig. 8.1. Flow configuration.

$$\frac{\partial u}{\partial x} + \frac{\partial v}{\partial y} + \frac{\partial w}{\partial z} = 0, \quad (8.1)$$

$$u \frac{\partial u}{\partial x} + v \frac{\partial u}{\partial y} + w \frac{\partial u}{\partial z} - 2\omega v = \nu_{hnf} \left( \frac{\partial^2 u}{\partial z^2} \right) - \frac{\nu_{hnf}}{K_p} u - F u^2, \quad (8.2)$$

$$u \frac{\partial v}{\partial x} + v \frac{\partial v}{\partial y} + w \frac{\partial v}{\partial z} + 2\omega u = \nu_{hnf} \left( \frac{\partial^2 v}{\partial z^2} \right) - \frac{\nu_{hnf}}{K_p} v - F v^2, \quad (8.3)$$

$$u \frac{\partial T}{\partial x} + v \frac{\partial T}{\partial y} + w \frac{\partial T}{\partial z} = \frac{k_{hnf}}{(\rho c_p)_{hnf}} \frac{\partial^2 T}{\partial z^2} + \frac{\nu_{hnf}}{K_p (c_p)_{hnf}} (u^2 + v^2) + \frac{Q(T-T_\infty)}{(\rho c_p)_{hnf}} \left. \vphantom{\frac{\partial T}{\partial z}} \right\} \quad (8.4)$$

$$+ \frac{\mu_{hnf}}{(\rho c_p)_{hnf}} \left[ \left( \frac{\partial u}{\partial z} \right)^2 + \left( \frac{\partial v}{\partial z} \right)^2 \right],$$

where  $(u, v, w)$  designate the respective velocity components in  $(x, y, z)$  directions,  $\nu_{hnf}$  the hybrid nanofluid kinematic viscosity,  $F = \frac{C_b}{x\sqrt{K_p}}$  the porous medium non-uniform inertia coefficient,  $K_p$  the permeability of porous space,  $C_b$  the drag coefficient  $(T, T_\infty)$  the liquid and ambient temperatures and  $Q$  heat absorption/generation.

### 8.1.1 Empirical relations and thermo-physical features for nanomaterials

**Table 8.1:** Empirical relations for thermo-physical features of nanofluid (CNTs – kerosene oil) and hybrid nanoliquid (SWNT – MWNT-kerosene oil).

Properties	Nanofluid	Hybrid nanofluid
Density	$\rho_{nf} = \rho_f(1 - \phi) + \rho_{CNT}\phi,$	$\rho_{hnf} = \rho_f(1 - \phi_2) \left( (1 - \phi_1) + \phi_1 \left( \frac{\rho_{SWCNT}}{\rho_f} \right) + \phi_2 \left( \frac{\rho_{MWNT}}{\rho_f} \right) \right)$
Viscosity	$\mu_{nf} = \frac{\mu_f}{(1-\phi_1)^{25/10}}$	$\mu_{hnf} = \frac{\mu_f}{(1-\phi_1)^{2.5}(1-\phi_2)^{2.5}}$
Heat capacity	$(\rho c_p)_{nf} = (\rho c_p)_f(1 - \phi) + (\rho c_p)_{CNT}\phi$	$(\rho c_p)_{hnf} = \phi_2 \left( \frac{(\rho c_p)_{MWNT}}{(\rho c_p)_f} \right) + (\rho c_p)_f(1 - \phi_2) \left( (1 - \phi_1) + \phi_1 \frac{(\rho c_p)_{SWCNT}}{(\rho c_p)_f} \right)$
Thermal conductivity	$\frac{k_{nf}}{k_f} = \frac{1-\phi+2\phi \frac{k_{CNT}}{k_{CNT}-k_f} \ln \frac{k_{CNT}+k_f}{2k_f}}{1-\phi+2\phi \frac{k_f}{k_{CNT}-k_f} \ln \frac{k_{CNT}+k_f}{2k_f}}$	$\frac{k_{hnf}}{k_{bf}} = \frac{1-\phi_2+2\phi_2 \frac{k_{MWNT}}{k_{MWNT}-k_f} \ln \frac{k_{MWNT}+k_f}{2k_f}}{1-\phi_2+2\phi_2 \frac{k_f}{k_{MWNT}-k_f} \ln \frac{k_{MWNT}+k_f}{2k_f}}$
		where
		$\frac{k_{bf}}{k_f} = \frac{1-\phi_1+2\phi_1 \frac{k_{SWCNT}}{k_{SWCNT}-k_f} \ln \frac{k_{SWCNT}+k_f}{2k_f}}{1-\phi_1+2\phi_1 \frac{k_f}{k_{SWCNT}-k_f} \ln \frac{k_{SWCNT}+k_f}{2k_f}}$

In above table  $(nf, hnf)$  manifest nanofluid and hybrid nanofluid,  $(\phi_1, \phi_2)$  the solid volume fractions of CNTs and hybrid CNTs,  $(\rho_f, \rho_{nf}, \rho_{CNT})$  the base fluid, nanofluid and carbon nanotubes densities,  $(\mu_f, \mu_{nf}, \mu_{hnf})$  the base liquids, effective nanofluid and hybrid nanofluid dynamic viscosity,  $((\rho c_p)_{nf}, (\rho c_p)_{hnf})$  the nanoliquid and hybrid nanoliquid effective heat capacity and  $(k_{hnf}, k_{nf}, k_f)$  the thermal conductivities of CNTs and hybrid CNTs and base liquid.

**Table 8.2:** Thermal and physical features of carbon nanotubes (SWCNT and MWCNT) and kerosene oil [110, 111].

Constituents	$\rho(kg/m^3)$	$c_p(J/kgK)$	$k(W/mk)$
<i>CWNT</i>	2600	425	6600
<i>MWNT</i>	1600	796	3000
Kerosene oil	783	2090	0.15

### 8.1.2 Boundary conditions

We have

$$\left. \begin{aligned} v = 0, \quad u = U_w(x) = ax, \quad w = 0, \quad -k_{hnf} \frac{\partial T}{\partial z} = h_f(T_f - T) \text{ at } z = 0, \\ u \longrightarrow 0, \quad v \longrightarrow 0, \quad T \longrightarrow T_\infty \text{ as } z \longrightarrow \infty. \end{aligned} \right\} \quad (8.5)$$

In physical sense, the convective condition elaborates that a uniform temperature is utilized from below the surface which relates the heat flux linearly to the difference between  $T_f$  (hot liquid temperature below the surface) and  $T$  (liquid temperature above the surface).

### 8.1.3 Dimensionless variables

The transformations are taken as

$$\left. \begin{aligned} u = axf'(\eta), \quad v = axg(\eta), \quad w = -(a\nu_f)^{1/2}f(\eta), \\ \theta(\eta) = (T - T_\infty)/(T_f - T_\infty), \quad \eta = \left(\frac{a}{\nu_f}\right)^{1/2}z. \end{aligned} \right\} \quad (8.6)$$

Expression (1) is fulfilled identically by invoking  $u = axf'(\eta)$ ,  $v = -axg(\eta)$  and  $w = -(a\nu_f)^{1/2}f(\eta)$ .

### 8.1.4 Transformed systems

With the aid of Eq. (8.6), Eqs. (8.2)-(8.3) are reduced to the following forms:

$$\frac{1}{A_1A_2}(f''' - \lambda f') + ff'' + 2\Omega g - (1 + F_r)f'^2 = 0, \quad (8.7)$$

$$\frac{1}{A_1A_2}(g'' - \lambda g) + fg' - f'g - 2\Omega f' - F_r g^2 = 0, \quad (8.8)$$

$$\frac{1}{\text{Pr}} \left( \frac{A_4 A_3}{k_f} \right) \theta'' + A_1 A_3 Ec (f''^2 + g'^2) - f\theta' + A_1 A_3 \lambda Ec (f'^2 + g^2) + A_3 \delta = 0, \quad (8.9)$$

$$\left. \begin{aligned} f(0) = 0, \quad f'(0) = 1, \quad g(0) = 0, \quad \theta'(0) = -\frac{k_f}{k_{hnf}} \gamma (1 - \theta(0)), \\ f'(\infty) \rightarrow 0, \quad g(\infty) \rightarrow 0, \quad \theta(\infty) \rightarrow 0, \end{aligned} \right\} \quad (8.10)$$

where  $\Omega = \frac{\omega}{a}$  refers to rotation parameter,  $F_r = \frac{C_b}{K_p^{1/2}}$  the inertia coefficient,  $\lambda = \frac{\nu_f}{a K_p}$  the porosity parameter,  $Ec = \frac{U_w^2}{(c_p)_f (T_f - T_\infty)}$  the Eckert number,  $\text{Pr} = \frac{(\rho c_p)_f}{k_f}$  the Prandtl number,  $\delta = \frac{Q}{a(\rho c_p)_f}$  the heat absorption/generation,  $\gamma = \frac{h_f}{k_f} \sqrt{\frac{\nu_f}{a}}$  the Biot number, prime symbolizes differentiation via  $\eta$  and  $(A_1) - (A_4)$  are expressed by

$$A_1 = (1 - \phi_1)^{2.5} (1 - \phi_2)^{2.5}, \quad (8.11)$$

$$A_2 = (1 - \phi_2) \left( (1 - \phi_1) + \phi_1 \left( \frac{\rho_{SWCNT}}{\rho_f} \right) \right) + \phi_2 \left( \frac{\rho_{MWCNT}}{\rho_f} \right), \quad (8.12)$$

$$A_3 = (1 - \phi_2) \left( (1 - \phi_1) + \phi_1 \frac{(\rho c_p)_{SWCNT}}{(\rho c_p)_f} \right) + \phi_2 \left( \frac{(\rho c_p)_{MWCNT}}{(\rho c_p)_f} \right), \quad (8.13)$$

$$A_4 = \left( \frac{1 - \phi_2 + 2\phi_2 \frac{k_{MWCNT}}{k_{MWCNT} - k_f} \ln \frac{k_{MWCNT} + k_f}{2k_f}}{1 - \phi_2 + 2\phi_2 \frac{k_f}{k_{MWCNT} - k_f} \ln \frac{k_{MWCNT} + k_f}{2k_f}} \right) \left( \frac{1 - \phi_1 + 2\phi_1 \frac{k_{SWCNT}}{k_{SWCNT} - k_f} \ln \frac{k_{SWCNT} + k_f}{2k_f}}{1 - \phi_1 + 2\phi_1 \frac{k_f}{k_{SWCNT} - k_f} \ln \frac{k_{SWCNT} + k_f}{2k_f}} \right). \quad (8.14)$$

### 8.1.5 Physical quantities

Physical quantities such as drag force ( $C_{fx}$ ) and temperature gradient ( $Nu_x$ ) satisfy

$$\left. \begin{aligned} C_{fx} &= \frac{2\tau_{wx}}{\rho_f U_w^2}, \\ Nu_x &= \frac{xq_w}{k_f (T_f - T_\infty)}, \end{aligned} \right\} \quad (8.15)$$

in which ( $\tau_{wx}$ ) the wall shear stress and ( $q_w$ ) heat flux are respectively equal to

$$\left. \begin{aligned} \tau_{wx} &= \mu_{hnf} \left( \frac{\partial u}{\partial z} \right) \Big|_{z=0}, \\ q_w &= -k_{nf} \left( \frac{\partial T}{\partial z} \right) \Big|_{z=0}. \end{aligned} \right\} \quad (8.16)$$



Employing Eq. (8.14) in Eq. (8.15) we have

$$\left. \begin{aligned} \text{Re}_x^{0.5} C_{fx} &= \frac{1}{(1-\phi_1)^{25/10}(1-\phi_2)^{25/10}} f''(0), \\ \text{Re}_x^{-0.5} Nu_x &= -\left(\frac{K_{hnf}}{k_f}\right) \theta'(0), \end{aligned} \right\} \quad (8.17)$$

where local Reynolds number is symbolized as  $\text{Re}_x = \frac{xU_w}{\nu_f}$ . It is important to mention that for  $\phi_2 = \phi_1 = 0$ , the conventional liquid (kerosene oil) situation is recovered. When  $\phi_1 \neq 0$  and  $\phi_2 = 0$ , then kerosene oil based CNTs nanomaterials has been achieved. The relation  $\phi_2 \neq \phi_1 \neq 0$  must be satisfied for SWCNT-MWCNT-kerosene oil hybrid nanofluid.

## 8.2 Second law analysis

Production of entropy demolish the present energy in the system of different industrial and engineering processes. Therefore it is significant to estimate the production rate of entropy in a system. For our considered study, it is assumed that generation of entropy occurs as a result of liquid friction, porous medium and irreversibility due to heat transport. Additionally the system is considered in a state of local thermodynamic equilibrium. The volumetric rate of entropy production can be written as

$$E_G = \frac{k_{hnf}}{T_\infty^2} \left(\frac{\partial T}{\partial z}\right)^2 + \frac{\mu_{nf}}{T_\infty} \Psi + \frac{\mu_{nf}}{T_\infty K_p} (u^2 + v^2), \quad (8.18)$$

where  $\Psi$  denotes viscous dissipation

$$\Psi = \left(\frac{\partial u}{\partial z}\right)^2 + \left(\frac{\partial v}{\partial z}\right)^2. \quad (8.19)$$

Using Eq. (8.19) in Eq. (8.17) one has

$$\left. \begin{aligned} E_G &= \frac{k_{hnf}}{T_\infty^2} \left(\frac{\partial T}{\partial z}\right)^2 + \frac{\mu_{nf}}{T_\infty} \left[ \left(\frac{\partial u}{\partial z}\right)^2 + \left(\frac{\partial v}{\partial z}\right)^2 \right] \\ &+ \left(\frac{\mu_{nf}}{T_\infty K_p}\right) (u^2 + v^2). \end{aligned} \right\} \quad (8.20)$$

Now we define the dimensionless entropy generation ( $N_G$ ) which is equal to generation rate of volumetric entropy ( $E_G$ ) to generation rate of characteristic entropy ( $E_0 = \frac{k_{nf}(T_f - T_\infty)}{T_\infty l^2}$ ) ratio.

Mathematically we have

$$N_G = \frac{E_G}{E_0}. \quad (8.21)$$

On utilizing variables (8.6), Eqs. (8.20) and (8.21) can be converted to the form

$$N_G = \frac{k_{nf}}{k_f} \theta'^2 \alpha_1 + \frac{1}{(1-\phi_1)^{25/10}(1-\phi_2)^{25/10}} \lambda \text{Pr} Ec (f'^2 + g^2) + \frac{\text{Pr} Ec}{(1-\phi_1)^{25/10}(1-\phi_2)^{25/10}} (f''^2 + g'^2). \quad (8.22)$$

Bejan number is

$$Be = \frac{\text{Entropy generation due to heat}}{\text{Total entropy generation}}, \quad (8.23)$$

or

$$Be = \frac{\left[\frac{k_{nf}}{k_f}\right] \theta'^2 \alpha_1}{\left[\frac{k_{nf}}{k_f}\right] \theta'^2 \alpha_1 + \lambda \text{Pr} Ec \frac{1}{(1-\phi_1)^{25/10}(1-\phi_2)^{25/10}} (f'^2 + g^2) + \frac{\text{Pr} Ec}{(1-\phi_1)^{25/10}(1-\phi_2)^{25/10}} (f''^2 + g'^2)}, \quad (8.24)$$

where  $\alpha_1 = \frac{(T_f - T_\infty)}{T_\infty}$  manifests the temperature ratio variable due to entropy generation. For  $Be = 0$  the entropy due to liquid friction dominates while for  $Be = 1$  the heat transfer irreversibility effects become predominates rate. Besides that for  $Be = \frac{1}{2}$  the production of entropy due to liquid friction and heat transfer are similar.

### 8.3 Computational scheme

The modeled problems (8.7) – (8.9) and (8.22) subject to boundary conditions (8.10) are computed using NDSolve technique. This technique attains exceptional accuracy and is stable unconditionally. For this computation we assign experimental values to Prandtl number ( $\text{Pr} = 21$ ) and other values are listed in Table (8.2). Boundary conditions  $f'(\eta)$ ,  $g(\eta)$  and  $\theta(\eta)$  for  $\eta \rightarrow \infty$  is converted to finite range ( $\eta = 4.0$ ).

### 8.4 Outcomes and discussion

In this section our emphasis is to visualize the obtained outcomes from non-linear systems after computations. In fact aim of these tables and figures is to analyze the feature of nanomaterials compared to hybrid nanomaterials. Here the combination of SWCNT/kerosene

oil as nanoliquid and SWCNT-MWCNT/kerosene oil as hybrid nanoliquid is used. In all these graphical illustrations (see Figs. (8.2)-(8.17)) the dotted and solid lines show the aspect of nanoliquid and hybrid nanoliquid respectively. The empirical relations and thermo-physical attributes of both types of CNTs and kerosene oil are highlighted in Tables (8.1) and (8.2). Further skin frictions  $((\text{Re}_x^{0.5} f_x))$  for both cases of CNTs nanofluids is computed and discussed (see Table 8.3). Additionally the ranges of pertinent variables for entropy generation ( $N_G$ ), temperature ( $\theta(\eta)$ ) and velocities ( $f'(\eta)$  and  $g(\eta)$ ) are  $0.0 \leq Fr \leq 1.3$ ,  $0.0 \leq \Omega \leq 0.4$ ,  $0.0 \leq \lambda \leq 0.6$ ,  $0.0 \leq \gamma \leq 1.0$ ,  $0.1 \leq \alpha_1 \leq 0.6$ ,  $0.1 \leq \delta \leq 0.4$ ,  $0.1 \leq Ec \leq 0.9$ ,  $0.01 \leq \phi_1 \leq 0.03$ , and  $0.1 \leq \phi_2 \leq 0.03$ .

### 8.4.1 Velocity

The behaviors of velocity distributions ( $f'(\eta)$  and  $g(\eta)$ ) against distinct physical variables are captured in Figs. (8.2)-(8.6). Role of  $Fr$  on ( $f'(\eta)$  and  $g(\eta)$ ) is declared in Figs. (8.2) and (8.3). From Fig. (8.2) it is clear that rising estimations of  $Fr$  decay  $f'(\eta)$  in both nano and hybrid phases. Physically an increment in  $Fr$  enhances the inertial force which is responsible for the reduction of velocity  $f'(\eta)$ . In Fig. (8.3) reverse feature is noticed for  $g(\eta)$  as a result of enhancing  $Fr$ . Figs. (8.4) and (8.5) present the behavior of ( $f'(\eta)$  and  $g(\eta)$ ) with the variation in rotation parameter  $\Omega$ . It depicts that velocity  $f'(\eta)$  grows when angular velocity is enhanced (see Fig.(8.4) for both cases of nanofluid (SWCNT/kerosene oil) and hybrid nanofluid (SWCNT-MWCNT/kerosene oil). In Fig. (8.5) the profile shows a decaying trend of  $g(\eta)$ . The negative values of  $g(\eta)$  indicate that flow is merely in the negative  $y$ -direction. Behavior of  $f'(\eta)$  for  $\lambda$  is disclosed in Fig. (8.6). Here velocity is diminished for both phases of nanofluid (SWCNT/kerosene oil) and hybrid nanofluid (SWCNT-MWCNT/kerosene oil). Further it is noteworthy to mention that throughout from figures (8.2)-(8.6), hybrid nanofluid (SWCNT-MWCNT/kerosene oil) has dominant features when compared with nanofluid (SWCNT/kerosene oil).

### 8.4.2 Temperature

Figs. (8.7)-(8.10) exhibit the influences of  $Ec$ ,  $\delta$ ,  $\phi_1/\phi_2$  and  $\gamma$  on dimensionless temperature  $\theta(\eta)$  for both nanofluid (SWCNT/kerosene oil) and hybrid nanofluid (SWCNT-MWCNT/kerosene

oil). Impact of temperature  $\theta(\eta)$  against Eckert number  $Ec$  is portrayed in Fig. (8.7). An enhancement in thermal field  $\theta(\eta)$  is observed for higher  $Ec$ . In physical sense it is credited to the argument that higher  $Ec$  provides more dissipative energy to liquid which intensifies the nanomaterials temperature. In addition it is remarkable to point out that hybrid nanofluid (SWCNT-MWCNT/kerosene oil) produces more dissipative energy in the fluid than traditional nanofluid (SWCNT/kerosene oil). Characteristics of  $\delta$  on thermal field is illustrated in Fig. (8.8). It is found that  $\theta(\eta)$  and thermal layer are increased for both nanofluid (SWCNT/kerosene oil) and hybrid nanofluid (SWCNT-MWCNT/kerosene oil). Further  $\theta(\eta)$  is higher in case of hybrid nanofluid (SWCNT-MWCNT/kerosene oil) comparative to nanofluid (SWCNT/kerosene oil). Curves in Fig. (8.9) are designed to disclose how fluid temperature is affected by the addition of nanoparticles and hybrid nanoparticles. From this figure three different types of variation can be seen i.e. pink line represents regular fluid, red line indicates nano phase and blue line shows hybrid phase. Comparative study of these lines depicted that hybrid phase has more contribution to intensify  $\theta(\eta)$  than nano phase. Fig. (8.10) illustrates outcome for  $\theta(\eta)$  in response to Biot number  $\gamma$ . Higher convection enhances the surface hotness which consequently rises the thermal field abruptly. Therefore selecting these two cases of nanofluid, thermal conductivity enhances more in hybrid phase when compared with nano phase.

### 8.4.3 Entropy generation

Variations in  $N_G$  versus different physical variables namely porosity parameter, temperature ratio parameter, Eckert number and Biot number for both hybrid phase (SWCNT-MWCNT/kerosene oil) and nano phase (SWCNT/kerosene oil) in the range of  $0 \leq \eta \leq 3.0$  are declared in Figs. (8.11)-(8.14). Here  $N_G$  enhances for an increase of porosity parameter, temperature ratio parameter, Eckert number and Biot number in both cases of nanofluids. These Figs. reflect that porosity parameter, temperature ratio parameter, Eckert number and Biot number contribute in intensifying strength of disorder within the system. Further it is noted that initially the behavior of hybrid phase dominates the nano phase but for higher values of parameters, nano phase behavior marginally dominates when compared with hybrid phase.

#### 8.4.4 Variations in physical quantities of interest ( $C_{fx}$ , $Nu_x$ )

In this subsection aspects of physical quantities of interest i.e skin friction ( $C_{fx}$ ) and temperature gradient ( $Nu_x$ ) for both cases of nanofluid and hybrid nanofluid are illustrated via table and plots. First in Figs. (8.15) and (8.16), an increment of  $\delta$  and  $Ec$  leads to decay the temperature gradient for both phases of nanomaterials. Reverse behavior is seen in Fig. (8.17) for higher estimations of Biot number  $\gamma$ . Additionally we clearly see the difference between Nusselt number of nanofluid (SWCNT/kerosene oil) and hybrid nanofluid (SWCNT-MWCNT/kerosene oil). Table 8.1 is computed numerically to disclose the impact of skin friction against influential variables ( $\Omega$ ,  $\lambda$  and  $Fr$ ). Form this table it is scrutinized that for both nanofluid (SWCNT/kerosene oil) and hybrid nanofluid (SWCNT-MWCNT/kerosene oil), the variables  $\Omega$ ,  $\lambda$  and  $Fr$  have direct link with  $C_{fx}$ . Each variation in parameter also anticipates comparison between nanofluid (SWCNT/kerosene oil) and hybrid nanofluid (SWCNT-MWCNT/kerosene oil). Clearly  $C_{fx}$  is higher for hybrid nanofluid (SWCNT-MWCNT/kerosene oil).

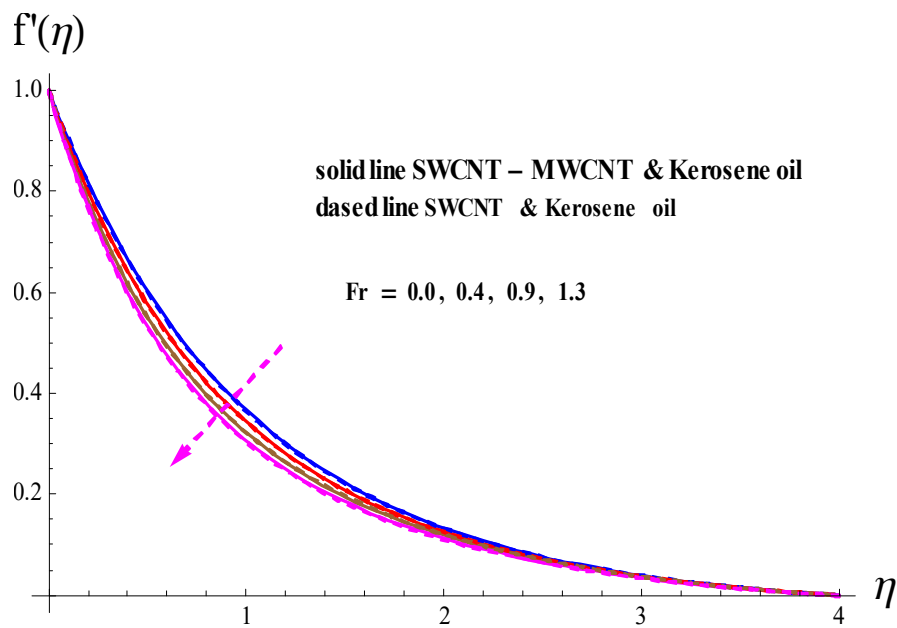


Fig. 8.2. Feature of  $Fr$  on  $f'(\eta)$ .

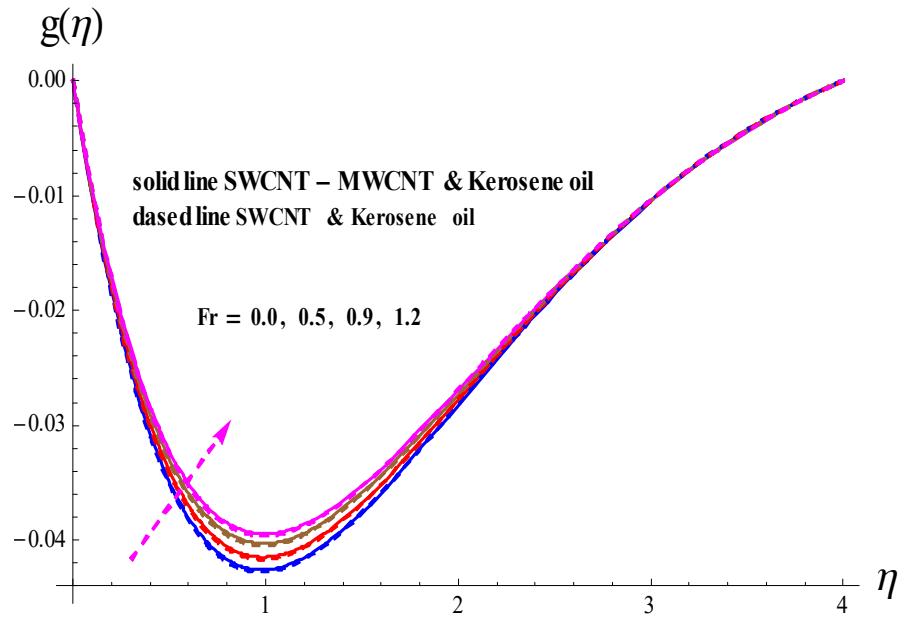


Fig. 8.3. Feature of  $Fr$  on  $g(\eta)$ .

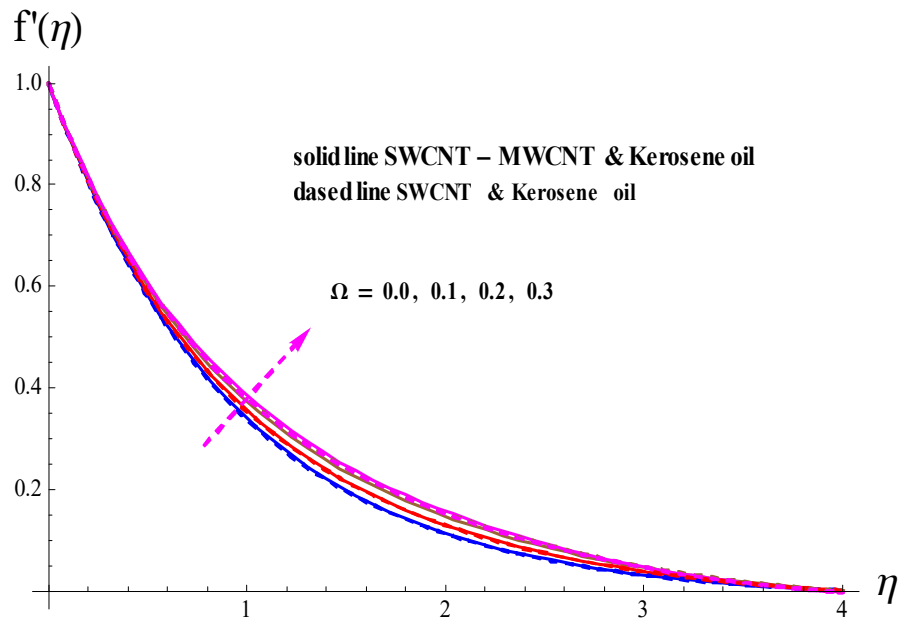


Fig. 8.4. Feature of  $\Omega$  on  $f'(\eta)$ .

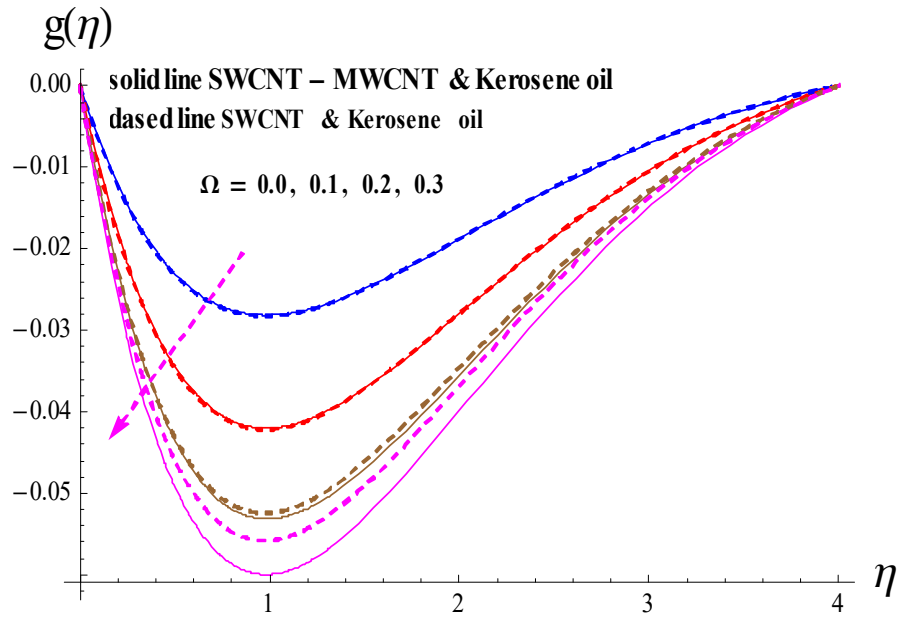


Fig. 8.5. Feature of  $\Omega$  vs  $g(\eta)$ .

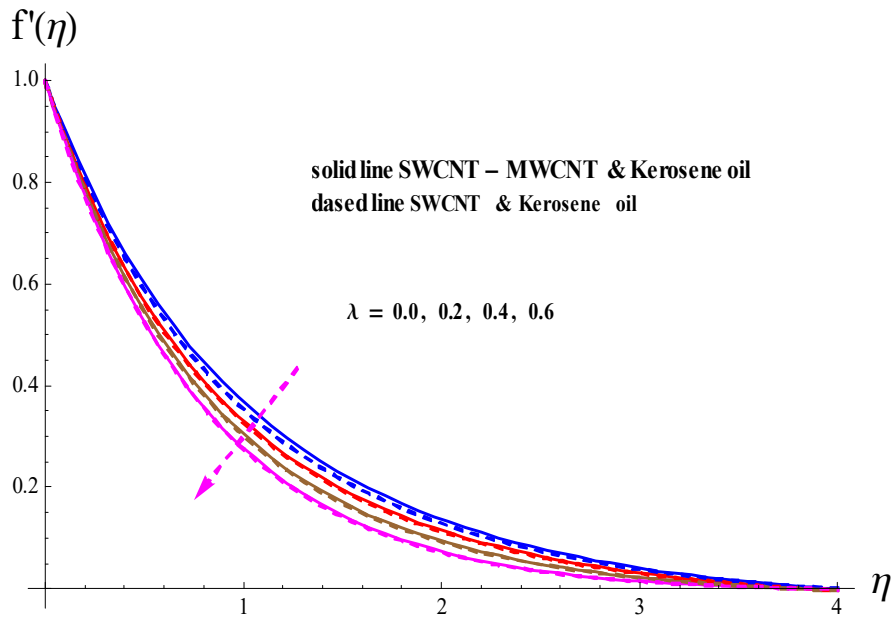


Fig. 8.6. Feature of  $f'(\eta)$  via  $\lambda$ .

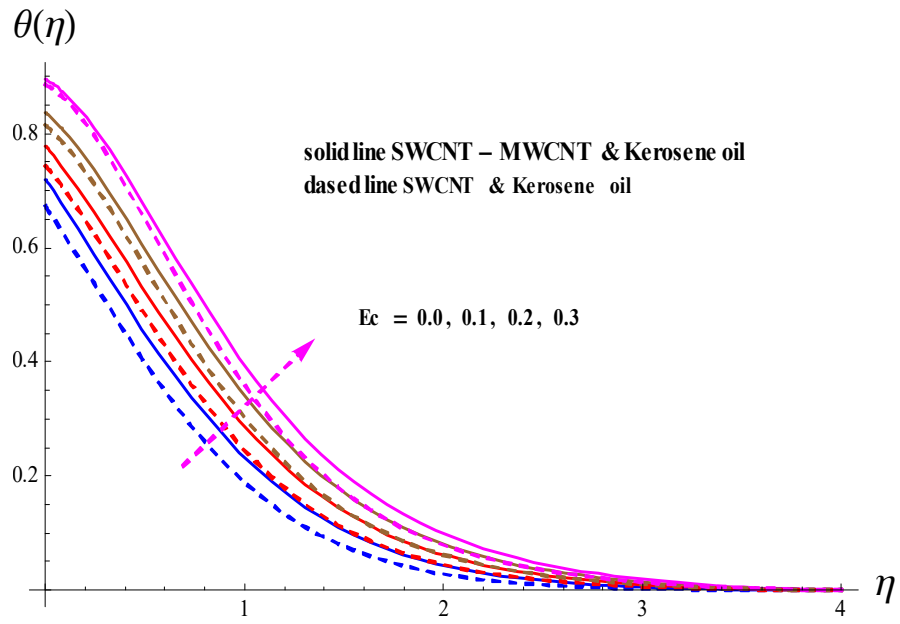


Fig. 8.7. Feature of  $\theta(\eta)$  vs  $Ec$ .

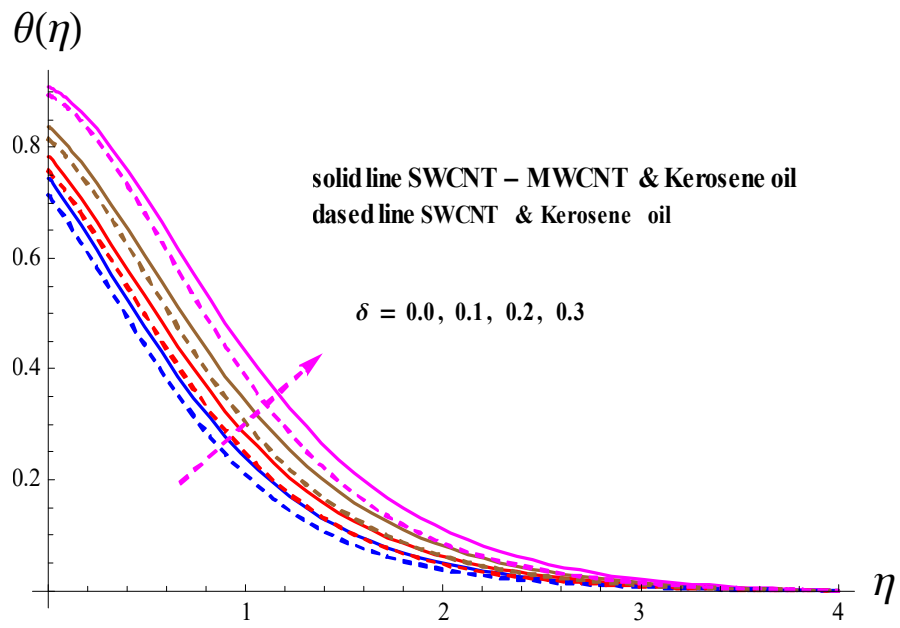


Fig. 8.8. Feature of  $\theta(\eta)$  vs  $\delta$ .



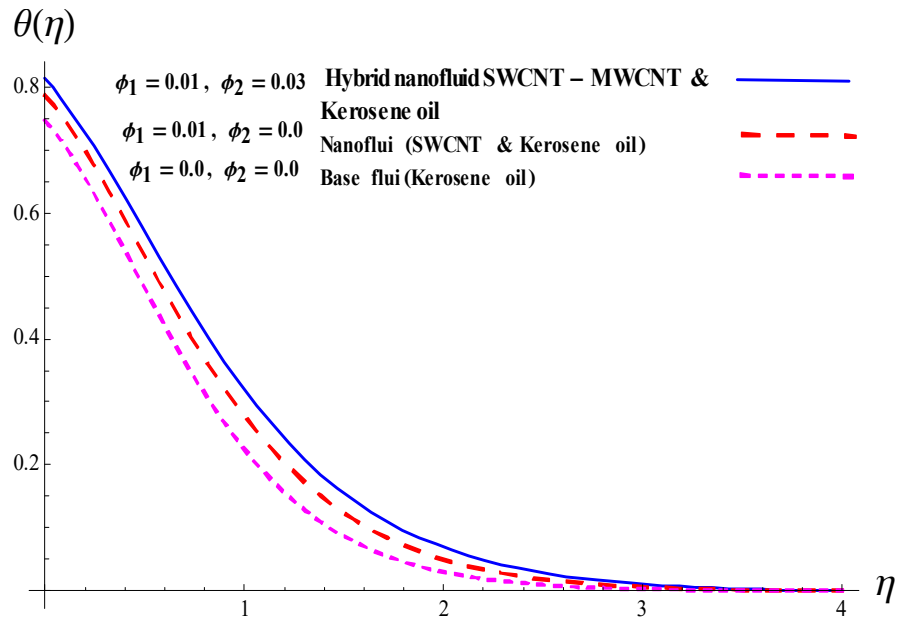


Fig. 8.9. Feature of  $\theta(\eta)$  vs  $\phi_1$  and  $\phi_2$ .

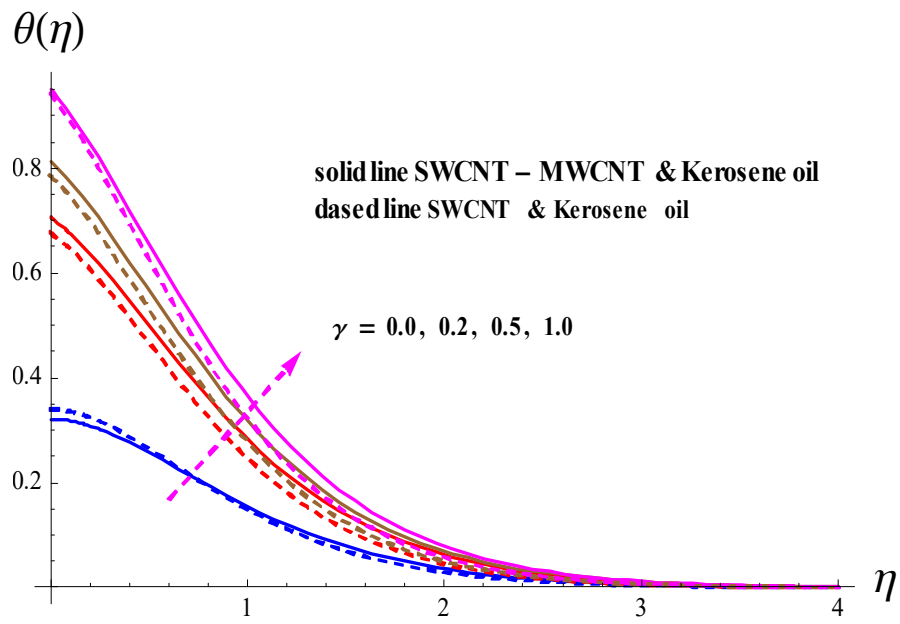


Fig. 8.10. Feature of  $\theta(\eta)$  vs  $\gamma$ .

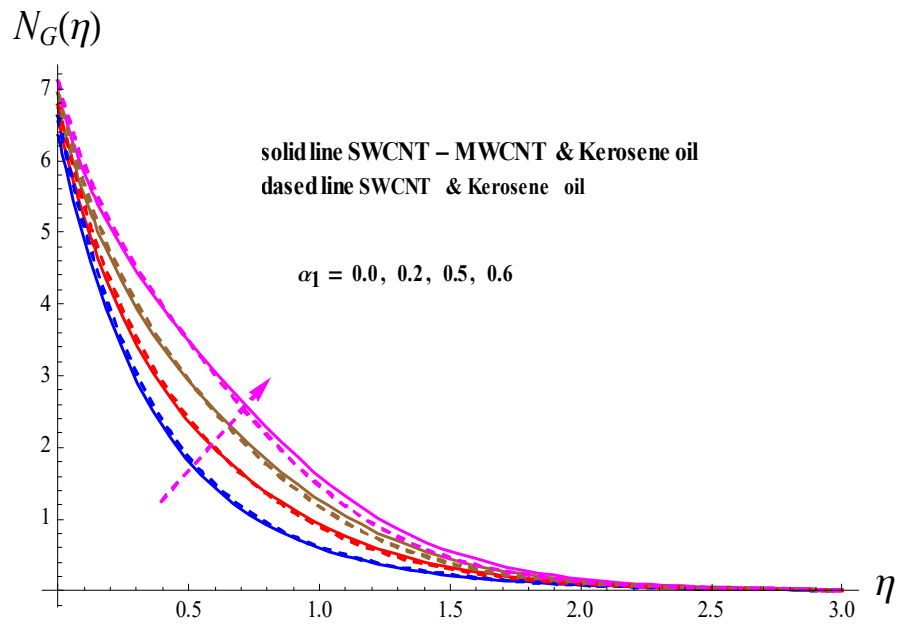


Fig. 8.11. Feature of  $\alpha_1$  on  $N_G(\eta)$ .

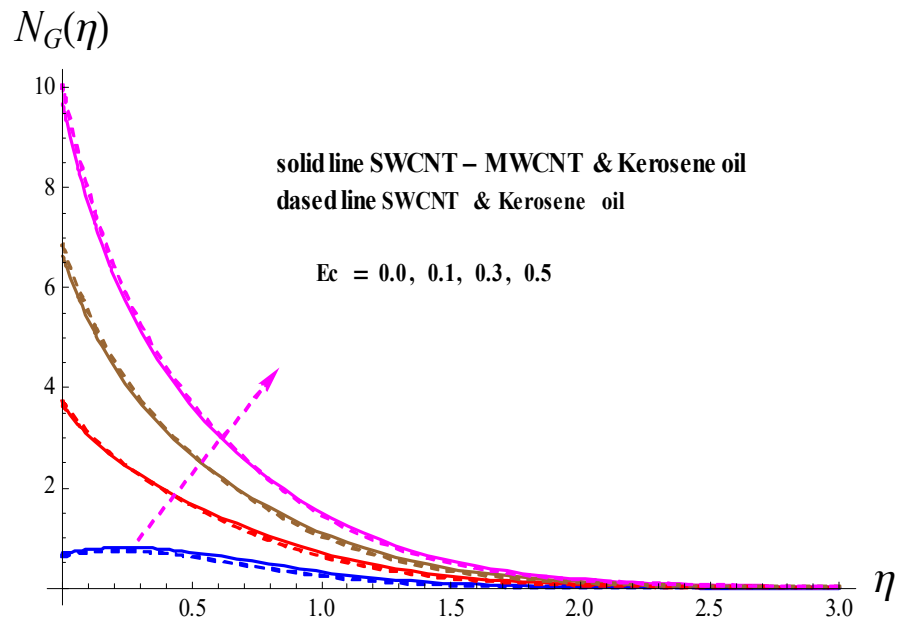


Fig. 8.12. Feature of  $Ec$  on  $N_G(\eta)$ .

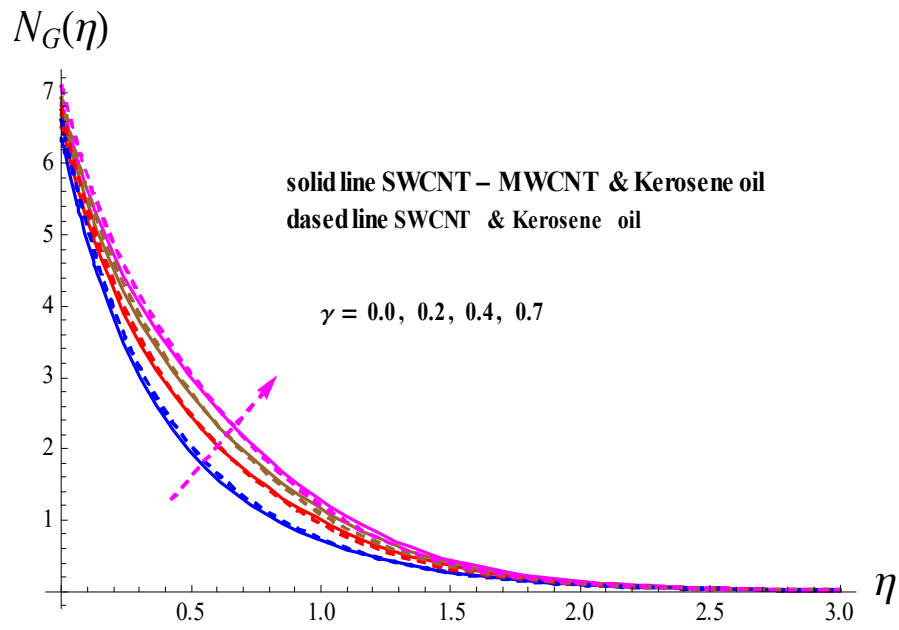


Fig. 8.13. Feature of  $\gamma$  on  $N_G(\eta)$ .

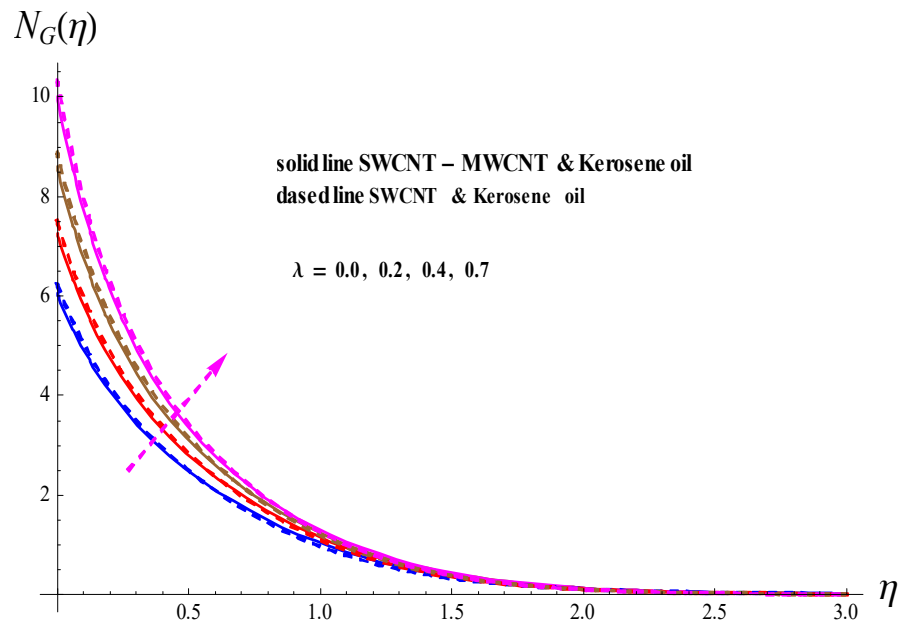


Fig. 8.14. Feature of  $\lambda$  on  $N_G(\eta)$ .

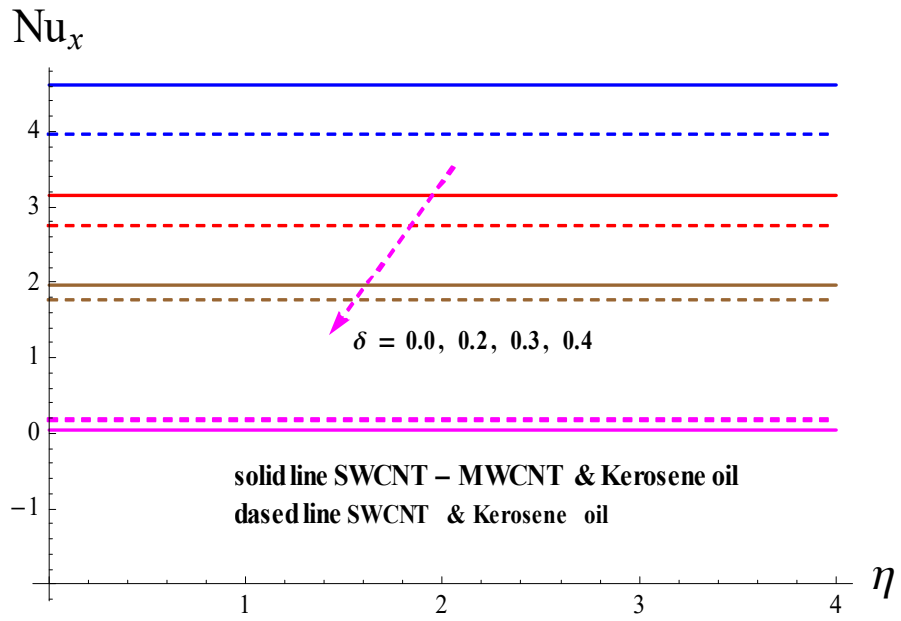


Fig. 8.15. Feature of  $\delta$  on  $Nu_x$ .

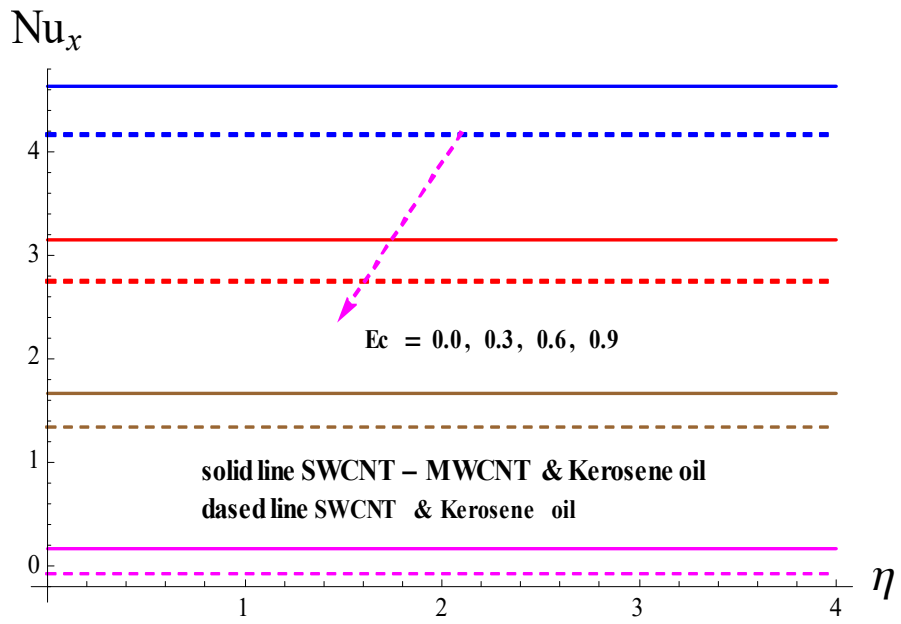


Fig. 8.16. Feature of  $Ec$  on  $Nu_x$ .

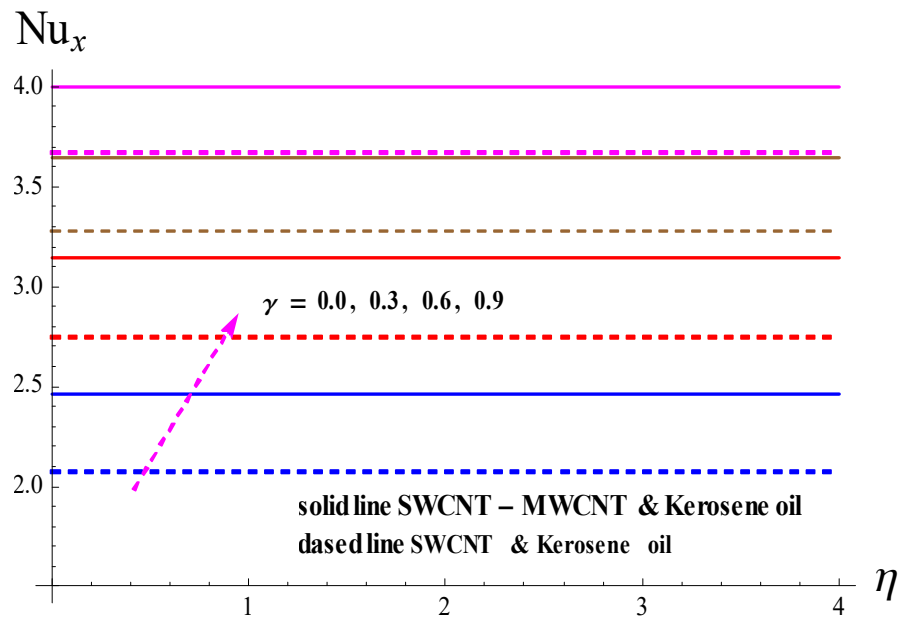


Fig. 8.17. Feature of  $Nu_x$  via  $\gamma$ .

**Table 8.3:** Variations of  $(\text{Re}_x^{0.5} C_{fx})$  through  $\phi$ ,  $Fr$ ,  $\lambda$  and  $\Omega$  for both MWCNTs-kerosene oil and SWCNTs-MWCNTs-kerosene oil.

Parameters (fixed values)	Variables	SWCNTs-kerosene oil		SWCNTs-MWCNTs-kerosene oil
			$-\text{Re}_x^{0.5} C_{fx}$	$-\text{Re}_x^{0.5} C_{fx}$
$\delta = Fr = Ec = 0.2,$ $\lambda = \phi_1 = \phi_2 = 0.1$	$\Omega$	0.0	1.13786	1.15881
		0.2	1.16024	1.18142
		0.4	1.21787	1.23983
$\delta = Ec = 0.2, \lambda = 0.1,$ $\Omega = \phi_1 = \phi_2 = 0.1$	$Fr$	0.0	1.08368	1.10366
		0.3	1.17255	1.19404
		0.5	1.22864	1.25108
$\delta = Fr = Ec = 0.2,$ $\Omega = \phi_1 = \phi_2 = 0.1$	$\lambda$	0.0	1.09794	1.11745
		0.3	1.23053	1.25432
		0.6	1.35141	1.37893

## 8.5 Final outcomes

Key points of presented analysis are listed below:

- Velocities show opposite response against  $Fr$  and  $\Omega$ .
- Higher  $\delta$  and  $Ec$  lead to improve the thermal field for both phases of nanomaterials.
- Skin friction enhances for  $\lambda$ ,  $Fr$  and  $\Omega$ .
- Implementing hybrid nanomaterials rather than traditional nanomaterials is much more effective.
- The magnitude of  $Nu_x$  for nanoliquid is also smaller than  $Nu_x$  for hybrid nanoliquid.

# Bibliography

- [1] A. Bejan, A study of entropy generation in fundamental convective heat transfer, *J. Heat. Transfer*, 101 (1979) 718–725.
- [2] A. Bejan, *Entropy generation through heated fluid flow*, Wiley, NewYork, 1982.
- [3] O. Mahian, S. Mahmud and S.Z. Heris, Analysis of entropy generation between co-rotating cylinder susing nanofluids, *Energy*, 44 (2012) 438–446.
- [4] A. Reveillere and A.C. Baytas, Minimum entropy generation for laminar boundary layer flow over a permeable plate, *Int. J. Exergy*, 7 (2010) 164–177.
- [5] M.M. Rashidi, N. Kavyani and S. Abelman, Investigation of entropy generation in MHD and slip flow over a rotating porous disk with variable properties, *Int. J. Heat. Mass Transf.*, 70 (2014) 892–917.
- [6] G. Ibanez, Entropy generation in MHD porous channel with hydrodynamic slip and convective boundary conditions, *Int. J. Heat. Mass Transf.*, 80 (2015) 274–280.
- [7] Y.J. Jian, Transient MHD heat transfer and entropy generation in a microparallel channel combined with pressure and electroosmotic effects, *Int. J. Heat Mass Transfer.*, 89 (2015) 193–205.
- [8] A.S. Butt, S. Munawar, A. Ali and A. Mehmood, Entropy generation in the Blasius flow under thermal radiation, *Phys. Scr.*, 85 (2012) 035008.
- [9] M. Mustafa, I. Pop, K. Naganthran and R. Nazar, Entropy generation analysis for radiative heat transfer to Bödewadt slip flow subject to strong wall suction, *Eur. J. Mech. B-Fluids*, 72 (2018) 179–188.

- [10] T. Hayat, S. Qayyum, M.I. Khan and A. Alsaedi, Entropy generation in magnetohydrodynamic radiative flow due to rotating disk in presence of viscous dissipation and Joule heating, *Phys. Fluid.*, 30 (2018) 017101.
- [11] M.I. Khan, T.A. Khan T. Hayat, M.I. Khan, S. Qayyum, A. Alsaedi and I. Ullah, Irreversibility analysis and heat transfer performance of Williamson nanofluid over a stretched surface, *Heat transf. Res.*, (2018), 10.1615/HeatTransRes.2018026342.
- [12] N. V. Ganesh, Q.M. Al-Mdallal and A. J. Chamkha, A numerical investigation of Newtonian fluid flow with buoyancy, thermal slip of order two and entropy generation, *Case Studies Therm. Eng.*, 13 (2019) 100376.
- [13] S.U.S. Choi, Enhancing thermal conductivity of fluids with nanoparticle, In proceedings of the ASME Int. Mech. Eng. Cong. Exposition, 66 (1995) 99–105.
- [14] J.A. Eastman, S.U.S. Choi, S. Li, W. Yu and L.J. Thompson, Anomalous increased effective thermal conductivity of ethylene glycol-based nanofluids containing copper nanoparticles, *Appl. Phys. Lett.*, 78 (2001) 718–720.
- [15] S.K. Das, S.U. Choi and H.E. Patel, Heat transfer in nanofluids a review, *Heat Transf. Eng.*, 27 (2006) 3–19.
- [16] Q. Xue and W.M. Xu, A model of thermal conductivity of nanofluids with interfacial shells, *Mater. Chem. Phys.*, 90 (2005) 298–301.
- [17] R. Ellahi, M. Hassan and A. Zeeshan, Shape effects of nanosize particles in Cu-H<sub>2</sub>O nanofluid on entropy generation, *Int. J. Heat Mass Transf.*, 81 (2015) 449–456.
- [18] M. Mustafa, A. Mushtaq, T. Hayat and A. Alsaedi, Rotating flow of magnetitewater nanofluid over a stretching surface inspired by nonlinear thermal radiation, *PLOS One*, 11 (2016) e0149304.
- [19] L. Yang and K. Du, A comprehensive review on heat transfer characteristics of TiO<sub>2</sub> nanofluids, *Int. J. Heat Mass Transf.*, 108 (2017) 11–31.



- [20] Z. Hussain, T. Hayat, A. Alsaedi and B. Ahmad, Three-dimensional convective flow of CNTs nanofluids with heat generation/absorption effect: A numerical study, *Comp. Methods Appl. Mech. Eng.*, 329 (2018) 40-54.
- [21] N.S. Shashikumar, B.J. Gireesha, B. Mahanthesh and B.C. Prasannakumara, Brinkman-Forchheimer flow of SWCNT and MWCNT magneto-nanofluids in a microchannel with multiple slips and Joule heating aspects, *Multidiscipline Mod. Mater. Structures*, 14 (2018) 769-786.
- [22] I.L. Animasaun, B. Mahanthesh, A.O. Jagun, T.D. Bankole, R. Sivaraj, N.A. Shah and S. Saleem, Significance of Lorentz force and thermoelectric on the flow of 29 nm CuO-water nanofluid on an upper horizontal surface of a paraboloid of revolution, *J. Heat Transfer*, 141 (2019) 022402.
- [23] Z. Boualahia, A. Wakif, A.J. Chamkha, C.H. Amanulla and R. Sehaqui, Effects of wavy wall amplitudes on mixed convection heat transfer in a ventilated wavy cavity filled by copper-water nanofluid containing a central circular cold body, *J. Nanofluids*, 8 (2019) 1170-1178.
- [24] T. Hayat, K. Muhammad, I. Ullah, A. Alsaedi and S. Asghar, Rotating squeezed flow with carbon nanotubes and melting heat, *Phys. Scr.*, 94 (2019) 035702.
- [25] R. Mohebbi, S.A.M. Mehryan, M. Izadi and O. Mahian, Natural convection of hybrid nanofluids inside a partitioned porous cavity for application in solar power plants, *J. Therm. Anal. Calorim.*, 137 (2019) 1719-1733.
- [26] N. Moghaddaszadeh, J.A. Esfahani and O. Mahian, Performance enhancement of heat exchangers using eccentric tape inserts and nanofluids, *J. Therm. Anal. Calorim.*, (2019) 1-13.
- [27] S. Rashidi, M. Eskandarian, O. Mahian and S. Poncet, Combination of nanofluid and inserts for heat transfer enhancement, *J. Therm. Anal. Calorim.*, 135 (2019) 437-460.
- [28] Q.Z. Xue, Model for thermal conductivity of carbon nanotube-based composites, *Physica B.*, 368 (2005) 302-307.

- [29] J. Wang, J. Zhu, X. Zhang and Y. Chen, Heat transfer and pressure drop of nanofluids containing carbon nanotubes in laminar flows, *Exp. Therm. Fluid Sci.*, 44 (2013) 716–721.
- [30] T. Hayat, M. Farooq and A. Alsaedi, Homogeneous-heterogeneous reactions in the stagnation point flow of carbon nanotubes with Newtonian heating, *AIP Adv.*, 5 (2015) 027130.
- [31] R. Ellahi, M. Hassan and A. Zeeshan, Study of natural convection MHD nanofluid by means of single and multi walled carbon nanotubes suspended in a salt water solutions, *IEEE Trans. Nanotechnol.*, 14 (2015) 726–734.
- [32] M. Imtiaz, T. Hayat, A. Alsaedi and B. Ahmad, Convective flow of carbon nanotubes between rotating stretchable disks with thermal radiation effects, *Int. J. Heat Mass Tran.*, 101 (2016) 948–957.
- [33] S. Farooq, T. Hayat, A. Alsaedi and S. Asghar, Mixed convection peristalsis of carbon nanotubes with thermal radiation and entropy generation, *J. Mol. Liq.*, 250 (2018) 451–467.
- [34] R. Kumar, R. Kumar, M. Sheikholeslami and A. J. Chamkha, Irreversibility analysis of the three dimensional flow of carbon nanotubes due to nonlinear thermal radiation and quartic chemical reactions, *J. Mol. Liq.*, 274 (2019) 379–392.
- [35] M.H. Hamzah, N.A.C. Sidik, T.L. Ken, R. Mamat and G. Najafi, Factors affecting the performance of hybrid nanofluids: a comprehensive review, *Int. J. Heat Mass Transf.*, 115 (2017) 630–646.
- [36] D.D. Kumar and A.V. Arasu, A comprehensive review of preparation, characterization, properties and stability of hybrid nanofluids, *Renew. Sust. Energ. Rev.*, 81 (2018) 1669–1689.
- [37] J. Sarkar, P. Ghosh and A. Adil, A review on hybrid nanofluids: recent research, development and applications, *Renew. Sust. Energ. Rev.*, 43 (2015) 164–177.
- [38] N.A.C. Sidik, M.M. Jamil, W.M.A.A. Japar and I.M. Adamu, A review on preparation methods, stability and applications of hybrid nanofluids, *Renew. Sust. Energ. Rev.*, 80 (2017) 1112–1122.

- [39] S. Suresh, K.P. Venkitaraj, M.S. Hameed and J. Sarangan, Turbulent heat transfer and pressure drop characteristics of dilute water based Al<sub>2</sub>O<sub>3</sub>-Cu hybrid nanofluids, *J. Nanosci. Nanotechnol.*, 14 (2014) 2563-2572.
- [40] S.S. Harandi, An experimental study on thermal conductivity of FMWCNTs-Fe<sub>3</sub>O<sub>4</sub>/EG hybrid nanofluid: effects of temperature and concentration, *Int. Commun. Heat Mass Transf.*, 76 (2016) 171-177.
- [41] S.S. Ghadikolaei, K. Hosseinzadeh and D.D. Ganj, Investigation on ethylene glycol-water mixture fluid suspend by hybrid nanoparticles (TiO<sub>2</sub>-CuO) over rotating cone with considering nanoparticles shape factor, *J. Mole. Liq.*, 272 (2018) 226-236.
- [42] M.N. Rostamia, S. Dinarvanda and I. Pop, Dual solutions for mixed convective stagnation-point flow of an aqueous silica-alumina hybrid nanofluid, *Chines J. Phys.*, 56 (2018) 2465-2478.
- [43] A. Ishak, R. Nazar and I. Pop, Uniform suction/blowing effect on flow and heat transfer due to a stretching cylinder, *Appl. Math. Model.*, 32 (2008) 2059-2066.
- [44] T. Hayat, M.I. Khan, M. Waqas and A. Alsaedi, Newtonian heating effect in nanofluid flow by a permeable cylinder, *Results Phys.*, 7 (2017) 256-262.
- [45] T. Hayat, M. Zubair, M. Waqas, A. Alsaedi and M. Ayub, Application of non-Fourier heat flux theory in thermally stratified flow of second grade liquid with variable properties, *Chin. J. Phys.*, 55 (2017) 230-241.
- [46] M. Turkyilmazoglu, Multiple solutions of heat and mass transfer of MHD slip flow for the viscoelastic fluid over a stretching sheet, *Int. J. Thermal Sci.*, 50 (2011) 2264-2276.
- [47] T. Hayat, I. Ullah, T. Muhammad and A. Alsaedi, Magnetohydrodynamic (MHD) three-dimensional flow of second grade nanofluid by a convectively heated exponentially stretching surface, *J. Mol. Liq.*, 220 (2016) 1004-1012.
- [48] T. Hayat, M. Zubair, M. Waqas, A. Alsaedi and M. Ayub, Impact of variable thermal conductivity in doubly stratified chemically reactive flow subject to non-Fourier heat flux theory, *J. Mol. Liq.*, 234 (2017) 444-451.

- [49] M.A. Zaky, An improved tau method for the multi-dimensional fractional Rayleigh–Stokes problem for a heated generalized second grade fluid, *Comp. Math. Appl.*, 75 (2018) 2243–2258.
- [50] A.W. Sisko, The flow of lubricating greases, *Ind. Eng. Chem. Res.*, 50 (1958) 1789–1792.
- [51] S. Abelman, T. Hayat and E. Momoniat, On the Rayleigh problem for a Sisko fluid in a rotating frame, *Appl. Math. Comput.*, 215 (2009) 2515–2520.
- [52] T. Hayat, R.J. Moitsheki and S. Abelman, Stokes’ first problem for Sisko fluid over a porous wall, *Appl. Math. Comput.*, 217 (2010) 622–628.
- [53] A. Munir, A. Shahzad, M. Khan, Convective flow of Sisko fluid over a bidirectional stretching surface, *PLos One*, 10 (2015) e0130342.
- [54] M. Khan and R. Malik, Forced convective heat transfer to Sisko nanofluid past a stretching cylinder in the presence of variable thermal conductivity, *J. Mol. Liqs.*, 218 (2016) 1–7.
- [55] T. Hayat, T. Muhammad, S.A. Shehzad and A. Alsaedi, On three-dimensional boundary layer flow of Sisko nanofluid with magnetic field effects, *Adv. Powder Technol.*, 27 (2016) 504–512.
- [56] R.V. Williamson, The flow of pseudoplastic materials, *Industrial Eng. Chem. Research*, 21 (1929) 1108–1111.
- [57] M. Kothandapani and J. Prakash, Effect of thermal radiation parameter and magnetic field on the peristaltic flow of Williamson nanofluids in a tapered asymmetric channel, *Int. J. Heat Mass Transfer*, 51 (2015) 234–45.
- [58] S.D. Cramer and J.M. Marchello, Numerical evaluation of models describing non-Newtonian behavior, *American Inst. Chem. Eng. J.*, 14 (1968) 980–983.
- [59] S.D. Cramer and J.M. Marchello, Numerical evaluation of models describing non-Newtonian behavior, *American Inst. Chem. Eng. J.*, 14 (1968) 980–983.

- [60] T. Hayat, I. Ullah, A. Alsaedi and B. Ahmad, Variable aspects of double stratified MHD flow of second grade nanoliquid with heat generation/absorption: A revised model, *Radiat. Phys. Chem.*, 157 (2019) 109-115.
- [61] E. Magyari and A. Pantokratoras, Note on the effect of thermal radiation in the linearized Rosseland approximation on the heat transfer characteristics of various boundary layer flows, *Int. Commun. Heat Mass Transfer*, 38 (2011) 554-556.
- [62] A. Pantokratoras, Natural convection along a vertical isothermal plate with linear and nonlinear Rosseland thermal radiation, *Int. J. Thermal Sci.*, 84 (2014) 151-157.
- [63] R. Cortell, Fluid flow and radiative nonlinear heat transfer over a stretching sheet, *J. King Saud Uni.-Sci.*, 26 (2014) 161-167.
- [64] M.I. Khan, M. Waqas, T. Hayat, A. Alsaedi and M.I. Khan, Significance of nonlinear radiation in mixed convection flow of magneto Walter-B nanoliquid, *Int. J. Hydrogen Energy*, 42 (2017) 26408-26416.
- [65] M. Irfan, M. Khan and W.A. Khan, Interaction between chemical species and generalized Fourier's law on 3D flow of Carreau fluid with variable thermal conductivity and heat sink/source: A numerical approach, *Results Phys.*, 10 (2018) 107-117.
- [66] P. Forchheimer, Wasserbewegung durch boden, *Zeitschrift Ver. D. Ing.*, 45 (1901) 1782-1788.
- [67] M. Muskat, *The flow of homogeneous fluids through porous media*, (1946) Edwards, MI.
- [68] J.C. Umavathi, O. Ojjela and K. Vajravelu, Numerical analysis of natural convective flow and heat transfer of nanofluids in a vertical rectangular duct using Darcy Forchheimer-Brinkman model, *Int. J. Therm. Sci.*, 111 (2017) 511-524.
- [69] M.A. Sadiq and T. Hayat, Darcy-Forchheimer flow of magneto Maxwell liquid bounded by convectively heated sheet, *Results Phys.*, 6 (2016) 884-890.
- [70] T. Hayat, A. Aziz, T. Muhammad and A. Alsaedi, An optimal analysis for Darcy-Forchheimer 3D flow of Carreau nanofluid with convectively heated surface, *Results Phys.*, 9 (2018) 598-608.

- [71] A.K. Alzahrani, Darcy–Forchheimer 3D flow of carbon nanotubes with homogeneous and heterogeneous reactions, *Phys. Letters A*, 382 (2018) 2787–2793.
- [72] T. Hayat, K. Rafique, T. Muhammad, A. Alsaedi and M. Ayub, Carbon nanotubes significance in Darcy–Forchheimer flow, *Results Phys.*, 8 (2018) 26–33.
- [73] J.D. Audu, F. Fairag and K. Mustapha, Mixed finite element analysis for generalized Darcy–Forchheimer model in porous media, *J. Comput. Appl. Math.*, 353 (2019) 191–203.
- [74] S.J. Liao, On the homotopy analysis method for nonlinear problems, *Appl. Math. Comput.* 147 (2004) 499-513.
- [75] M. Sheikholeslami, M. Hatami and D.D. Ganji, Micropolar fluid flow and heat transfer in a permeable channel using analytic method, *J. Mol. Liq.*, 194 (2014) 30–36.
- [76] T. Hayat and M. Sajid, On analytic solution for thin film flow of a fourth grade fluid down a vertical cylinder, *Phys. Lett. A*, 361 (2007) 316-322.
- [77] A. Mastroberardino, Homotopy analysis method applied to electrohydrodynamic flow. *Commun. Nonlinear Sci. Numer. Simulat.*, 16 (2011) 2730–2736.
- [78] O. A. Beg, M. M. Rashidi, T. A. Beg and M. Asadi, Homotopy analysis of transient magneto-bio-fluid dynamics of micropolar squeeze film in a porous medium: A model for magneto-bio-rheological lubrication, *J. Mech. Medicine Biology*, 12 (2012) 1250051.
- [79] T. Hayat, M. Farooq and A. Alsaedi, Inclined magnetic field effect in stratified stagnation point flow over an inclined cylinder, *Z. Naturforsch.*, 70 (2015) 317-324.
- [80] T. Hayat, I. Ullah, A. Alsaedi and B. Ahmad, Radiative flow of Carreau liquid in presence of Newtonian heating and chemical reaction, *Results Phys.*, 7 (2017) 715-722.
- [81] S. Abbasbandy, T. Hayat, A. Alsaedi and M. M. Rashidi, Numerical and analytical solutions for Falkner-Skan flow of MHD Oldroyd-B fluid, *Int. J. Numer. Methods Heat Fluid Flow*, 24 (2014) 390-401.

- [82] T. Hayat, I. Ullah, A. Alsaedi, and B. Ahmad, Modeling tangent hyperbolic nanoliquid flow with heat and mass flux conditions, *Eur. Phys. J. Plus*, 132 (2017) 112.
- [83] M. Turkyilmazoglu, Parametrized Adomian decomposition method with optimum convergence, *Trans. Model. Comput. Simul.*, 27 (2017), doi:10.1145/3106373.
- [84] T. Hayat, I. Ullah, A. Alsaedi and B. Ahmad, Simultaneous effects of non-linear mixed convection and radiative flow due to Riga-plate with double stratification, *J. Heat Transfer*, 140 (2018) 102008.
- [85] Liao, S. J. Liao, An optimal homotopy-analysis approach for strongly nonlinear differential equations. *Commun. Nonlinear Sci. Numer. Simul.*, 15 (2010) 2003-2016.
- [86] N. S. Akbar, S. Nadeem, R. U. Haq and Z. H. Khan, Numerical solutions of magnetohydrodynamic boundary layer flow of tangent hyperbolic fluid towards a stretching sheet, *Indian J. Phys.*, 87 (2013) 1121-1124.
- [87] Hashim and M. Khan, A revised model to analyze the heat and mass transfer mechanisms in the flow of Carreau nanofluids, *Int. J. Heat Mass Transfer*, 103 (2016) 291-297.
- [88] Hashim and M. Khan, On Cattaneo-Christov heat flux model for Carreau fluid flow over a slendering sheet, *Results Phys.*, 7 (2017) 310-319.
- [89] A.H. Hashim and M. Khan, Numerical simulation for heat transfer performance in unsteady flow of Williamson fluid driven by a wedge-geometry, *Results Phys.* 9 (2018) 479-485
- [90] T. Fang, J. Zhang and S. Yao, *Commun. Nonlinear Sci. Numer. Simul.*, 14 (2009) 3731.
- [91] S. Abelman, T. Hayat and E. Momoniat, On the Rayleigh problem for a Sisko fluid in a rotating frame, *Appl. Math. Comput.*, 215 (2009) 2515-2520.
- [92] M. Molati, T. Hayat and F. Mahomed, Rayleigh problem for a MHD Sisko fluid, *Nonlin Analysis: Real World Appl.*, 10 (2009) 3428-3434.
- [93] T. Hayat, N. Aslam, A. Alsaedi and M. Rafiq, Numerical study for MHD peristaltic transport of Sisko nanofluid in a curved channel. *Int. J. Heat Mass Transfer*, 109 (2017) 1281-1288.

- [94] T. Hayat, R.J. Moitsheki and S. Abelman, Stokes' first problem for Sisko fluid over a porous wall, *Appl. Math. Comput.* 217 (2010) 622-628.
- [95] N. Ali, A. Zaman and M. Sajid, Unsteady blood flow through a tapered stenotic artery using Sisko model, *Comput. Fluids*, 101 (2014) 42-49.
- [96] M.M. Rahman, Locally similar solutions for hydromagnetic and thermal slip flow boundary layers over a flat plate with variable fluid properties and convective surface boundary condition, *Meccanica*, 46 (2011) 1127–1143.
- [97] E. Magyari and B. Keller, Heat and mass transfer in the boundary layers on an exponentially stretching continuous surface, *J. Phys. D. Appl. Phys.*, 32 (1999) 577–585.
- [98] M. Khan and A. Shahzad, On boundary layer flow of a Sisko fluid over a stretching sheet, *Quaest. Math.*, 36, (2013) 137–151.
- [99] E. Sanjayanand and S.K. Khan, On heat and mass transfer in a viscoelastic boundary layer flow over an exponentially stretching sheet, *Int. J. Therm. Sci.*, 45 (2006) 819–828.
- [100] S.V. Subhashini, N. Samuel and I. Pop, Double-diffusive convection from a permeable vertical surface under convective boundary condition, *Int. Commun. Heat Mass transfer*, 38 (2011) 1183-1188.
- [101] P.D. Ariel, Generalized three-dimensional flow due to a stretching sheet, *Z. Angew. Math. Mech.*, 83 (2003) 844–852.
- [102] A. Munir, A. Shahzad and M. Khan, Convective flow of Sisko fluid over a bidirectional stretching surface, *PLos One* 10 (2015) e0130342.
- [103] D. Sarma and K.K. Pandit, Effects of Hall current, rotation and Soret effects on MHD free convection heat and mass transfer flow past an accelerated vertical plate through a porous medium, *Ain Shams Eng. J.*, (2018) 9, 631–646.
- [104] J.A. Shercliff, *A textbook of magnetohydrodynamics*, Pergamon Press, (1965) 45.
- [105] T.G. Cowling, *Magnetohydrodynamics*, New York: Interscience Publishers; 1957.



- [106] B. Mahanthesh, B.J. Gireesha, B.C. Prasannakumara and P.B.S. Kumar, Magneto-Thermo-Marangoni convective flow of Cu-H<sub>2</sub>O nanoliquid past an infinite disk with particle shape and exponential space based heat source effects, *Results Phys.*, 7 (2017) 2990–2996.
- [107] U. Khan, Adnan, N. Ahmed and S. T. Mohyud-Din, Heat transfer enhancement in hydromagnetic dissipative flow past a moving wedge suspended by H<sub>2</sub>O-aluminum alloy nanoparticles in the presence of thermal radiation, *Int. J. Hydrogen Energy*, 42 (2017) 24634-24644.
- [108] N. Sandeep, R.P. Sharma and M. Ferdows, Enhanced heat transfer in unsteady magneto-hydrodynamic nanofluid flow embedded with aluminum alloy nanoparticles, *J. Mol. Liq.*, 234 (2017) 437-443.
- [109] S.S. Ghadikolaei, Kh. Hosseinzadeh, M. Hatami, D.D. Ganji and M. Armin, Investigation for squeezing flow of ethylene glycol (C<sub>2</sub>H<sub>6</sub>O<sub>2</sub>) carbon nanotubes (CNTs) in rotating stretching channel with nonlinear thermal radiation, *J. Mol. Liq.*, 263 (2018) 10–21.
- [110] T. Hayat, F. Haider, T. Muhammad and A. Alsaedi, On Darcy-Forchheimer flow of carbon nanotubes due to a rotating disk, *Int. J. Heat Mass Transfer*, 112 (2017) 248–254.
- [111] M. Mustafa, I. Pop, K. Naganthran and R. Nazar, Entropy generation analysis for radiative heat transfer to Bödewadt slip flow subject to strong wall suction, *Eur. J. Mech. B-Fluids*. 72 (2018) 179-188.
- [112] T. Hayat, S. Qayyum, M. I. Khan and A. Alsaedi, Entropy generation in magnetohydrodynamic radiative flow due to rotating disk in presence of viscous dissipation and Joule heating, *Phys. Fluid.*, 30 (2018) 017101.

## Turnitin Originality Report

Flows of Nanomaterials by Stretching Boundaries  
From DRSM (DRSM L)

by Ikram Ullah .



- Processed on 28-Sep-2020 09:17 PKT
- ID: 1398919238
- Word Count: 26382

Similarity Index  
9%  
Similarity by Source:

Internet Sources:  
4%  
Publications:  
6%  
Student Papers:  
3%

*3/11/2020*  
*3/x/2020*

*Ikram Ullah*

**Focal Person (Turnitin)**  
**Quaid-i-Azam University**  
**Islamabad**

*Ikram Ullah*

**sources:**

- 1 < 1% match (Internet from 05-Oct-2017)  
<http://pr.hec.gov.pk/Thesis/2927S.pdf>
- 2 < 1% match (student papers from 10-Jan-2017)  
[Submitted to Higher Education Commission Pakistan on 2017-01-10](#)
- 3 < 1% match (student papers from 10-Oct-2009)  
[Submitted to Higher Education Commission Pakistan on 2009-10-10](#)
- 4 < 1% match (publications)  
[Tasawar Hayat, M. Ijaz Khan, Tufail Ahmad Khan, M.I. Khan, Salman Ahmad, Ahmed Alsaedi. "Entropy generation in Darcy-Forchheimer bidirectional flow of water-based carbon nanotubes with convective boundary conditions", Journal of Molecular Liquids, 2018](#)
- 5 < 1% match (student papers from 12-Mar-2018)  
[Submitted to Institute Vinca on 2018-03-12](#)
- 6 < 1% match (student papers from 21-Sep-2015)  
[Submitted to Higher Education Commission Pakistan on 2015-09-21](#)
- 7 < 1% match (publications)  
[Shehzad, Sabir Ali, Tasawar Hayat, Ahmed Alsaedi, and Mustafa Ali Obid. "Nonlinear thermal radiation in three-dimensional flow of Jeffrey nanofluid: A model for solar energy", Applied Mathematics and Computation, 2014.](#)
- 8 < 1% match (publications)